

# Sheffield Hallam University

*Processing and rheological studies of cellulosic materials.*

TSANG, Sideny C.N.

Available from the Sheffield Hallam University Research Archive (SHURA) at:

<http://shura.shu.ac.uk/20456/>

## A Sheffield Hallam University thesis

This thesis is protected by copyright which belongs to the author.

The content must not be changed in any way or sold commercially in any format or medium without the formal permission of the author.

When referring to this work, full bibliographic details including the author, title, awarding institution and date of the thesis must be given.

Please visit <http://shura.shu.ac.uk/20456/> and <http://shura.shu.ac.uk/information.html> for further details about copyright and re-use permissions.

PROCESSING AND RHEOLOGICAL  
STUDIES OF CELLULOSIC MATERIALS

by

SIDNEY C N TSANG

This thesis submitted to the Council for National Academic Awards in partial fulfilment of the requirements for the award of the Degree of Doctor of Philosophy.

Sponsoring Establishment : Department of Applied Physics  
Sheffield City Polytechnic  
Sheffield, U.K.

Collaborating Establishment : Ministry of Defence  
Royal Ordnance Explosives Division  
Waltham Abbey, U.K.

February 1987

ProQuest Number: 10701102

All rights reserved

INFORMATION TO ALL USERS

The quality of this reproduction is dependent upon the quality of the copy submitted.

In the unlikely event that the author did not send a complete manuscript and there are missing pages, these will be noted. Also, if material had to be removed, a note will indicate the deletion.



ProQuest 10701102

Published by ProQuest LLC (2017). Copyright of the Dissertation is held by the Author.

All rights reserved.

This work is protected against unauthorized copying under Title 17, United States Code  
Microform Edition © ProQuest LLC.

ProQuest LLC.  
789 East Eisenhower Parkway  
P.O. Box 1346  
Ann Arbor, MI 48106 – 1346

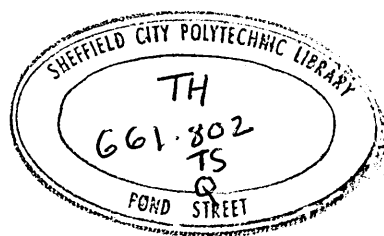
Processing and rheological studies  
of cellulosic materials

by

C N Tsang

Abstract

The present studies are concerned with the modelling of the manufacturing process of nitrocellulose-base propellant in which cellulose acetate is substituted as a model for the explosive nitrocellulose. An investigation of the inter-relationships between processing and rheological and morphological properties has been carried out on cellulose acetate doughs, using modified torque and capillary extrusion rheometers. Some of the doughs show a yield stress and behave as Herschel-Bulkley fluids. The yield stress is found to be smaller than that of nitrocellulose doughs, and there is some evidence of shear heating. Mixing time and mixing temperature showed no influence on the rheological parameters of the doughs. These results suggest that the change in rheological properties of propellant doughs is attributed to the change in crystallinity and fibrosity after processing. The rheological properties of doughs are greatly affected by extrusion temperature, solvent, plasticiser and filler content. The interaction between the solvents and plasticisers with cellulose acetate was explained by adopting a model consisting of a rigid backbone chain from which protruded flexible side groups. In good solvents these side groups extend causing interactions between molecules, giving rise to dough up and elasticity. In poor solvents, dough up becomes difficult and the elasticity is low because the flexible side groups retract towards the stiff backbone chain. The morphology of solvated doughs are examined using solution viscometry, infrared spectroscopy, scanning electron microscope, differential scanning calorimetry, x-ray diffraction and dynamic mechanical thermal analysis. All these techniques showed that the solvation process had no significant effect on the molecular architecture of the cellulose acetate, in which the original crystallinity of the material is low. From this it was concluded that changes in the rheological properties of nitrocellulose doughs as a function of the process variables was due to changes induced in the crystallites rather than in the amorphous regions.



### ACKNOWLEDGEMENTS

The author would like to express his sincere gratitude for assistance, advice and encouragement from Director of Studies, Dr. A A Collyer; otherwise this thesis would not possibly have been completed, especially during the initial set-backs in the first year.

Thanks are also due to Dr. F S Baker,<sup>Dr</sup> D W Clegg, Dr. K Dodgson, and Dr. R M Wood for their helpful discussion.

Parts of the work were carried out at the Royal Ordnance Explosives Division, for which many thanks are due to Mr G Privett for his technical assistance.

A special thanks goes to all members of the Sheffield City Polytechnic technical, secretarial and library staff who have helped in a variety of ways; especially to Mr G France and S Lee for their assistance in computing.

The author is indebted to the Ministry of Defence (United Kingdom), for financing the research project.

## ABSTRACT

1 : Introduction	1
1.1 Research ideas	1
1.2 Aim of project	2
1.3 Cellulose	2
1.4 Cellulose acetate	4
1.4.1 Sythesis	4
1.4.2 Chemical structure of cellulose acetate	6
1.4.3 Properties of cellulose acetate	7
1.5 Processing of cellulose acetate	11
1.5.1 Introduction	11
1.5.2 General review of mixing mechanisms	12
1.5.3 Flow mechanism inside the torque rheometer	14
1.5.4 Control and scaling-up of mixing	15
1.6 Rheological properties of doughs	17
1.6.1 General consideration	17
1.6.2 Flow properties of various ideal rheological fluids	17
1.6.3 Mechanics of flow in capillaries	22
1.6.4 A review of flow properties of propellant dough	28
2 : Rheological measurement	37
2.1 Introduction	37
2.2 Torque rheometry	37
2.2.1 Machine specification and modification	37
2.2.2 Measurement techniques	40
2.2.3 Data analysis	40
2.3 Capillary extrusion rheometry	41
2.3.1 Machine specification and modification	41
2.3.2 Measurement technique	43
2.3.3 Data processing of rheological results	48
2.4 Computer-controlled rheometer	49
2.4.1 Capillary extrusion rheometer	49
2.4.2 Torque rheometer	50
3 : Morphological studies of cellulose acetate doughs	53
3.1 Determination of combined acyl in CA	53
3.1.1 Introduction	53
3.1.2 Experimental and result	53
3.2 Thermal studies of CA	55
3.2.1 Theory	55
3.2.2 Experimental	55
3.2.3 Results and discussion	56
3.3 Mechano-degration studies of CA doughs	68
3.3.1 Introduction	68
3.3.2 Experiment and data processing	69

3.3.3 Results and discussion	71
3.4 Infrared analysis of CA	74
3.4.1 Theory	74
3.4.2 Experimental	75
3.4.3 Results and discussion	76
3.5 Electron microscopic studies of CA doughs	82
3.5.1 Theory	82
3.5.2 Experiment	83
3.5.3 Results and discussion	83
3.6 Dynamic mechanical analysis of CA	90
3.6.1 Theory	90
3.6.2 Experimental	91
3.6.3 Results and discussion	93
3.7 X-ray diffraction of CA	104
3.7.1 Theory	104
3.7.2 Experimental	105
3.7.3 Results and discussion	105
4 : Rheological studies of CA doughs	109
4.1 Introduction	109
4.2 Selection of a suitable fill factor	109
4.3 A study of the rate of gelation of CA	112
4.4 Flow behaviour of CA doughs	115
4.5 Effect of extrusion temperature	122
4.6 Effect of mixing parameters	132
(A) Effect of mixing time	132
(B) Effect of solvent concentration	133
(C) Effect of mixing temperature	136
4.7 Effect of fibrous cellulose acetate	151
4.8 Effect of plasticisers	158
5 : Conclusion	169
6 : Future work	173
REFERENCES	
APPENDICES	
A : Computer program for extrusion rheometer	A1
B : Computer program for torque rheometer	B1
C : Computer program for intrinsic viscosity	C1

Processing and rheological studies  
of cellulosic materials

by

Sidney C N Tsang

Abstract

The present studies are concerned with the modelling of the manufacturing process of nitrocellulose-base propellant in which cellulose acetate is substituted as a model for the explosive nitrocellulose. An investigation of the inter-relationships between processing and rheological and morphological properties has been carried out on cellulose acetate doughs, using modified torque and capillary extrusion rheometers. Some of the doughs show a yield stress and behave as Herschel-Bulkley fluids. The yield stress is found to be smaller than that of nitrocellulose doughs, and there is some evidence of shear heating. Mixing time and mixing temperature showed no influence on the rheological parameters of the doughs. These results suggest that the change in rheological properties of propellant doughs is attributed to the change in crystallinity and fibrosity after processing. The rheological properties of doughs are greatly affected by extrusion temperature, solvent, plasticiser and filler content. The interaction between the solvents and plasticisers with cellulose acetate was explained by adopting a model consisting of a rigid backbone chain from which protruded flexible side groups. In good solvents these side groups extend causing interactions between molecules, giving rise to dough up and elasticity. In poor solvents, dough up becomes difficult and the elasticity is low because the flexible side groups retract towards the stiff backbone chain. The morphology of solvated doughs is examined using solution viscometry, infrared spectroscopy, scanning electron microscope, differential scanning calorimetry, x-ray diffraction and dynamic mechanical thermal analysis. All these techniques showed that the solvation process had no significant effect on the molecular architecture of the cellulose acetate, in which the original crystallinity of the material is low. From this it was concluded that changes in the rheological properties of nitrocellulose doughs as a function of the process variables was due to changes induced in the crystallites rather than in the amorphous regions.

## CHAPTER 1 : Introduction

### 1.1 Research Ideas

Early in the seventeenth century, gunpowder was still manufactured from potassium nitrate, sulphur and carbon. This explosive material was known as 'Low ' explosive [1,2] and had the disadvantages that it produced large volumes of smoke, rapidly fouled gun barrels and deteriorated quickly in humid atmospheres. As a result, new gun propellant systems were developed. The most successful propellant, which consisted of a mixture of nitrocellulose (NC) and nitroglycerine(NG), was discovered by Alfred Nobel in 1888. Nowadays, gun propellant systems are generally composed of NC, plasticised with NG, filled with materials such as picrite and stabilised with carbamate [3]. The manufacturing process of the double- and triple-base NC propellants, which is in many ways similar to the processes in food, plastic and rubber industries, involves incorporating the ingredients with volatile solvents such as a mixture of acetone and ethanol to form a dough. The dough is extruded through a die of suitable geometry. The resulting extrudate is cut to length and the solvent is removed by drying. The traditional gun propellant manufacturing process in England has not changed significantly during the past fifty years. The process is inefficient in terms of output, use of energy and in the quality and consistency of the product. Advance in other aspects of modern weapons systems has meant that controlling the variation in consistency of the propellant is essential. In the future of the gun propellant manufacturing industry, a continuous process based on a screw extrusion machine is on the way. An inert material that will simulate as far as possible the rheology of the gun propellant doughs is required to test the validity of the proposed equipment for processing explosive materials. Such a material is cellulose acetate.

Apart from these technological problems there is a considerable

academic interest in the morphological study of cellulose acetate, since many of the fundamental properties relating to its molecular structure still remain unresolved.

## 1.2 Aim of Project

The present study is concerned with the modelling of the processing behaviour of solvent-processed NC-base propellant in which cellulose acetate (CA) is substituted as a model for the explosive NC. It represents part of an ongoing research programme in ROF committed to understanding those physical and chemical factors during mixing which are likely to influence the flow behaviour and morphological properties of NC propellant. The aim of this study is that through an investigation of the inter-relationships between processing, morphology, rheology and physical behaviour of CA it may prove possible to understand some of problems associated with the processing and performance of NC propellants. This may lead to improvements in the existing methods of manufacture of gun propellants.

## 1.3 Cellulose

Cellulose is the chief constituent of the cell walls of higher plants. It is the world's most abundant organic compound and serves as a chemical feedstock for several commercially important polymer industries.

The basic unit of cellulose is anhydro-D-glucose with an empirical formula of  $C_6H_{10}O_5$ . These units are linked together through  $\beta$ -(1,4)-glycosidic bonds to form a linear and extended polymer chain as shown in Fig. 1.1.

The adoption of the bi-(anhydro-D-glucose) unit as the repeating unit rather than the chemically equivalent single anhydro-D-glucose unit has become universally accepted in order to show that the consecutive units are not simply repeated along the chain axis but are helically displaced with respect to one another. The anhydro-D-glucose unit has the stable chair form and successive

units are twisted about the glycosidic bonds by approximately  $65^\circ$  giving the molecule five-fold helical symmetry [4] as shown in Fig. 1.2.

Fig. 1.1 Repeating unit of cellulose (bi-anhydro-D-glucose)

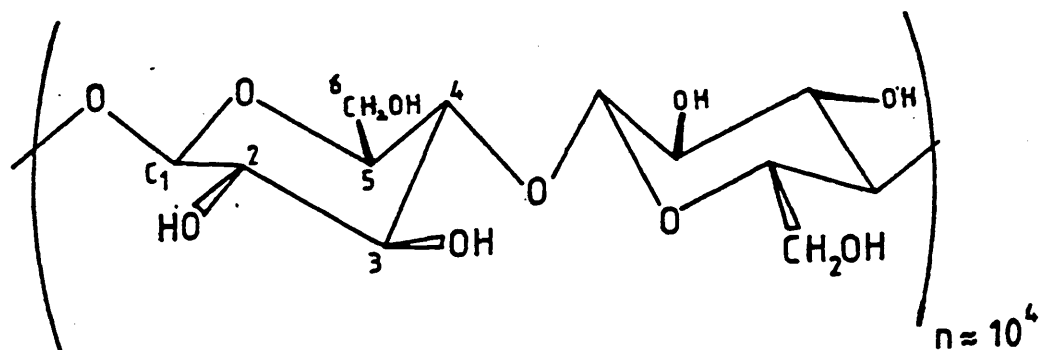
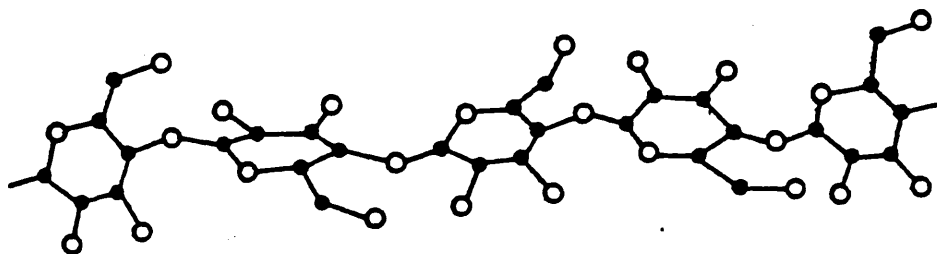


Fig. 1.2 5-fold helical structure of the cellulose chain



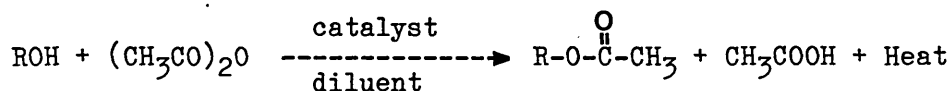
Cellulose chains have the opportunity of forming extensive intra- and intermolecular hydrogen bonds due to the presence of the three hydroxyl groups in the anhydro-D-glucose unit. The resulting high intermolecular forces plus the regular structure enables the cellulose chains to crystallize into different forms. This is confirmed by Pertsin and co-workers, indicating the existence of cellulose polymorphism [5,6]. Cotton cellulose or native cellulose, usually known as cellulose I, possesses a higher degree of crystallinity than cellulose II, which is formed by the swelling of cellulose I by a swelling agent. Cellulose III and IV do not occur in nature and are not as well characterized as the other forms. The full details of cellulose polymorphism are not discussed here, and the readers should refer to the book written by Bikales [7] for further information. From the x-ray pictures of cellulose, there is evidence for crystalline and amorphous regions as suggested by the fringed-micelle model. The degree of order affects the accessibility of the hydroxyl groups of the anhydro-D-glucose units to chemical reagents. Owing to its high crystallinity, cellulose is a tough, rigid and non-thermoplastic material which cannot be plasticised.

#### 1.4 Cellulose Acetate

##### 1.4.1 Synthesis

Cellulose is a polyhydric alcohol consisting of three hydroxyl groups in each anhydro-D-glucose unit for esterification. The basic chemical reaction involved in the acetylation of cellulose is a simple acid-catalyzed esterification of hydroxyl groups with acetic anhydride in the presence of a catalyst and a diluent [8]. In spite of the vast amount of important catalysts that have been described in the patent literature [9], concentrated sulphuric acid is almost universally adopted nowadays. Acetylation of cellulose is exothermic and the presence of the diluent makes the reaction temperature more controllable. The diluent is usually a

non-solvent for cellulose but may or may not be a solvent for the acetylated product. In the case of the non-solvent method, larger quantities of diluent are required for the ease of heat dissipation from the reaction mixture. The acetylation equation is shown as below:



The resulting product is often called primary cellulose acetate with all the hydroxyl groups substituted by acetyl groups. The morphology of primary cellulose acetate shows variation depending not only upon the cellulose source but also upon the conditions employed in the the systhesis. In homogeneous acetylation the acetate product passes into the diluent, the consequence of which is the complete breakdown of the original fibre structure. The fibrous nature of the native cellulose to a great extent can be retained by the heterogeneous acetylation in which no dissolution step is involved in the esterification. Thus, the resulting cellulose triacetates, having the same bulk chemical compositions, exhibit markedly different physical characteristics.

At this intermediate stage, cellulose triacetate (CTA) dissolves only in chlorinated hydrocarbons, such as methylene chloride, which has the disadvantage of extreme volatility and undesirable toxicity. As a result, primary CA is hydrolyzed to commerical cellulose diacetate, which has a maximum solubility in acetone [10]. In the conversion of fibrous acetone-insoluble cellulose acetate into acetone-soluble cellulose diacetate, the saponification process involves loss of the fibrous structure of CTA. It should be stressed that although fibrous CTA is not produced commercially, it is a better model for nitrocellulose in the propellant industry, since both of the cellulose esters are in a fibrous form.

Direct acetylation of cellulose to produce uniformly substituted cellulose diacetate is not possible because of the differences in

accessibility of the hydroxyl groups in cellulose, so that the surface may be fully substituted while molecules disposed in the the centre of the fibre will be completely unreacted. Thus, the commerical manufacture of uniformly substituted cellulose diacetate involves complete acetylation of cellulose in a medium in which the esters dissolve, followed by uniform removal of some of the substituted groups by back-hydrolysis.

The commerical manufacture procedures of cellulose acetate involve the following operations:

Pretreatment → Acetylation → Saponification → Precipitation

#### 1.4.2 Chemical Structure of Cellulose Acetate

The fundamental unit of cellulose acetate is shown in the following figure:

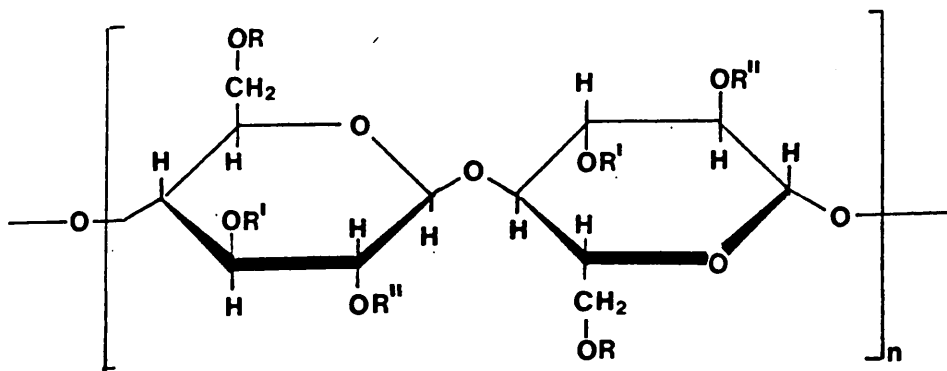


Fig. 1.3 Chemical structure of the monomeric unit in cellulose acetate

The hydroxyl groups (R,R',R'') may be partly or completely replaced by acetyl groups in the glucose unit of the cellulose chain. The degree of polymerisation is given by the value of n and the above unit molecular weight can be calculated by the following equation [11] :

$$\text{unit M.W.} = 162 + 42 \text{ D.S} \quad \text{-----(1)}$$

where D.S is the degree of substitution and is defined as the average number of hydroxyl groups per anhydroglucose unit that

have been replaced by the substituting groups [12]. Thus, an approximate average molecular weight is found by multiplying the unit molecular weight by the degree of polymerization as below:

$$\text{Molecular Weight} = n * \text{Unit M.W.} \quad \text{-----}(2)$$

Cellulose acetate is characterized mainly by its degree of polymerization, its degree of substitution and the distribution of unesterified hydroxyl groups among the primary (6-) and secondary (2- and 3-) positions.

#### 1.4.3 Properties of Cellulose Acetate

Although Fig. 1.3 represents the chemical nature of one chain, it is likely that such a structure would be somewhat modified in the solid state as a result of interaction with other chains. Thus, the physical and chemical behaviour of the structure cannot be described in terms of the properties of a single chain only, and the degree of aggregation of polymer chains will contribute more or less towards the eventual observations of a particular type of physical or chemical response. The morphology of unplasticised cellulose acetate is mainly dependent on the degree of substitution and its distribution. This is because replacement of hydroxyl groups by acetyl groups makes the polymer less polar and increases the inter-chain separation, thus reducing the extent of inter-chain hydrogen bonding. Moreover, the distribution of acetyl groups also plays an important part as it may affect the ordering of the cellulose molecules. Consequently, cellulose acetate with varying degrees of thermoplasticity [8] is obtained.

From the results of x-ray studies of cellulose and its derivatives, Pethrick [13] and other workers [14,15] have shown that the formation of cellulose esters leads to a marked loss of crystalline structure, as evidenced by the broad distribution in CTA. In a similar study, Conrad [16] revealed that CA which has a high DS is readily crystallizable by simple heat treatments in the ranges of 220 to 280<sup>o</sup>C, and the x-ray diffraction traces of heat-treated CTA shows a distinct crystal pattern. Also, a number of

workers [17,18] have shown that the well-known cellulose polymorphisms can be extended to cellulose derivatives, and is noticeable in the case of CTA I and II. Sprague et al [19] stated that the fibrous acetylation of cellulose I and cellulose II yields triacetate I and II respectively. Upon saponification both the crystalline and amorphous CTA I and II are always converted to a cellulose I and II respectively.

The x-ray diffraction technique has been used by Boy and co-worker [20] to study the crystal structure of secondary CA. The x-ray diffraction picture gave a very diffuse pattern, which was slightly indicative of crystalline structure, and this material would not crystallize by simple heat treatment.

The thermal behaviour of CA has been studied by a number of workers [16,20,21]. From the DTA thermograms, Conrad et al have indicated an endothermic peak at about  $310^{\circ}\text{C}$ , which is due to the crystalline melting ( $T_m$ ) of CTA. It has been shown that CTA has the highest  $T_m$  and its value decreases to a minimum of about  $230^{\circ}\text{C}$  at a DS of 2.3-2.4 [12].

In a similar study of CA, Boy has shown conclusively that secondary CA passes through endothermic transitions when it is heated. The similarity of the transitions of CA to the melting transitions of crystalline CTA leaves no doubt that CA possesses a greater degree of crystallinity than x-ray diffraction patterns indicate.

Unplasticised CA melts at such a high temperature that it cannot be processed by heat without excessive decomposition. Plasticisers have a dual action on CA. Compounding with plasticisers is necessary in order to lower its melting point to a reasonable temperature range. Besides, they improve polymer properties such as flow, flexibility, toughness and elasticity.

The effect of plasticiser on the mechanical relaxation behaviour of CA has been studied extensively. Scandola et al [22] stated that three relaxations common to all different DS of unplasticised

CA were found ( $\alpha$ ,  $\beta$  and  $\gamma$ ), in which the high temperature  $\alpha$  transition is the glass transition temperature ( $T_g$ ) of CA. The change in modulus associated with the  $\alpha$  transition is much smaller than that generally observed for a glass to a rubber in a completely amorphous polymer. Woods [23] has observed a similar change in modulus at the  $T_g$  of a partially crystalline terephthalate polyester. This observation has suggested that the crystallinity and probably the less flexible nature of the cellulosic chain will account for the small change in modulus at this transition.

The variation of  $T_g$  with DS of CA has been studied by Nakamura [24] who showed that the  $T_g$  and the activation energy of the transition decrease with increasing DS.

Plasticisation occurs through a specific type of plasticiser and polymer interaction, which lowers  $T_g$ , suppresses the  $\gamma$  relaxation and gives rise to a new loss process,  $\beta$ . The characteristics of the  $\beta$  relaxation depend on the nature and concentration of the plasticiser; more flexible plasticisers or higher concentration of them lowers the  $\beta$  temperature. The mechanism of such an effect may involve the breakdown of the intermolecular interactions, especially hydrogen bonding, within the cellulose chains by the plasticiser molecules. This is because the affinities of some of the hydroxyl groups are expended on the plasticiser rather than on each other. Thus some of the interactions are broken. As a result, the cellulose ester chains are pushed farther apart, resulting in an increase in molecular mobility at temperatures lower than that associated with the mobility of the pure polymer [12].

Because the plasticiser acts at a molecular level, the primary requirement is that the plasticiser should be compatible with CA. Since the solubility parameter,  $\delta$ , is often used as a guide to the solubility behaviour, this approach has also been used in the polymer-plasticiser system, while bearing in mind the inherent polarity of CA.

CA can be dissolved in a variety of solvents. However, a solvent

for CA with a particular DS would be unlikely to dissolve other CA of a different DS. The solubility characteristics of CA with different DS in various organic solvents is given in Table 1.1 [9].

From the Small's attraction constant [25], the solubility parameter of cellulose diacetate and triacetate can be estimated to be 22.3-23.1 (MJ/m<sup>3</sup>)<sup>0.5</sup> and 20.0-20.4 (MJ/m<sup>3</sup>)<sup>0.5</sup>. Good solvents for the triacetate are chloroform ( $\delta = 19.0$ ) and methylene chloride ( $\delta = 19.8$ ) as expected. By comparison methyl ethyl ketone ( $\delta = 19.0$ ) and acetone ( $\delta = 20.4$ ) should also be expected to dissolve CTA but if specific interactions such as polar and hydrogen bonding effects occur, then the use of solubility parameters as a guide becomes less reliable. Hence, a three-dimensional approach to solubility based on dipole moment, hydrogen bonding and solubility parameter values for solvents has been set up by Crowley [26] in order to predict precisely the solubility of polymer in organic solvents.

Table 4.8 (page 160) illustrates the three solution parameters of a number of organic solvents [26]. From this table, it can be seen that CTA dissolves in nonpolar and poorly hydrogen-bonded solvents. This can easily be understood as all the hydroxyl groups in the anhydro-D-glucose unit of CTA have been substituted by acetyl groups. The presence of free hydroxyl groups in secondary CA makes the polymer more polar in nature, and hence they can be dissolved in polar and moderately hydrogen-bonding solvents such as acetone and methyl formate. By similar reasoning, the compatibility of CA and plasticiser should also be influenced by the aforementioned three solution parameters. In general, it would be expected that dimethyl phthalate (DMP) is more compatible with secondary CA than diethyl phthalate (DEP) and dibutyl phthalate (DBP), in decreasing order. In fact, it has been found that the maximum compatibility of DMP, DEP and DBP with CA are 80, 50 and 25 pph respectively [22,27]. This observation will be discussed in

Table 1.1 Solubility characteristics of CA with different DS in various organic solvents

Acetyl content	13-19	24-32	36.5-38	38-39.5	39.5-41.5	41.5-44
DS solvent	0.6- 0.9	1.2- 1.8	2.2- 2.3	2.3- 2.4	2.4- 2.6	2.8- 3.0
Water	S	I	I	I	I	I
2-methoxy ethanol	I	S	I	I	I	I
Acetone	I	I	S	S	SW	I
Methyl ethyl ketone	I	I	S	PS	I	I
Chloroform	I	I	I	I	I	S
Methylene chloride	I	I	I	I	I	S

\*  
 Note: I - insoluble  
 S - soluble  
 PS - partly soluble  
 SW - swell

## 1.5 Processing of Cellulose Acetate

### 1.5.1 Introduction

There are two basic methods of processing CA powders into plastics, namely a hot-rolling and a solvent incorporation process [12]. Of particular interest in the present study is the incorporation of solvent and other additives into CA using the solvent method, since this is the way in which most propellants are prepared.

In the technological application of solvent to cellulosic derivatives in solvent-processed explosive industry, it has become conventional to refer to the process of incorporation of solvent as 'gelatinisation'. This process involves the uptake of solvent by the cellulose esters, usually with mechanical aid, and the gradual formation of a dough, which may or may not be entirely homogeneous. The term of mixing or compounding used in this

project is defined as a process in which CA and other ingredients become more intimately intermingled through the gelatinisation process, more or less to a continuum of polymer, which has the properties of machinability and mouldability. Such operations are invariably involved in the first place in the processing of gun propellant. A good mixing operation is essential to ensure a suitable degree of homogeneity in composition and, to some extent, morphological structure during the manufacture of products. This is an important consideration because the physical and chemical properties of the propellant are extremely sensitive to the composition homogeneity and morphology.

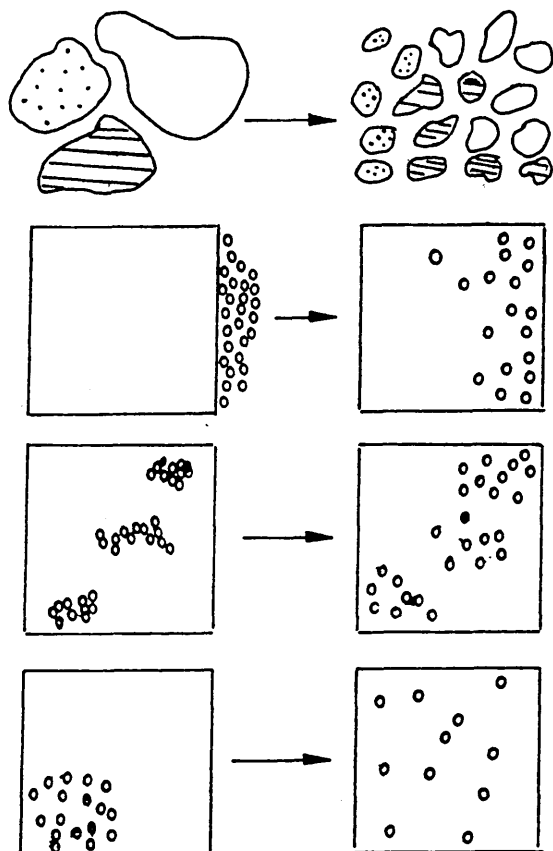
#### 1.5.2 General Review of Mixing Mechanisms

The mechanism of mixing is discussed in a number of excellent texts [28,29]. Several authors have described mechanisms of mixing in broad conceptual terms. However, the mechanisms of mixing suggested by Palmgren and Tadmor are generally accepted. Palmgren, regarding mixing as the concept of increasing entropy of a mixture [30], has designated four steps in mixing as shown in Fig 1.4

- (1) Subdivision in which large individual components are broken down into small elements.
- (2) Incorporation in which elements of one component are dispersed into the space occupied by another.
- (3) Dispersion in which elements of a component which were assembled in congregations become segregated.
- (4) Simple mixing in which elements of a component approach a random distribution amongst other components.

In an actual mixing process, these steps may overlap, although some subdivision may be necessary before incorporation can commence. It would be expected that simple mixing is determined mainly by the shear deformation whilst dispersion largely depends on the shear stress during the process.

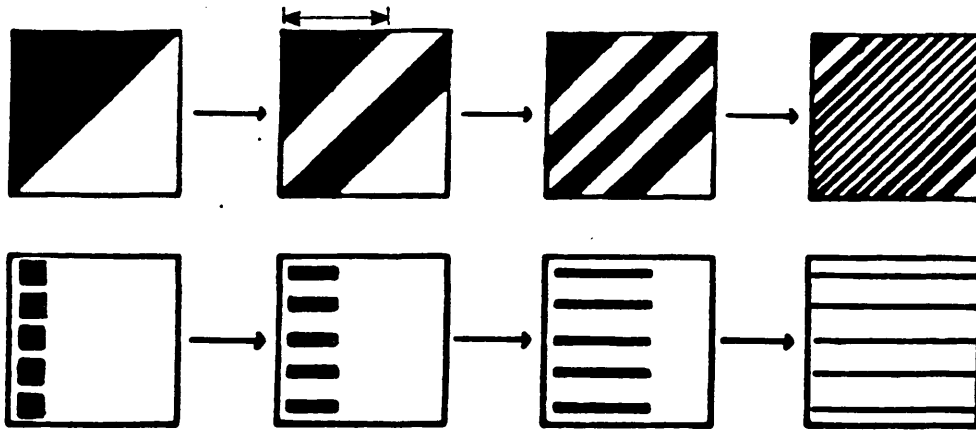
Fig 1.4 Sketches showing the various steps in mixing  
----- Palmgren theory



Tadmor considers mixing as the concept of redistributing volume elements of the components in space [31]. Convective mixing is the dominant mixing mechanism. It can arise by two different mechanisms, namely simple mixing and laminar mixing.

- (1) Simple mixing involves simple bulk rearrangement of material by plug type flow, and no continuous deformation of the material is observed. The repeated rearrangements can be ordered or random.
- (2) Laminar mixing involves deformation of the system by laminar flow, in which the viscosity ratio of the two components plays an important role. Interfacial area between components is increased whereas striation thickness is decreased when a strain is imposed on the system, as shown in Fig. 1.5.

Fig 1.5 Effect of shear on the striation thickness

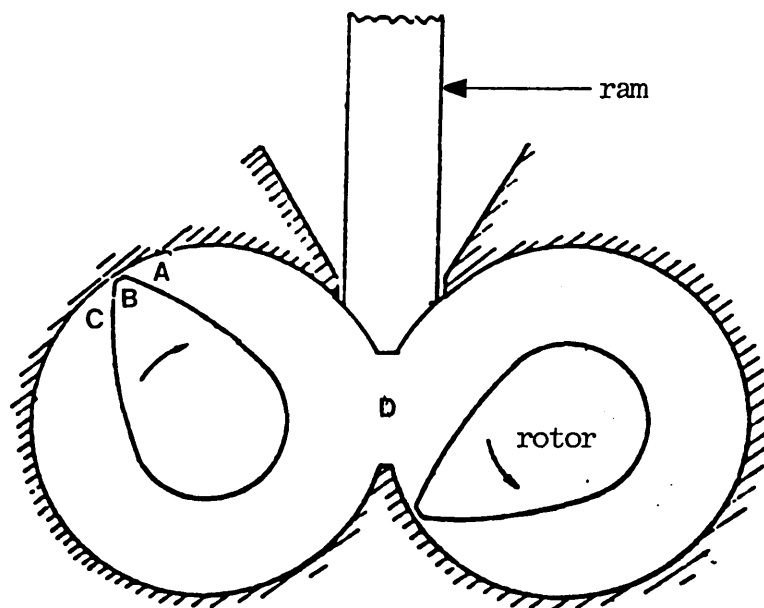


Direction of shear →  
( striation thickness ←→ )

### 1.5.3 Flow Mechanism inside the Torque Rheometer

Recent studies of the mechanics of flow in the mixing chamber by a dynamic visualization method have been carried out by Freakley et al [32]. They identified that there are five separate regions of the mixing chamber, which are defined as follows: (A) in front of the rotor tip, (B) the tip region, (C) behind the rotor tip, (D) on the bridge, and (E) between two adjacent wings of a rotor (axial flow) as shown in Figure 1.6.

Fig. 1.6 Cross section of the mixing chamber in a torque rheometer



A detailed study of the flow pattern can be made by considering the five regions and their interactions with one another. Owing to the motion of the rotor, region (A) is constantly filled with material. This results in a streamlined flow, which is composed of pressure and drag flow due to the convergence of the flow path and the motion of the rotor relative to the chamber wall respectively. It is in the tip region that the major mechanism for breakdown of particle aggregates occurs. Region (C) is not completely filled with material. The existence of the voids behind the rotor tip is important for a disordering of the flow regimes to increase the efficiency of mixing. The flow in the region (D) is essential to provide a mechanism for the effective exchange of material between the lobes of the chamber. In the final region (E), each rotor has been specially designed so that the rotor tips are angled to give an axial and circumferential flow. It should be noted that the flow patterns inside the chamber depend <sup>on</sup> the amount of material being processed. From a molecular viewpoint, during the initial stage of mixing the interface between the components is small, a situation characteristic of the unmixed state, and surface tension does not play an important role. Deformation caused by the local stress field, which is inhomogeneous as CA and solvent have different rheological properties, results in enlargement of the interface and an improvement of the state of mix. Once the mixing process has progressed and the interfacial areas have increased sufficiently, the degree of miscibility of the components may play an important role. In miscible systems, inter-diffusion aids the mixing process down to the molecular level.

#### 1.5.4 Control and Scaling-up of Mixing

Mixing of the cellulose esters is generally done in a batch process using high-shear mixers, such as torque rheometers. The materials have traditionally been mixed according to time-temperature specifications [33]. These specifications, however,

are extremely sensitive to the mixer type, size and mixing condition. Control specifications of time-temperature do not always achieve batch-to-batch uniformity in the same mixer, due to the differences in the mixers' cooling system. Besides, these specifications are certainly difficult to translate to different pieces of equipment. As a result, the work unit parameter is proposed for quantifying mixing over wide ranges of mixer capacity, rotor speed, time and temperature. This simple technique as the preferred basis for quantifying mixing is shown to be independent of mixer capacity or speed of operation, thus providing a way of controlling and scaling up between laboratory and factory mixers [34].

To simplify the complex combination of shearing, deforming, pumping and compressing actions which occur in the mixer, it is necessary to make certain assumptions [35-37]:

- (1) The total work (  $W_t$  ) of mixing is predominantly shear work and
- (2) Shear work is directly proportional to the rate of electrical power consumption per unit mass of material being mixed.

The work unit is defined by the following equation:

$$W_u = \frac{W_t}{M} = 2\pi S_R * 9.8 * 10^{-6} \int_{t_1}^{t_2} (T) dt / M \quad \text{-----(3)}$$

where  $S_R$  = rotor speed in rpm

$T(t)$  = torque in Kgm, which is a function of time and is taken as the top of the torque trace

$t$  = time in minute

However, there are some limitations to this technique. Certain precautions have been found to be necessary if reproducible results are to be obtained with the work unit technique. Operationally, the temperature-time profile should be matched as closely as possible, the same loading procedure should be used and

the batch size should be kept at the same loading volume. It is also assumed that the energy going into mixing is not lost in giving rise to shear heating.

## 1.6 Rheological properties of doughs

### 1.6.1 General Consideration

Polymer rheology is the science of deformation and flow behaviour of polymeric materials. Of particular interest in the present study is the investigation of the rheological properties of a dough system, since most propellants are processed as doughs. Cellulose esters are rigid polymers and are incapable of flow below their decomposition temperatures. Incorporation of large amounts of solvent and plasticiser render the polymer matrix into a mobile dough, which is capable of flowing at a reasonable temperature. The rheological behaviour of such a dough system is very complicated and is mainly governed by the chemical formulation and the associated morphology, which may be manipulated by the subsequent processing conditions.

Rheology is concerned with the relationship between stress, strain and time to give a constitutive equation, which describes the constitution of the material.

$$\tau = f ( \gamma, t ) \quad \text{-----(4)}$$

The detailed theory of rheology is dealt with in many excellent texts [38-43] and the following discussion reviews those aspects of rheological properties relevant to the present research work.

### 1.6.2 Flow properties of various ideal rheological fluids

Several types of rheological fluids have been recognized. These different types of behaviour can be easily visualized by plotting shear stresses versus shear rates as shown in Fig. 1.7.

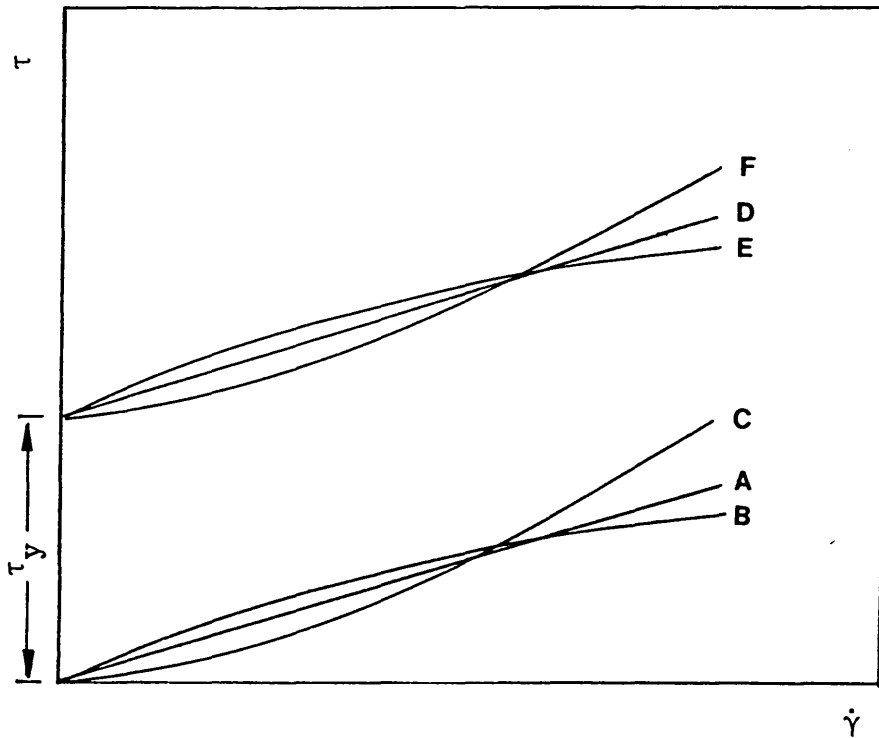
The classical Newtonian fluid (curve A) is characterized by the constant viscosity, which is independent of the shear rate at constant temperature and pressure. The constitutive equation for

this fluid is simple and is expressed by:

$$\tau = \eta \dot{\gamma} \quad \text{-----}(5)$$

The viscosity of the fluid is given by the slope of the line. Once the viscosity is measured, a complete rheological characterization of the fluid is obtained.

Fig. 1.7 Flow Curves of time-independent fluids



Certain materials must be exposed to a finite shear stress before any deformation occurs. Once this yield stress ( $\tau_y$ ) has been exceeded, a linear relationship between shear stress and shear rate may be obtained. These fluids are called Bingham plastics (curve D). The constitutive equation is given as:

$$\tau - \tau_y = \eta \dot{\gamma} \quad \text{-----}(6)$$

Although single phase, low molecular weight liquids behave experimentally as Newtonian fluids in laminar flow, polymer solutions and melts approximate to this Newtonian behaviour only at very low shear rates or shear stresses. Such a system is termed

non-Newtonian and the viscosity is commonly referred to as apparent viscosity ( $\eta$ ). At higher shear rates, such a system may deviate from ideal Newtonian behaviour in one of several ways, as illustrated by the curves B,C,E and F in Fig 1.7.

When the shear rate increases more than in proportion to the shear stress, as shown by curve B, the material is called a pseudoplastic or a shearing-thinning liquid. On the other hand, a material is called a dilatant or a shearing-thickening fluid when the rate of shear increases less than in proportion to the shear stress, as illustrated in curve C. The above flow curves have a common feature in that they pass through the origin showing no yield stress ( $\tau_y$ ). A variety of rheological models have been proposed to describe these types of non-Newtonian behaviour as discussed in detail by Holdsworth [44]. The Power Law model is generally adopted to describe the flow properties of polymer melts, solution and the dough system. It is represent by:

$$\tau = k\dot{\gamma}^n \quad \text{-----}(7)$$

where  $\tau$  = shear stress ( $N/m^2$  )

$k$  = consistency index ( $Ns^n /m^2$  )

$\dot{\gamma}$  = shear rate ( $s^{-1}$  )

$n$  = flow behaviour index or shear thinning index

Another form of expressing the Power Law equation is given as follow:

$$\eta = \eta_0 \left[ \frac{\dot{\gamma}}{\dot{\gamma}_0} \right]^{n-1} = \eta_0 \left[ \frac{\tau}{\tau_0} \right]^{\frac{n-1}{n}} \quad \text{-----}(8)$$

where  $\dot{\gamma}_0$  and  $\tau_0$  represent values of shear rate and shear stress in some arbitrarily chosen standard state and  $\eta_0$  is the viscosity in this state. For convenience,  $\dot{\gamma}_0$  is chosen as  $1 s^{-1}$ .

It states that the shear stress is proportional to the shear rate raised to the power  $n$ . The viscosity level of the non-Newtonian fluid can be specified by the value of consistency index. The flow

behaviour index may be considered to be a measure of the non-Newtonian character of a polymer melt. For shear thinning fluids, the flow index is smaller than unity and it becomes smaller as the deviation from Newtonian behaviour becomes greater.

Also, pseudoplastic fluids exhibiting a yield value show plastic flow (curve E), which is found in most cases of gun propellant doughs. Curve F represents a dilatant fluid with a yield stress. In order to account for the existence of a yield stress in the non-Newtonian fluid, the power law model has also been modified with an additional term. Such a form is called the Herschel-Bulkley model.

$$\tau - \tau_y = k\dot{\gamma}^n \quad \text{-----}(9)$$

The Power Law model has a limitation in fitting the experimental data at both very low and very high shear rates. Careful examination of shear-thinning polymer melts indicates that they do not follow a power function throughout an extended range of shear rates. Instead, the logarithmic function appears to fit that part of the curve lying between two limiting straight portions. This behaviour may be seen clearly in Fig 1.8, in which the logarithm of the apparent viscosity is plotted against the logarithm of the shear rate.

In this figure the low shear rate range (range A) is Newtonian because little or no molecular orientation has occurred (ie random orientation). As the shearing proceeds, the molecules align themselves along the streamlines, thus reducing the shear viscosity (region B). If the alignment becomes complete while the flow is still laminar, a second Newtonian region occurs (region C). The regions A and C represent the constant low-shear and high-shear limiting Newtonian viscosities respectively, and the region B shows the range of shear rates in which the Power law can be applied. Therefore, this model cannot adequately represent the flow behaviour over any very extensive shear rate range, an

extension of the empirical expression to a quadratic form with three constants has been developed for fitting the experimental data over a much wider range of shear rates.

$$\log \tau = c_0 + c_1 \log \dot{\gamma} + c_2 [ \log \dot{\gamma} ]^2 \quad \text{-----}(10)$$

However this equation is much more complex because 3 parameters must be determined. Owing to its simplicity and ability to correlate observed rheological behaviour over the shear rate range (10 to 200 s<sup>-1</sup>), of interest in extrusion processes, the Power law model has found extensive use as a constitutive equation for non-Newtonian fluids.

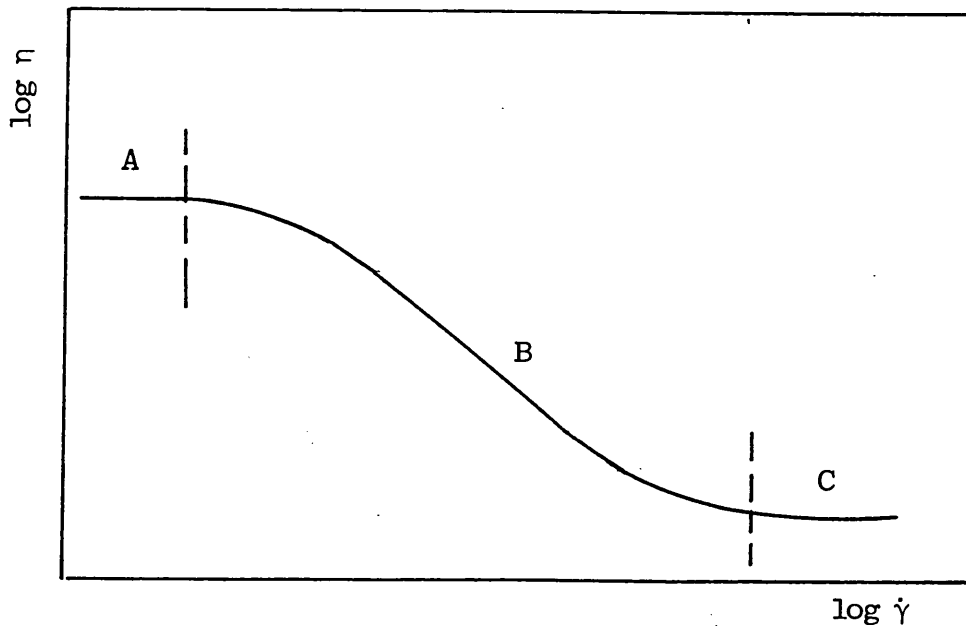


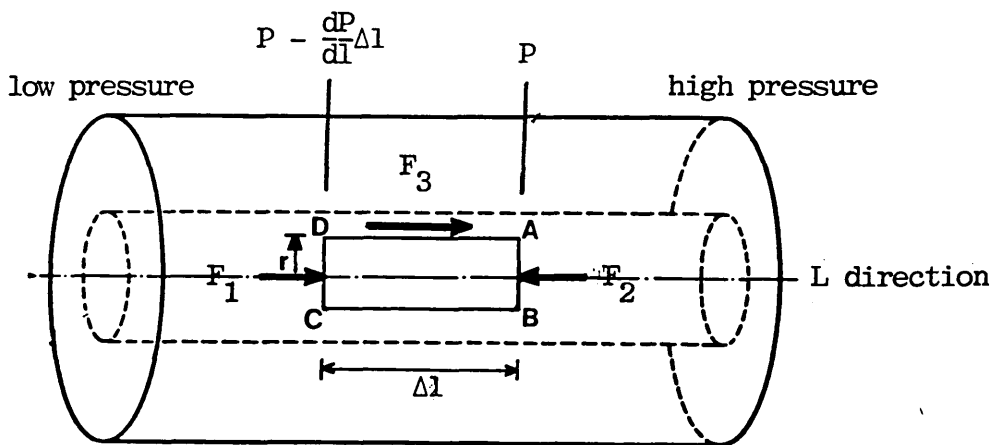
Fig. 1.8 Viscosity versus shear rate for shear-thinning fluid

### 1.6.3 Mechanics of Flow in Capillaries

In general, most polymer processing methods involve flow through straight (horizontal) tubes. It is, in practical, of interest to study the flow mechanism inside the capillaries. In the analysis of non-Newtonian flow in capillaries the following assumptions are made [41]:

- (1) There is no slip at the wall;
- (2) The melt is incompressible;
- (3) The flow is steady, laminar and time independent;
- (4) Fluid viscosity is not affected by pressure changes along the capillary; and
- (5) Isothermal conditions prevail throughout.

Fig. 1.9 Force vector for a element of fluid inside a capillary



Consider the force acting on an element of fluid (ABCD) in Fig. 1.9

$$F_1 = \pi r^2 \left( P - \frac{dP}{dl} \Delta l \right)$$

$$F_2 = \pi r^2 P$$

$$F_3 = 2\pi r * \Delta l (\tau)$$

Since the flow is steady, the pressure-induced force ( $F_2 - F_1$ ) tending to move the element in the direction of flow is balanced against the viscous force  $F_3$  resisting the motion of the element of fluid. Thus,

$$F_3 = F_2 - F_1$$

$$\tau = \frac{r}{2} \left( \frac{dP}{dl} \right)$$

In many cases, the pressure gradient is uniform so that the shear stress at the wall for a pressure drop  $P$  over a length of  $l$  is given by:

$$\tau_w = \frac{PR}{2L} \text{-----(11)}$$

Also since

$$\tau = \eta \dot{\gamma} = \eta \frac{dv}{dr}$$

$$\tau = \frac{r}{2} \left( \frac{dP}{dl} \right) = \eta \left( \frac{dv}{dr} \right)$$

$$\frac{dv}{dr} = \frac{r}{2\eta} \left( \frac{dP}{dl} \right)$$

From equation (8) for power law fluids

$$\eta = \eta_0 \left[ \frac{\dot{\gamma}}{\dot{\gamma}_0} \right]^{n-1} = \eta_0 \left[ \frac{dv/dr}{\dot{\gamma}_0} \right]^{n-1}$$

$$\frac{dv}{dr} = \frac{r}{2\eta_0 \left[ (dv/dr) / \dot{\gamma}_0 \right]^{n-1}} \left( \frac{dP}{dl} \right)$$

Rearranging this equation gives

$$dv = \left[ \frac{\dot{\gamma}_0^{n-1}}{2\eta_0} \left( \frac{dP}{dl} \right) \right]^{1/n} r^{1/n} dr$$

$$\int_0^v dv = Z \int_R^r r^{1/n} dr$$

$$\text{where } Z \equiv \left[ \frac{\dot{\gamma}_0^{n-1}}{2\eta_0} \left( \frac{dP}{dl} \right) \right]^{1/n}$$

$$v = Z \left( \frac{n}{n+1} \right) \left[ r^{\frac{n+1}{n}} - R^{\frac{n+1}{n}} \right]$$

At  $r=0$   $V=V_0$

$$V_0 = -Z \left( \frac{n}{n+1} \right) R^{\frac{n+1}{n}}$$

$$V = V_0 \left[ 1 - \left( \frac{r}{R} \right)^{\frac{n+1}{n}} \right]$$

This equation predicts the velocity profile at any radius

The volume flow rate,  $Q$ , is given by:

$$dQ = 2\pi V r dr$$

$$Q = 2\pi V_0 \int_0^R \left[ 1 - \left( \frac{r}{R} \right)^{\frac{n+1}{n}} \right] r dr$$

Integrating gives

$$Q = \left( \frac{n+1}{3n+1} \right) \pi R^2 V_0$$

$$V_0 = \left( \frac{3n+1}{n+1} \right) \frac{Q}{\pi R^2} \quad \text{-----(12)}$$

Also shear rate,

$$\dot{\gamma} = \frac{dv}{dr} = \frac{d}{dr} V_0 \left[ 1 - \left( \frac{r}{R} \right)^{\frac{n+1}{n}} \right]$$

$$\dot{\gamma} = - \frac{V_0 [(n+1)/n]}{R} \left( \frac{r}{R} \right)^{1/n}$$

From equation (12), the shear rate at the wall ( $r=R$ ) is expressed as:

$$\dot{\gamma}_t = - \left( \frac{3n+1}{n} \right) \frac{Q}{\pi R^3} \quad \text{-----(13)}$$

where  $\dot{\gamma}_t$  = true shear rate at the wall

Equation (11) shows that the shear stress is directly proportional to the distance from the centre of the capillary and to the pressure gradient. It should be noted that the shear stress at the centre of the capillary is zero and increases to a maximum value at the wall. This linear relation of the shear stress to the radius of the capillary is valid regardless of the nature of the fluid. The analysis of capillary flow assumes that the theoretical pressure drop occurring down the length of the capillary is as represented schematically in the following figure.

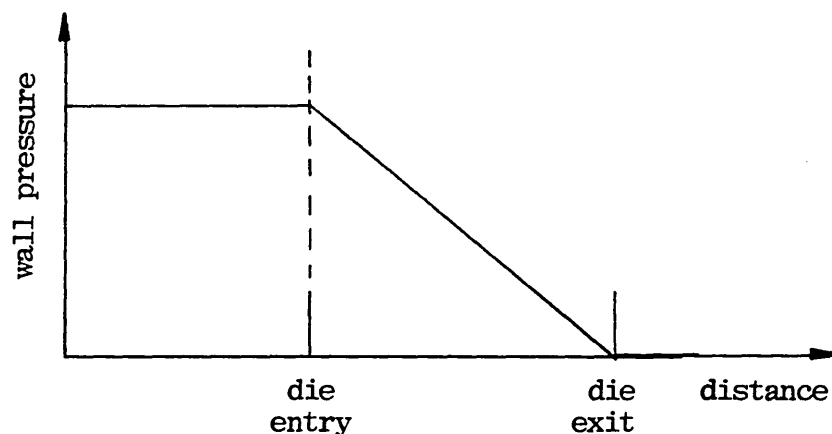


Fig. 1.10 Theoretical pressure drop in and around the capillary

This figure shows that

- (1) Pressure is independent of position in the reservoir;
- (2) There is a linear change in pressure with respect to the axial position along the whole length of capillary;
- (3) The pressure drops to zero at the exit of the capillary.

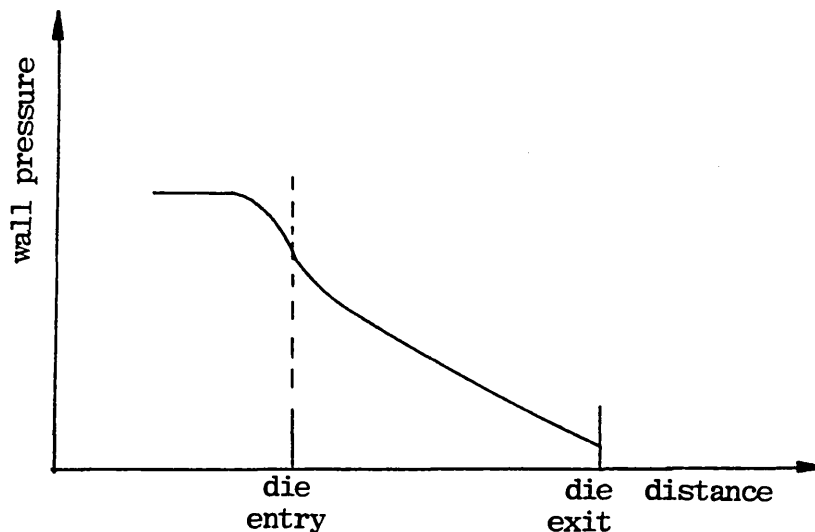
However, studies with polymer melts have found that the measured pressure drop across the die is usually higher than the expected theoretical value. This is because the pressure measured at the die entrance is a combination of an entrance pressure and the pressure used in giving flow.

An experimental pressure profile of polymer melts [39] in a capillary shows the following features that are at variance with

the aforementioned assumptions: (Fig 1.11)

- (1) A substantial pressure drop at the die entrance, the magnitude of which depends on shear rate;
- (2) Some degree of non-linearity just downstream of the capillary entrance;
- (3) An extrapolated non-zero value for the pressure at the exit of the capillary

Fig 1.11 Schematic diagram of the pressure distribution in the reservoir and capillary



The entrance pressure drop effect is the most important and may arise from a combination of 3 effects:

- (1) A viscous dissipation of energy due to the converging flow prior to entry into the capillary;
- (2) A viscous dissipation of energy due to the development of a velocity profile near the die entry; and
- (3) Chain uncoiling leading to a storage of elastic energy, some of which may be recoverable.

Failure to make the correction for the entrance effect will shift the flow curves upward towards a higher shear stress. The correction for the entrance effect will be discussed in Chapter 2. As with the shear stress, the shear rate also varies with radius of the capillary. The mode of variation depends on the radial

velocity distribution which, in turn, is determined by the nature of the fluid.

For a non-Newtonian fluid described by the power law, the velocity distribution depends on the value of flow index (Fig 1.12). For pseudoplastic fluids ( $n < 1$ ), the velocity profiles flatten as  $n$  decreases. For dilatant fluids ( $n > 1$ ), the velocity profiles sharpen as  $n$  increases.

For the sake of simplicity, the wall shear rate and wall shear stress are always taken. For a Newtonian fluid the wall shear rate is given by:

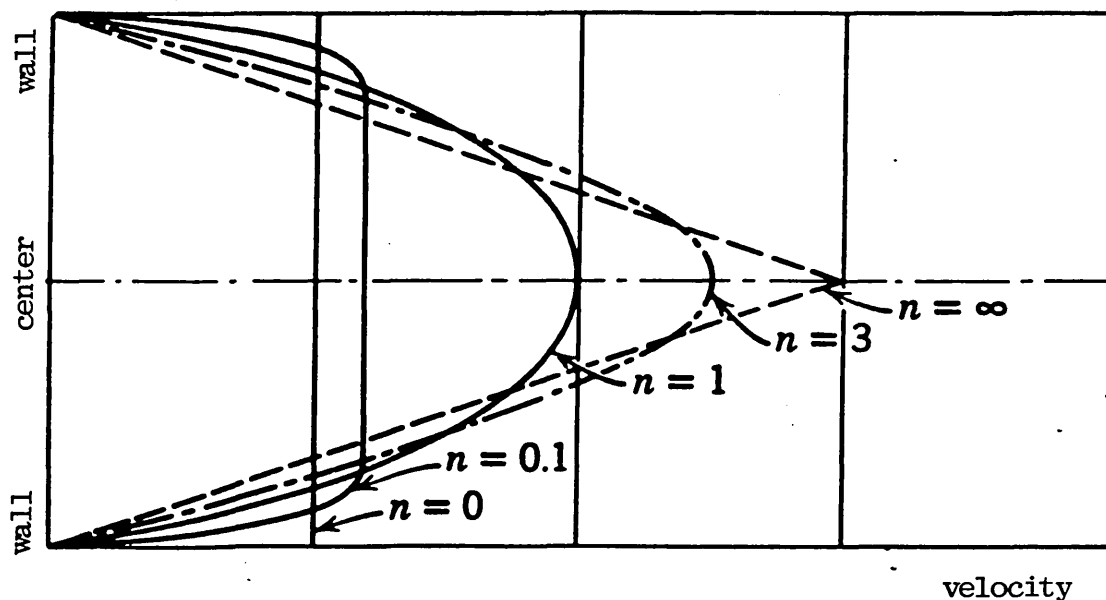
$$\dot{\gamma} = \frac{4Q}{\pi R^3} \quad \text{-----(14)}$$

However, the shear rate at wall must be corrected to allow for the non-Newtonian behaviour, and the true wall shear rate,  $\dot{\gamma}_t$ , is given by :

$$\dot{\gamma}_t = \left(\frac{3n+1}{4n}\right)\dot{\gamma} \quad \text{-----(15)}$$

The quantity  $(3n+1)/4n$  is commonly referred to the Rabinowitsch correction for non-Newtonian behaviour and becomes unity for Newtonian fluids.

Fig 1.12 Velocity profiles of non-Newtonian fluids



#### 1.6.4 A Review Of Flow Properties of Propellant Dough

The manufacture of nitrocellulose (NC) based propellant involves the mixing of NC with solvent and other additives until a dough is formed. This is then extruded to the required shape and dried [45-57]. The effect of mixing parameters on mixing behaviour of NC doughs were studied. It was found that there was a linear dependence between work unit and mixing time as shown in Fig.1.13. The variation of torque with mixing temperature is shown in Fig. 1.14 in which the type of variation depends on the solvent concentration. On the other hand, a plot of work unit against solvent content showed a logarithmic-linear relationship over a range of 5 to 21 pph of solvent as seen in Fig. 1.15.

$$\log (Wu) = 1.02 - 0.055 * C$$

where C is the solvent concentration in pph.

The observed logarithmic flow curves of NC doughs deviate from the power law at high and low shear rates giving 'S' shaped curves as shown in Fig. 1.16. The reasons for these deviations at low and high shear rates are different in nature. It has been shown that the deviation at lower shear rates is due to the existence of yield stress, and hence the doughs behave as Herschel-Bulkley materials. The deviation at high shear rate is due to shear heating. As the material temperature increases there is a reduction in its viscosity, giving the deviation from linearity. This argument is further supported by the results from an experiment in which a propellant dough is extruded through dies of constant diameter but increasing length. The deviation of the logarithmic flow curve from the power law is greater and starts at lower shear rates as shown in Fig. 1.17. This is because at a given flow rate, the material inside a longer die will be subjected to shear for a longer time, and thus the frictional heating becomes more severe.

The nature of the rheological behaviour of the gun propellant changes as a function of plasticiser, filler and temperature. As would be expected, the flow properties of the propellant doughs are strongly dependent on temperature, being more viscous at a lower temperature as shown in Fig. 1.18.

There is ample evidence that wall slip effect is observed in gun propellant doughs containing low molecular weight liquids, especially water and ether, because both are relatively incompatible with the propellant. These liquids form a lubricating layer at the wall or close to it, giving a characteristically shaped flow curve as shown in Fig. 1.19. Such an effect will increase the difficulty in the analysis of the flow behaviour parameters.

The effect of mixing time and solvent concentration on the yield stress, consistency index ( $k$ ) and flow behaviour index ( $n$ ) are shown in figures 1.20 and 1.21 respectively. Fig. 1.20 shows that all the flow parameters decrease as a function of time, however the decrease in flow behaviour index is relatively smaller than that of yield stress and consistency index. Fig. 1.21 shows that yield stress and consistency index increase with decreasing solvent content, but the flow behaviour index remains reasonably constant over the range.

It is suggested that the molecular state of NC/NG in the matrix was best reflected by the changes in flow behaviour index. It is because flow behaviour index is neither sensitive to mixing time nor solvent concentration. Even at 10 pph solvent there is still sufficient acetone present to gelatinize most of the matrix and hence flow behaviour index would not be a sensitive function of solvent content in the range investigated. The shear-thinning index may be more dependent on the mixing conditions for concentrations of less than 10 pph.

The values of yield stress and the consistency index could be a measure of the degree of wetting and breaking down of the fibrous NC and the picrite crystals. The greater the solvent concentration

the greater is the wetting and breaking down of the matrix. This would lower the yield stress and the consistency index of the dough. It has been shown that solvent concentration of less than 15 pph had a more profound influence on yield stress and consistency index than higher concentrations.

Since both the yield stress and the consistency index decrease as a function of mixing time and solvent concentration, this suggests that long mixing times and high solvent concentrations cause changes in the NC fibres and the picrite crystals.

Both solvent concentration and time of incorporation have an appreciable effect on the mechanical properties of the dried cord. A maximum was observed when tensile strength was plotted as a function of mixing time. The initial increase in tensile strength was attributed to the progressive homogenisation and wetting of the dry ingredients. Prolonged mixing was thought to break down the crystalline regions to give a more amorphous mass, thereby reducing the overall modulus of NC. In extreme cases the tensile strength is reduced drastically. Moreover, both the initial modulus and the tensile strength of the dried cord decrease with solvent content as shown in Fig 1.22 and 1.23 respectively. The NC/solvent matrix becomes stiffer as the solvent concentration is reduced. The stiffness would decrease the ability to homogenise the ingredients. The dried cord would therefore become progressively weaker and more porous with decreasing solvent content.

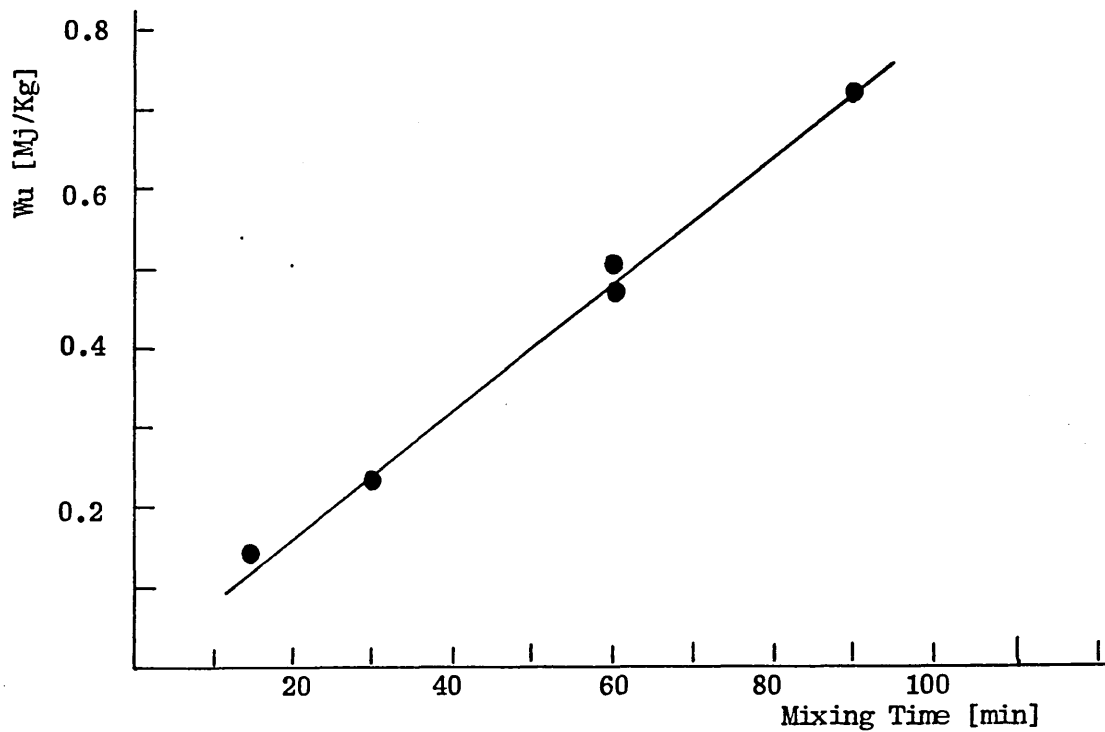


Fig. 1.13 Relationship of work unit against time of propellant dough

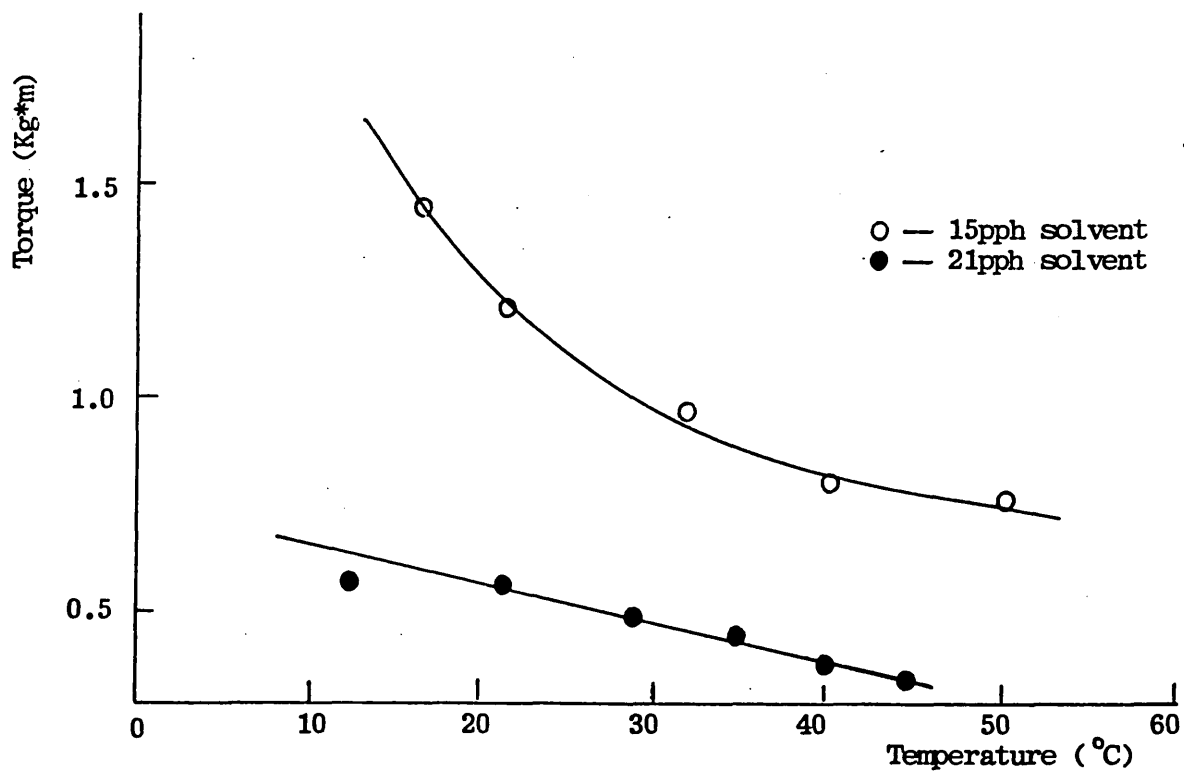


Fig. 1.14 Effect of mix temperature on torque with different solvent content

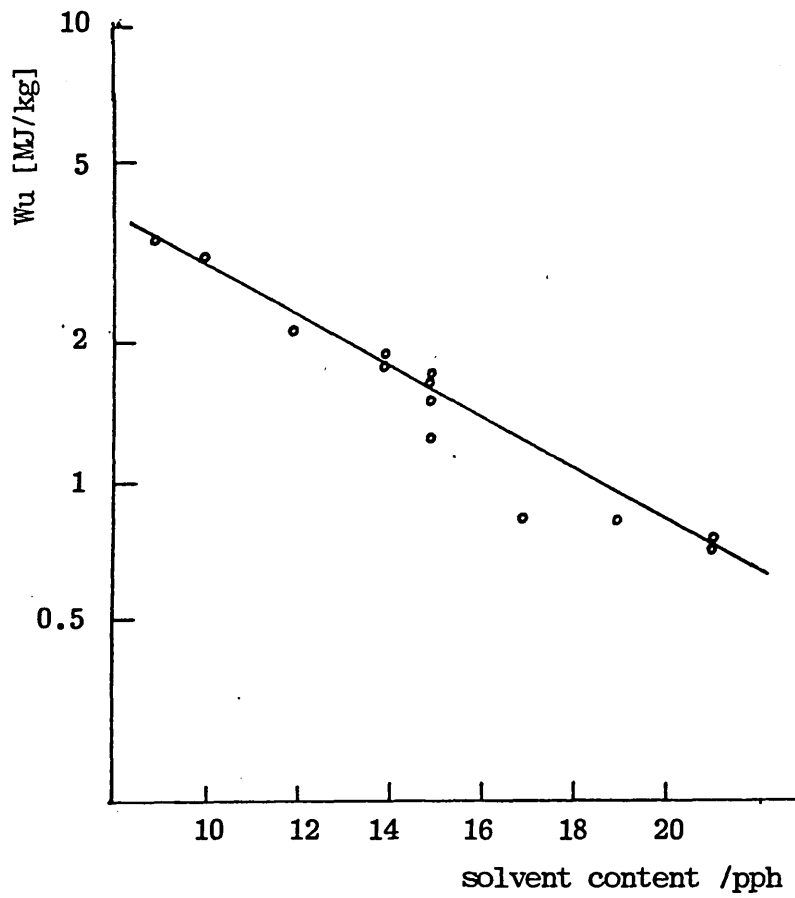


Fig. 1.15 Effect of solvent content on work unit of propellant dough

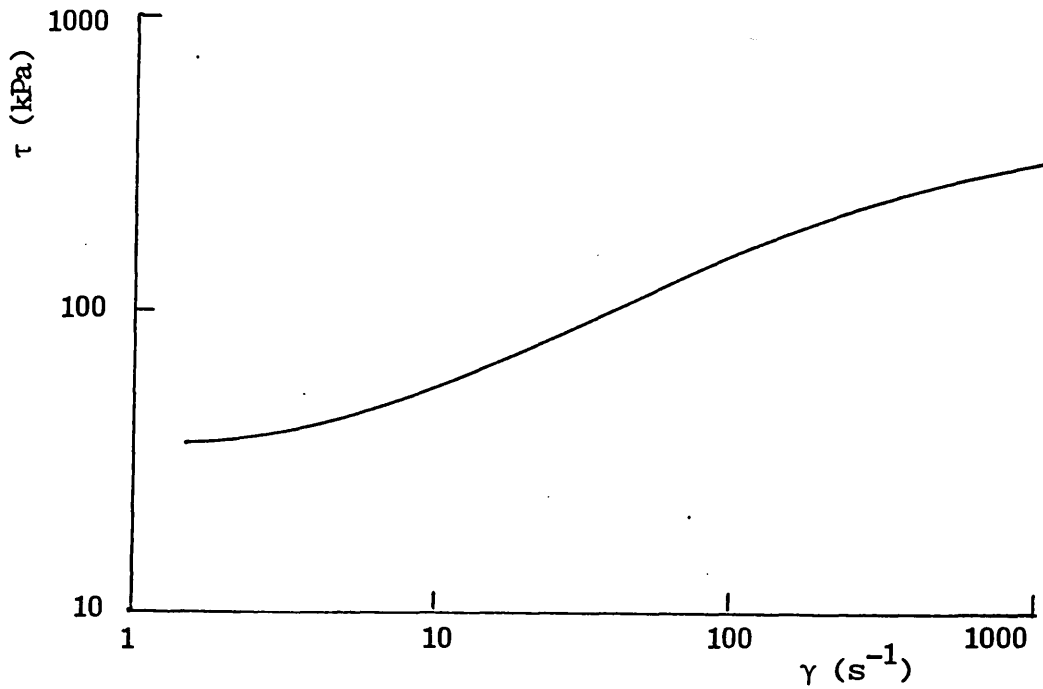


Fig. 1.16 Typical flow curve of nitrocellulose-base propellant dough

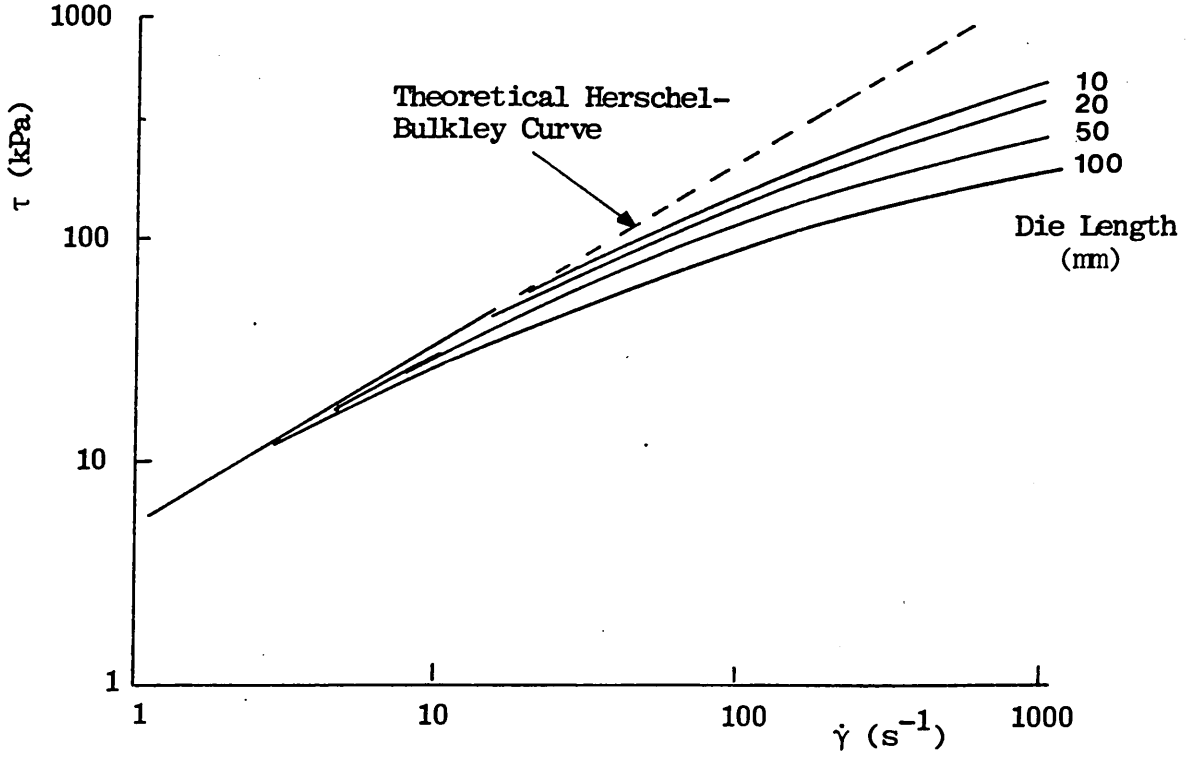


Fig. 1.17 Relationship between die length and viscous heating

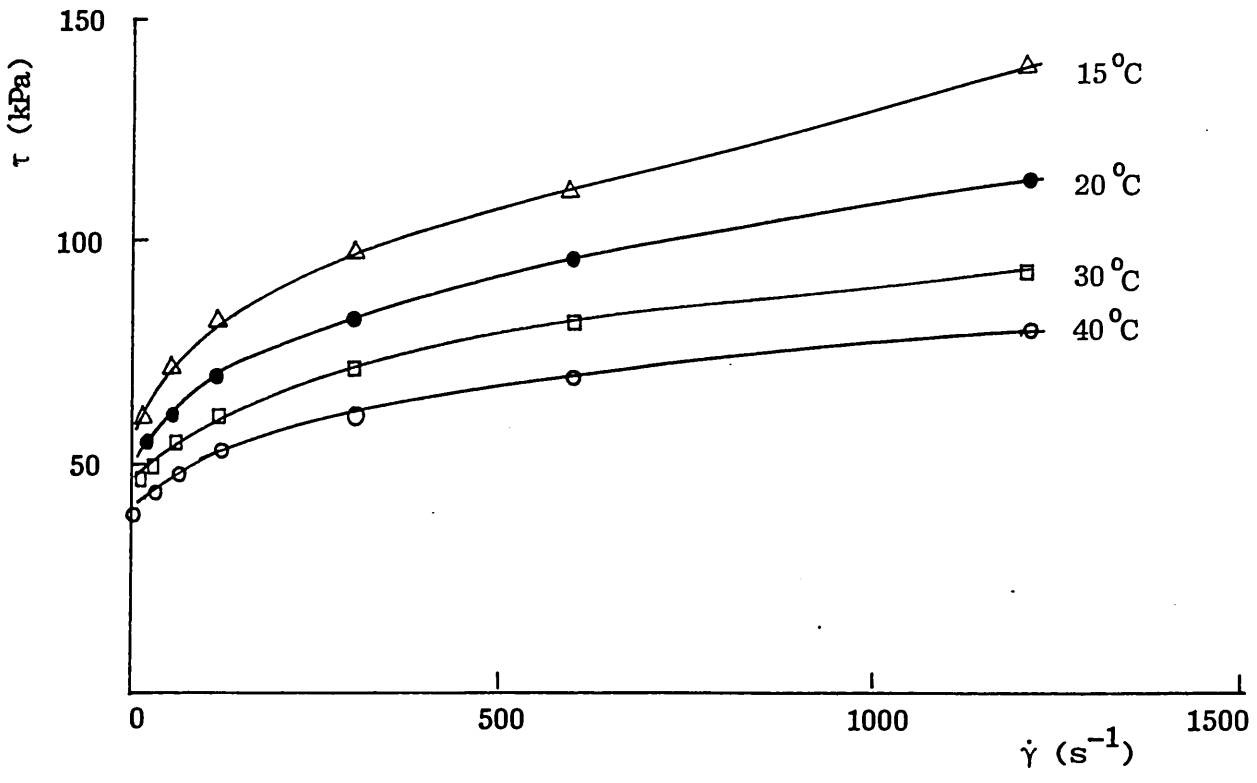


Fig. 1.18 Effect of temperature on the flow curve of propellant dough

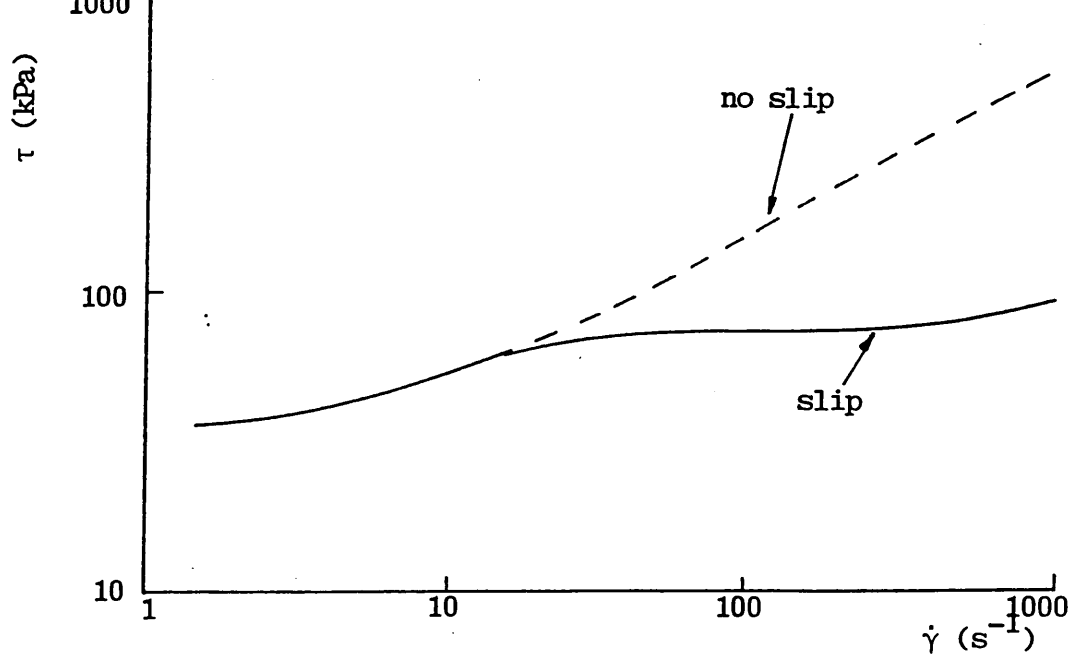


Fig. 1.19 Effect of wall slip on the flow curve

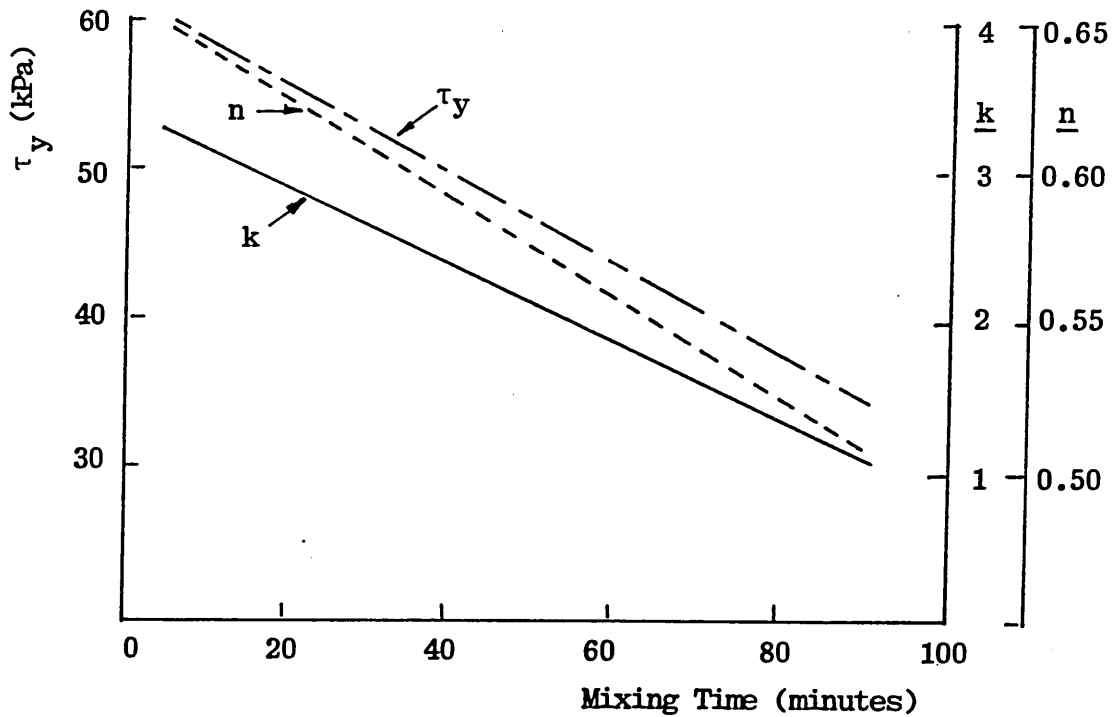


Fig. 1.20 Change in Herschel-Bulkley flow parameters as a function of mixing time

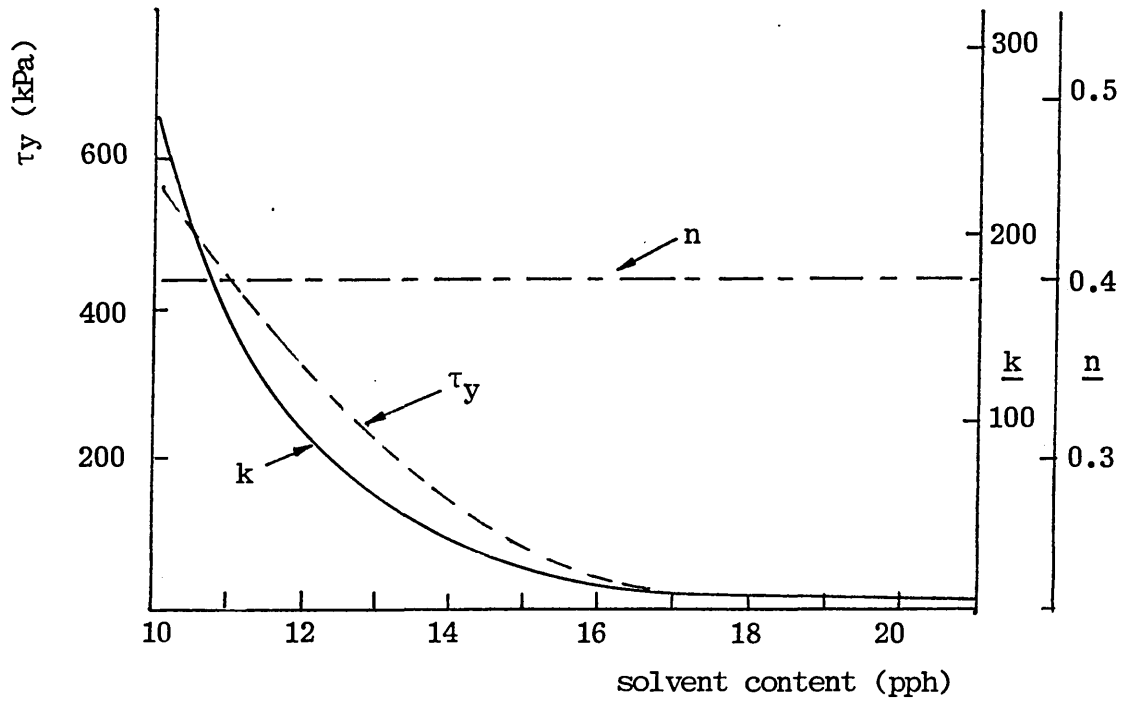


Fig. 1.21 Change in Herschel-Bulkley flow parameters as a function of solvent content

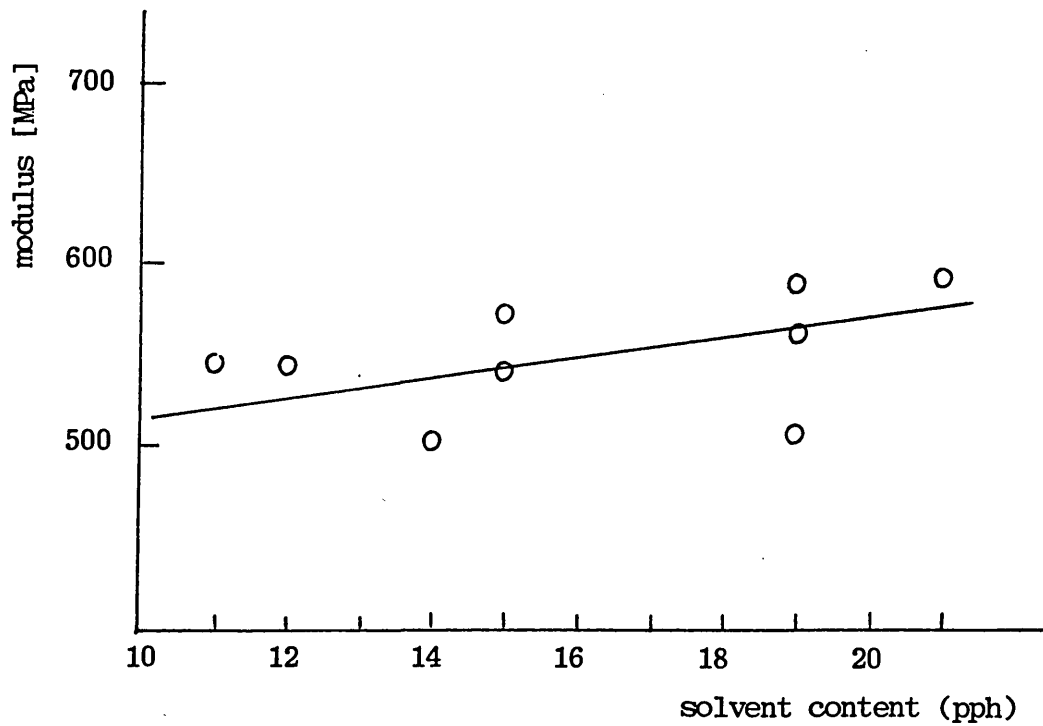


Fig. 1.22 Variation of the initial modulus of dried propellant as a function of solvent content

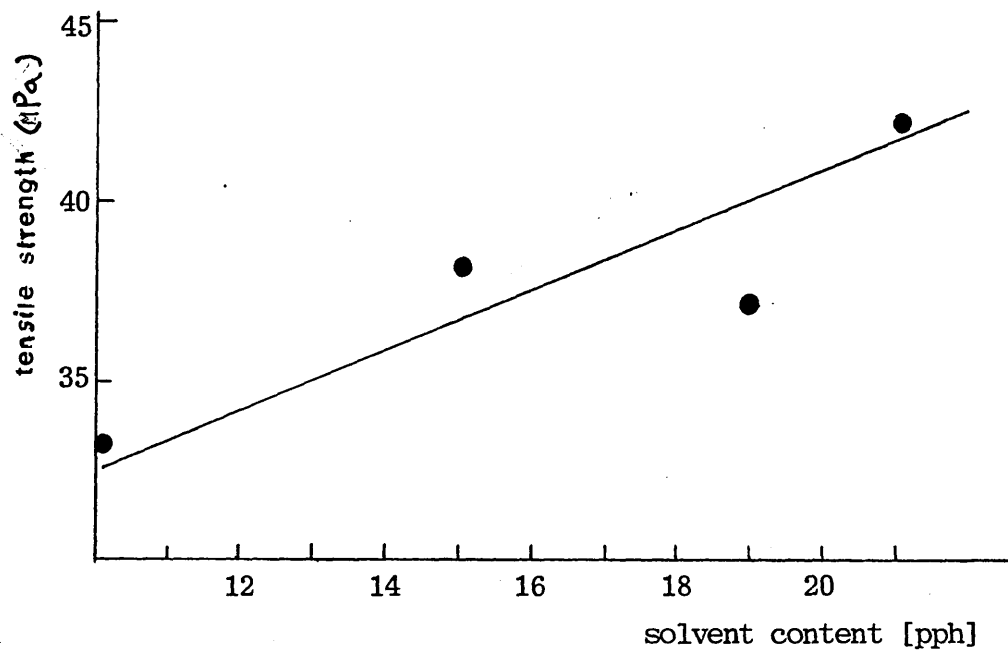


Fig. 1.23 Variation of the ultimate tensile strength of dried propellant as a function of solvent content

## CHAPTER 2 : Rheological Measurement

### 2.1 Introduction

The current propellant production process has two distinct areas which involve the flow of materials, namely incorporation and pressing. A variety of laboratory scale rheological instruments are available; but almost all have limited application to the propellant industry with respect to the control of solvent loss during the processing stages. To overcome this problem, modified torque and capillary extrusion rheometers have been adopted, since solvent loss can be minimized by processing the ingredients inside an enclosed chamber of the individual batch processor. In addition, they best represent conditions prevailing in propellant processing equipment, covering the shear rate range of interest, and they are most suitable for automation.

### 2.2 Torque Rheometry

#### 2.2.1 Machine Specification and Modification

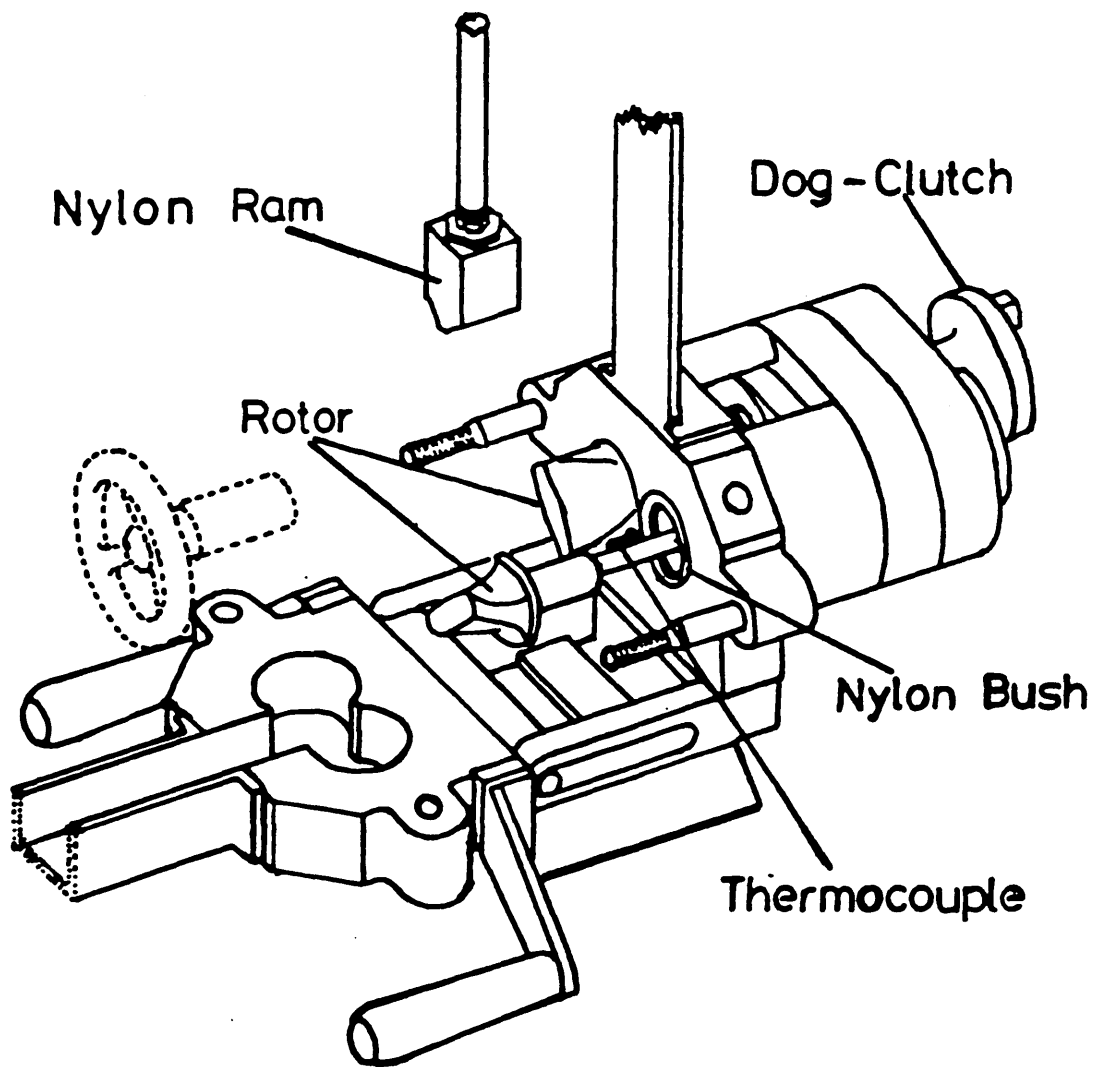
The torque rheometer used in this project is the Hampden Variable Torque Rheometer, Model TR-1 [48]. It is essentially a small laboratory internal mixer. It was originally designed by RAPRA for the purpose of compounding rubber stocks, and therefore it had to be modified to suit the research purpose [49].

Figure 2.1 shows the mixer unit of the torque rheometer. It comprises two blocks of chromium-plated steel which are clamped together to form the mixer chamber with a capacity of 40 ml. The mixing action is conducted by a pair of parallel kneading rotors driven in a contra-rotating sense downwards into the nip. The rotation direction of the drive shaft is modified by fitting a reversing switch to the motor. This is important to reduce the number of undispersed aggregates of CA simply by reversing the rotation direction during the filling period. The gap between the rotor blade and the chamber wall is about 1.7mm. A v-shaped, air operated ram rests on the upper central region of the mixing

chamber and its position inside the chamber can be adjusted by means of the air pressure. The function of this ram is used to define the chamber volume and to prevent the solvent loss during mixing. The gearbox with a gear ratio of 1.5 to 1 is situated between the mixing head and a two-speed (30 and 60 rpm) constant torque electric motor. Due to the complex geometry of the mixer head and the gear ratio, a distribution of shear rates is set up inside the mixer, with the maximum shear rate at the rotor tip. It is found that a maximum shear rate of  $68 \text{ s}^{-1}$  is created when the rotor is rotating at 30 rpm. A torque measuring system consisting of a linear voltage displacement transducer is rigidly connected to the suspended motor so that the torque exerted on the rotor blades by the materials as they are being processed gives a D.C voltage output corresponding to the torque level. The temperature control system of the torque rheometer has also been modified since the temperatures of interest for the present work range from about 10 to  $60^{\circ}\text{C}$ , which are far below the normal compounding temperatures of plastics and rubbers. Therefore a mixture of water and ethylene glycol (antifreeze agent) instead of oil is circulated from a thermocirculator through the side walls of the mixing chamber. The thermocirculator, which is basically a Churchill O2/CTCV series, is also modified so that the controller senses the mix temperature via a platinum resistance thermometer inserted into the mixing chamber just above the two rotors. Thus, the temperature of the mix is controlled instead of that of the water. Also, the mix temperature is accurately measured by a copper-constantan thermocouple which protrudes 3mm into the mixer chamber from a nylon plug. The DC voltage output from the thermocouple is connected to an interface unit before it is directly coupled to the chart recorder. In addition, the temperature of circulating water before and after passing through the mixing chamber is measured by means of a platinum resistance thermometer located at the end of both the inlet and outlet nylon

tubing of the mixing chamber.

Fig. 2.1 Sketch of the mixer head



### 2.2.2 Measurement Techniques

When all the experimental conditions have been attained, the mixing chambers are firmly tightened. 30% of cellulose acetate [47] is loaded into the mixer, which is rotating at 30 rpm, with the assistance of a paint brush. The solvent is then added very slowly to the centre of the chamber through a dropper and the direction of rotation is changed at least twice for short periods within this feeding time. The remaining ingredients are pushed into the chamber by means of the hydraulic ram. The feeding time should be within 2-3 minutes. While mixing is carried out, cooling is often necessary because a considerable amount of internal heat is generated from the internal frictional work between the material and chamber wall. When the pre-determined dumping condition has been reached, the computer will give out a signal to stop the experiment. The dough is obtained by unscrewing the chamber clamps and mechanically separating the chamber walls by a pair of screw jets. It is transferred to a polyethylene container with a tight top to minimize solvent loss.

It should be noted that a considerable amount of the mix (particularly the solvent) is able to leak through the rotor shafts. This problem is minimized by wrapping PTFE tape round the rotor shaft at its skirt. The rotors are then fixed into position and run until a fixed low torque value is obtained, indicating that the PTFE has flowed round the shaft to form a good seal between the shaft and the steel bearing.

### 2.2.3 Data Analysis

The data obtained from the torque rheometer consists of measured values of torque and temperature at a constant rotational speed as a function of time. Mixing curves yield a lot of information about the changes in rheological properties during mixing. This is because inherent transitions, which occur when a material is sheared and mixed, such as the gelatinisation process, lead to changes in the consistency and consequently cause variations in

torque level.

The gelatinisation process is an essential stage of propellant processing. The torque rheometer is used to make qualitative and comparative measurements of this process. This technique provides information on resistance to flow, heat generation and time-scale to consolidate under the processing conditions. Thus the shape of the mixing curve is used to characterize a propellant system. A typical torque versus time curve is shown in Fig. 2.2.

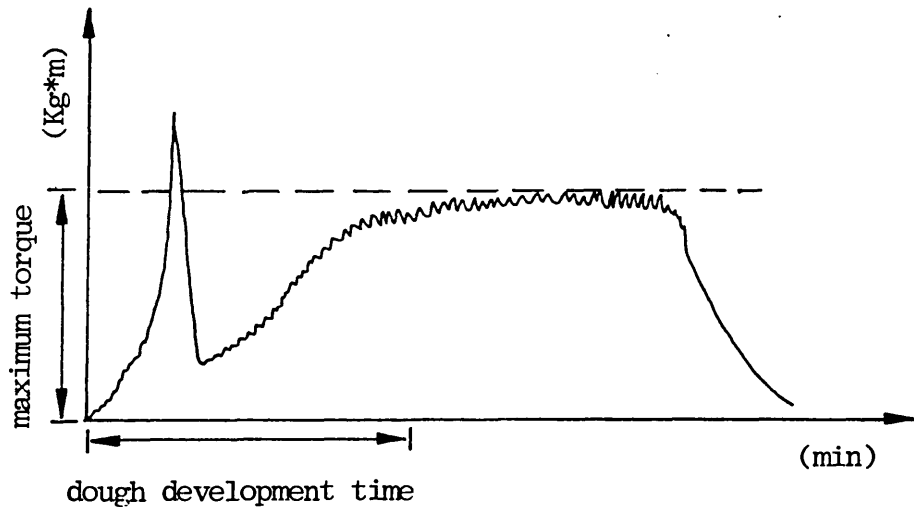


Fig. 2.2 Torque versus time trace of a mixing process

The peak of the mixing curve is called maximum torque and is expressed in torque unit ( $\text{Kg}\cdot\text{m}$ ). The reciprocal of torque is called mobility. The torque and mobility of doughs apparently are analogous to viscosity and fluidity. The time required to form the dough with maximum torque is defined as the dough development time and after this period, the torque of the dough remains at a constant level. The area under the mixing curve corresponds to the amount of energy used for mixing.

## 2.3 Capillary Extrusion Rheometry

### 2.3.1 Machine Specification and Modification

Unlike the torque rheometer, the flow curve under a given set of extrusion conditions can be obtained easily by the capillary

extrusion rheometer. Among the currently available constant extrusion rate capillary rheometers, the Davenport Capillary Rheometer (serial no. ZR406/31) is selected for this project [50]. In this method, a fluid is forced through a die and the viscosity of the liquid is determined from the measured volumetric flow rate, applied pressure and die dimensions. Originally, the Davenport Capillary Extrusion Rheometer was designed for the characterization of the flow properties of plastics materials. For the scope of this research, this machine is also modified to meet the requirements of processing of gun propellant [51]. A complete modified capillary extrusion rheometer consists of the following five essential units:

(A) Extrusion Unit

This unit contains a fluid circulating extrusion barrel 24.55 cm long and of inner diameter of the bore of 21.92 mm. The die is retained in the barrel by a threaded plug. The thread of the barrel is specially designed by machining the thread on the outside of the lower part of the barrel rather than on the inside.

(B) Capillary Unit

This unit is in fact a series of flat-entry capillary dies of known dimensions which are specified in terms of length and diameter of the die capillary.

(C) Temperature Control Unit

Direct electrical heating is not desirable for gun propellants. Consequently, a fluid circulation modified Churchill thermocirculator is used to control the extrusion temperature from about 10 to 60 °C with accuracy of  $\pm 1$  °C. The control of the Churchill unit is redesigned so that the temperature of the extrusion barrel is controlled rather than the temperature of the heat exchanger in the thermocirculator. To achieve this, a platinum resistance thermometer which steers this control is installed in a silicone-oil filled pocket in the wall of the rheometer barrel.

#### (D) Drive Unit

The piston is driven vertically into the barrel by a variable-speed D.C motor acting through a gear train which is modified by installing a single speed gearbox rather than a two speed gearbox. The speed of the piston can be set for any rate from 0.125 to 25 cm/min and the actual speed is directly indicated on a tachometer. In addition, this unit is also modified to gain access for external control of speed by the input of  $\pm 5V$  for speed control.

#### (E) Pressure Measurement Unit

The driving pressure is monitored by means of a pressure transducer mounted in the wall of the barrel just above the die so that errors due to pressure losses down the barrel are eliminated. The maximum working pressure is 10000 p.s.i.

A chart recorder is connected to the transducer so that the extrusion pressure is continuously displayed as a function of extrusion time. This proved to be essential, owing to the difficulty in deciding when the extrusion pressures in these materials were steady.

#### 2.3.2 Measurement Technique

It is essential to know the volumetric flow rate under a given set of extrusion pressures to calculate the viscosity of a material through a capillary with a well-defined geometry. As a result, either the extrusion pressure or the volumetric flow rate may be controlled as the independent variable with the other being the measured dependent variable.

Using a constant pressure rheometer, the volumetric flow rate is obtained by the knowledge of the density and mass of the extrudate over a known period of time. The general equation is

$$Q = \frac{W}{t\rho}$$

where Q = volumetric flow rate  
W = weight of extrudate  
t = time of extrusion  
 $\rho$  = extrudate density at a specific temperature

However, the modelling system to be studied contains volatile solvent. The above technique would be impractical as errors due to solvent loss would be introduced. Thus a constant extrusion rate rheometer is more suitable to the present system because the volumetric flow rate is easily obtained by the expression:

$$Q = \pi r^2 s$$

where r = piston radius  
s = piston speed

The extrusion pressure is measured by a pressure transducer fitted at the entrance to the die.

In operation, extrusion is normally carried out at the lowest required rate first, and the rate increased in increments as the extrusion progresses. The extruded cord is collected for each shear rate and the diameter of the cord is measured for die swell determination.

The major problems associated with the extrusion process have been found in:

(1) Loading the Dough

By the traditional packing of the barrel, it is found that air is trapped in the dough and the process of solvent losses are considerable. As a result, a loading device is used to minimize these problems. This loading device which is kindly provided by Baker & Carter [52] is in fact a loading barrel resting on top of the extrusion barrel. The materials are injected into the extrusion barrel by the loading ram fitted to the drive unit. As soon as the loading device is removed from the rheometer, the extrusion ram is fitted and lowered to contact the top of the dough, thus sealing the cylinder to prevent solvent loss.

(2) Temperature Equilibrium of the Dough

Temperature uniformity within the sample is difficult to achieve

quickly because the thermal conductivity of the dough is low. Besides, sufficient time must be allowed for the imposed stresses which are created during mixing to relax completely. To overcome this problem, the dough is conditioned for at least 30 minutes before extrusion commences.

(3) Sample Size

The batch size of the torque rheometer is very small compared to that of the extrusion rheometer. Therefore, a narrow range of shear rates is obtained.

(4) Piston speed

Since the capillary extrusion rheometer is originally designed to cover extrusion rate ranges of commercial interest, the accuracy of shear rates below  $1 \text{ s}^{-1}$  is low.

(5) Entrance Effects

As mentioned in Chapter 1, determination of the entrance pressure is fundamental to the validity of the viscosity measurements. In practice, there are 3 methods of correcting the entrance pressure.

(a) Bagley Correction [53]

This theory assumes that the effective length ( $L+eR$ ) of the capillary is greater than its true length ( $L$ ). The product,  $eR$ , is the length of the fully-developed capillary flow having a pressure drop equal to the excess pressure drop resulting from end effects. Thus, the true shear stress  $\tau_t$  may be written as:

$$\tau_t = \frac{PR}{2(L+eR)} = \frac{P}{2(L/R+e)}$$

Dies of the same radius  $R$  and different  $L/R$  ratios are used in the measurement. The total pressure drop across each die is measured as a function of uncorrected shear rate ( $\dot{\gamma}$ ). A graph is drawn for several shear rates of pressure drops versus  $L/R$  ratio. This is known as a Bagley plot. The graph is straight for a given uncorrected shear rate. From this curve, where  $P=0$ , the value of

e can be read off from the negative intercept, i.e,  $e = -L/R$ . Any increase in shear rate increases the values of e up to a limiting value.

#### Merits

- (i) It is the most accurate method;
- (ii) It corrects the shear stress to give a true value for a given shear rate.

#### Shortcomings

- (i) A lot of data is needed to obtain the true shear stress.
- (ii) The plots may be non-linear at high shear rates due to
  - (a) viscous heating
  - (b) wall slip
  - (c) increase in viscosity due to hydrostatic pressure
- (iii) There has been much debate over the correction of exit pressure drop by this method.

#### (b) Orifice Die Method

In this theory, the entrance effect may be thought of as a "polymer die" in series with the metal die.

Extrusions are carried out in two dies of the same radius but a die of length L and of zero length respectively. The pressure P obtained with the orifice die is assumed to embrace both entrance and exit corrections. If the flow rate is the same for both extrusions using a long die ( $L/R=32$ ) and an orifice die ( $L/R=0$ ), it can be assumed that the pressure required for the orifice can be subtracted from the total pressure drop obtained with the long metal die to give the true wall shear stress:

$$\tau_t = \frac{(P_L - P_0)R}{2L}$$

where  $P_L$  and  $P_0$  are the pressure drops across the long and orifice dies respectively.

#### Advantages

It is the simplest method of obtaining true wall shear stress while permitting the study of elongational flow from the entrance pressure drop. However, there is now some doubt about the validity

of this method to study the elongational flow behaviour.

Disadvantages

Values of P obtained have been found to be slightly higher than predicted by the conventional Bagley plot, indicating that the flow is never fully-developed. Also, for polymers that distort by melt fracture rather than sharkskin, the distortion will set in at very much lower shear rates for the orifice die. This confirms that the flow in the two dies is dissimilar.

(c) Couette-Hagenbach Method

This is a "different method" in which two dies of length  $L_1$  and  $L_2$  are used, for each of which the output Q and the pressure drop value P are obtained. Since, at a given shear rate, the entrance pressure drop is the same for each die, the pressure and length values of the shorter die can be subtracted from those of the longer die so that the true shear stress is given by:

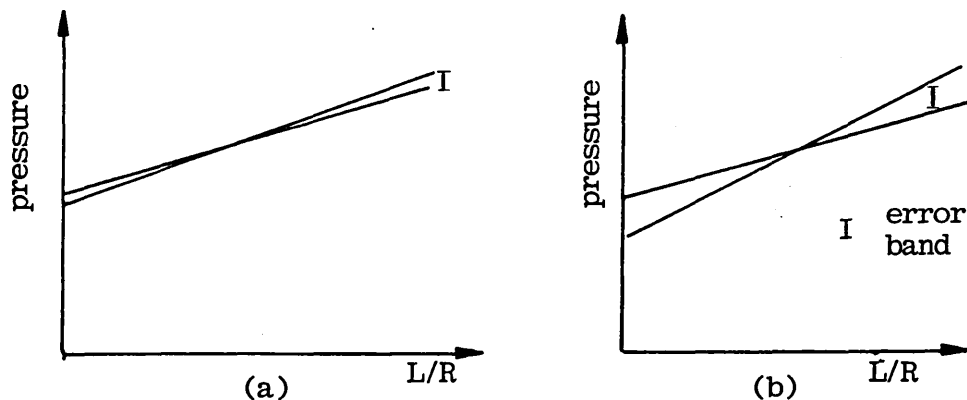
$$\tau_t = \frac{(P_1 - P_2)R}{2(L_1 - L_2)}$$

where the suffices 1 and 2 refer to the longer and shorter dies respectively.

This method offers the same advantages as that obtained in the orifice die method. It gives no idea of either total or relative magnitudes of the entrance and exit corrections. It has no indication on the recoverable tensile strain and the error in pressure measurement may be increased as shown in Fig 2.3.

Fig 2.3 Determination of Pressure Gradient

(a) Preferred (b) Dies of too similar L/R ratio



In conclusion, the fully-developed flow problem is common to all methods. Although the Bagley method theoretically offers the most accurate result, the hydrostatic pressure effect and the viscous heating of the modelling system render this method more complicated to use. Hence, the orifice die method is generally adopted because of its simplicity in application.

### 2.3.3 Data Processing of Rheological Results

The extrusion pressure across the die is determined by using a long die and an orifice die. This will eliminate the entrance pressure loss of the die. Thus, the true shear stress is given by:

$$\tau_t = \frac{(P_L - P_O) R}{2L}$$

The true shear rate is obtained by the application of Rabinowitsch correction to the apparent shear rate

$$\dot{\gamma}_t = \left(\frac{3n+1}{4n}\right)\dot{\gamma}$$

By using the Power law model,

$$\tau_t = k\dot{\gamma}_t^n$$

and taking logarithms of both sides

$$\log \tau_t = \log k + n \log \dot{\gamma}_t$$

A plot of  $\log \tau_t$  versus  $\log \dot{\gamma}_t$  gives a straight line. The slope and the intercept of this line gives the flow behaviour index and consistency index of the material respectively.

The corrected viscosity is determined by

$$\eta_t = \frac{\tau_t}{\dot{\gamma}_t}$$

The diameter of the extrudate for each shear rate is measured and the die swell is given by the equation:

$$B_R = \frac{\text{diameter of extrudate}}{\text{diameter of die}}$$

where  $B_R$  is the swelling ratio

If the die is long and tensile stress has relaxed, the die swell is due to the sudden release of the shear stresses at the exit. For a zero length die the shear stresses are not as significant as the tensile stresses built up in the entrance flow, and the swelling is due to the sudden removal of the tensile stress. For short dies both tensile and shear stresses are present at the capillary exit.

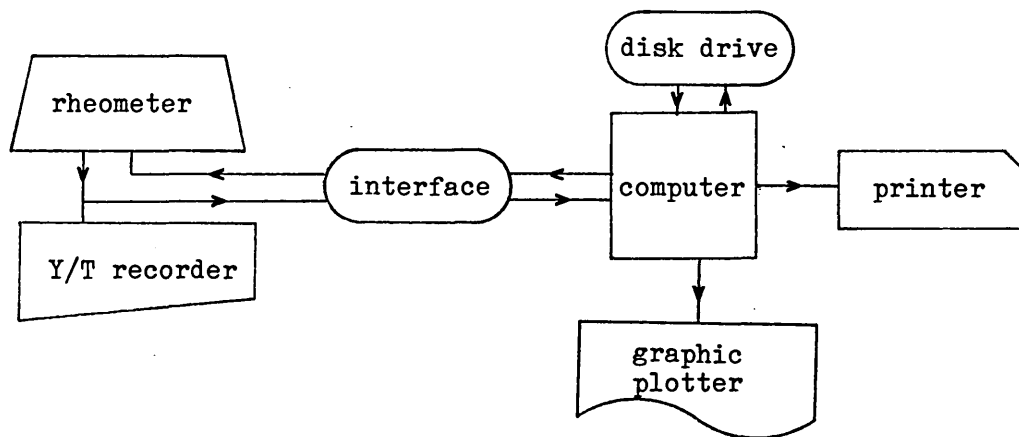
#### 2.4 Computer-controlled Rheometer

Computerisation of both the capillary extrusion rheometer and the torque rheometer are necessary in order to reduce the manpower and time involved in both measurements and the data interpretation processes. Complete automation of the capillary extrusion rheometer has been employed but the major setback is the relatively long set-up time involved for automation. This progressed gradually throughout the project.

##### 2.4.1 Capillary extrusion rheometer

The general layout of the system is shown below in Fig. 2.4.

Fig. 2.4 Layout of the computer-controlled rheometer



The computer is used to control the rheometer and to monitor and analyse the measured data. The interface provides two-way communication between the rheometer and the computer, i.e. extrusion rate has to be controlled and measured, and the stress has to be monitored. By achieving this, a purpose-built 12 bit D/A and A/D converter and the controller are used. Initially, the shear rate range within the experiment is selected. For each particular shear rate the computer selects a particular voltage level to the motor controller via a digital to analogue converter. In return, the voltage level from the pressure transducer is monitored via an analogue to digital converter. Thus, the motor speed is controlled and the corresponding pressure is monitored by the computer via the interface unit.

Various software packages had been developed by France (Sheffield City Polytechnic) for the control and data treatment before this particular research started. Therefore, some of the packages had to be modified in order to suit my research requirement. In general, the flow chart of control program for the data acquisition is shown in Fig 2.5 (Appendix A).

#### 2.4.2 Torque Rheometer Program

A computer program has been devised by Lee (Sheffield City Polytechnic) for routine use to calculate the work unit during the mixing cycles. A 6502 Apple IIe microprocessor computer is used for this purpose. It is connected to a 12 bit AI13 A/D converter with conversion time of approximately 20 micro-second. Both the signals of the temperature and torque are conveyed to the computer memory via the A/D converter. The data are then processed and stored in a sequential text file.

The essential features of the computer program are:

(a) A program which is called "SIDCODE" is written in low-level programming language for taking data. It performs the following functions:

- (1) It takes a temperature and energy channel reading from the rheometer via the AI13 A/D converter.

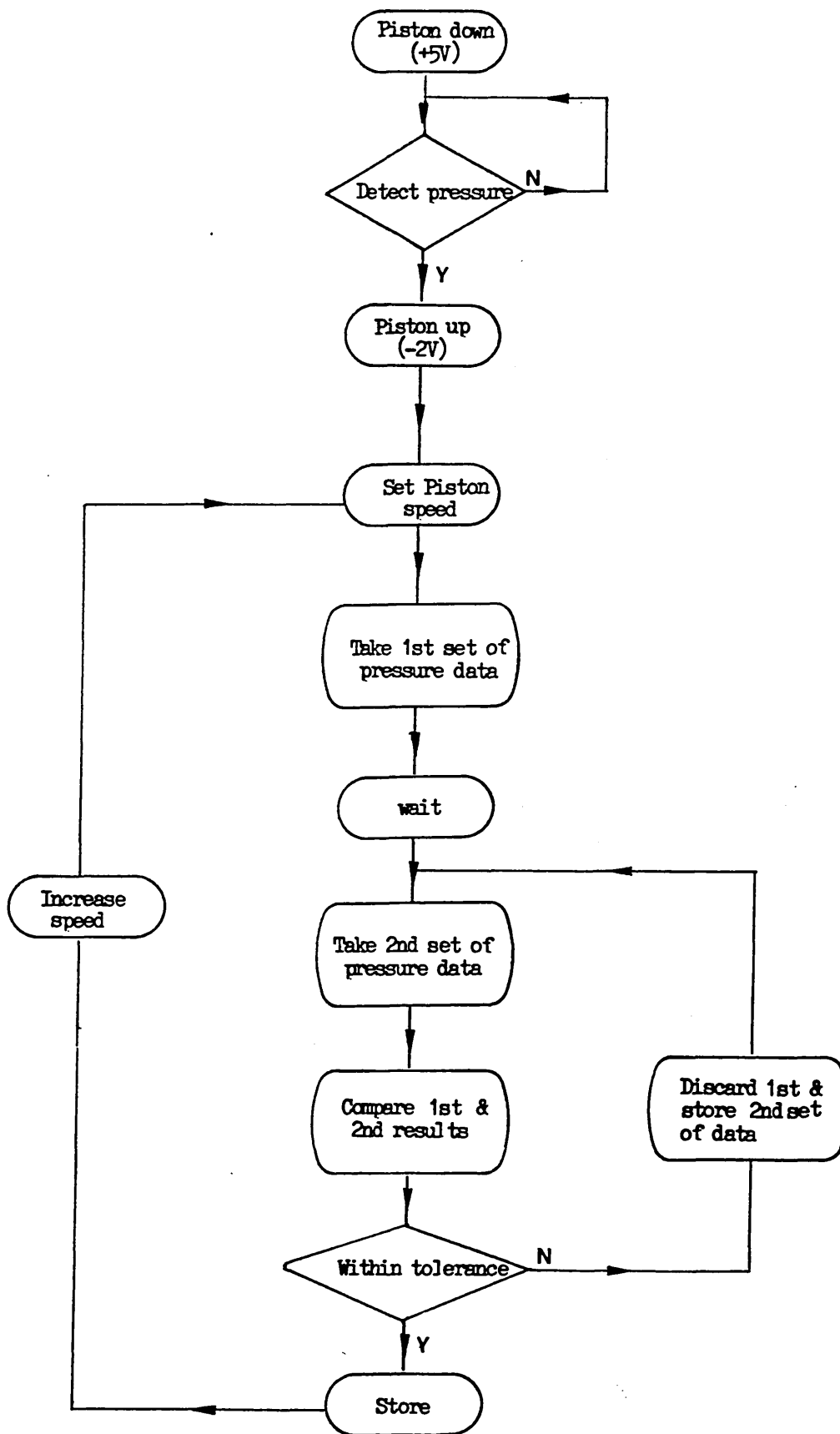
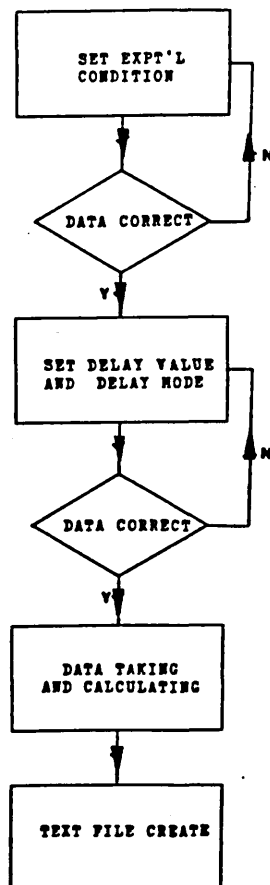


Fig. 2.5 Flow chart of extrusion program

- (2) The readings are stored as a 12 bit binary number in memory.
- (3) The pointers to memory are incremented and a value is read off from the new memory location. (This value is the time allocated to the next reading)
- (4) A timing clock is generated by a "do nothing" delayed loop. This loop is performed to give the appropriate delay.
- (5) The above processes are repeated until the required number of readings are taken.

(b) A program which is called "SID 3" is written in high-level programming language. It is able to communicate with the users for them to assign the values of the mixing parameters for the required functioning of the "SIDCODE" program. Such parameters include number of readings, delay value, delay mode, temperature and energy channels. Moreover, the program also allows for the calculation work unit from the 12 bit binary data in memory, and a text file is created from the permanent record. A flow chart of this program is shown in Figure 2.6 (Appendix B).

Figure 2.6 Flow chart of "SID 3" program



3.1 Determination of combined acyl in cellulose acetate

3.1.1 Introduction

The importance of the mean combined acyl of CA in influencing the solubility of the materials has often been mentioned, and numerous methods for its determination have been advocated. The methods fall into two general classes; saponification with alkaline reagents, or decomposition and hydrolysis by acids. Summaries of the literature have been presented by Marsh & Wood [54], and recent additional references are given by Howlett et al [55]. In this study, the total combined acyl in CA is determined by the modified Ebserstadt method because this method has proved to be the most accurate, reliable and satisfactory for the analysis of CA and other cellulose esters of relatively low molecular weight organic acids [56]. It involves the method of hydrolysing CA with a known amount of sodium hydroxide solution, and determining the excess alkali by titration with standard HCL. However, this method is found to be unsuitable owing to absorption of alkali by cellulose acetate, resulting in a poor end-point. This is improved by adding a known amount of acid at the end-point of the first titration, and after a suitable period of time for allowing the absorbed alkali to soak out from CA. The excess acid is back-titrated with standard alkali. The per cent acyl is calculated by:

$$\% \text{ acyl} = \frac{(V_a - V_s) * N * E_w}{10 * S_w}$$

where  $V_a$  = ml. of acid for blank  
 $V_s$  = ml. of acid for sample  
 $N$  = acid normality  
 $E_w$  = equivalent weight  
 $S_w$  = sample weight

3.1.2 Experimental & Result

Four samples were dried at 110<sup>o</sup>C for 2 days before they were tested by this method. 40 ml. of 75% ethyl alcohol as a swelling agent was added to CA at 50-60<sup>o</sup>C for 1/2 hour. Afterwards, 40 ml.

of 0.5N NaOH was added to the mixture for 15 minutes at the same temperature, and finally this solution was allowed to stand at room temperature for 48 hours. At the end of this time the excess alkali was back-titrated with HCL. The results of these titrations are shown in Table 3.1, and the mean combined acyl of CA was determined to be 38.5%. The degree of substitution (DS) of CA can be calculated from the acyl content as follow [57] :

$$DS = \frac{3.86 * \% \text{ acyl}}{102.4 - \% \text{ acyl}}$$

The degree of substitution of CA was found to be 2.33.

Table 3.1 Combined acyl of cellulose acetate

sample number	combined acyl /%
1	38.66
2	38.17
3	38.59
4	38.59
mean	38.50

## 3.2 Thermal studies of cellulose acetate

### 3.2.1 Theory

The thermal behaviour of CA was carried out by differential scanning calorimetric (DSC) and thermogravimetric analysis (TGA). DSC is an instrumental technique for studying the effects of heat on a small sample that is heated in a controlled manner inside a furnace (Fig. 3.1). Physical and chemical changes of the sample may occur. The sample and the inert reference sample are continuously maintained at the same temperature by automatic balancing of the power fed to each. The differential power is thus measured and plotted against temperature. The lower and upper portions of the DSC thermogram as shown in Fig. 3.2 represent transitions which are endothermic and exothermic in nature respectively. Quantitative determination of the energy involved for the transition can easily be obtained by evaluation the area under the curve for that transition. The glass transition is observed as only a shift in the base line because it is neither exothermic nor endothermic, but is a change in the specific heat. TGA is a technique for measuring the thermal stability of a material. The sample is coupled to a small furnace with an accurate balance so that the weight change can be displayed continually against temperature. The loss or gain of weight of a sample as a function of temperature or as a function of time at a fixed temperature is determined.

### 3.2.2 Experimental

Samples in a form of powder or tiny small doughs were inserted into an alumina pan in the case of the DSC measurement or into a crucible in the case of the TGA measurement. The Mettler TA 3000 thermal analysis system was used. It consists of the TC 10 TA processor, DSC 30 measuring cell and TG 50 thermobalance. The operation conditions for DSC and TGA were given as follows:

Scan parameter	DSC	TG
start temp. / °C	10	30
rate /K/min	10	10
end temp. / °C	280	500
time isothermal	0	0

In order to obtain a high precision in the measurement of the sensible heat, the signal is referred to a baseline determined separately. In this way, minor asymmetries in the measurement cell and differences in the pan weights can be compensated for. For this purpose a DSC curve is recorded with the blank function in which an empty sealed pan is inserted as a sample [58].

### 3.2.3 Results & Discussion

A typical DSC thermogram of unprocessed CA is shown in Fig. 3.3. This figure shows that the broad endothermic peak, which appears between 30 °C and 130 °C, is due to the endothermic moisture desorption. To clarify this observation, a sample was cooled to room temperature after a DSC scan over the range 0-250 °C and immediately rescanned over the same range. The endothermic peak almost disappeared, as shown in Fig. 3.4. Heating during the first DSC scan drove off essentially all of the moisture in CA, indicating that the first endothermic peak is due to dehydration. A second endothermic peak occurs with a peak maximum at about 234 °C, and the first exothermic peak at about 310 °C is observed. It should also be noted that a poorly defined transition is observed at about 200 °C.

The DSC thermogram of quenched CA from 240 °C is shown in Fig. 3.5. Comparison of the first DSC curve (Fig. 3.3) with that recorded during the second run (Fig. 3.5) clearly shows that the endothermic peak at about 234 °C has disappeared and there is a change in the base line observed at 190 °C. This implies that the crystalline regions in the sample are destroyed by the quenching process, with the formation of a glass transition ( $T_g$ ) at 190 °C, which is characteristic of an amorphous polymer. The endothermic

peak at 234 °C in the first DSC thermogram is identified as the crystalline melt temperature ( $T_m$ ) of CA.

The thermal behaviour of CTA is shown in Fig. 3.6. By comparison with Fig. 3.3, it reveals that the endotherm of CTA (45.5 J/g) is more pronounced as those obtained in CA (13.2 J/g), and the crystalline melting temperature of the former (311 °C) is higher than that of the later (234 °C). An exothermic peak at about 190 °C is also observed in Fig. 3.6. It is well known that CTA is readily crystallizable by simple heat treatments at temperatures higher than its glass transition temperature. Although the exotherm observed at 190 °C is small (ca 1.1 J/g), there is no doubt of its presence, and is due to the crystallization of CTA. These results are in good agreement with a number of investigators [16,20,59]. The poorly defined transition at about 190 °C as shown in Fig. 3.3 may be attributed to  $T_g$  of CA, which is following by an exothermic effect probably due to crystallization and by a subsequent melting endotherm. Owing to the unavoidable inhomogeneities in ester substitution, the CA sample under investigation contains some amount of CTA, and hence gives rise to an exothermic effect, disorting the well-defined  $T_g$  transition.

A thermogravimetric analysis has also been carried out in order to understand the origin of the exothermic peak in the high temperature region of the DSC thermogram. From the TGA curve shown in Fig. 3.7, it is readily seen that a significant weight loss begins in the temperature range (320-420 °C), where the exothermic phenomena appear, suggesting that CA undergoes exothermic thermal decomposition at temperatures higher than 320 °C, in accordance with previous results [21,22,66]. Also, a less substantial weight loss is observed at 40 °C to 120 °C, which coincides with the same temperature range of the endothermic dehydration peak in the DSC scan. Quantitative analysis of the moisture content of CA by thermogravimetry reveals that the moisture content of CA is reduced from about 3.2% to 1.5% after drying at 110 °C for 24

hours.

Some DSC measurements were made on the unprocessed and processed CA doughs. Figure 3.8 shows how the DSC thermograms change with progressive drying in an oven. The first thermogram shows a melt endotherm at  $233.7^{\circ}\text{C}$  for the unprocessed CA. If the processed CA dough is not sufficiently dried, two more endotherms appear (labelled  $\alpha$  and  $\gamma$ ). The size of these endotherms decreases gradually from stage I to III. On complete removal of the solvent, the  $\beta$  peak remains.

As a result, all the processed doughs are manually ground down to a fine powder and they are dried in a vacuum oven until a single crystalline melting transition is observed as shown in Fig. 3.9. This figure reveals that a less pronounced crystalline melting endotherm at  $227^{\circ}\text{C}$  is observed after mixing. A decrease in the size of this endotherm produces a corresponding shift of base line at about  $190^{\circ}\text{C}$ . The smaller endotherm and the occurrence of a glass transition in the DSC scan of processed CA may indicate fewer crystalline blocks or perhaps a lower degree of perfection of the crystalline structure of CA after mixing. Solvent (MEK) penetrates both the amorphous fraction of the CA and possibly a portion of the smaller and less perfect crystallites in the CA. This leaves an insoluble portion consisting of larger crystalline areas of CA that are not readily disrupted by the solvent.

The results of DSC thermograms of processed CA at different mixing times are summarized in Table 3.2. No value for the heat of fusion of completely crystalline CA has been reported in the literature and only relative crystallinity can be estimated. It should be noted that CA undergoes decomposition just after  $T_m$ , which introduces considerable uncertainty in the location of the base line of the fusion endotherm, and as a result, only approximate  $H$  values of these transitions are quoted in Table 3.2.

Table 3.2 Enthalpy of fusion, melting temperatures, relative crystallinities of CA from DSC

CA mixed at different time	$T_m$ / $^{\circ}$ C	H /J/g	relative crystallinity
0 min	233.7	13	1.00
1 min	228.5	11	0.85
5 min	228.5	9	0.69
20 min	227.9	8	0.62
60 min	227.0	8	0.62

This table shows both the crystalline melting temperature and the enthalpy of fusion decrease as the mixing time increases from 0 to 60 minutes, indicating that mixing reduces the degree of order in CA.

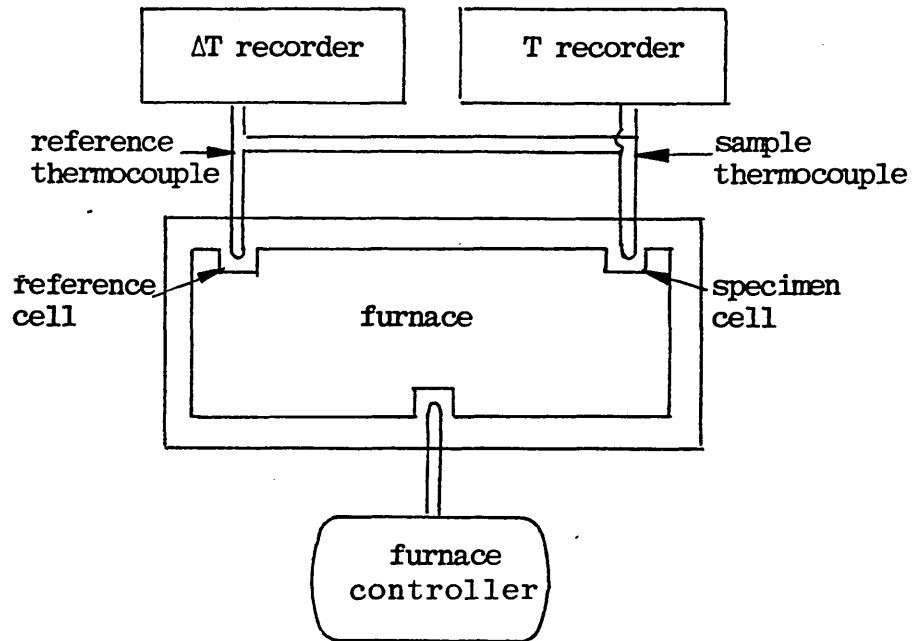


Fig 3.1 Sketches showing the layout of DSC

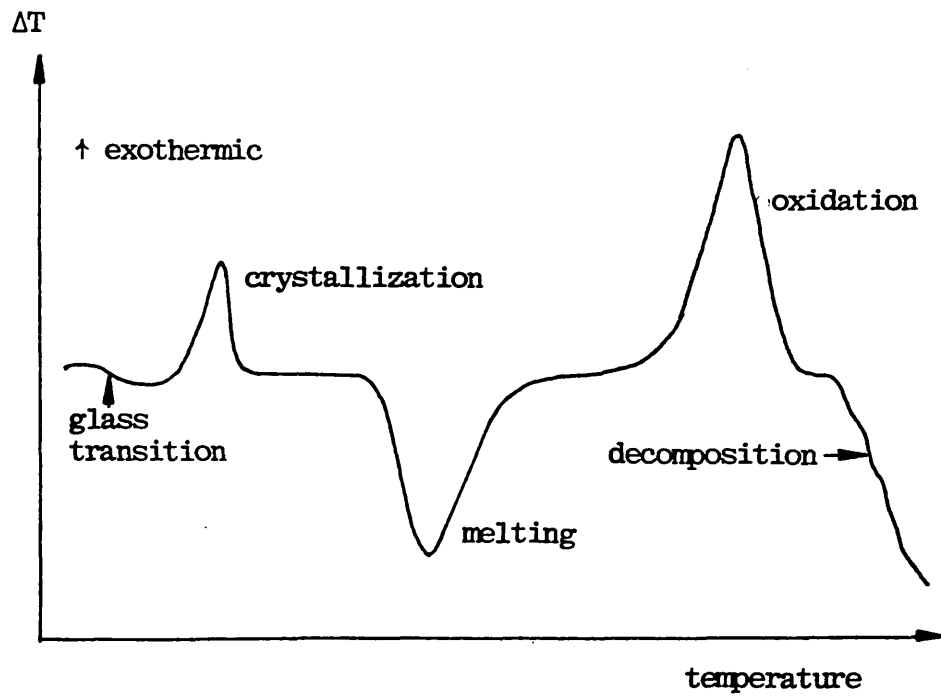


Fig. 3.2 A typical DTA thermogram

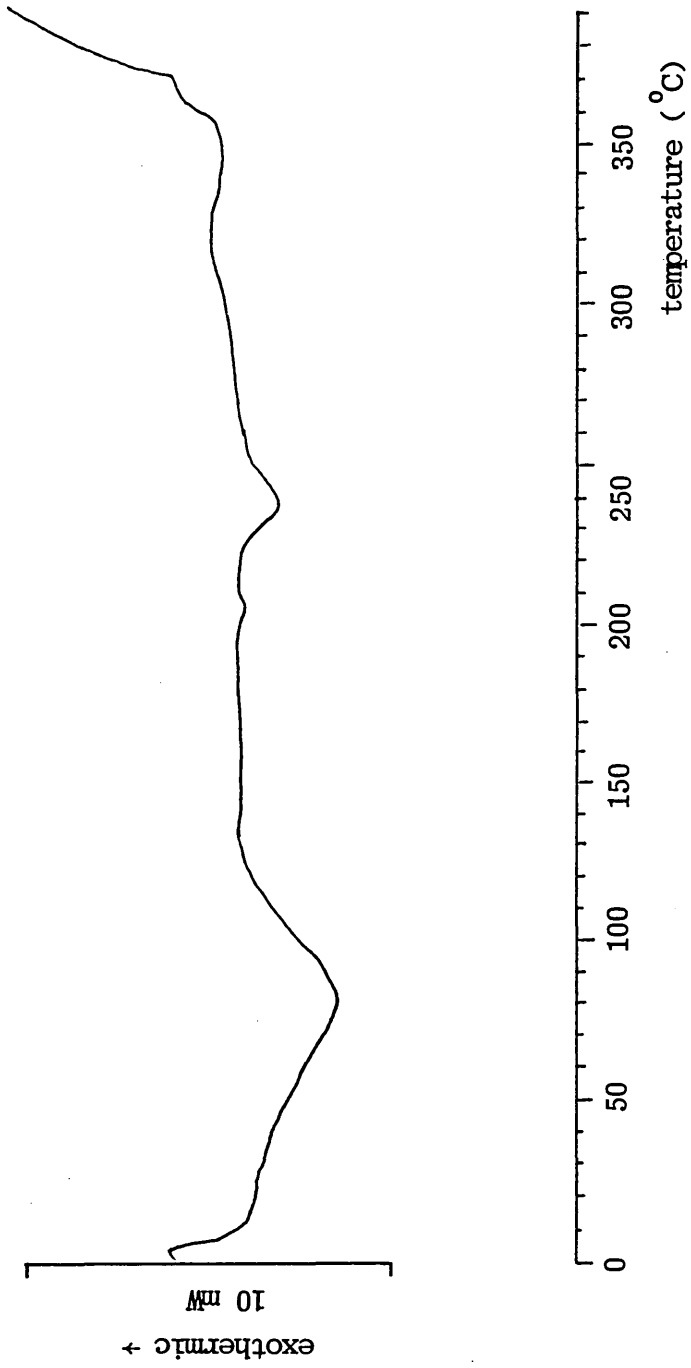


Fig. 3.3 DSC thermogram of unprocessed cellulose acetate

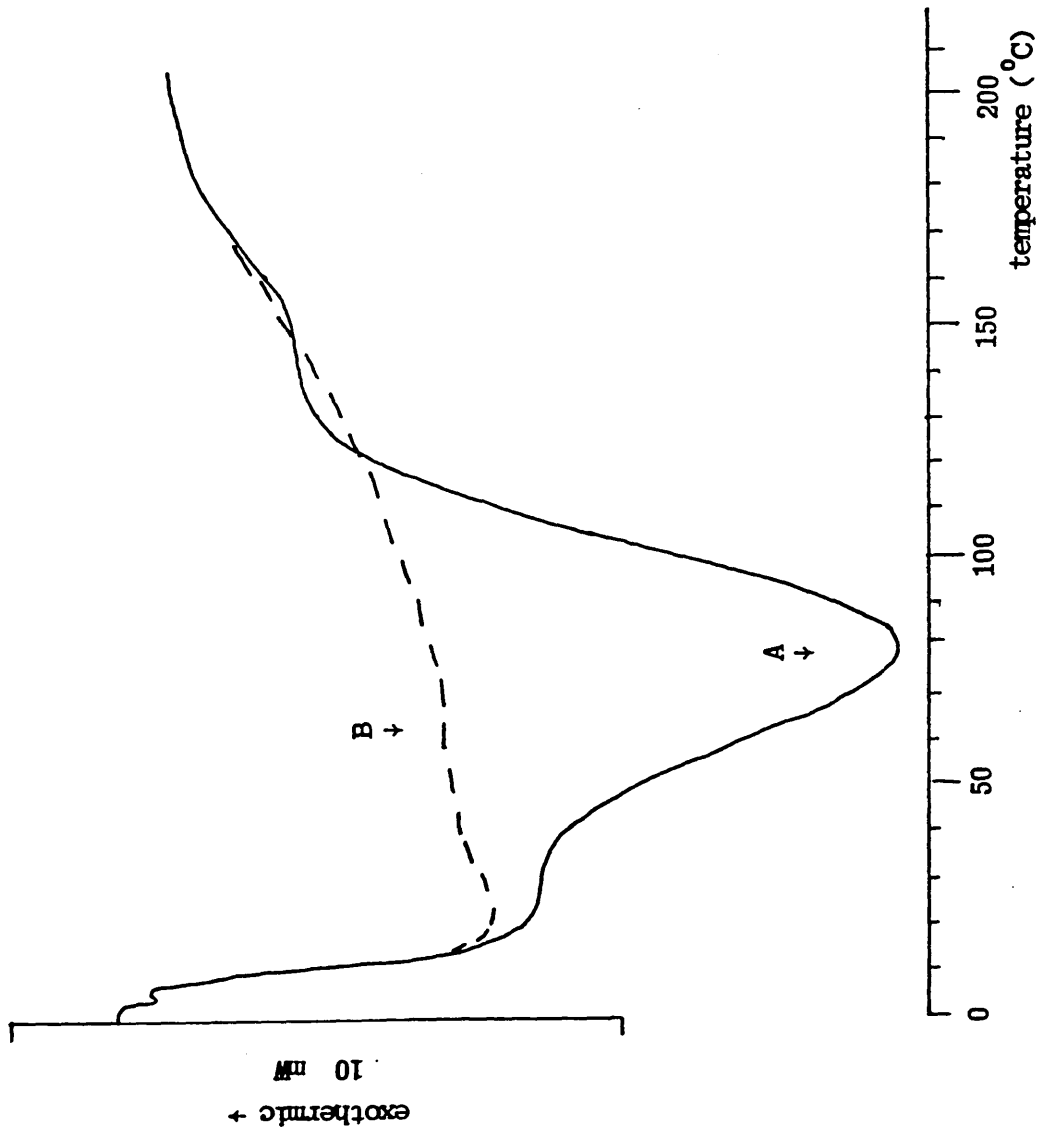


Fig. 3.4 DSC thermogram of unprocessed CA (A) before and (B) after driving off the water

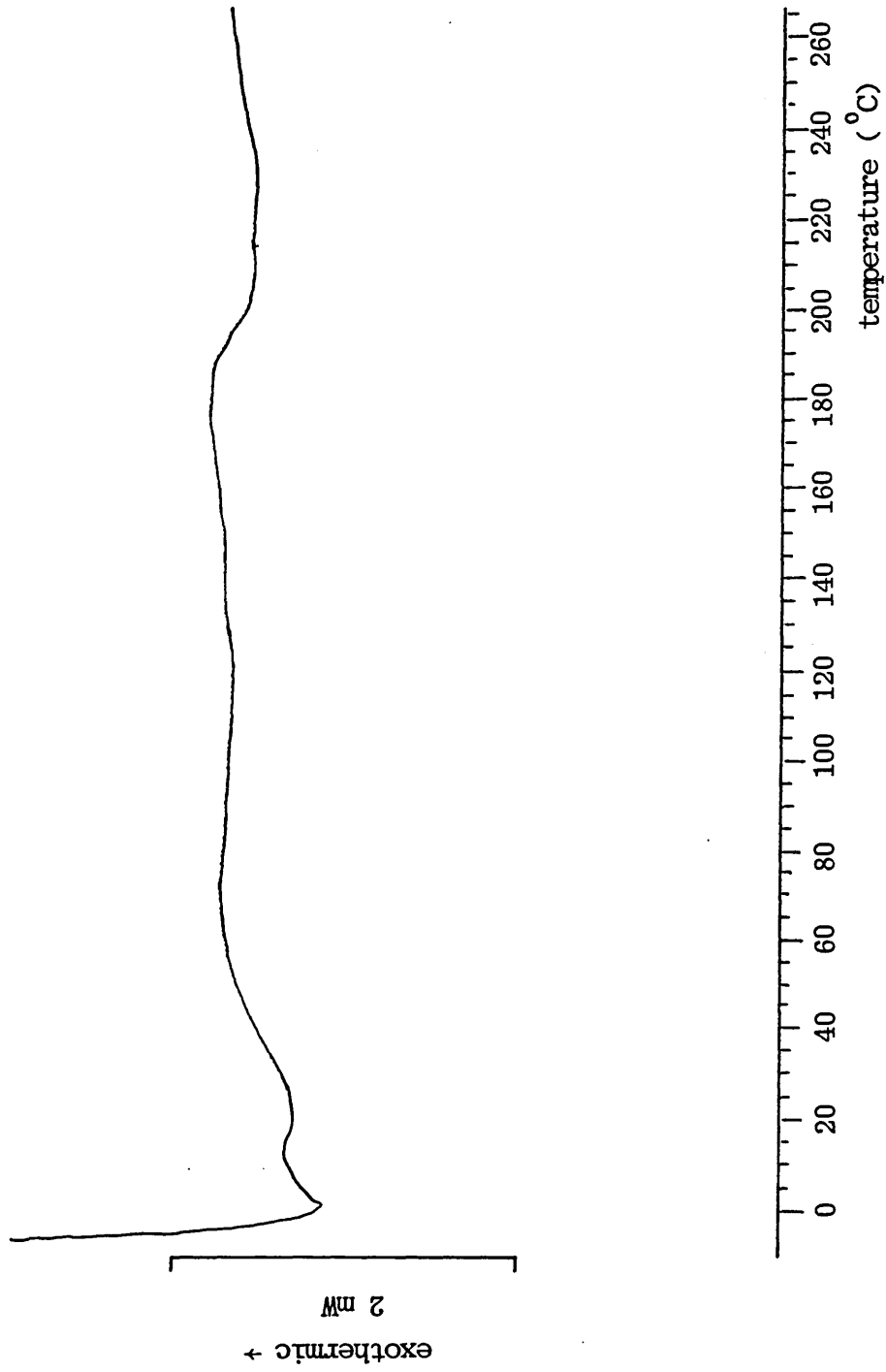


Fig. 3.5 DSC thermogram of quenched cellulose acetate

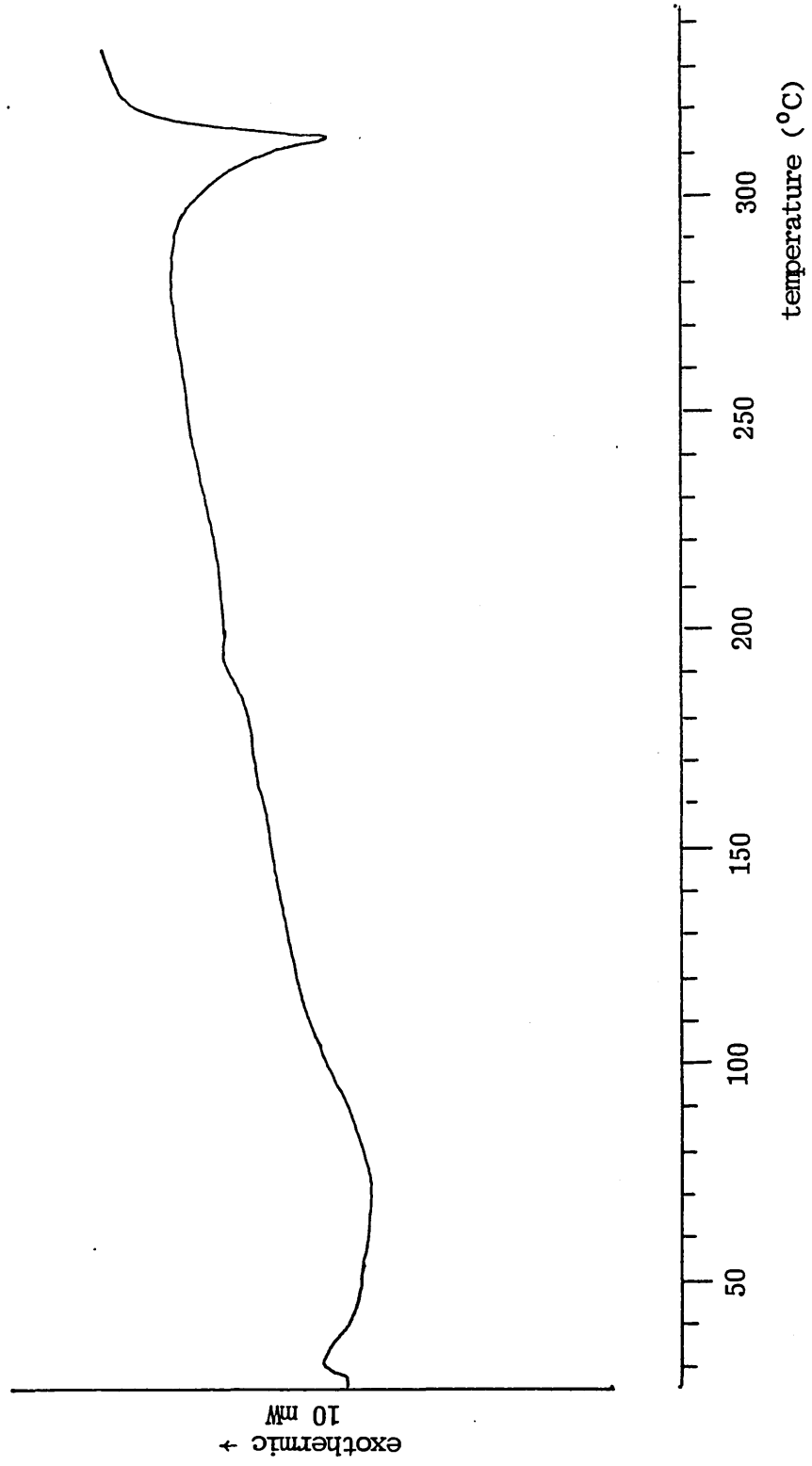


Fig 3.6 DSC thermogram of unprocessed cellulose triacetate

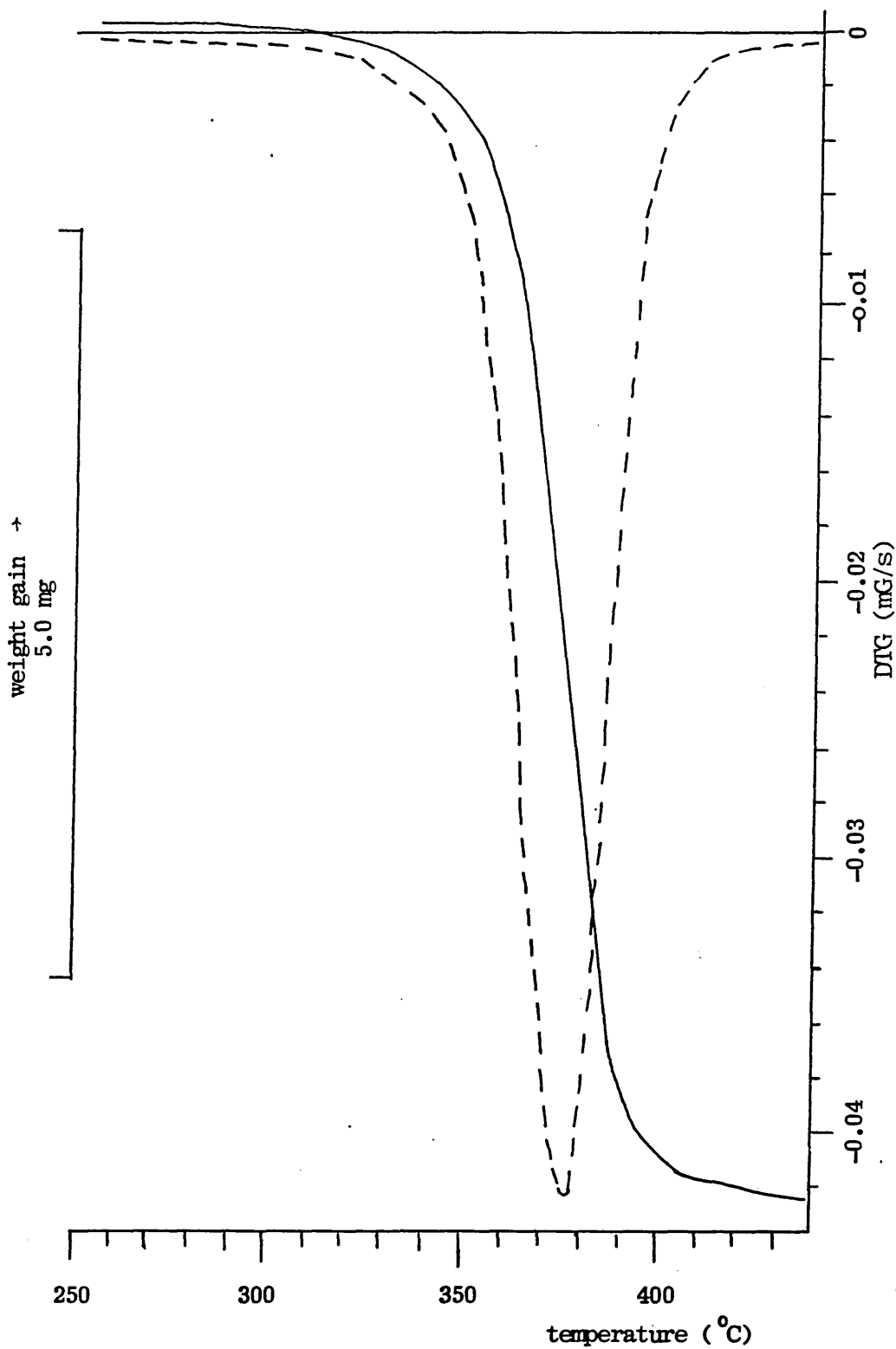


Fig. 3.7 TGA curve of unprocessed cellulose acetate

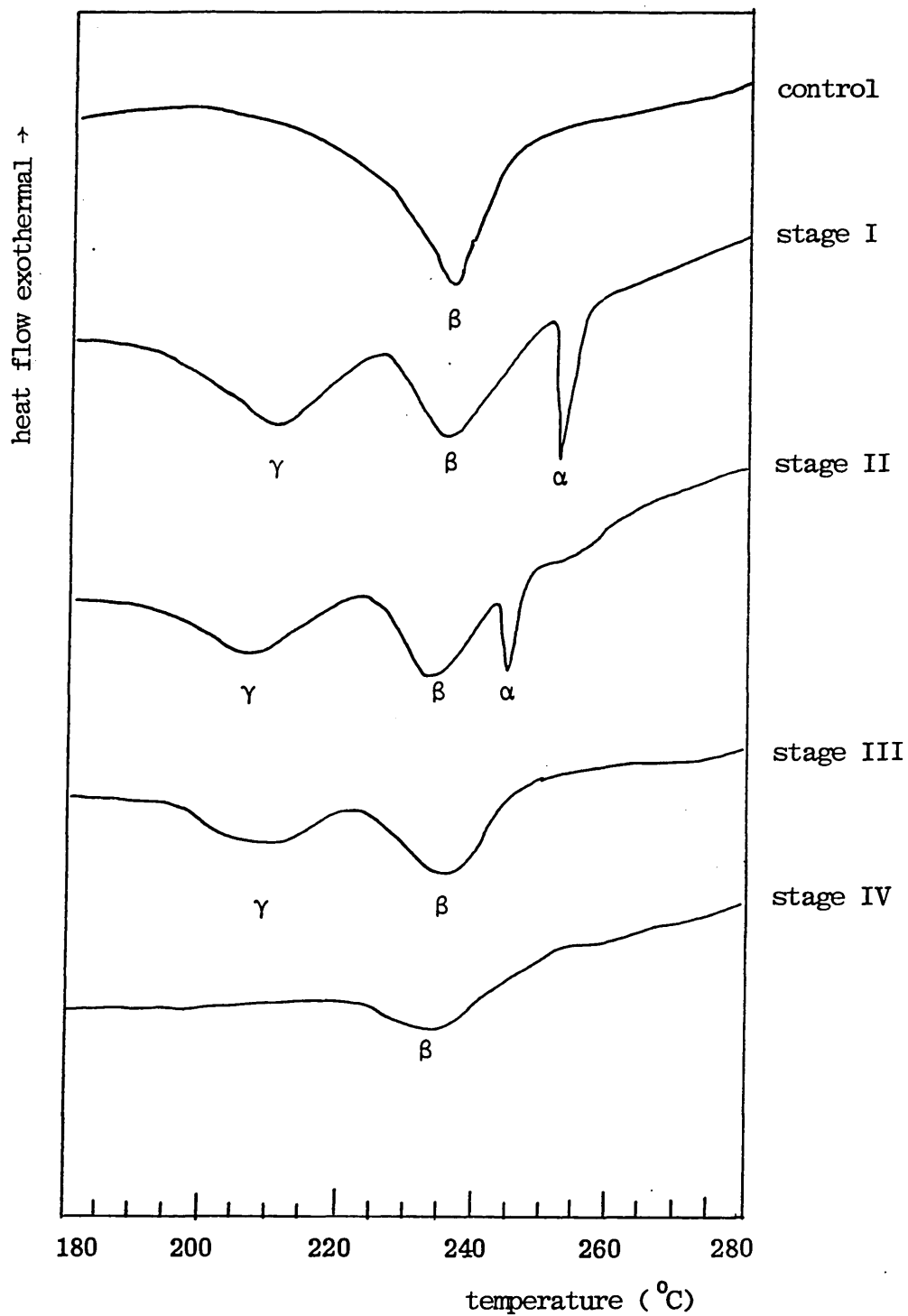


Fig. 3.8 DSC thermograms of processed CA as a function of drying condition

Note - I — 3 days at 60 °C  
 II — 3 days at 60 °C under vacuum  
 III — 3 days at 80 °C under vacuum  
 IV — 6 days at 80 °C under vacuum

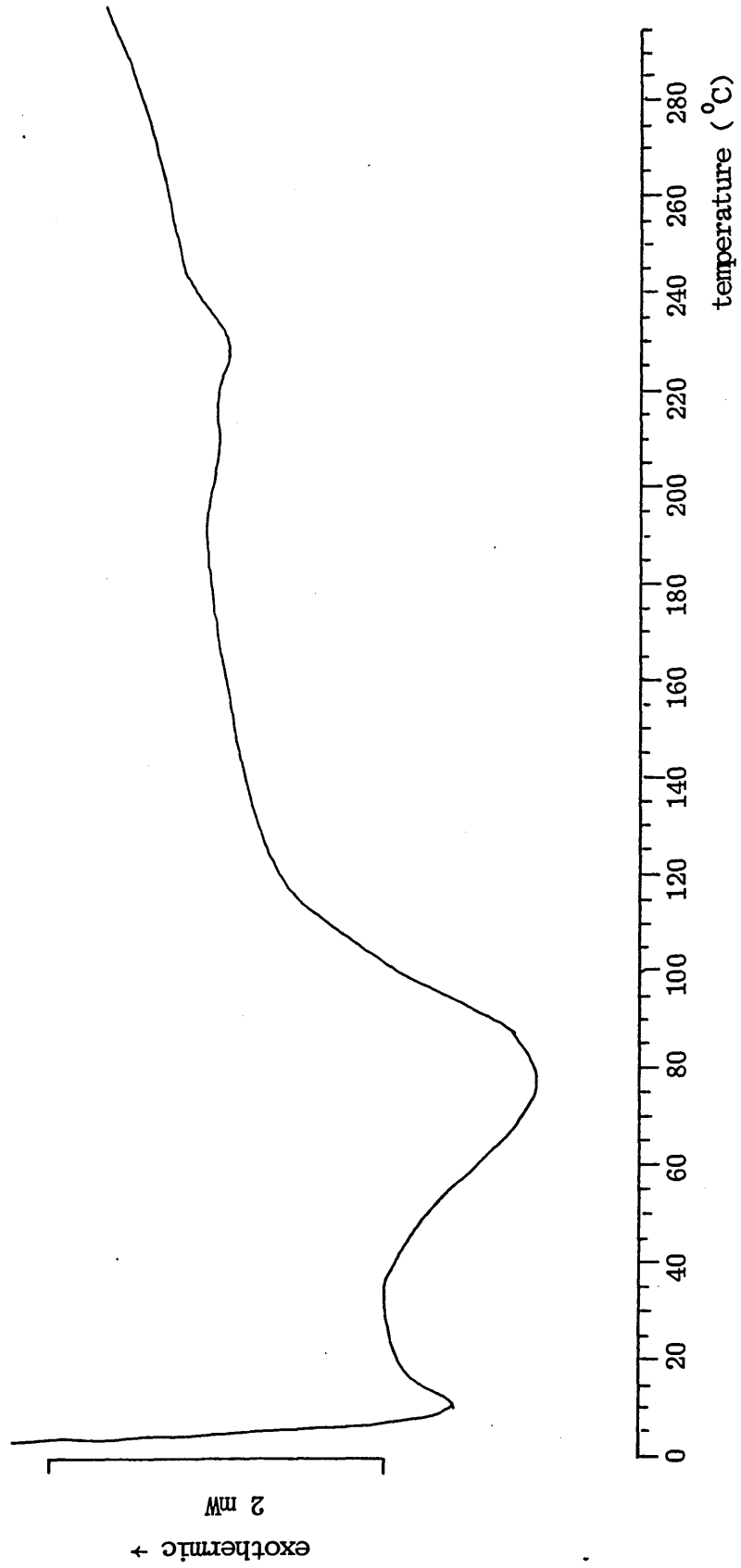


Fig. 3.9 DSC thermogram of processed solvent-free cellulose acetate

### 3.3 Mechano-degradation studies of cellulose acetate doughs

#### 3.3.1 Introduction

Scission of molecular chains under applied force is not a rare phenomenon, but it has been observed in the comminution of cellulose. The detailed mechanisms of mechano-degradation of high polymers was studied by Watson [60].

Mechano-degradation of CA might possibly occur during the mixing process, leading to a decrease in the mean molecular weight of CA. The earliest viscosity-molecular weight relationship for CA was developed by Staudinger [61]. Solution viscosity is basically a measure of the extension in space or hydrodynamic volume of polymer molecules.

Flory and Fox [62] studied the relationship between intrinsic viscosity and unperturbed mean square end-to-end distance  $\langle r_0^2 \rangle$  for a polymer chain, as shown as follows :

$$[\eta] = \frac{\bar{\Phi} V_h}{M} = \frac{\bar{\Phi} \langle r_0^2 \rangle^{3/2} \alpha^3}{M}$$

where  $[\eta]$  is the intrinsic viscosity  
 $\bar{\Phi}$  is the universal constant  
 $M$  is the molar mass of polymer  
 $\alpha$  is the linear expansion factor  
 $V_h$  is the hydrodynamic volume

The above equation can be rearranged as below:

$$[\eta] = \bar{\Phi} \left( \frac{\langle r_0^2 \rangle}{M} \right)^{3/2} M^{1/2} \alpha^3$$

It should be noted that the quantity  $(\langle r_0^2 \rangle / M)^{3/2}$  is a constant which is dependent on the chain structure and the linear expansion factor is equal to unity at the theta condition. This equation can be simplified under the theta condition.

$$[\eta]_{\theta} = K_{\theta} M^{0.5}$$

The above equation can be extended to the non-theta condition and is known as the Mark-Houwink equation [63]:

$$[\eta] = K M_V^{\alpha}$$

where  $K$  and  $\alpha$  are the Mark-Houwink constants.

The values of  $K$  and  $\alpha$  are determined from experimental measurement of  $[\eta]$  and molecular weight. The system of CA in acetone has been studied extensively. However, it has been found that the results of different investigators differ significantly. A review of the literature gives values of  $K$  and  $\alpha$  for the CA/ACE system as shown in Table 3.3 [64].

It should be noted that the Mark-Houwink constants are a function of temperature, solvent, molecular weight and degree of substitution of CA. Although Howlett [65] has demonstrated that the values of  $K$  and  $\alpha$  remain constant for the CA/ACE system at 25 °C. This relationship is only limited to some cellulose acetates with acyl content of 39.4-39.8%, in the molecular weight range of 30,000 to 62,000.

In order to avoid confusion, intrinsic viscosity of the polymer solution is used as a relative measure of the molecular weight of the samples. A drop in intrinsic viscosity indicates the mechano-degradation of the sample during mixing, and this approach has been used throughout this project.

Table 3.3 Literature values of Mark-Houwink constants for the CA/ACE system [63]

Range of m.wt. ( $10^4$ )	Range of /dl/g	DS	K /dl/g	$\alpha$
1.1-13.0	0.2-2.8	2.32	0.254	1.0
2.0-10.4	0.5-2.5	2.32	0.238	1.0
1.0-18.4	0.3-3.1	2.38	0.897	0.9
2.6-26.9	0.8-5.1	2.25-2.38	1.600	0.82
3.1-36.0	0.6-3.5	2.38	1.49	0.82
3.4-10.4	0.9-2.3	2.25	2.80	0.78
2.9-30.8	0.5-6.0	/	3.51	0.76
0.4-10.5	1- 3	2.32	8.90	0.67

### 3.3.2 Experiment and data processing

Viscosity measurements were made in a Cannon-Ubbelohde number 75 (No. 1783) viscometer at  $25 \pm 0.1$  °C. The maximum polymer concentration used in the determination of intrinsic viscosity was 1.0 g/dl. Several efflux times consistent to  $\pm 0.1$  s for the pure solvent and the polymer solution ( $t_0$  &  $t_1$ ) were determined.

Successive dilutions of the stock solutions were made by pipetting 2 ml of fresh acetone into the viscometer. Hence, a series of polymer concentrations and efflux times were obtained.

The specific viscosities ( $\eta_{sp}$ ) of polymer solutions are determined from the relative values of the viscometrically measured solution and solvent flow times by means of the equation.

$$\eta_{sp} = \frac{t}{t_0} - 1$$

According to the Huggins equation,

$$\frac{\eta_{sp}}{c} = [\eta] + k' [\eta]^2 c$$

The intrinsic viscosity is usually determined by a graphical method in which the values of reduced viscosities are plotted against concentration. A typical reduced viscosity versus concentration curve for unprocessed CA in acetone is shown in Fig. 3.10. This plot is essentially linear in the lower ranges of the concentrations studied, and it is extrapolated to zero concentration to determine the corresponding intrinsic viscosity, which is defined as

$$[\eta] = \lim_{c \rightarrow 0} \frac{\eta_{sp}}{c}$$

A computer program is set up by Holfreiter et al [66] in order to calculate a least-square-derived intrinsic viscosity from the raw data. In addition to eliminating errors inherent in graphic solutions, the computer output provides a 95% confidence interval (CI) of the intrinsic viscosity. This program is used in my work and a list of the program is shown in Appendix C. It should be noted that the value of intrinsic viscosity for any sample with 95% C.I. index higher than 0.1 should be disregarded, and the viscosity molecular weight determination of such sample should be repeated.

### 3.3.3 Results & Discussion

The effect of the process variables time, concentration and temperature on work unit and intrinsic viscosity of the CA doughs are shown in Table 3.4.

The intrinsic viscosity of unprocessed CA is higher than that of all processed CA doughs, indicating the possibility of mechano-degradation of CA during the mixing process. Thus, it should be expected that intrinsic viscosity is a function of work unit. However, no strong correlation between intrinsic viscosity and work unit is observed in this particular study. The results in Fig. 3.8 suggest that the drop in intrinsic viscosity of processed CA may be due to the presence of solvent in the doughs. The difficulties in removing the chemisorbed solvent completely from CA doughs may be due to the formation of an impermeable skin on the surface, enhancing the energy barrier of the solvent evaporation process. As a result, the trapped solvent can only escape at high temperatures because of the high molecular mobility of CA chains.

Quantitative analysis of the trapped solvent was carried out by means of the thermogravimetric technique. The relationship between weight loss and temperature is shown in Fig. 3.7. It has been mentioned that unprocessed CA can withstand temperatures of up to 320 °C without any significant loss in weight due to thermal decomposition. The weight loss at temperatures lower than 320 °C, particularly in the range of the T<sub>m</sub> of CA, is mainly due to the evaporation of solvent from doughs, as shown in Fig. 3.11.

Quantitative analysis of the trapped solvent was determined by this method, and the calculated solvent contents are shown in Table 3.4. It should be noted that the intrinsic viscosity of all the processed CA doughs after solvent correction are roughly of the same magnitude of unprocessed CA. Thus, the presence of solvent inside the doughs accounts for the drop in intrinsic viscosities of the processed CA doughs, and mechano-degradation of CA during mixing is not observed in this study.

Table 3.4 Intrinsic viscosities of unprocessed and processed cellulose acetates

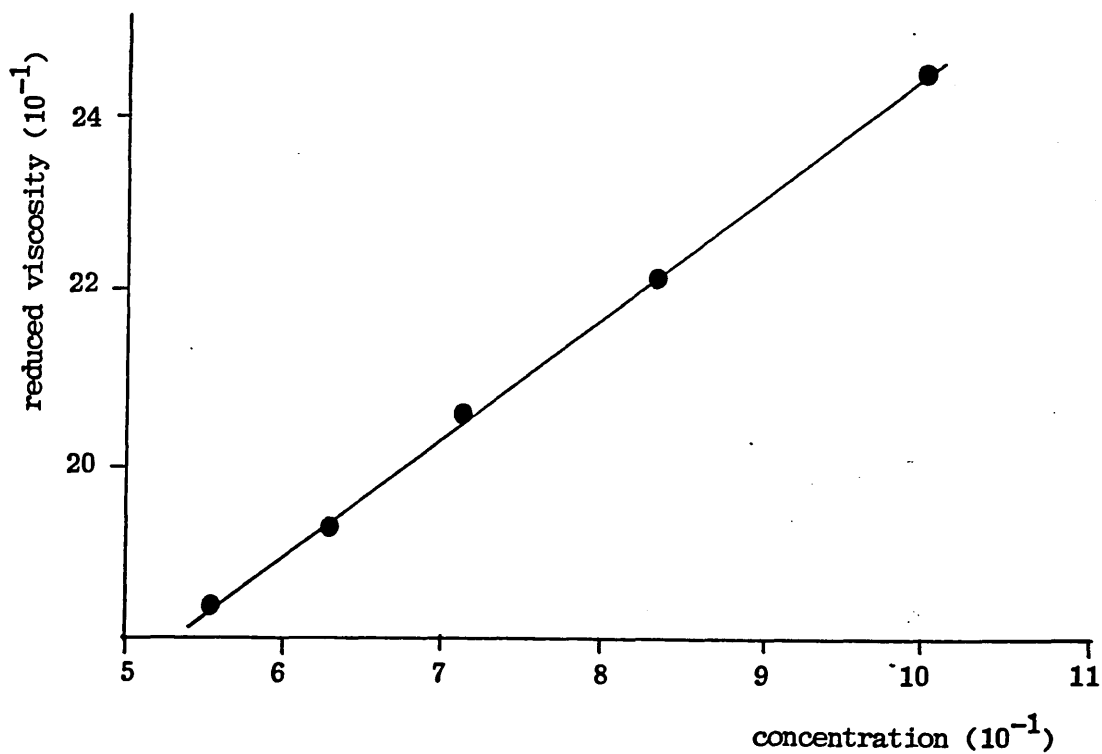
Mixing Variables	Work unit /MJ/Kg	$[\eta]_0$ /dl/g	Solvent Content	$[\eta]$ /dl/g
1 min	0.074	1.067	4.7%	1.120
5 min	0.4	1.062	5.7%	1.126
20 min	2.2	1.076	4.7%	1.116
60 min	6.767	1.066	5.4%	1.127
120 min	13.92	1.076	6.6%	1.115
60 pph	2.68	1.097	3.1%	1.132
70 pph	2.2	1.076	4.7%	1.116
80 pph	1.5	1.103	4.0%	1.162
90 pph	0.75	1.088	4.8%	1.143
10 C	2.622	1.088	5.6%	1.153
20 C	2.2	1.076	4.7%	1.116
30 C	1.33	1.086	4.4%	1.136
40 C	0.791	1.099	3.0%	1.134
unprocessed	0	1.121	1.4%	1.163

Note:

$[\eta]_0$  - intrinsic viscosity before solvent correction

$[\eta]$  - intrinsic viscosity after solvent correction.

Fig. 3.10 Relationship between reduced viscosity and concentration of unprocessed cellulose acetate



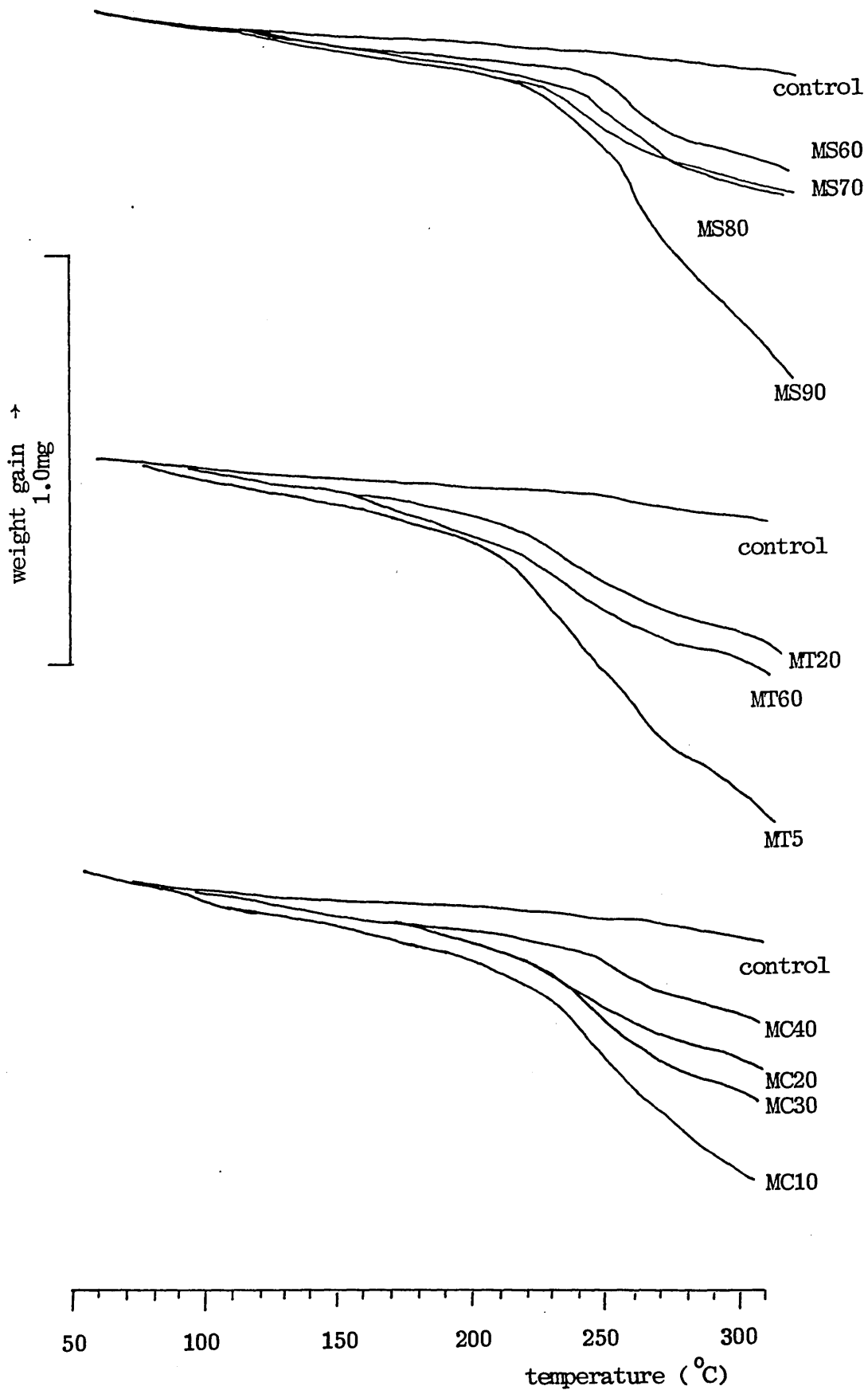


Fig. 3.11 Quantitative determination of trapped solvent in doughs by thermogravimetric analysis

### 3.4 Infrared analysis of cellulose acetate

#### 3.4.1 Theory

Emission or absorption spectra arises when molecules undergo transitions between quantum states corresponding to two different internal energies. The energy difference  $\Delta E$  between the states is related to the frequency of the radiation emitted or absorbed by the quantum relation  $\Delta E = h * \gamma$ .

Infrared frequencies in the wavelength range 1-50  $\mu\text{m}$  (10000-200  $\text{cm}^{-1}$ ) are associated with molecular vibration and vibration-rotation spectra.

A molecule containing N atoms has 3N normal vibration modes, including rotational and translational motions of the entire molecule. For highly symmetrical molecules with very few atoms, the entire infrared spectrum can be correlated to and explained by the vibrational modes, but even for low-molecular weight substances, N is too large for such analysis. Useful information can still be obtained because some vibration modes involve localized motions of small groups of atoms and give rise to absorption bands at frequencies characteristic of these groups and the type of motions they undergo. With regard to polymers, the infrared absorption spectrum is often surprisingly simple considering the large number of the atoms involved. This simplicity results from the fact that many of the normal vibrations have almost the same frequency and therefore appear in the spectrum as one absorption band.

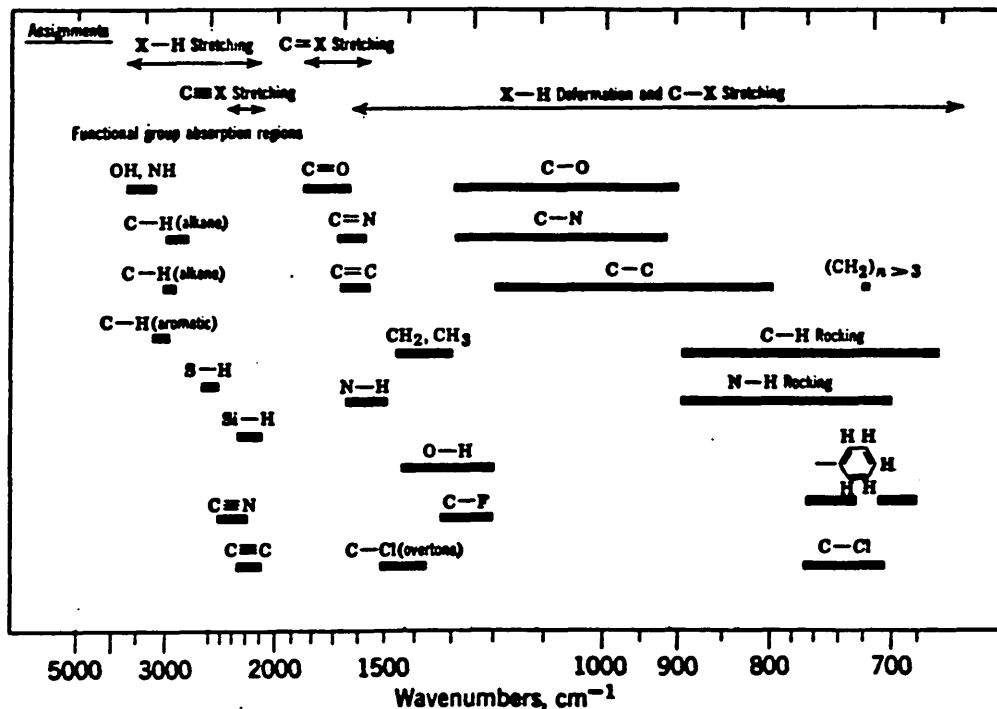
The approximate wavelengths of some infrared absorption bands arising from functional group and atomic vibrations found in polymers are shown in Fig. 3.12.

Infrared spectroscopy may be used to elucidate the structure of cellulose esters including [67]:

- (1) Identification of the type of cellulose esters;
- (2) Analysis of hydrogen bonding of free hydroxyl group;
- (3) Elucidation of the structural features of a product, depending on the conditions of esterification or hydrolysis;

- (4) Investigation of the extent of substitution of hydroxyl groups;
- (5) Studies on the kinetics of esterification or hydrolysis and
- (6) Establishment of the existence of ester bonds.

Fig 3.12 Infrared absorption bands by the functional groups of interest in polymers



### 3.4.2 Experimental

Solvent-free cellulose acetate dough was broken down into small pieces and was ground into a fine powder. This powder was then mixed with dried potassium bromide and was again ground to a very fine powder in order to make a KBr disc by the standard press and pressure method. A Perkin Elmer 783 IR Spectrophotometer, which is connected to a Perkin Elmer Infrared 3600 Data Station, was used.

The samples were scanned under the following conditions:

slit program	3
scan time	6 minutes
wave number	4000 to 200 cm <sup>-1</sup>
reference	air

### 3.4.3 Results and Discussion

Before discussing the effect of shear on the morphology of CA, it is essential to understand the origin of the absorption bands in the CA spectrum.

The infrared spectra of unprocessed CA and FCA are shown in Fig. 3.13, spectrum A and spectrum B respectively. The region 2000-4000  $\text{cm}^{-1}$  of the CA spectrum contains the main stretching vibration frequencies of the groups OH ( $3490 \text{ cm}^{-1}$ ),  $\text{CH}_2$  and CH ( $2950$  &  $2890 \text{ cm}^{-1}$ ). Although Tsuboi considered that absorption in the region 2800-3000  $\text{cm}^{-1}$  of the cellulose spectrum was due mainly to CH as the ratio of CH to  $\text{CH}_2$  group in the cellulose structure is 5:1, it is later proved that this region is due mainly to absorption by  $\text{CH}_2$ . This is confirmed by the marked reduction in intensity in the 2800-3000  $\text{cm}^{-1}$  region when the  $\text{CH}_2\text{OH}$  groups are oxidized by oxides of nitrogen [67]. The stretching vibration frequency of the C=O group in CA is at  $1750 \text{ cm}^{-1}$ , and this band is little affected by the chain length of the organic acid residue. This absorption band is used for following the kinetics of processes such as esterification. The symmetric deformation vibrations of the water molecule correspond to a band at  $1635 \text{ cm}^{-1}$ , and this band is convenient for checking the extent of drying of CA. The deformation vibrations of the  $\text{CH}_2$  group and the OH group of CA are at  $1430 \text{ cm}^{-1}$  and  $1370 \text{ cm}^{-1}$  respectively [68]. The origin of the absorption band at  $1370 \text{ cm}^{-1}$  is confirmed by the disappearance of the band when cellulose is treated with a solution of NaOD in  $\text{D}_2\text{O}$ . The 950-1250  $\text{cm}^{-1}$  region of the CA spectrum shows not less than two quite well-defined absorption bands at  $1235 \text{ cm}^{-1}$  and  $1030 \text{ cm}^{-1}$ . Differences in the spectra of cellulose ethers and esters are clearly distinguished in this region because the former shows a broad diffuse absorption band, without any well-defined structure. However, with increasing size of the organic acid residue in cellulose esters, such as cellulose acetate, propionate and butyrate, the resolution of the two main bands between 1000

and  $1250\text{ cm}^{-1}$  becomes less distinct. Interpretation of the absorption bands in this region by Thompson et al [67] revealed that the band in the  $1100\text{-}1250\text{ cm}^{-1}$  was due to vibration of the bond  $\text{-O}-\overset{\parallel}{\text{C}}\text{-}$ , and the band in the  $1000\text{-}1100\text{ cm}^{-1}$  region was due to alcoholic C-O.

The spectral region  $400\text{-}950\text{ cm}^{-1}$  of CA is difficult to interpret. CA shows a sharp spectral band at  $900\text{ cm}^{-1}$ , with an inflection at  $880\text{ cm}^{-1}$ , and a weaker band at  $840\text{ cm}^{-1}$ . It is possible that some of the bands in this region reflect structural features of the cellulose derivatives, caused by the introduction of new functional groups.

It seems probable that during the mixing process of CA, the dual action of shear and solvation may reduce the crystallinity of CA due to the destruction of hydrogen bonds between chain molecules, with the formation of some unassociated hydroxyl groups. For cellulosic substances, the group responsible for the hydrogen bonding is the OH group [69]. It has been observed that the acetylation and mercerization of cellulose result in a weakening of the degree of hydrogen bonding, and a shift in the OH stretching vibration band from  $3400\text{ cm}^{-1}$  to  $3480\text{ cm}^{-1}$  [67] and to  $3450\text{ cm}^{-1}$  [70] were recorded respectively. It should be noted that in the spectra of highly substituted cellulose esters [67] the relatively small variation in frequency of the hydroxyl group band with the nature of the esterifying groups gives grounds for supposing that the variation is mainly due to intramolecular hydrogen bonding as shown in Fig. 3.14.

By a similar reasoning, the change in frequency of the main maximum of the OH group band, in the  $3200\text{-}3600\text{ cm}^{-1}$  region, can be used to study the structural modification of CA because hydrogen bonding may affect the conformational and crystalline characteristics of CA. Thus, a change in the hydrogen bond structure may be an important criterion in the study of special features of CA. This is supported by the result as shown in Fig. 3.13. The infrared spectrum of CTA is very similar to the spectrum

of CA except in the absorption region  $3200-3600\text{ cm}^{-1}$ . Since all the hydroxyl groups in cellulose have been substituted by the acetyl groups in CTA, it should be expected that the degree of hydrogen bonding should be smaller, compared to the partial substituted CA. Indeed, the spectrum of CTA from Fig. 3.13 reveals a weak band with a shift of the OH stretching vibration band from  $3490\text{ cm}^{-1}$  to  $3450\text{ cm}^{-1}$ , and the shape of this band is more diffuse and broader than the well-defined peak of CA. This weak absorption band of CTA is due to the presence of a few unesterified hydroxyl groups in CTA.

The effect of shear on the structure of CA was investigated through the analysis of the hydroxyl absorption band in the region of  $3200-3600\text{ cm}^{-1}$ . Infrared spectra of unprocessed CA and one of the processed CA doughs are shown in Fig. 3.15. By comparison of the shape and the frequency of the main maximum of the OH group band of all processed CA, the shape and the position of OH group absorption bands ( $3480\text{ cm}^{-1}$ ) are very similar to that of the unprocessed CA, and in fact the deviation of this absorption band for all the samples is only about  $10\text{ cm}^{-1}$ , indicating that there is no significant change in the conformational characteristics of the CA after the mixing process.

Establishment of the presence of definite types of double bonds can be of great value in the analysis of the possibility of degradation of CA during the mixing process [60]. This idea is also supported by Chugaev [67] who found that cellulose methylxanthate undergoes thermal decomposition with the formation of C=C double bonds in the products. The  $1500-2000\text{ cm}^{-1}$  region contains the frequencies corresponding to the stretching vibrations of the double bonds (N=O, C=O, C=C). Analysis of all the spectra of processed CA in this region reveals that no appearance of new bands is observed. This indicates the absence of new double bonds, which would most likely arise from the degradation mechanism of cellulosic materials. This result is well corroborated by the

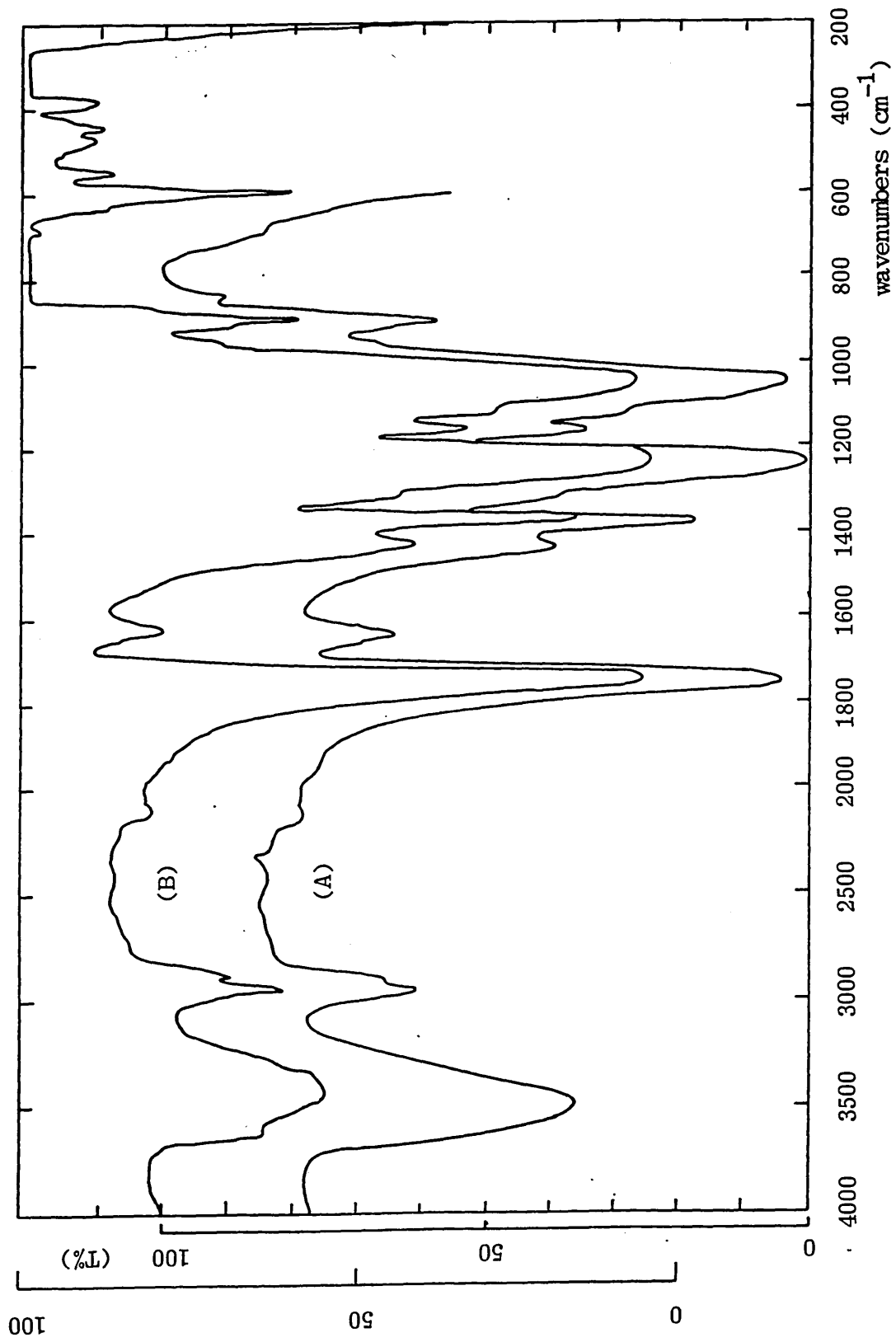
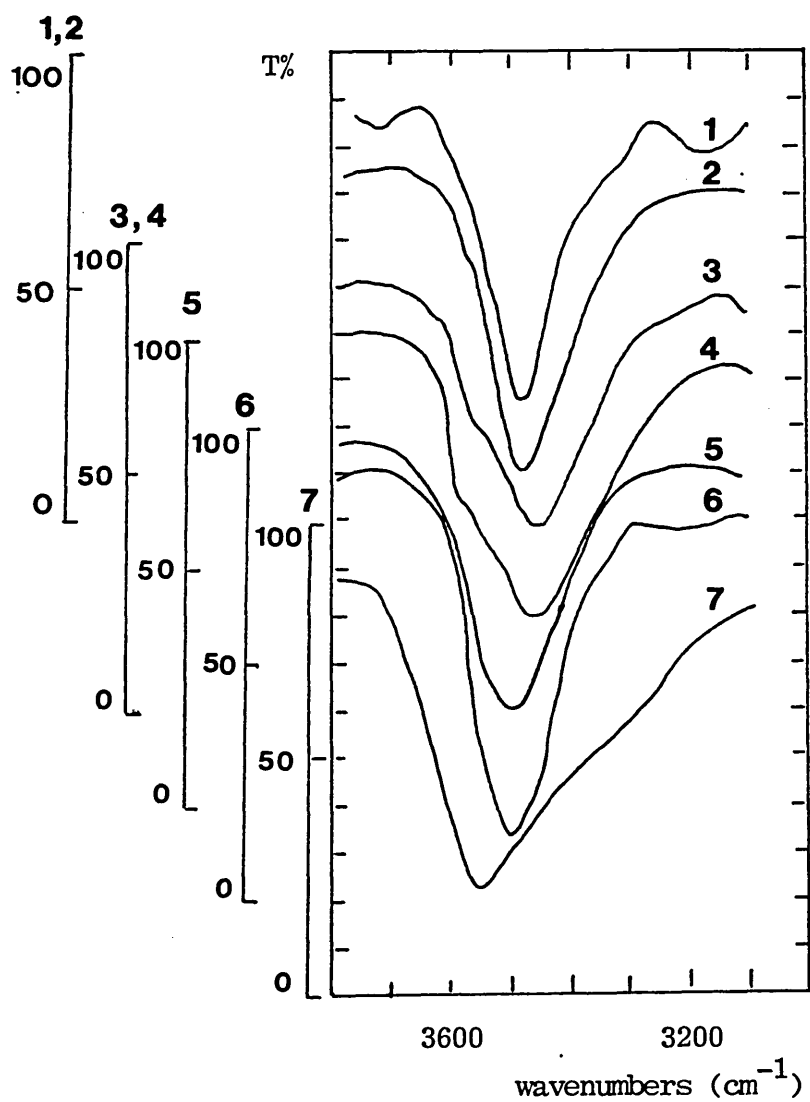


Fig. 3.13 Infrared spectra of unprocessed CA (A) and FCA (B)

result of solution viscosity of CA.

Fig.3.14 Spectra of highly substituted cellulose esters and ethers

- (1) Ethylcellulose
- (2) Nonylcellulose
- (3) Benzylcellulose
- (4) Tritylcellulose
- (5) Cellulose acetoacetate
- (6) cellulose 2-dimethyl propionate
- (7) Nitrocellulose



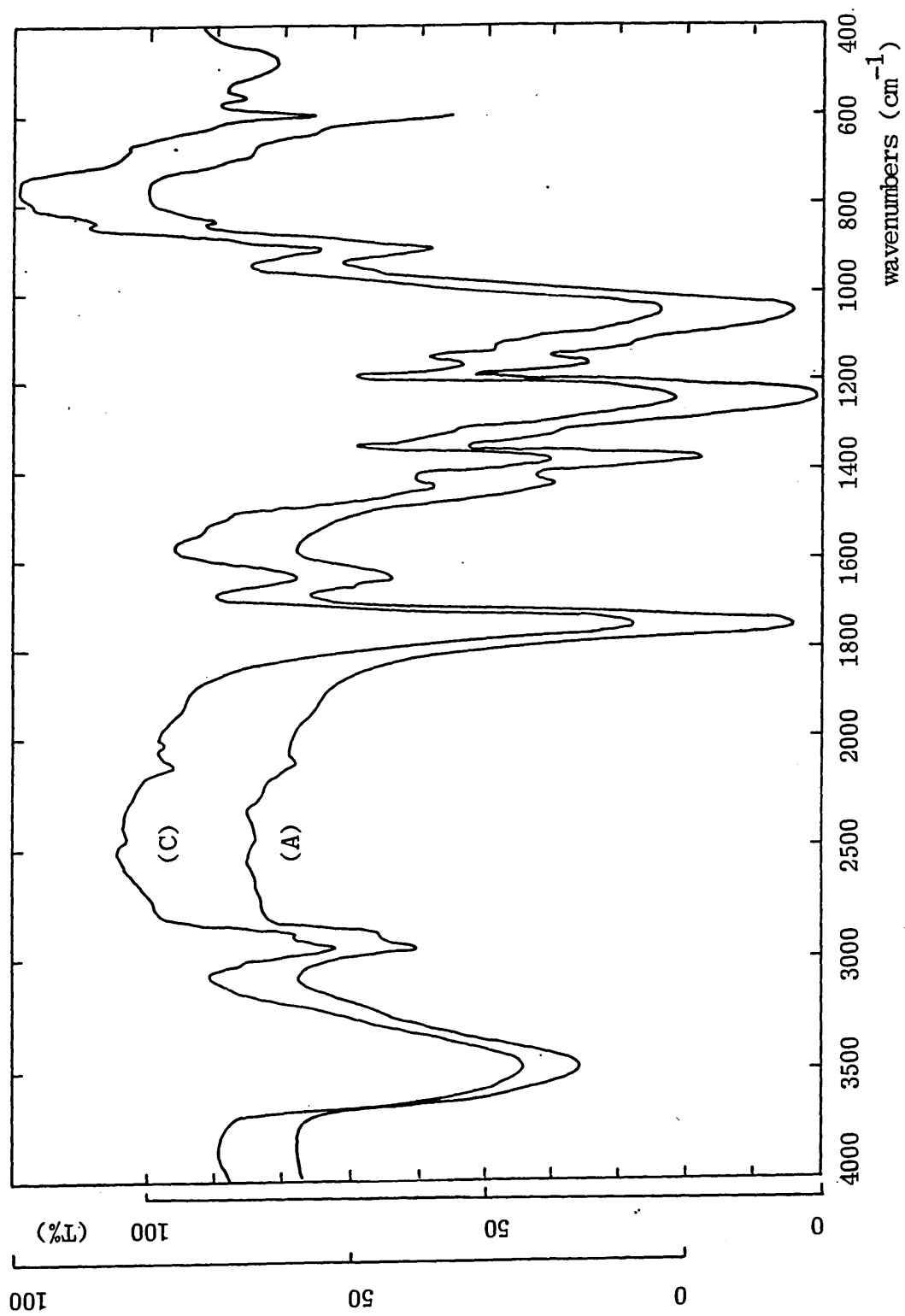


Fig. 3.15 Infrared spectra of unprocessed CA (A) and processed CA (C)

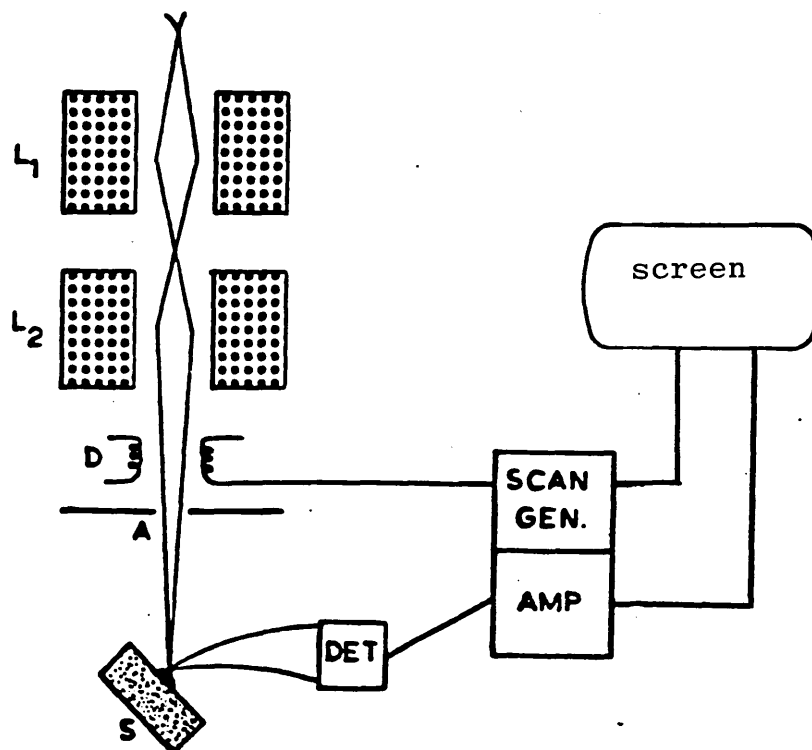
### 3.5 Electron microscopic studies of cellulose acetate doughs

#### 3.5.1 Theory

The transmission electron microscope (TEM) and the scanning electron microscope (SEM) have been traditionally used as investigatory tools to study the surface topology of a sample [71-73]. However, SEM is selected for use in this project because specimen preparation limits the application of the TEM to the present studies. Most problems arise from the removal of the carbon replica film from the surface of the specimen in a single-stage replica technique. When the specimen is gradually dissolved by the solvent, tension is set up in different parts of the carbon replica film as a result of the great variation in specimen surface smoothness, and hence the delicate replica film tends to break away due to the different intrinsic surface tension.

The scanning electron microscopy is used primarily for the examination of thick (i.e. electron-opaque) samples by employing a beam of electrons directed at the specimen. A schematic diagram illustrating the operation of an SEM is shown in Fig. 3.16.

Fig.3.16 Schematic diagram for the operation of SEM



The electron beam is focussed on the specimen (S) by the condenser lens (L1 & L2) and scanned across the specimen by the deflector coils (D). An electron detector counts the number of secondary electrons given off at each point on the surface and converts them into a current. This current is then amplified and used to control the brightness of the cathode-ray tube. The contrast arises from the change in the surface topology of the sample provided that only secondary electrons are collected. Because the parts of the specimen which have the most direct path to the detector appear brightest, the image of a rough specimen appears as if it is viewed from above, when being illuminated from the detector. The fact that the low energy secondary electrons are bent into the detector from regions which do not have a direct line of sight into the detector allows details within holes and shaded regions to be observed. However, it does not offer any information about the chemical constitution of the materials being investigated.

### 3.5.2 Experimental

The surface morphological structure of CA dough was studied by scanning electron microscope (Phillips Instrument Co.). The CA doughs were coated with a very thin layer of metal (about 10 nm). Such a thin layer did not alter the surface detail in the actual sample, but it was thick enough to conduct away the excess charge. The coating unit was an Em-scope Sputter.

### 3.5.3 Results and Discussion

Examination of the surface of CA doughs by electron microscopy reveals that no fibre morphology such as finer fibrils and microfibrils is observed as shown by some workers [74,75], but all the micrographs of CA doughs have a similar appearance to that of a typical microstructure of a fracture surface [76].

In general, three common features are observed on the surface of CA doughs that are processed in the torque rheometer. They are:

- (a) irregularities in shapes;
- (b) different orientations of shear bands within the sample and
- (c) the occurrence of rough and smooth surfaces.

The efficiency of gelatinisation of CA doughs can be identified from the scanning electron micrograph. This is illustrated by Fig. 3.17 in which the undispersed CA is surrounded by the solvated CA gel. This figure shows that the area inside the circle is more rough and porous than the area outside the circle. This is again supported by the porous surface as shown in Fig 3.18 in which the aggregate of CA is highly magnified. Therefore, this leads to the conclusion that poorly gelatinised dough has a rough and porous surface while well gelatinised dough has a smooth and continual surface.

The effect of solvent concentration on the surface morphology of CA doughs is shown in Figs 3.19 to 3.22. These micrographs reveal that solvent concentration plays an important role in the efficiency of gelatinisation of the CA doughs because the micrographs change from an undulating to a smooth appearance as a function of solvent concentration. Again, this is confirmed by highly magnified micrographs (Figs 3.23-3.25) of CA doughs containing 30, 50 and 60 pph solvent concentrations in which the change in surface topology follows the aforementioned observation. The effect of mixing time on the surface morphology of CA doughs is not as sensitive as that of solvent concentration. Nevertheless, there is a general trend for formation of a well gelatinised dough with increasing mixing time.

The micrographs of CA doughs in terms of bulk properties have given a significant insight into the mechanical properties and performance of the product. When the product fails by fracture, the crack normally starts at weak boundary layers. In the case of poorly gelatinised CA doughs, there are stress concentrations created around the internal voids which subsequently act as weak boundary layers, and hence give rise to poor mechanical properties. The number of voids for the well gelatinised doughs is

small, and therefore no or fewer stress concentrations are created on the application of stress. This argument is further supported by Baker [47] in which he reported that the ultimate tensile strength of dried propellant cord increases as a function of solvent concentration as shown in Fig. 1.23 (Chapter 1).

Fig. 3.17 Micrograph of CA showing aggregate of undispersed CA in the central region

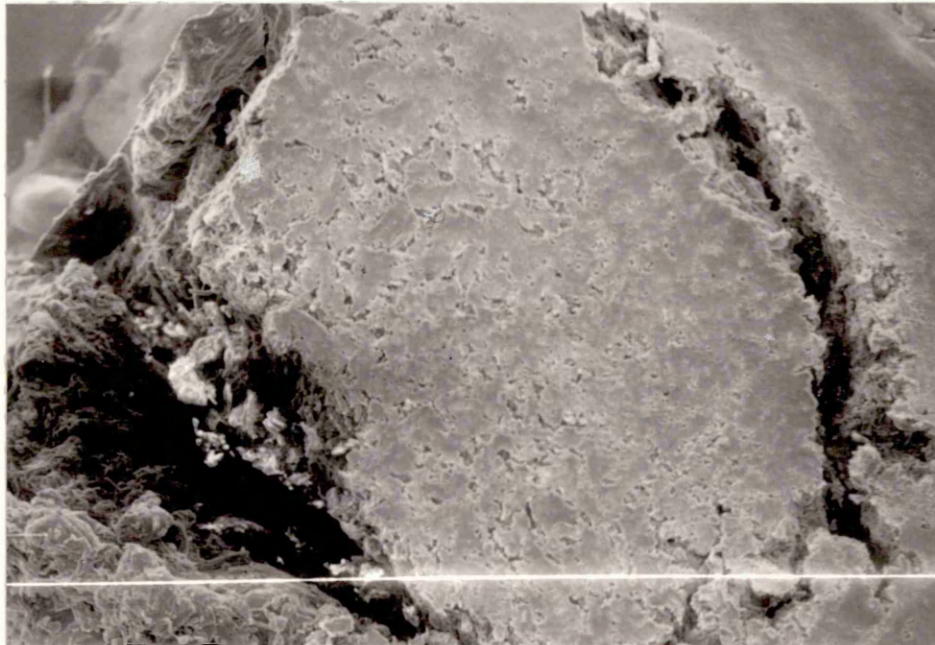


Fig. 3.18 Micrograph of CA with high magnification (400x)  
of the central region

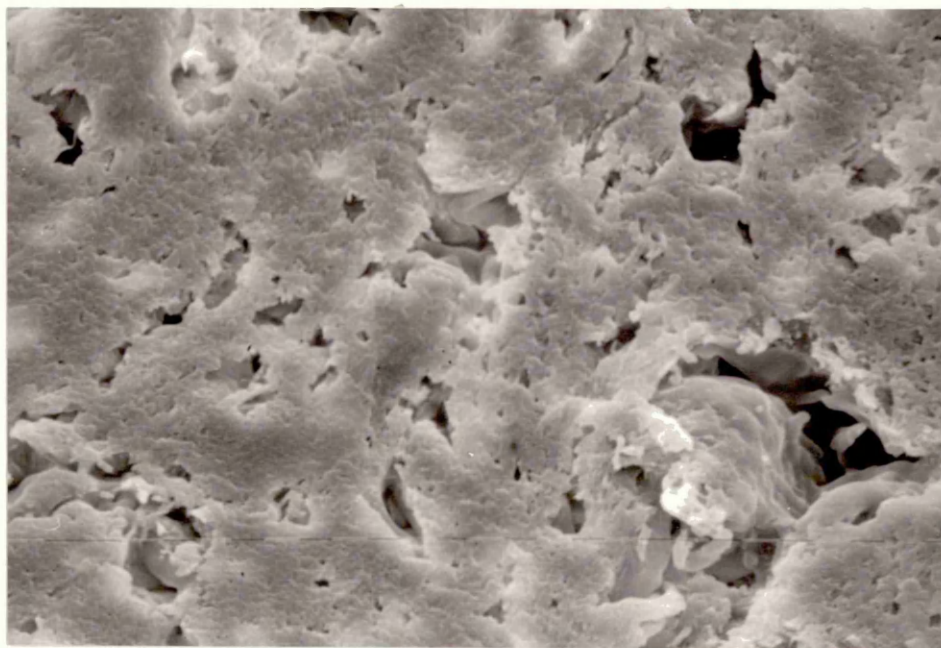


Fig. 3.19 Micrograph of CA with 10% acetone (50x)



Fig. 3.20 Micrograph of CA with 30% acetone (100x)



Fig. 3.21 Micrograph of CA with 50% acetone (100x)



Fig. 3.22 Micrograph of CA with 60% acetone (100x)

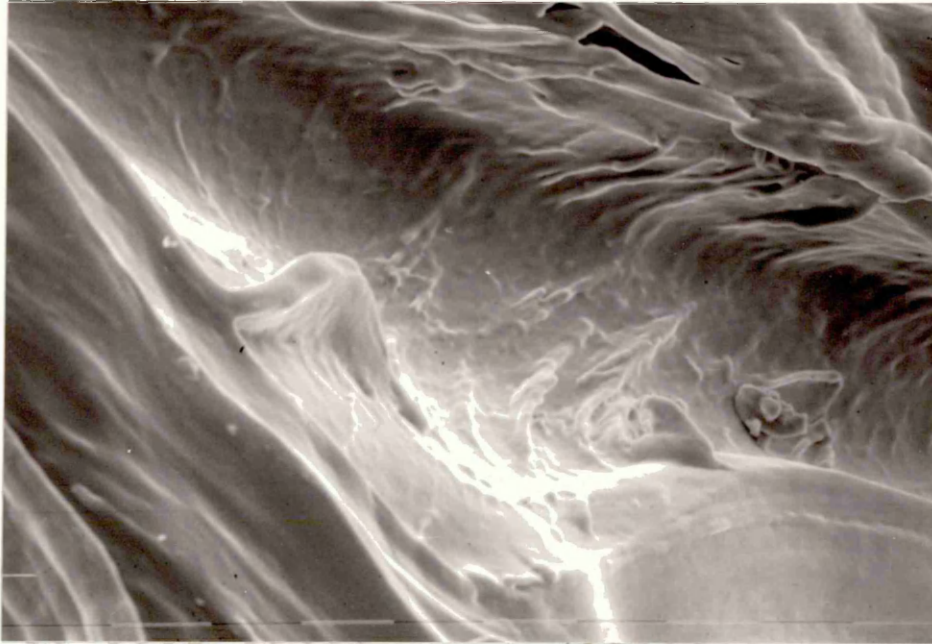


Fig. 3.23 Micrograph of CA with 30% acetone showing a porous appearance (400x)



Fig. 3.24 Micrograph of CA with 50% solvent showing a smooth appearance (400x)

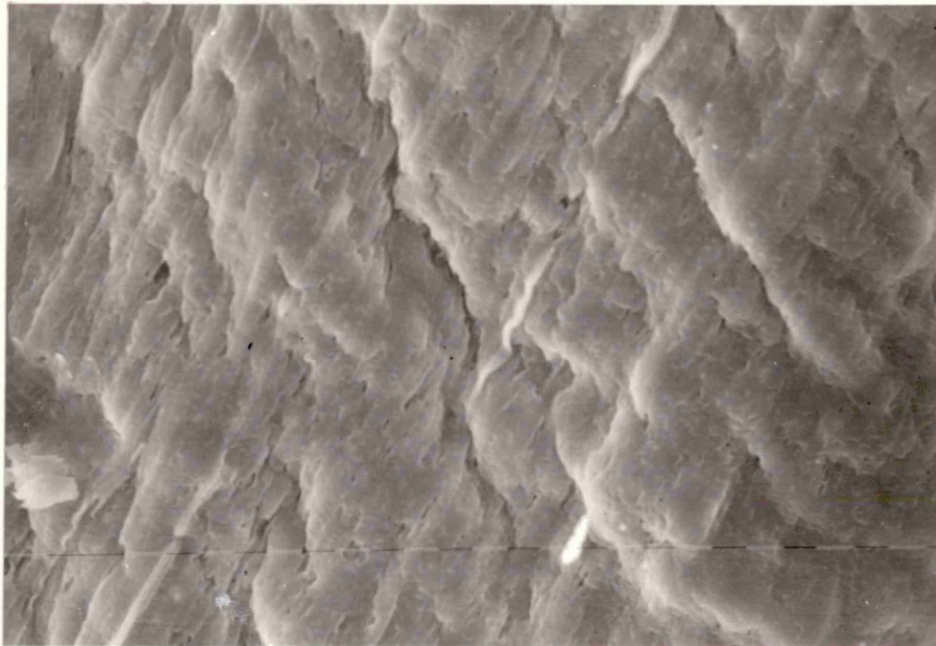
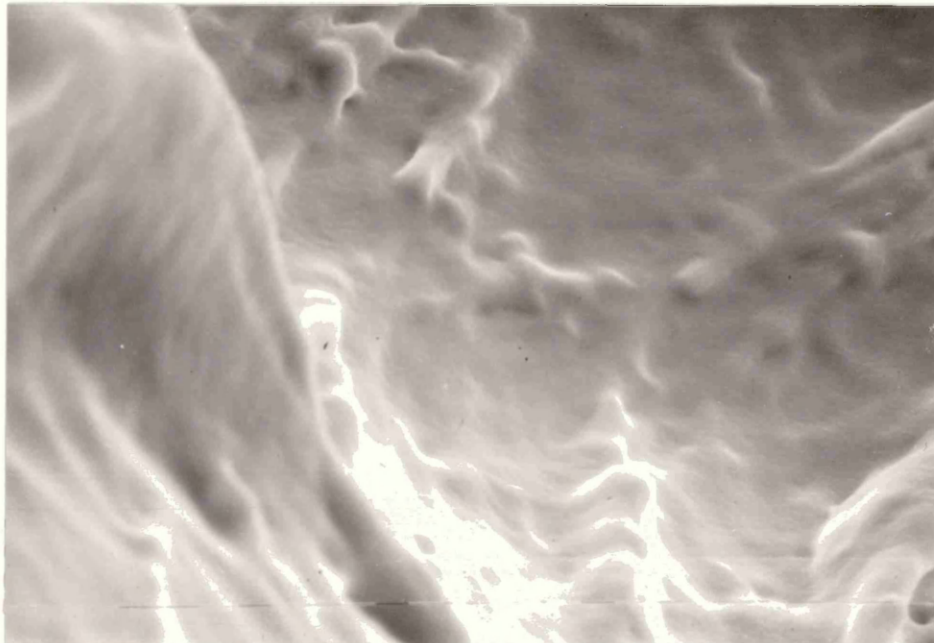


Fig. 3.25 Micrograph of CA with 60% solvent showing a smooth appearance (400x)



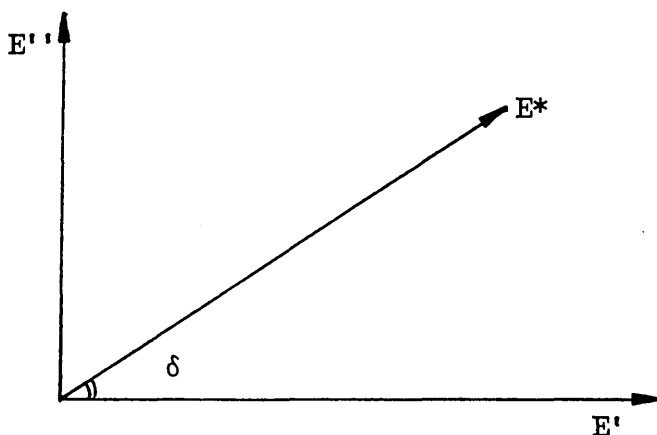
### 3.6 Dynamic mechanical analysis of cellulose acetate

#### 3.6.1 Theory

The stress response of polymers is greatly affected by additives such as plasticisers and fillers etc., and perhaps to some extent by the processing method. It is of importance both technologically and academically to understand how such factors bring about the observed changes in the mechanical properties of these materials. Dynamic mechanical analysis (DMA) is a particularly direct way of sensing all motional transitions, and hence all molecular relaxation processes in polymers, as a result of an applied mechanical stress over a wide temperature range and over a large time-scale [77-80].

In the dynamic mechanical technique, a small sinusoidal mechanical stress is applied to the sample and the resulting sinusoidal strain is detected. For a perfectly elastic solid the strain occurs exactly in phase with the stress. Comparison of the amplitude of the signals yields the complex dynamic young's modulus  $E^*$  in the bending mode. Owing to the intrinsic viscoelastic nature of polymers, the strain response lags behind the stress. The phase lag ( $\delta$ ) of strain behind stress allows the complex modulus to be resolved into two parts, the storage ( $E'$ ) and loss ( $E''$ ) moduli. A more useful parameter is the dimensionless ratio,  $\tan \delta = E''/E'$ , often referred to as the damping factor or mechanical loss tangent. The vector relationship between storage and loss moduli is shown in Fig. 3.26.

Fig 3.26 Relationship between storage ( $E'$ ) and loss ( $E''$ ) moduli in the Argand diagram.



In the case of CA the effects of mechanical stress produced by mixing or extrusion can be highly significant in determining the performance of the product, and the analysis of such stress is vital if the material is to be relied upon under various operational conditions [81].

A number of papers have been devoted to understand the origin of the molecular groups responsible for the viscoelastic relaxations of cellulose derivatives [81-84]. Recently, dynamic mechanical and dielectric studies on cellulose acylates has been carried out by Morooka et al [85] who reported more than one relaxation process below room temperature, and hence investigation of the second-order transitions becomes as significant as the first-order transitions in order to understand all the molecular motions resulting from the applied stress. This is of great important in the present study because all the extrusion processes have been carried out at low temperatures.

### 3.6.2 Experimental

The dynamic mechanical measurements were carried out by means of a dynamic mechanical thermal analyser (DMTA, Polymer Laboratories), using the dual cantilever geometry. In normal operation a sample in the form of an extruded cord with a dimension of 2\*20 mm was clamped rigidly at both ends, and its central point vibrated sinusoidally by the drive clamp inside the mechanical head, as shown in Fig. 3.27. Two types of drive clamp, namely bar sample and spreader clamps, were used in the studies of molecular relaxation process as in the low and high temperature regions respectively, as shown in Fig 3.28. A wide range of temperatures (-120°C to 200°C) and frequencies (0.33, 3.0 30 Hz) were selected at a heating rate of 1-3 °C /minute. The results were obtained in graphical form on the screen of a CBM 3032 microcomputer. The dynamic mechanical spectrum is presented as plots of the log E' and tan  $\delta$  as a function of temperature. This work is carried out at Royal Ordnance Explosives Divison, Waltham Abbey.

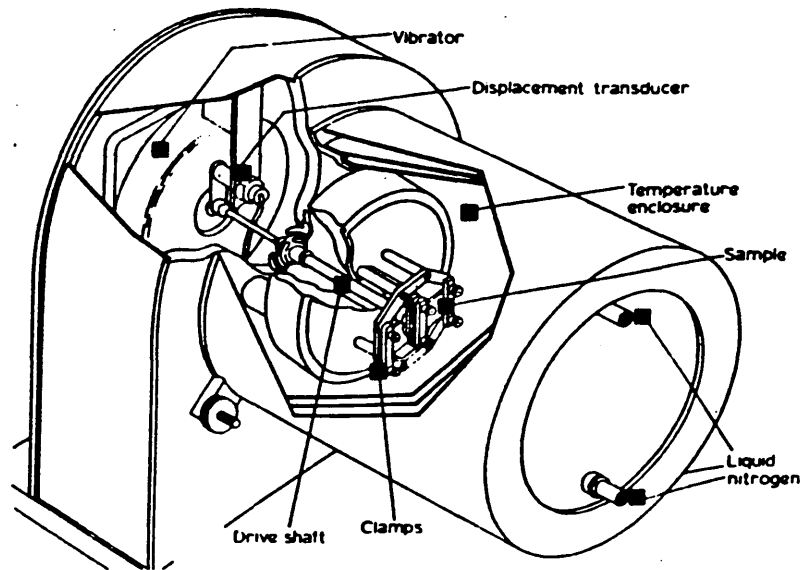


Fig. 3.27 Mechanical head of the dynamic mechanical thermal analyser ( After Wetton et al )

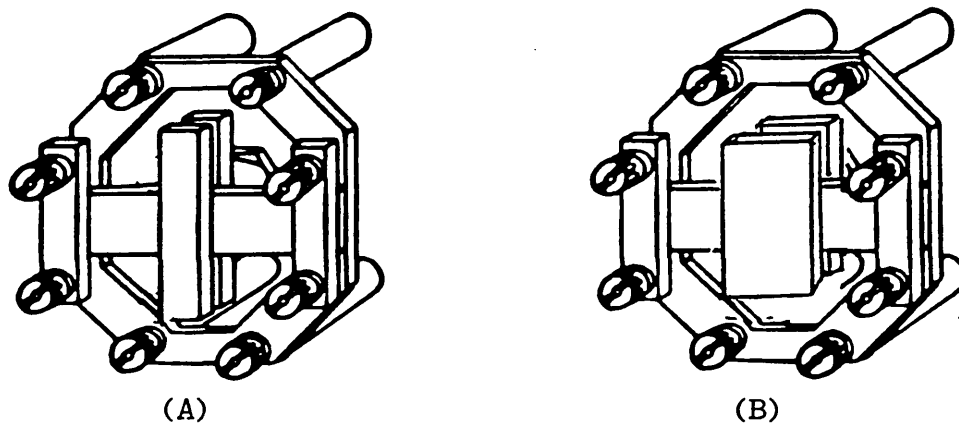


Fig. 3.28 Dual cantilever clamps showing the bar sample (A) and the spreader (B) clamps

### 3.6.3 Results and Discussion

The dynamic mechanical behaviour of CA as shown in Fig. 3.29 is surprisingly simple, with a single  $\alpha$  transition at about 189 °C, and no other pronounced low temperature relaxations are observed. Increasing the sample length by replacement of the 'spreader' clamp with a 'bar' clamp enhances the magnitude of all the relaxation transitions, as shown in Fig. 3.30. This figure shows that two transitions and one shoulder centred at about 100 °C are observed in the low temperature range, the absorption regions being named  $\beta^*$  (shoulder),  $\beta$  and  $\gamma$  in order of decreasing temperature. However, the mechanical loss tangent increases rapidly at high temperatures without giving a well-defined  $\alpha$  peak. As a result, the present discussion consists of two parts involving the higher and lower temperature relaxations.

The main  $\alpha$  relaxation in Fig. 3.29, which occurs in the same temperature range as the calorimetric glass transition (Fig 3.6), shows a very intense absorption maximum associated with a very steep modulus drop. The partially overlapping  $\beta$  and  $\gamma$  peaks are secondary relaxations of moderate intensity, associated with a fairly small decrease of the storage modulus. It is interesting to compare the dynamic mechanical loss behaviour in the  $\beta^*$  shoulder region to the DSC curves reported in Fig. 3.4. In the temperature range of interest, the first DSC scan is characterized by a broad endotherm and this phenomenon is absent from the second thermal scan. This may suggest that the dynamic mechanical  $\beta^*$  shoulder and the related calorimetric phenomenon are due to the presence of absorbed moisture, and specifically to evaporation of water from samples. Such a conclusion is also supported by Scandola et al [86-88] who reported a scan to 130 °C is sufficient to suppress the  $\beta^*$  shoulder from the dynamic mechanical spectrum. Owing to the complex molecular structure of CA and the unavoidable inhomogeneities in ester substitution, the identification of the molecular groups responsible for the low-temperature relaxations of CA is made particularly difficult. As

far as the present  $\beta$  relaxation is concerned, there has been much debate over the origin of this relaxation. Bradley [89] and Kimura [90] had suggested that the origin of the relaxation was attributed to motion of the water molecules between hydrogen bonding sites and motion of the hydroxyl or methylol groups. However, Seymour et al [91] reported that the  $\beta$  peak also occurred in CTA. This material contains no unesterified OH, and the assignment to OH-related motion must therefore be rejected. He suggested the present  $\beta$  relaxation was assigned to motion of the glucopyranose rings in the polymer backbone. This explains why CA at ambient temperature is certainly not in a glassy state and in fact possesses some inherent flexibility. Such a conclusion is also supported by Doyle [75] and Fong [81]. The influence of water on the secondary relaxations of CA has been investigated by Scandola who shows that the  $\beta$  relaxation is unaffected by water concentration, which does not agree with Bradley and Kimura [89,90]. A contribution from the motion of side groups to the  $\beta$  relaxation cannot be excluded since the motion may involve rather complex relaxing units. The  $\gamma$  absorption is identified as a water-dependent relaxation process whose molecular origin is attributed to motions of water associated with CA through interactions with polar groups. It is believed that at low hydration degrees the relaxing units involve water molecules bound to the unesterified hydroxyls of CA, so that the relaxation is mainly originated by motion of the methylol-water complex units. Increasing amounts of water will interact with the remaining polar parts of the macromolecule as well as with water molecules already bound to the polymer, as suggested by Crofton and Pethrick [92].

The effect of different plasticisers, dimethyl phthalate (DMP), diethyl phthalate (DEP) and dibutyl phthalate (DBP) on the relaxation behaviour of CA is studied. Figures 3.31 and 3.32 show the high temperature relaxation in CA cords containing increasing

quantities of DMP and DBP respectively. The relaxation is well defined, the storage modulus being constant up to the transition region and then falling by over three orders of magnitude from about  $10^8$  to about  $10^5 \text{ Nm}^{-2}$  over the temperature span of the relaxation. A summary of the  $\alpha$  transition is given in Table 3.5. As would be expected the addition of plasticisers to CA shifts the transition and corresponding modulus drop to lower temperature. Generally, the incremental plasticisation effect on CA as measured by the quantity of  $\Delta T_g/T_g$  decreases as the plasticiser level is increased as shown in Fig. 3.33. These results show that the magnitude of relative change in  $T_g$  of plasticised CA is substantially higher with DMP than with DBP. This difference in the effect of plasticisation suggests that CA does not interact with DMP in the same way as it does with DBP. This is clearly illustrated in Figs. 3.34 & 3.35, which show that the  $\alpha$  peak of CA containing the same concentration of plasticiser decreases in the order of DBP, DMP and DEP. The efficiency of plasticisation is therefore dependent on the nature of plasticiser and its concentration.

The effect of plasticiser on sub- $T_g$  relaxations is also studied. The nature of the interaction between DBP and CA is shown by the changes of the dynamic mechanical curve on the sub- $T_g$  relaxations. These changes are the depression of both the  $\beta$  and  $\beta^*$  shoulder relaxation, and the appearance of a new relaxation, designated as the  $\beta'$  peak. The low-temperature  $\gamma$  relaxation becomes less pronounced with increasing extent of plasticisation. These changes are shown in Fig. 3.36 and Fig. 3.37. In the previous discussion, the  $\gamma$  relaxation and  $\beta^*$  shoulder relaxation were tentatively attributed to motions involving water associated with the unesterified methylol groups of CA cord and the evaporation of water from the sample respectively. During the sample preparation (dried at  $90^\circ\text{C}$  under vacuum for 6 days), it may be assumed that no moisture is present, so that no interaction may occur between water and CA. The plasticiser, on

the other hand, can interact with the polymer and give rise to hydrogen-bond formation between the hydroxyls of CA and the polar ester groups of DBP. When the temperature is lowered, water absorbed from the environment is able to interact only with the remaining 'free' hydroxyls. This results in the hinderance of the motion that causes the  $\gamma$  relaxation and the  $\beta^*$  shoulder relaxation, as shown in Fig. 3.36 and 3.37 respectively.

As far as the  $\beta$  relaxation is concerned, the addition of DBP gives rise to a new  $\beta'$  process occurring at a higher temperature. Originally, the  $\beta$  relaxation of CA was tentatively attributed to local motions of the sugar rings. DBP and CA interact in such a way as to produce new modes of relaxing units, probably due to the interaction of DBP to the glucopyranose ring through the acetate groups. This may lead to an increase in size of the motional units responsible for the  $\beta$  relaxation, as supported by Seymour [91] and Scandola [86-88]. Generally, plasticisers that raise the value of a physical property such as relaxation temperature have been termed antiplasticisers [93-95]. The results from Figs 3.36 and 3.32 suggest, however, that antiplasticisation or plasticisation is merely a matter of the temperature at which the test is made. As far as  $\beta$  relaxation is concerned (Fig.3.36), DBP would be considered as an antiplasticiser for CA while at  $\alpha$  relaxation (Fig. 3.32) it would be considered as a plasticiser. A plot of the  $\beta'$  relaxation temperature as a function of DBP concentration is shown in Fig. 3.38. This figure shows that the peak temperature of  $\beta'$  process increases as a function of DBP content up to about 10 %, and thereafter an inversion occurs with higher DBP content. This may due to the compatibility limit of the CA/DBP. The amount of DBP above that which is compatible forms a separate plasticiser-rich phase giving rise to another motional loss mechanism, as visually apparent from the opacity of the CA cord. The plasticiser-rich phase may possibly have a great influence on the  $\beta'$  relaxation.

The effect of fibrous CA and mixing variables such as time and solvent concentration on the  $\beta$  relaxation of CA are also studied. Table 3.6 shows that the  $\beta$  peak shifts to slightly lower temperatures as the fibre content increases. The  $\beta$  peak of the cord remains fairly constant with respect to the mixing time, but it increases gradually with increasing solvent content as shown in Table 3.7. Owing to the complex motional mechanism of the  $\beta$  peak and the mixing process, identification of the molecular groups responsible for the difference in  $\beta$  peak of processed CA is made particularly difficult. Further work is required to determine the cause of the differences observed in  $\beta$  peak as a consequence of processing conditions.

Table 3.5 Effect of plasticisers and concentration on the  $\alpha$  relaxation of CA

Nature of plasticiser	concentration / pph	$\alpha$ -peak / °C
DMP	5	174.3
	8	165.7
	10	161.4
	20	153.9
DBP	5	175.3
	8	172.1
	10	169.4
	20	164.6
DEP	10	159.6
Control	0	189.2

Table 3.6 Effect of fibrous CA on the  $\beta$  relaxation of CA

Fibre content / %	mixing conditions	$\beta$ -peak / °C
0	Time = 20 min	-27.6
1	Sol. = 80 pph	-26.8
5	Temp. = 20 °C	-31.9
15		-32.7

Table 3.7 Effect of mixing variables on the  $\beta$  relaxation of CA

Mixing Variables	Mixing Condition	$\beta$ -peak / °C
T 1 min	Sol. = 80 pph	-27.6
I 5 min	Temp. = 20 °C	-22.3
M 20 min		-27.6
E 60 min		-24.1
S		
O 60 pph	Time = 20 min	-41.6
L 70 pph	Temp. = 20 °C	-34.4
V 80 pph		-27.6
E 90 pph		-25.1
N		
T		

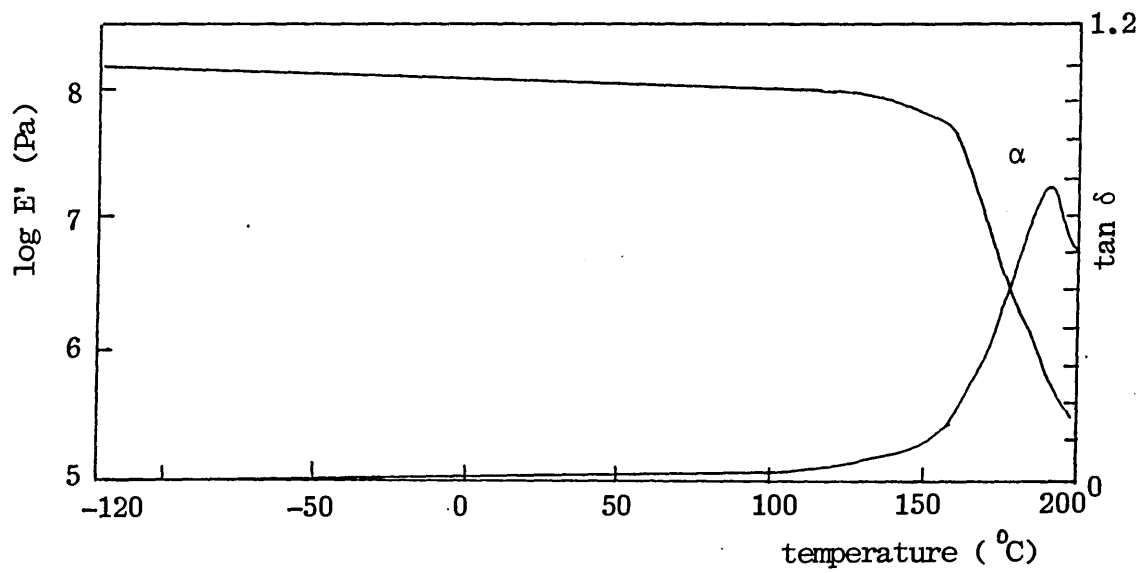


Fig. 3.29 Dynamic mechanical relaxation of CA using a spreader clamp

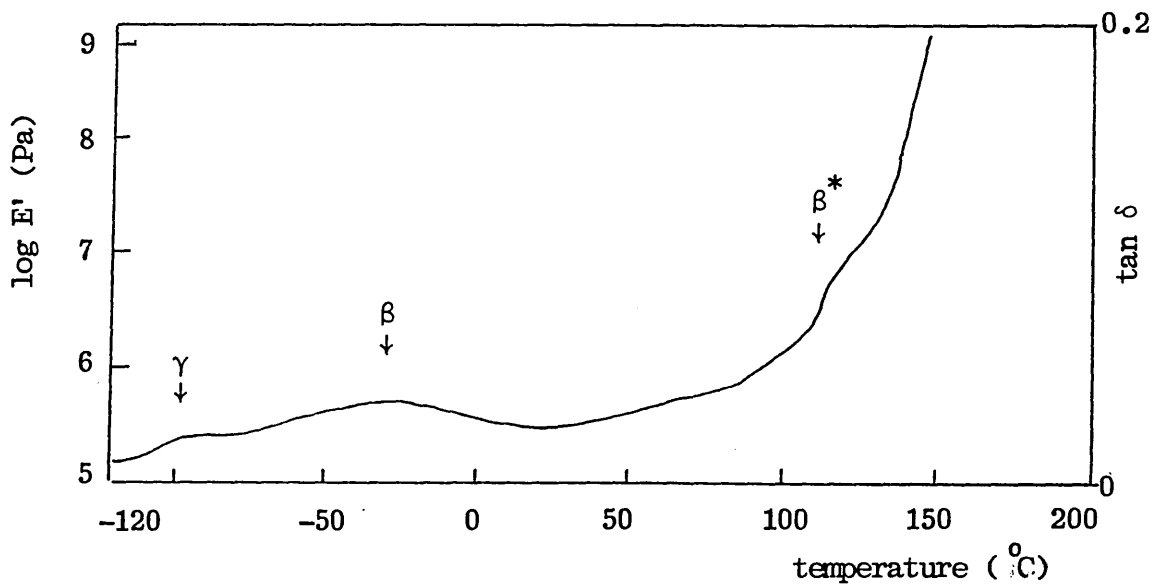


Fig. 3.30 Dynamic mechanical relaxation of CA using a bar sample clamp

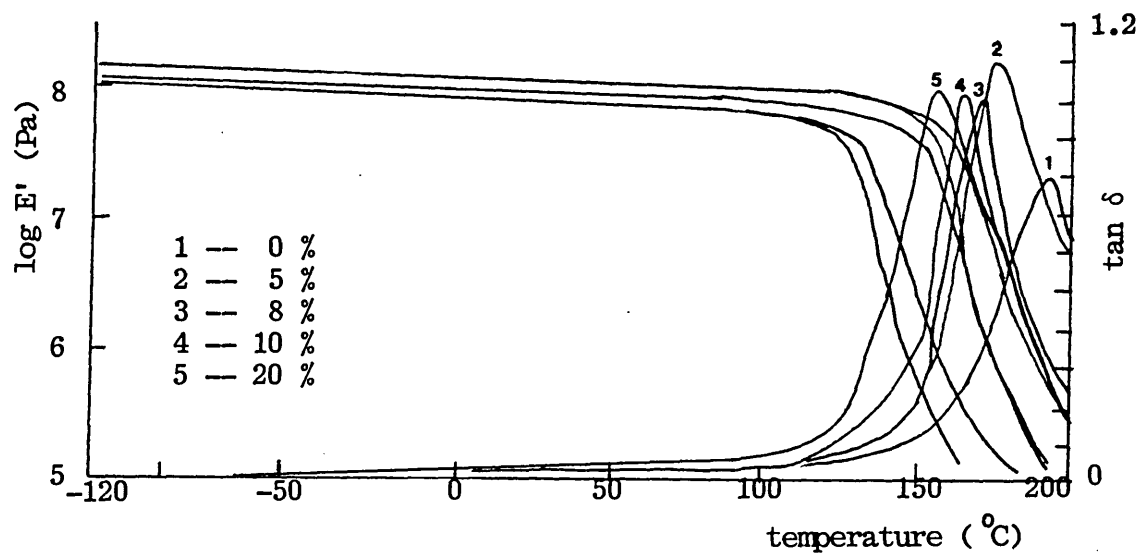


Fig. 3.31 Mechanical relaxation of plasticised CA/DMP as a function of DMP content

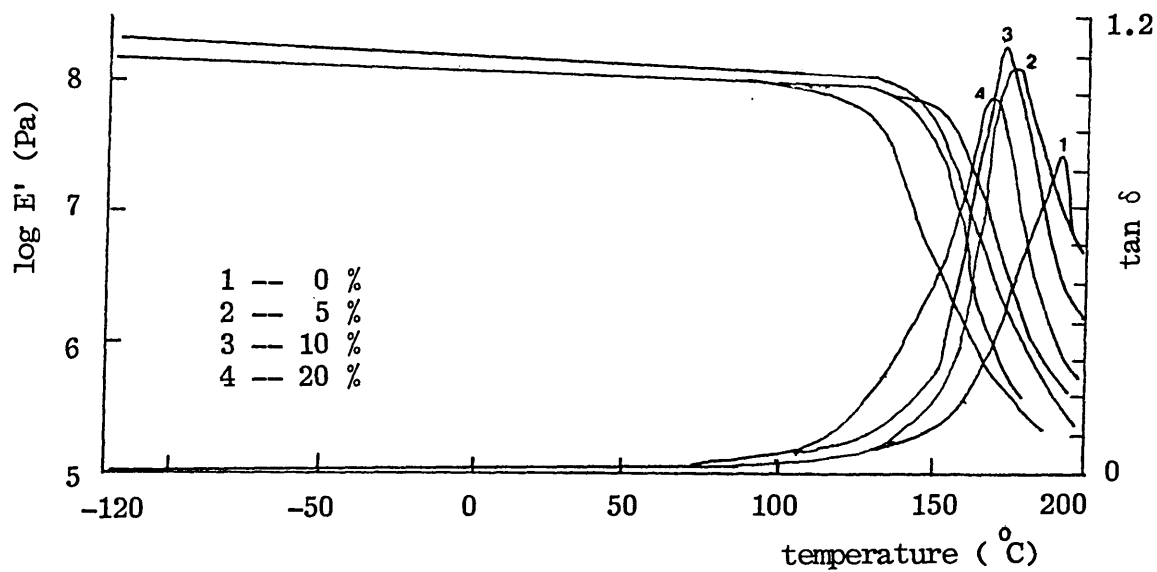


Fig. 3.32 Mechanical relaxation of plasticised CA/DBP as a function of DBP content

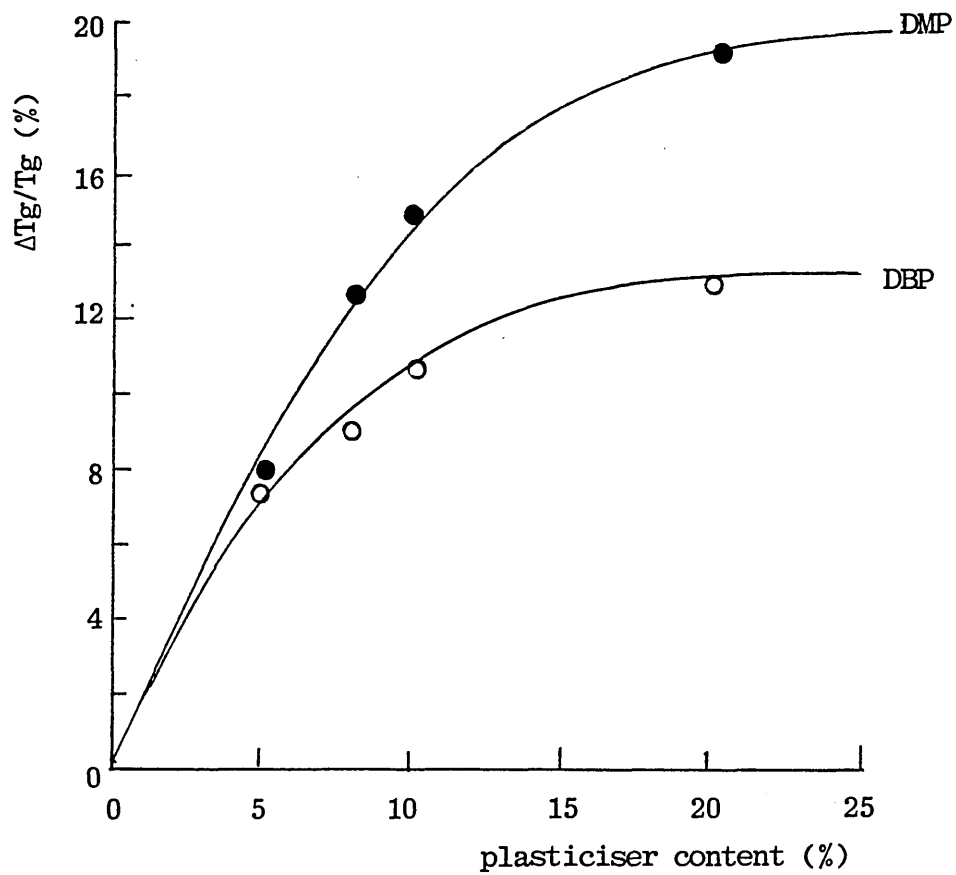


Fig. 3.33 Relative change in Tg caused by plasticisation with DMP and DBP

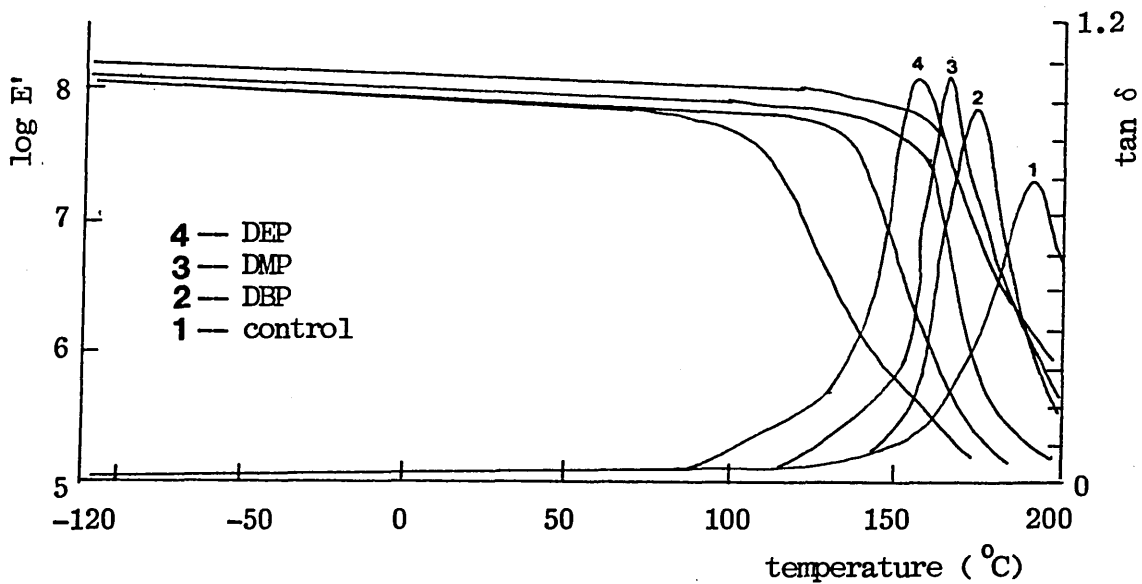


Fig. 3.34 Mechanical relaxation of CA with different type of plasticisers

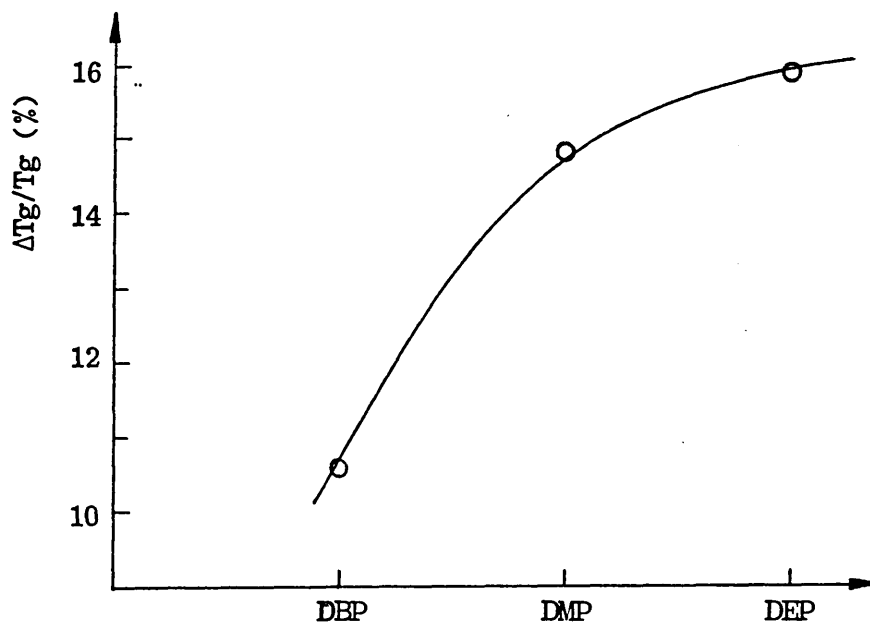


Fig. 3.35 Relative change in Tg of CA with different type of plasticisers

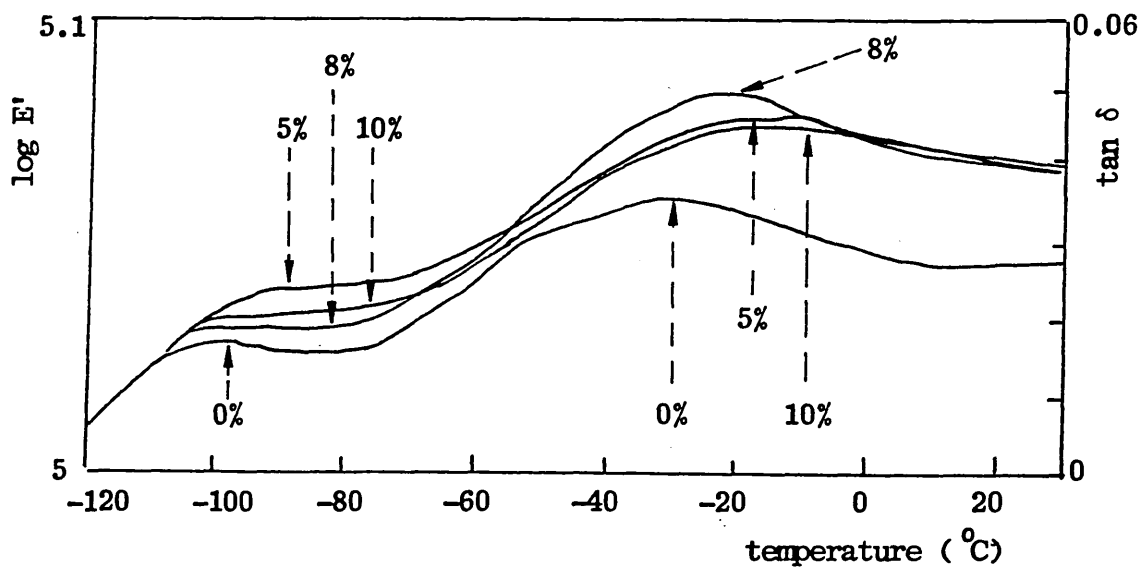


Fig. 3.36 Mechanical relaxation of plasticised CA/DEP at low temperature range

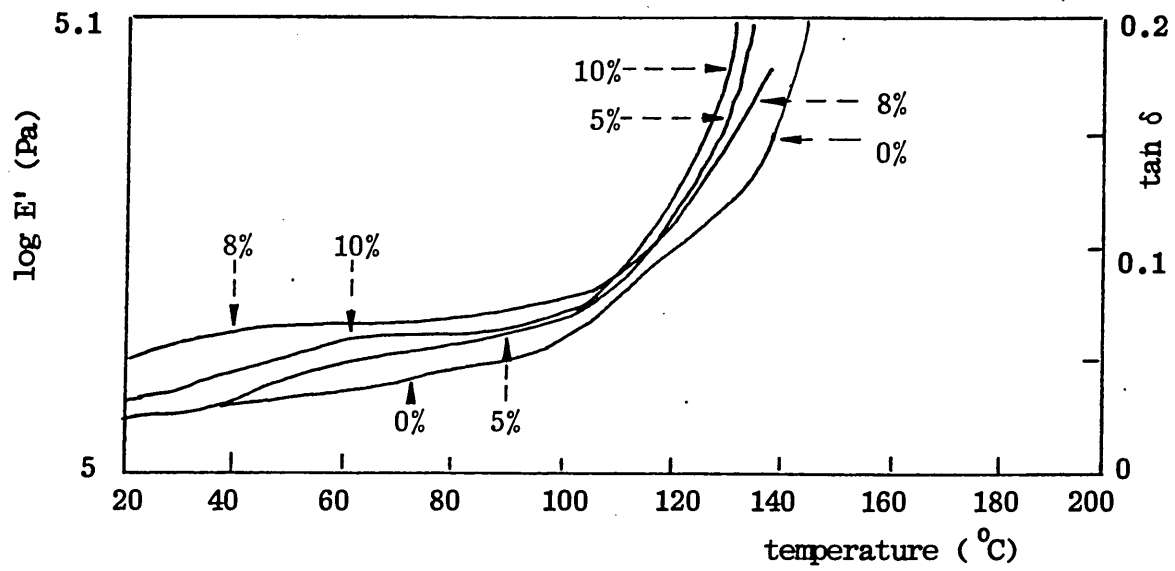


Fig. 3.37 Mechanical relaxation of plasticised CA/DBP showing the shoulder region

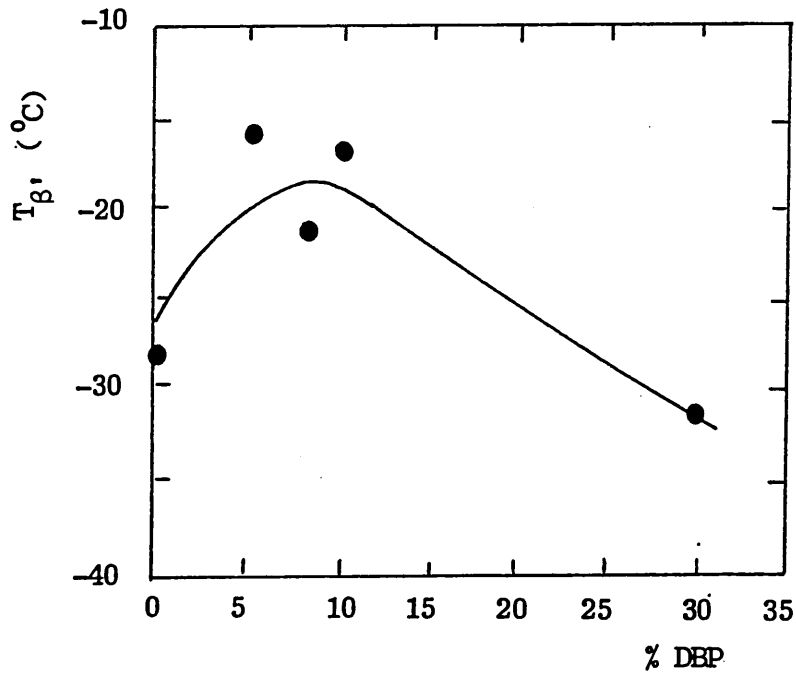


Fig 3.38 Effect of the concentration of DEP on the  $\beta'$  relaxation temperature of cellulose acetate dough

### 3.7 X-ray diffraction studies of cellulose acetate

#### 3.7.1 Theory

X-ray diffraction is a powerful technique to elucidate the chemical structure in the solid state. From the analysis of the lattice spacings and the diffraction intensities for a crystalline solid, the molecular structure of the crystal can usually be constructed as followings:

- (a) size of the unit cell and its shape,
- (b) positions of atoms in unit cell and
- (c) size of diffracting unit.

The technique has been widely applied in polymer science [96], and much of our knowledge of polymer structure comes from diffraction studies. It is unfortunately the case that polymer single crystals of a size sufficient for x-ray studies are impossible to obtain due to the difficulty with which polymers crystallise. As a result of the molecular constraints imposed upon them polymers which do crystallise to any degree give rise to a particular type of diffraction pattern which shows the polymer matrix to be a more or less imperfectly oriented arrangement of polymer chains. The typical x-ray diffraction patterns of an amorphous polymer, an unoriented polymer, and an oriented polymer are shown in Fig. 3.39. An amorphous polymer will simply scatter x-rays in all directions (Fig. 3.39a). A crystalline material will diffract x-rays at specific angles. The main differences between polymer x-ray photographs and those derived from single-crystal is the diffuseness and arclike character of the reflection often derived from polymers. The diffuseness and arclike character of the reflections in polymer x-ray photographs is partly a consequence of nonideal orientation of the crystallites (Fig. 3.39c). Totally random crystallite orientation results in an extension of the arcs into complete circles as shown in Fig. 3.39b. Thus, in theory, if the sharp diffraction can be compared with the general scattering from a polymer, a measure of the degree of crystallinity can be

obtained.

### 3.7.2 Experimental

X-ray specimens were prepared by grinding the extrudate to a thickness of generally around 1mm. Forward-reflection technique for the analysis of polymer samples is used. The beam of x-rays, usually is filtered by an iron filter, and subsequently collimated by a pinhole collimator of 0.5mm diameter. The beam passes through the sample, which is rotated at 1 rpm in order to increase the number of randomly oriented particles contributing to the reflections. The diffracted rays are recorded on a film located a short distance of about 7cm from the sample. The main undiffracted beam strikes a lead stop, thereby preventing blackening of the film due to high intensity of the undiffracted x-rays. X-ray exposures were made for 24 hours using Co radiation of wavelength  $K_{\alpha}$  1.7902 Å. The intensity profiles of the x-ray photographs are measured by means of an optical microdensitometer (Wooster Mark III MODIII Series).

### 3.7.3 Results & Discussion

Owing to the very low degree of order in CA and very small size of crystallites and because their orientation with respect to x-rays is not ideal, the diffraction patterns obtained from unprocessed CA tend to be more diffuse and the arclike features tend to be extended into complete circles. For this sample the photograph shown in Fig. 3.40 is about as good as can be achieved. The presence of the layer lines is also less obvious in the CA photograph, making it difficult to calculate the size of the unit cell of CA.

All the diffraction patterns of processed CA as a function of mixing time and the effect of plasticiser type and their concentration show a series of diffuse rings, and their relative breadth is attributed to poorer crystallinity. The resulting intensity profiles obtained from these photographs are given in

figure 3.41. The patterns were recorded using an optical microdensitometer. A peak is observed from the intensity profile as shown in Fig. 3.41. The relationship between the width of the peak ( $t$ ) and the dimensions of the crystallite domains ( $\epsilon$ ) is given by the following equation [97].

$$t = \frac{\lambda}{\epsilon \cos\theta}$$

This equation shows that the width of the peak is inversely proportional to the dimension of the domain. The investigation of the domain dimension by x-ray diffraction, although in theory rather simple, results in practice in substantial limitations on our interpretation of the measurements without recourse to sophisticated and possibly arbitrary computation. The intention in the present study has therefore been to obtain a qualitative estimate of the size of the crystallite domains in CA by a relatively crude analysis of the width of the peaks under the measured intensity profiles. This method reveals that the size of the domains decreases as a function of time and plasticiser content [98]. This may be attributed to the penetration of organic liquids such as solvent and plasticiser into possibly the portion of less perfect crystallites in CA, which disruptes both the intra- and intermolecular hydrogen bonding, and consequently lowers the degree of order of CA after the solvation process. It should be noted that DMP has a greater effect on influencing the structure of CA than DBP, as evidenced by the constancy of the size of domain of the two CA doughs containing 10pph DMP and 30pph DBP. The results tentatively indicate that the DMP penetrates more into the crystallites of CA than DBP does. However, a clear-cut conclusion cannot be drawn from these primitive results and further investigation is essential.

It should be realized that the present observation can only be regarded as indicating a trend towards greater disorder after the solvation process.

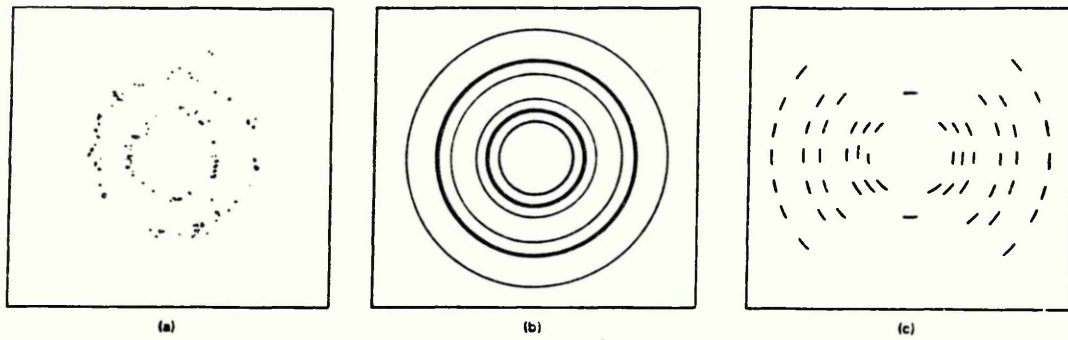


Fig 3.39 X-ray diffraction patterns of (a) an amorphous polymer, (b) an unorientated polymer and (c) an oriented polymer

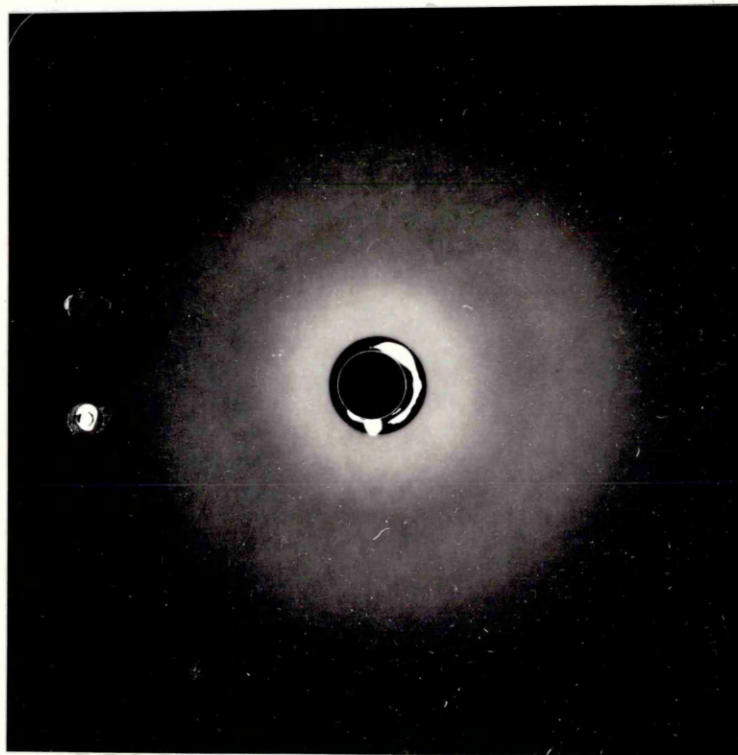


Fig 3.40 X-ray photograph of unprocessed cellulose acetate

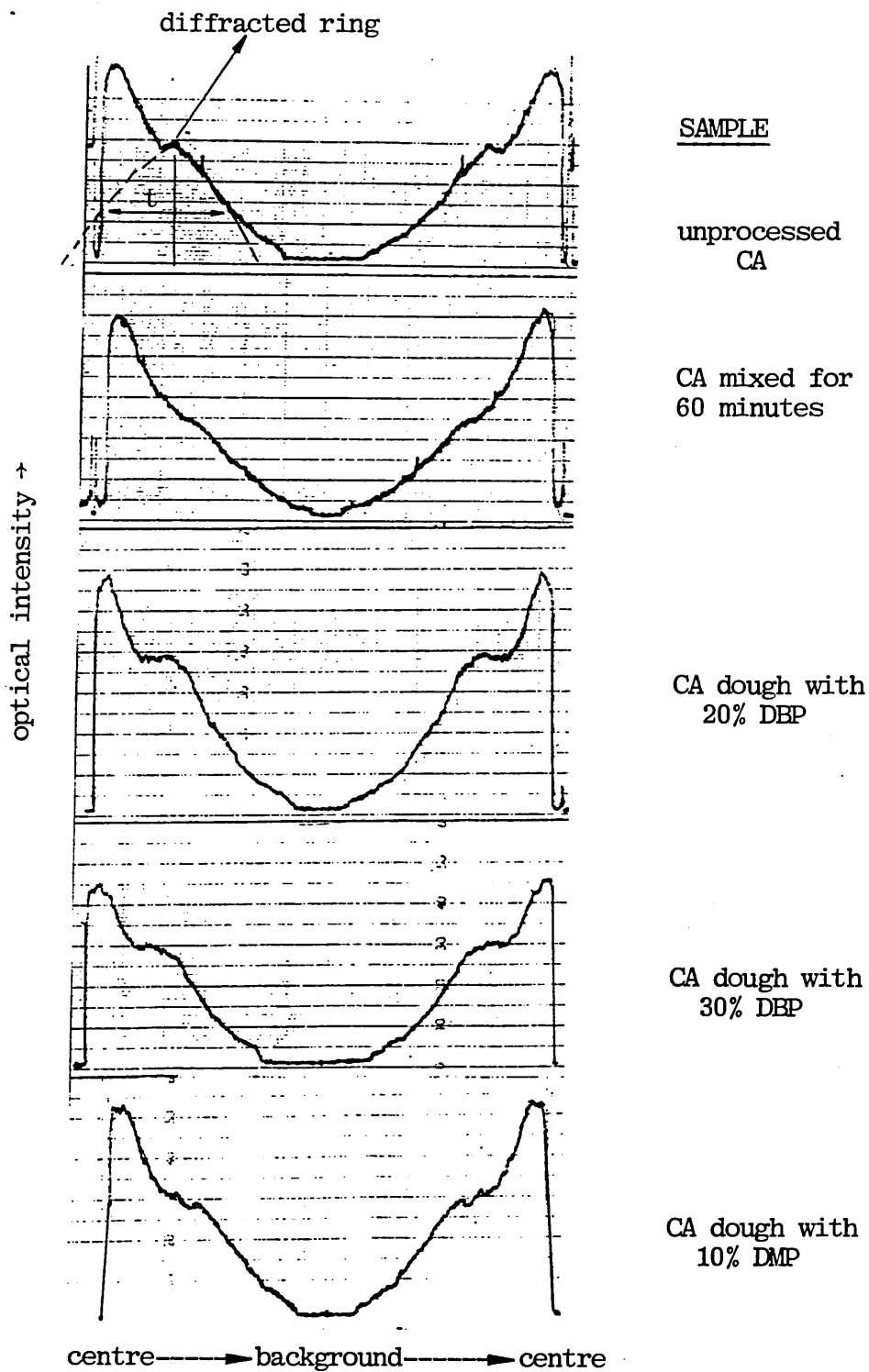


Fig. 3.41 X-ray diffraction intensity profiles for a series of processed CA doughs

4.1 Introduction

The rheological properties of CA doughs are studied using both torque rheometry and capillary extrusion rheometry. Owing to the complex geometry of the rotors and the design of the gearbox in the torque rheometer, a very complicated shearing motion is set up in the sample. Qualitative indications of viscosity and viscosity-temperature dependence may be obtained, but the interpretation of the torque rheometer data in absolute rheological units is difficult. Goodrich and Porter [99] attempted a quantitative analysis of the torque-time data and their results indicated a certain degree of success. However, their theory is still subject to strong criticisms. This is because they failed to take into account the distribution of shear rates that exists at each roller, and they did not allow for the non-Newtonian behaviour of the polymer melts.

4.2 Selection of a suitable fill factor

Fill factors ranging from 0.6-0.9 are commonly employed for mixing in torque rheometers. However, a different fill factor is used for different types of raw materials. As a result, fill factors of 0.6, 0.7, 0.8 and 0.9 were investigated while other mixing conditions were held constant. CA/MEK doughs with a solvent concentration of 70% were mixed at 20<sup>o</sup>C for 8 minutes.

The fill factor is identified as one of the key variables influencing mixing uniformity. Freakley et al [100] found that fill factor has a profound effect on viscous heating in the mixer. In general, fill factor, F, is defined as the ratio of the batch volume, V<sub>b</sub>, to the chamber volume, V<sub>c</sub>. For a system consisting of n components, the fill factor is given by the simple expression:

$$F = \frac{V_b}{V_c} = \frac{V_1 + V_2 + \dots + V_n}{V_c}$$

If a suitable fill factor has been selected, the amount of each

component can be determined provided that the density of the individual component and the chamber volume are known.

The chamber volume is determined by filling the chamber up to its neck with a viscous oil, which will not readily penetrate into the rotor shaft. The volume of oil inside the chamber is taken as the chamber volume and was found to be 40 ml.

Fig. 4.1 describes the gross appearance of the doughs mixed using different fill factors. Pictures of the surface and a cross-section through the dough are shown from left to right as a function of fill factor. It can be seen that there are some undispersed aggregates of CA powder on the surface of the doughs with the fill factors 0.6 and 0.9. No aggregates of CA are observed with the fill factors 0.7 and 0.8. The cross-section pictures of all the doughs reveal that the interior of the doughs are well gelatinised but they contain different amounts of air bubbles, depending on the fill factors. Again, the fill factors of 0.7 and 0.8 give the best mix, with fewer air bubbles present. Hence, a fill factor of 0.8 is selected for the mixing process, and this has been supported by Baker & Carter in a similar study on a gun propellant system [47].

The reasons for this phenomenon are complex. Freakley and Wan Idris [32] have demonstrated that the motion of material under the ram is highly dependent upon fill factor. At a fill factor of unity, no apparent movement of material under the ram is observed and the absence of voids behind the rotor tips gives rise to very little exchange of material between the lobes of the chamber. As a result, a fill factor of unity will give a poor dispersion of CA. The mix under the "dead area" at a fill factor of unity is shown in Fig. 4.2. However, at a fill factor below 0.7, it would appear that the amount of material is not sufficient to fill the front of the rotor tip continuously, so that axial flow of material is inadequate to achieve a good mix uniformity.

The consistency of CA doughs at fill factors of 0.7-0.8 may be due to an adequate and continual filling of the region in front of the

rotor tip and the presence of voids behind the rotor tip for promoting effectively the axial transfer of material.

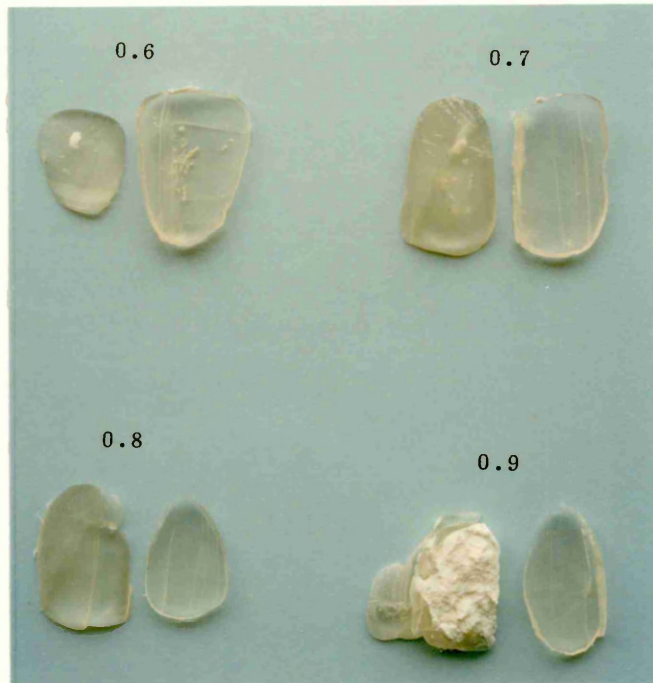


Fig. 4.1 Gross appearance of the surface (left) and the x-section (right) of the dough as a function of fill factor



Fig. 4.2 Dead area under the ram at a fill factor of unity

#### 4.3 A study of the rate of gelatinisation of cellulose acetate

The rate of gelatinisation is defined as the time interval between the addition of solvent and the binding-up of the CA powder with solvent.

In order to measure the rate of gelatinisation of CA in a torque rheometer, a static visualization method is used as described by Dizon & Papazian [101]. A series of mixes are dumped at specific time intervals, such as 0.5, 1, 1.5, 3, 4, 5 and 20 minutes. The mixing conditions were similar to that described in section 4.2.

Fig. 4.3 illustrates the variation in the extent of gelatinisation with different mixing times. Again, the surface and the cross-section area of the doughs are observed from left to right respectively as a function of processing time. These pictures clearly show that there are three key components in a dough system. They are the gelatinised matrix, the undispersed CA aggregates and the microvoids. It can be seen that there is quite a lot of CA powder on the surface as well as inside the dough after the initial one-minute period, which is corroborated by the observation of the presence of CA powder in the mixing chamber. The transparency of the dough is very low and this may probably be due to the presence of a large amount of CA powder and air bubbles inside the dough. After this initial phase of mixing, there is a progressive decrease in the size of CA aggregates and the amount of air bubbles as mixing continues. On the other hand, the degree of transparency of the dough increases with the mixing time, indicating that the degree of gelatinisation increases with time. It can be deduced from Fig. 4.3 that CA powder is consolidated within 3-4 minutes after the loading of the material. This almost corresponds to the time required to reach the peak of the mixing curve. A typical torque versus time curve is shown in Fig. 4.4. The shape of this curve indicates that three transitions occur during mixing, in which the incorporation, dispersion and homogenization stages are identified as zones I, II and III respectively [102,103].

In zone I, the initial torque level is low before the addition of solvent as the CA powder is tumbled around in the mixer with little energy being spent. With the introduction of solvent into the material, there is a gradual increase of torque level due to solvent incorporation into CA to form coherent doughs and the increase in volume of the material being mixed. The torque momentarily increases when the solvent is added and the ram is closed.

In zone II, the rise of torque to a maximum reflects the viscosity build-up due to the formation of well-gelatinised doughs. The increasing torque is required to shear the CA doughs and to break down and disperse the discrete unsolvated CA particles throughout the doughs.

In zone III, the torque level tends to flatten out and remains at a constant level, indicating the achievement of homogeneous doughs.

Fig. 4.3 Gross appearance of the surface (left) and the x-section (right) of the dough as a function of mixing time

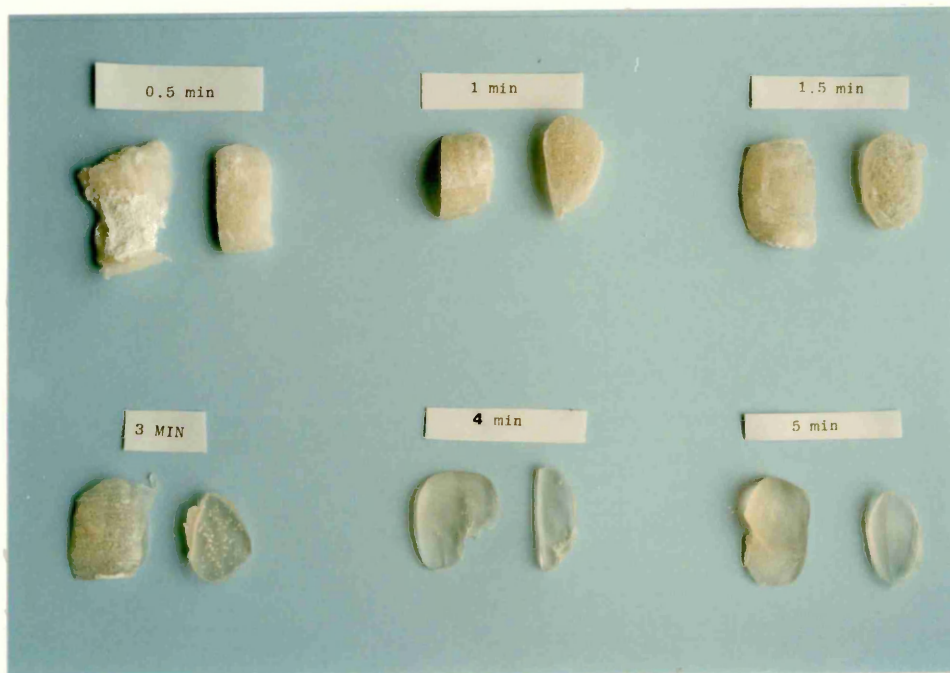
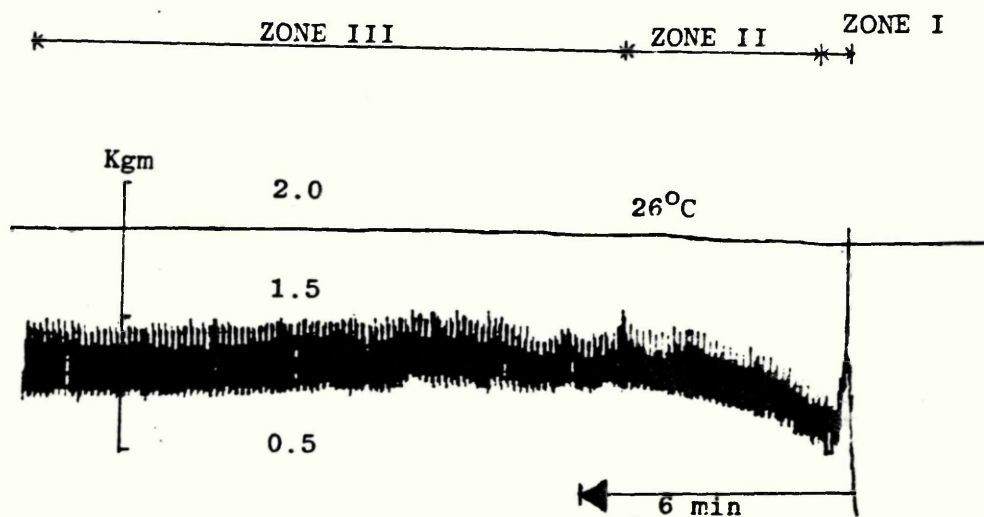


Fig. 4.4 A typical torque versus time curve of cellulose acetate



ZONE I - Solvent Incorporation

ZONE II - Solvent Dispersion

ZONE III - Homogenization

#### 4.4 Flow behaviour of cellulose acetate doughs

CA with a solvent concentration of 70% and 80% were mixed at 20<sup>o</sup>C for 20 minutes in the torque rheometer. These doughs were used as test materials in the capillary extrusion rheometer. Both the mixing and extrusion experiments were carried out at the Royal Ordnance, Explosive Division, Waltham Abbey.

The apparent flow curves of the CA doughs in Fig. 4.5 show that shear stress increase most rapidly in the low shear rate range, 0 s<sup>-1</sup> to 50 s<sup>-1</sup>. Following this initial shear rates range, the rate of increase in shear stresses with shear rate decreases gradually until at about 300 s<sup>-1</sup>, after which there is little change in shear stress. The flow behaviour of CA doughs, therefore, illustrates the classic flow properties of shear-thinning fluids.

According to the Power Law model, a double logarithmic plot of shear stresses versus shear rates of a pseudoplastic material should give a straight line of slope less than unity. However, the observed flow curves of CA doughs, in common with many double- and triple-phase propellant doughs, deviate from the Power Law at low and high shear rates, as shown in Fig. 4.6. Deviations from the straight line at high and low shear rates may depend on the extent of the shear heating effect and the value of yield stress respectively. Fig. 4.6 shows that viscous heating reduces shear stresses at high shear rates. Also, this effect is greater and starts earlier for the poorly gelatinised doughs which have higher shear viscosities, i.e., the doughs with lower solvent concentrations.

The surface temperatures of the extrudates through the 20 mm long die were measured by the IR pyrometer and the results are displayed as a function of shear rate as shown in Fig. 4.7. These results show that the surface temperatures of the cords, at low shear rates in which shear heating is not significant, are lower than the extrusion temperature (30<sup>o</sup>C). The reason for this phenomenon may be due to the drift in the measurement of the IR

pyrometer or the onset of another process, namely solvent evaporation. As the solvent evaporates from the dough surface, the surface temperature of the cord decreases because of the uptake of latent heat of evaporation by the solvent. Since, only a few experiments are carried out at Waltham Abbey, a final conclusion cannot be drawn for this observation, and this is left for further investigation. Nevertheless, the surface temperatures of the cords at high shear rates are higher than the extrusion temperature, indicating the occurrence of shear heating, which becomes more significant above shear rates of about  $10 \text{ s}^{-1}$ . It should be noted that the surface temperatures of the cords at shear rates below  $1 \text{ s}^{-1}$  are very close to ambient temperature. It is because at very low shear rates there is plenty of time for the cords to attain the ambient temperature before measurements were made by the IR pyrometer.

In order to understand the deviation from the Power Law at low shear rates, CA doughs with a higher solvent concentration (100%) is mixed under the same conditions and is extruded at  $20^\circ\text{C}$  by Privett (Royal Ordnance, Explosives Division). The apparent flow curve of this dough is also shown in Fig. 4.6. From this figure, it is observed that the deviation from the Power Law at low shear rates is not observed in the dough containing 100% solvent content. The apparent flow curves of doughs with solvent concentrations 70 pph, 80 pph and 100 pph were analysed, and apparent yield stresses of 24, 19.7 and 0 kPa were obtained respectively. The logarithmic plots of  $(\tau - \tau_y)$  against  $\dot{\gamma}$  for the doughs with solvent content of 70 pph and 80 pph are linearised at low shear rates as shown in Fig. 4.8, confirming that the deviation at low shear rates is due to the presence of yield stress, which provides adequate green strength to maintain the shape of the cords prior to drying. However, the cords extruded through a 2 mm diameter die collapsed after half an hour. This can be explained by the fact<sup>that</sup> the aforementioned apparent

yield stresses do not take into account the entrance effect during extrusion. If this effect is allowed for, CA doughs should have insignificant yield stresses. It is becoming clear that a more fibrous form of CA is required to simulate the effect of the nitrocellulose and give the composition a definite yield stress that can be modified by gelatinisation. However, it is found that commercial CA produced in the U.K. today differs from explosive-grade NC in that the CA does not retain the fibrous structure of the original cotton fibres from which it is produced.

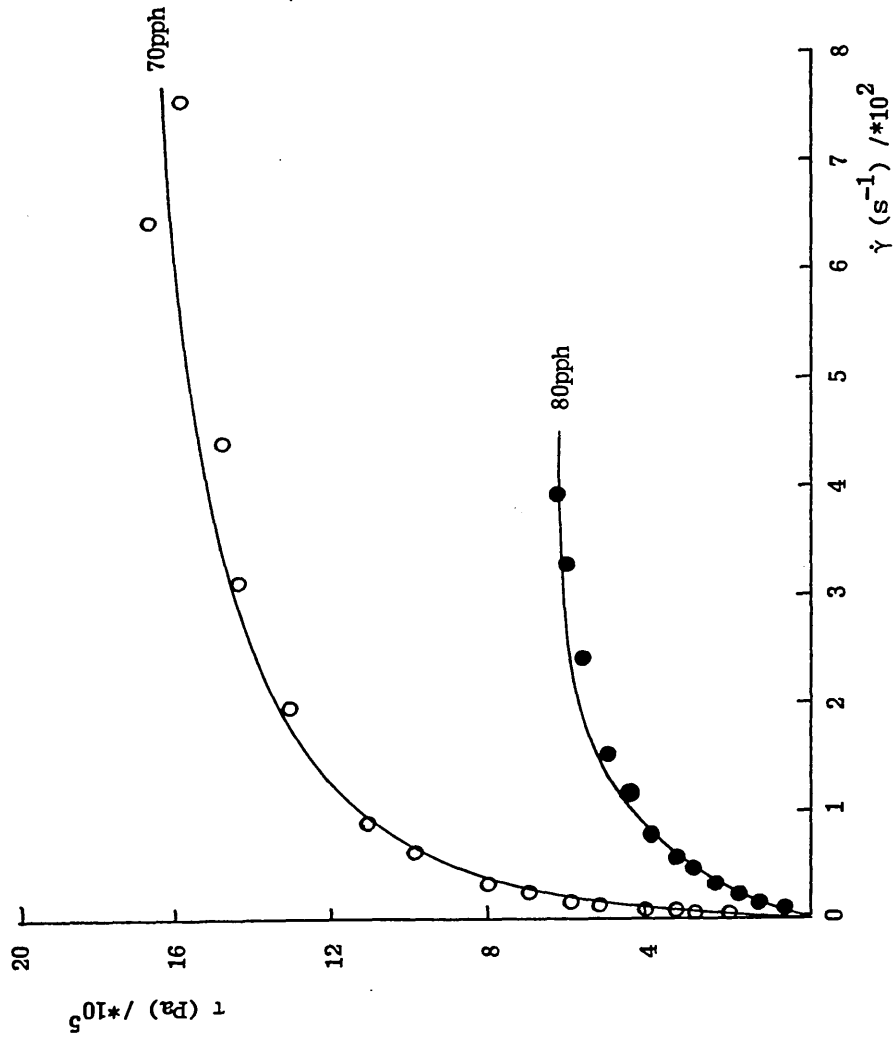


Fig. 4.5 Shear-thinning behaviour of CA doughs with different amount of solvent content

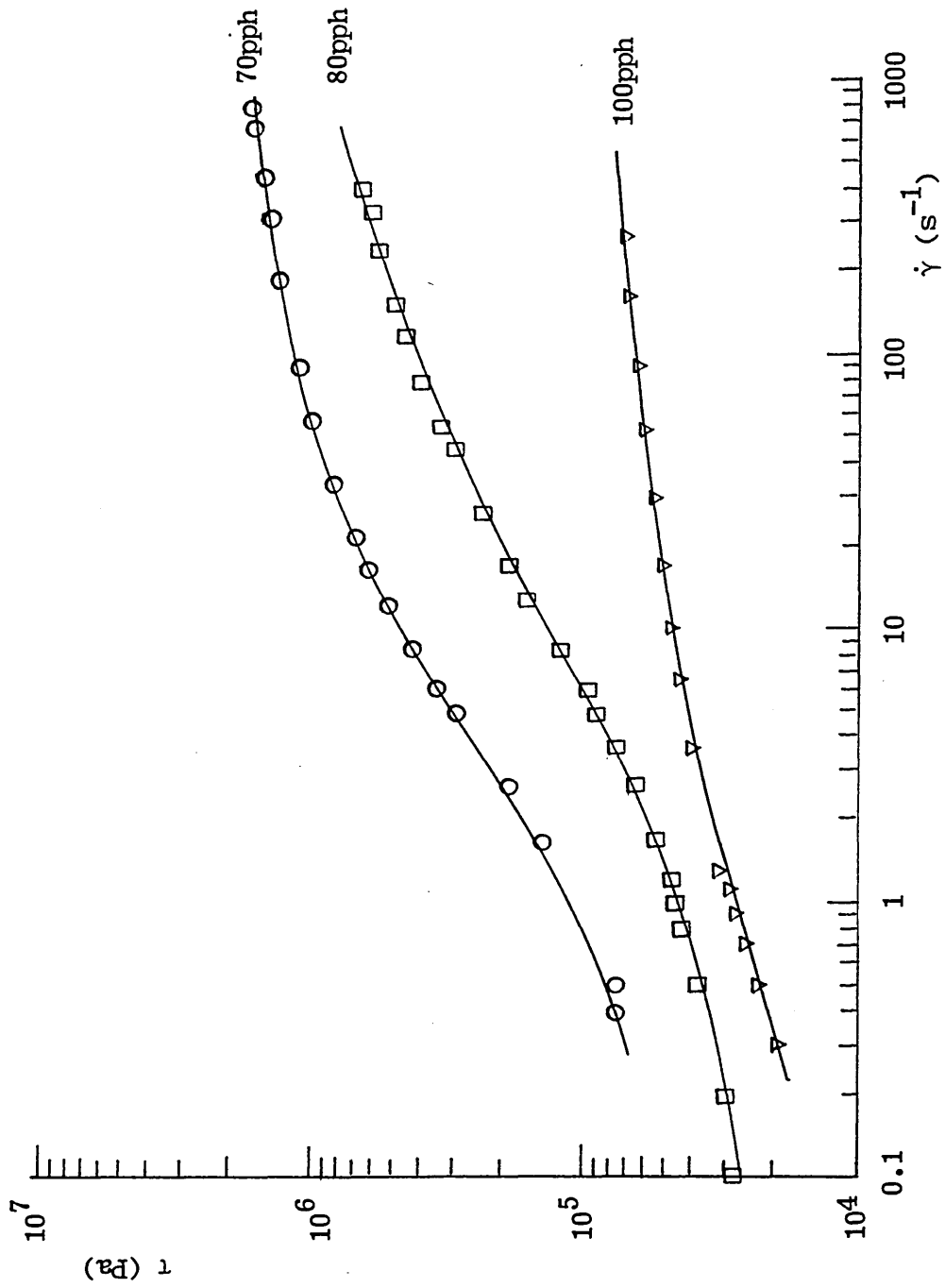


Fig. 4.6 A double logarithmic plot of shear stress versus shear rate of CA doughs at 30 °C

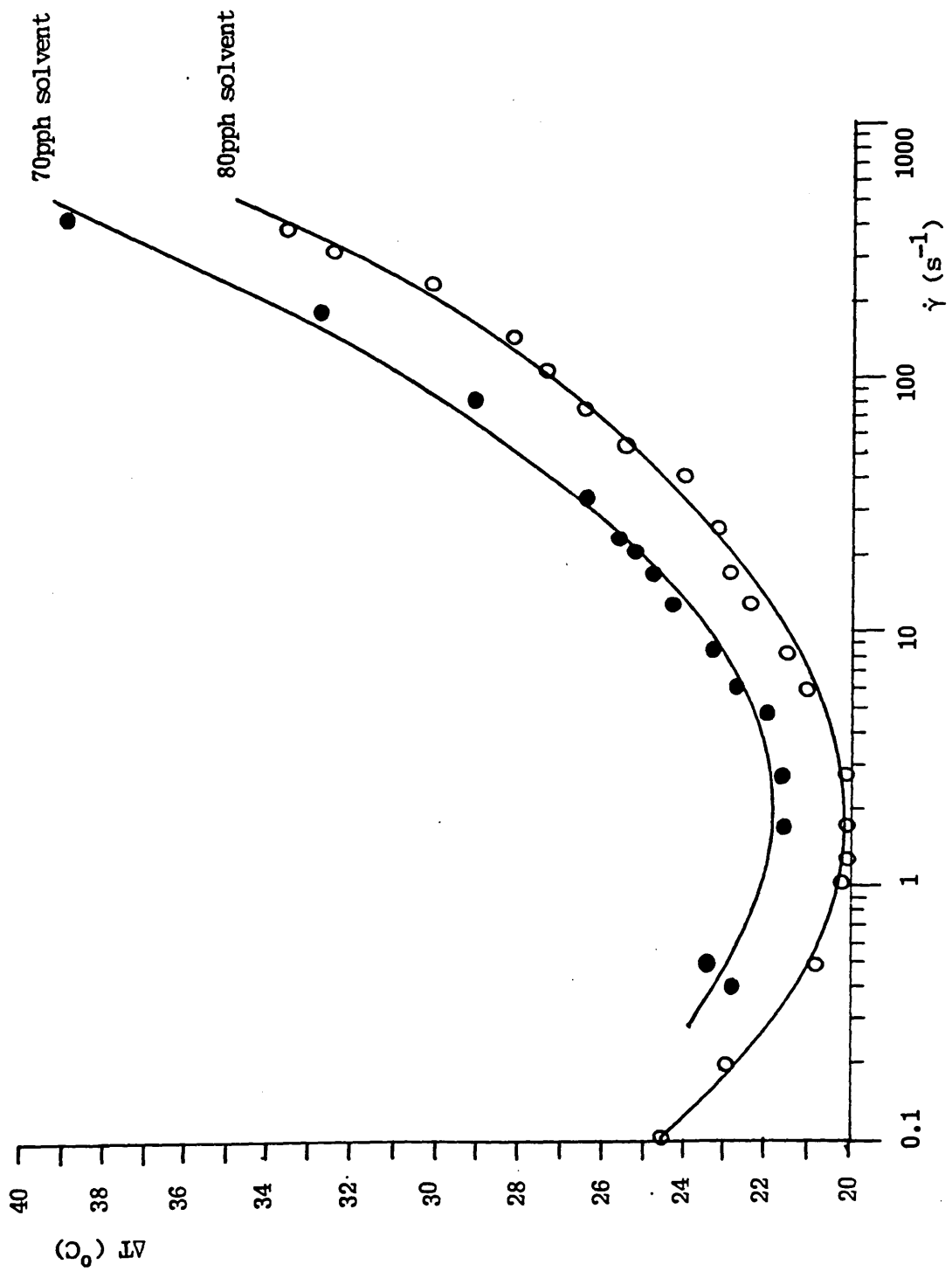


Fig. 4.7 Change of surface temperature of the cord as a function of shear rate

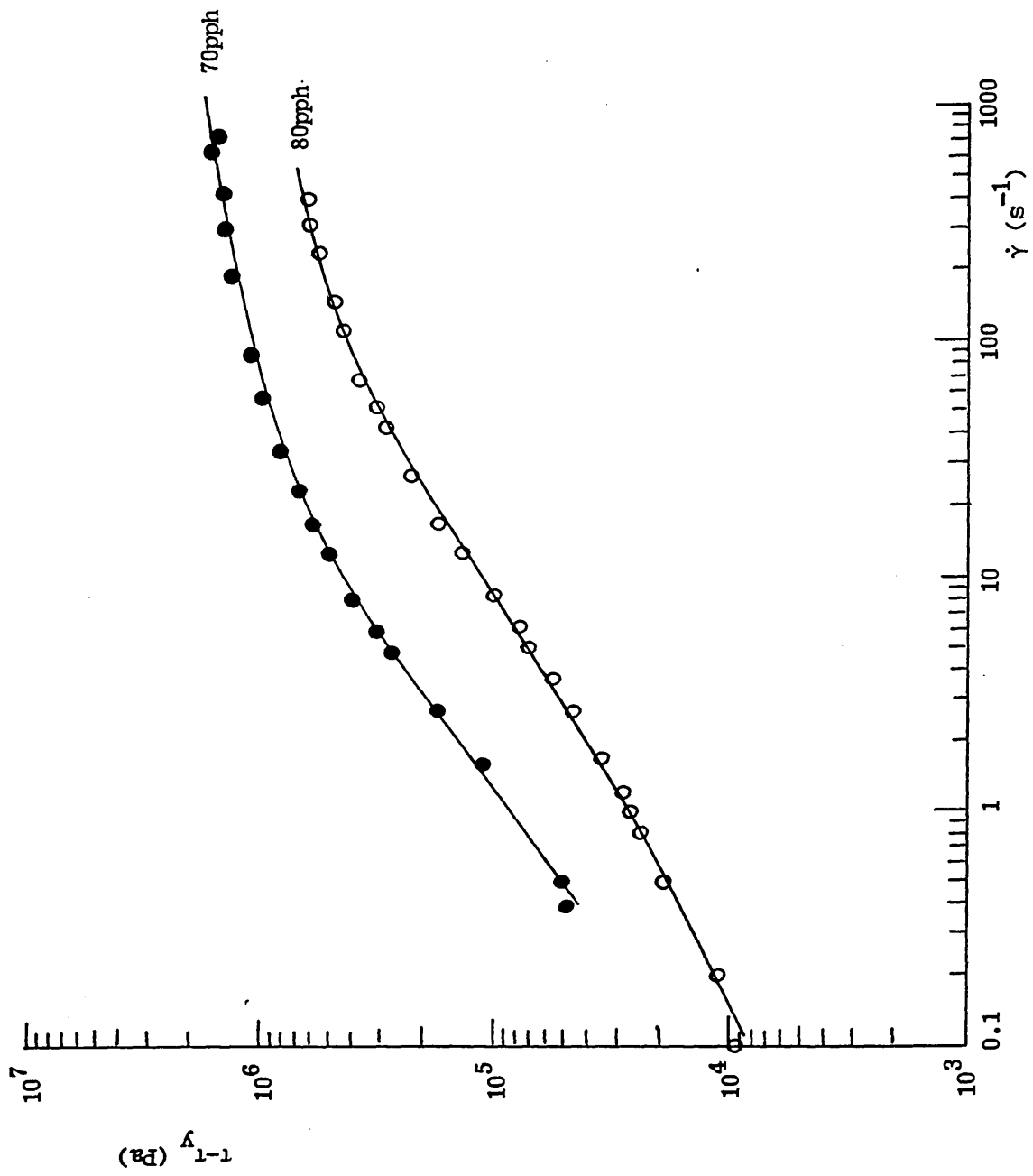


Fig 4.8 Apparent flow curves of CA doughs after correcting the yield stress

CA doughs containing 70% solvent concentration were mixed at 20°C for 20 minutes. These doughs were used to see the effect of extrusion temperature on the rheological properties of the solvated CA doughs, using the capillary extrusion rheometer at Sheffield City Polytechnic.

Fig. 4.9 shows the logarithmic flow curves as a function of extrusion temperature. It can be seen that at a wall shear stress of about  $2.5 \times 10^5 \text{ Nm}^{-2}$  the curves deviate from linearity. The curve for 20°C has a low value of  $n$  throughout and is almost horizontal for shear stress of about  $7 \times 10^5 \text{ Nm}^{-2}$ , whereas for temperatures of 35, 40 and 45°C the flow curves are linear throughout. For these temperatures, the shear stress remains below  $2.5 \times 10^5 \text{ Nm}^{-2}$  even at the highest shear rates studied. This phenomenon may possibly be due to the shear heating effect as mentioned in section 4.4, and this effect becomes prominent at a critical wall shear stress. The viscosity of the dough at low extrusion temperature is high and therefore shear heating will develop at lower shear rates than in those doughs extruded at higher temperatures.

Since the capillary extrusion rheometer in Sheffield cannot go down to shear rates below  $10 \text{ s}^{-1}$ , it is therefore not possible to determine the value of yield stress by our equipment. The deviation from linearity of the flow curves is therefore not observed. However, the extrudates do not hold their shape well before drying, and for this reason it is assumed that the yield stresses of these doughs are very small.

A study of the relationship between viscosity and extrusion temperature of CA dough is carried out in order to understand the flow mechanism. Both Arrhenius-Frenkel-Eyring (AFE) and Williams-Landel-Ferry (WLF) equations can be used for this purpose. However, solvent loss from the solvated dough during Tg determination is difficult to control, and hence the use of WLF equation cannot be applied in this project.

The AFE formula [104] is given as follows:

$$\eta = K \exp ( E/RT_k )$$

where  $\eta$  = viscosity  
E = activation energy  
K = constant  
R = gas constant (8.314 J/mol/K)  
 $T_k$  = kelvin temperature

According to this formula, a plot of logarithmic viscosity versus reciprocal kelvin temperature should give a straight line. Figure 4.10 shows <sup>an</sup> Arrhenius plot at a shear rate of  $200 \text{ s}^{-1}$  for all the extrusion temperatures. However, the data in this figure could not be adequately described by one straight line. Two distinct regions exist, and there is a gradual change of activation energy at a temperature of  $35^\circ\text{C}$ , determined by the intersection of two straight lines drawn from the low and high temperature ranges. This means that there are two activation energies of flow and hence two different types of flow are possible. This gradual change in activation energy may be due to two mechanisms with a decrease in importance in one accompanied by a gradual increase of the other. Thus, the change is a continuous function. Such an observation is further supported by Collins et al [105] in which they have observed two distinct flow activation energies in the low and high temperature regions of poly (vinyl chloride). Again, the presence of two distinct flow activation energies has been found in polyisobutylene [106] and polystyrene [107].

The curve in the Arrhenius plot at a shear rate of  $200 \text{ s}^{-1}$  is attributed to shear heating. If the points for the lower temperatures are shifted on to the straight line extrapolated from the higher temperature measurements, shearing heating of  $2.3^\circ\text{C}$ ,  $6.6^\circ\text{C}$  and  $8.9^\circ\text{C}$  have been observed at the extrusion temperatures of  $30^\circ\text{C}$ ,  $25^\circ\text{C}$  and  $20^\circ\text{C}$  respectively. The lowest extrusion temperature to remain on the Arrhenius plot is the one at  $35^\circ\text{C}$ , which is confirmed by the rise in temperature of the dough with 70% solvent in Fig. 4.7. This figure shows that shear heating of

2.8°C is measured by the IR camera, which is very close to the calculated value of 2.3°C. It is, therefore, likely that lower extrusion temperatures and hence higher material viscosities could give rise to shear heating.

The value of energy of activation (E) depends strongly on whether the viscosities at various temperatures are evaluated at constant shear stress or at constant shear rate. If E is evaluated at a constant shear stress, it is found that E is essentially a constant independent of what value is chosen for shear stress. However, if E is evaluated at a constant shear rate, the energy of activation generally decreases with increasing rate of shear [108]. As a result, the former method is selected to calculate the activation energy of CA doughs.

It would appear from Fig 4.9 that the flow curves start to deviate from the power law at a critical shear stress of  $2.5 \times 10^5 \text{ Nm}^{-2}$  or above. Therefore, a constant shear stress of  $10^5 \text{ Nm}^{-2}$  for the three higher temperature extrusions only is selected in order to eliminate the shear heating effect, and the Arrhenius plot gives a straight line with a slope of  $9.29 \pm 1.10 \times 10^3$  as shown in Fig. 4.10. The activation energy of flow for CA doughs with 70% solvent concentration is found to be  $178 \pm 23 \text{ kJ/mol}$ , and this high value is due to the inherent stiffness of the CA main chain, which dominates the flow behaviour of the doughs.

The variation of apparent viscosity,  $\eta$ , of polymer melts with shear rate,  $\dot{\gamma}$ , can be represented by a master curve in which  $\log(\eta / \eta_0)$  is plotted against  $\log(\dot{\gamma} t)$ , where  $t$  is a relaxation time [109,110]. Reasonable estimation of zero shear viscosity in the present case by extrapolating the non-Newtonian flow data was found to be in serious error because all the flow curves are measured at a relatively high shear rates. Hence, this technique is difficult to use, and the method which was proposed by Mendelson [111-113] is used here. The master curve is obtained by plotting  $\log \tau$  against  $\log(\dot{\gamma} a_T)$ , where  $a_T$  is called the shift factor.

It is mathematically defined as:

$$a_T = \frac{\dot{\gamma}(\text{reference})}{\dot{\gamma}(T)}$$

where  $\dot{\gamma}(\text{reference})$  is the shear rate for a given shear stress at a reference temperature of 40°C and  $\dot{\gamma}(T)$  is the shear rate at the same shear stress at a temperature T.

Owing to the uncertainty arising from shear heating as suggested by Chee [114], it was decided to fit the higher temperature data only to a master curve. The shift factor for the doughs extruded at 35°C, 40°C and 45°C are 4.18, 1.0 and 0.4 respectively. The resulting shifted data lies on the same line as shown in Fig. 4.11.

Analysis of the flow curves as a function of extrusion temperature gives the information on both flow index and consistency index as shown in Fig. 4.12. The result shows that the flow index value (n) is proportional to extrusion temperature. The experimentally determined relationship is :

$$n = 0.026T_c - 0.35$$

where  $T_c$  is the Celsius temperature.

However, the consistency index (k) decreases in an exponential manner as extrusion temperature increases. A linear relationship is obtained by taking the logarithmic consistency index versus reciprocal kelvin temperature as shown in Fig. 4.13. The observed relationship is given by :

$$\log k = 10^4 / T_k - 28.25$$

where  $T_k$  is in kelvin temperature.

The slope of this straight line ( $10^4$ ) is very similar to the slope in Fig. 4.10 (constant shear stress), suggesting that the consistency index reflects the viscosity of the dough and it can also be used in the Arrhenius equation in this particular system. The curve fitted equations representing experimental flow curves

of CA doughs which were extruded at different temperatures are given in Table 4.1.

Table 4.1 Curve fitted equations for flow of doughs extruded at different temperatures.

Extrusion temperature	Curve fitted equation for flow
20	$Y=4.769+0.957X-0.200X^2$
25	$Y=4.265+1.222X-0.258X^2$
30	$Y=4.167+1.221X-0.243X^2$
35	$Y=3.707+1.345X-0.242X^2$
40	$Y=3.451+0.979X-0.078X^2$
45	$Y=3.839+0.064X-0.256X^2$

where  $Y = \log \tau$  and  $X = \log \dot{\gamma}$

Figure 4.14 shows plots of die swell ratio versus shear rate for CA doughs at two extrusion temperatures. It can be seen that the data are not well correlated because of the difficulties in controlling solvent evaporation and extrudate distortion. As a result, errors may arise in the measurement of the extrudate diameter and the results of die swell ratio are not very accurate. Nevertheless, it can be seen in Fig. 4.14 that the die swell ratio increases with increasing shear rate at low rates, then tends to peak and decreases at high shear rates. The values are small, indicating that the amount of recoverable elastic energy of the dough is small. Besides, the die swell ratio increases with the extrusion temperature increases from 20 °C to 30 °C. These results are in good agreement with NC doughs [115]. It can be interpreted that the elasticity of molecules increases as a function of temperature. It is because temperature has a great influence on the degree of gelatinisation of the dough. At high temperatures, the doughs are well solvated and all side groups extend from the rigid backbone chain, causing interactions between molecules (Fig. 4.15). Consequently, the elasticity of the dough increases with a higher temperature.

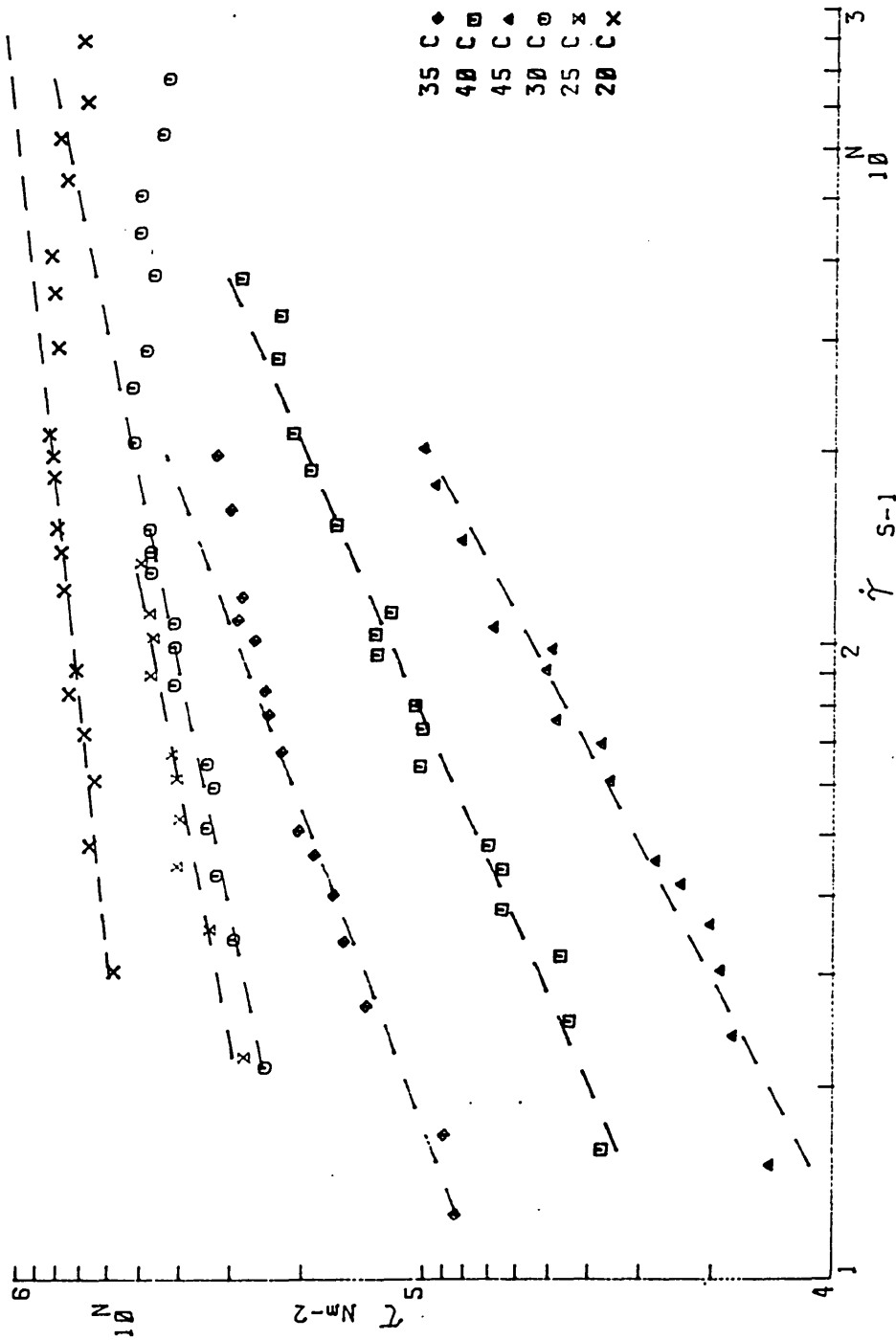


Fig. 4.9 Logarithmic flow curves of CA doughs as a function of extrusion temperature

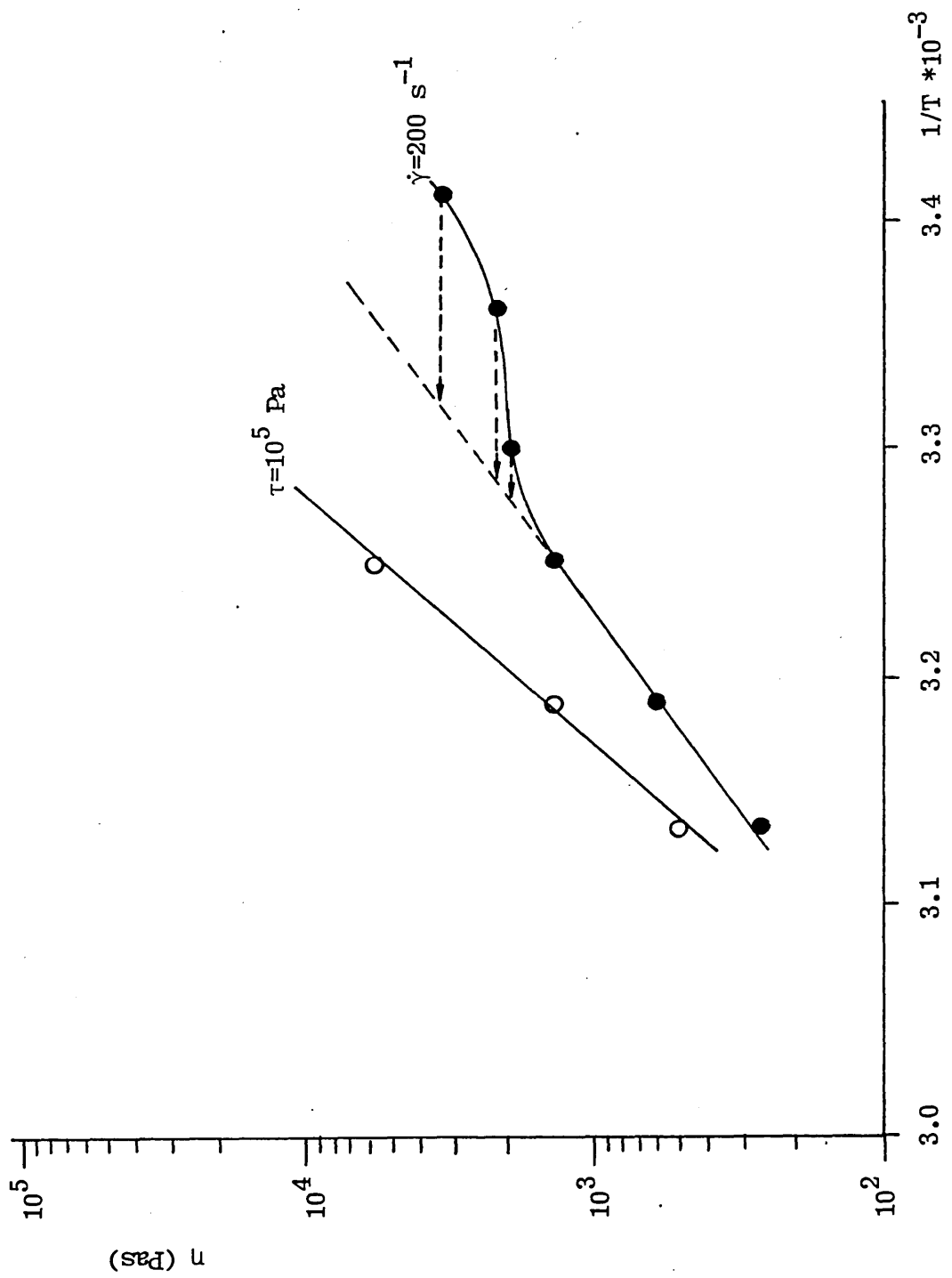


Fig. 4.10 Temperature dependence of viscosity at constant shear stress ( $10^5$  Pa) and constant shear rate ( $200$  s $^{-1}$ )

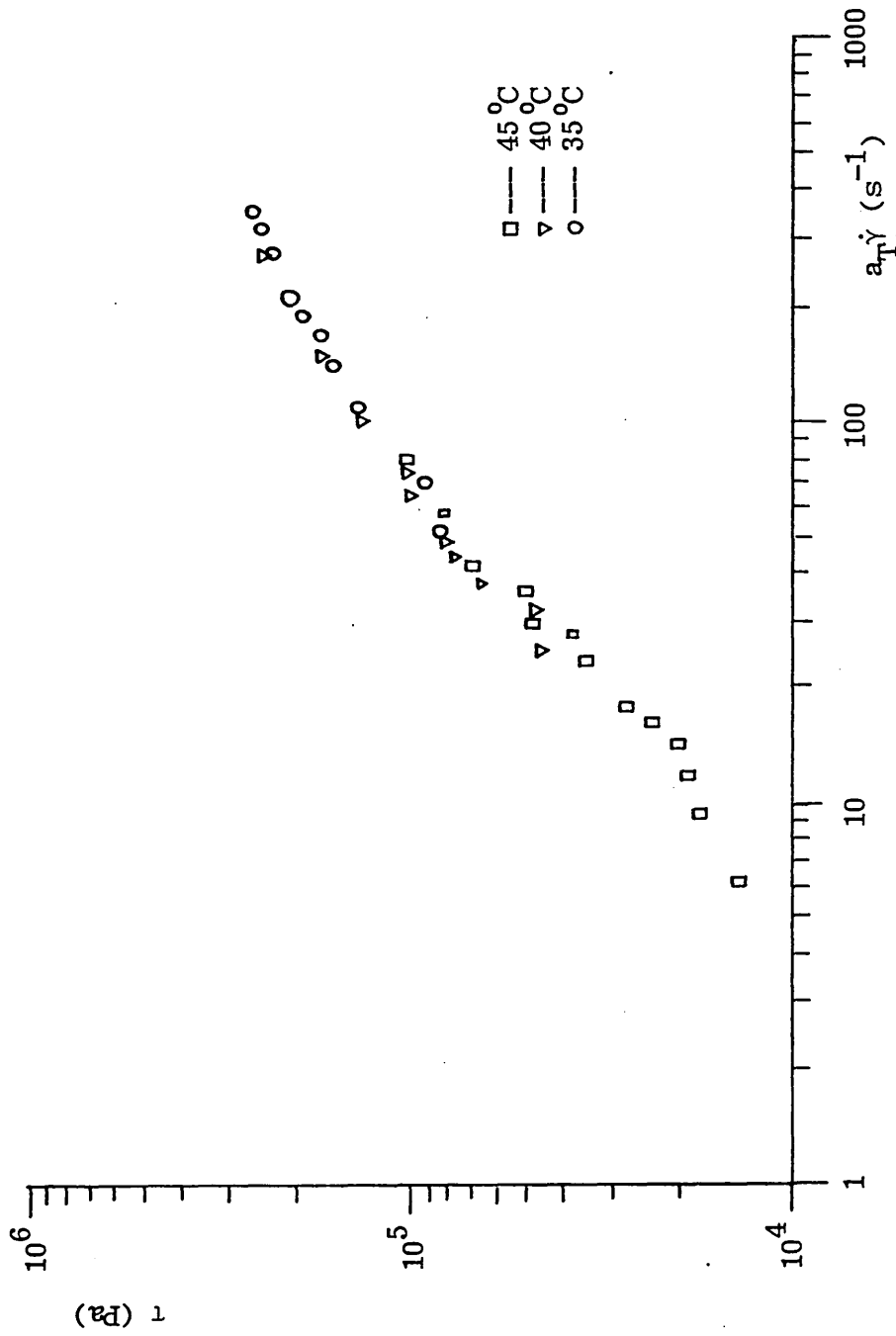


Fig. 4.11 Master curve of CA doughs at different extrusion temperatures

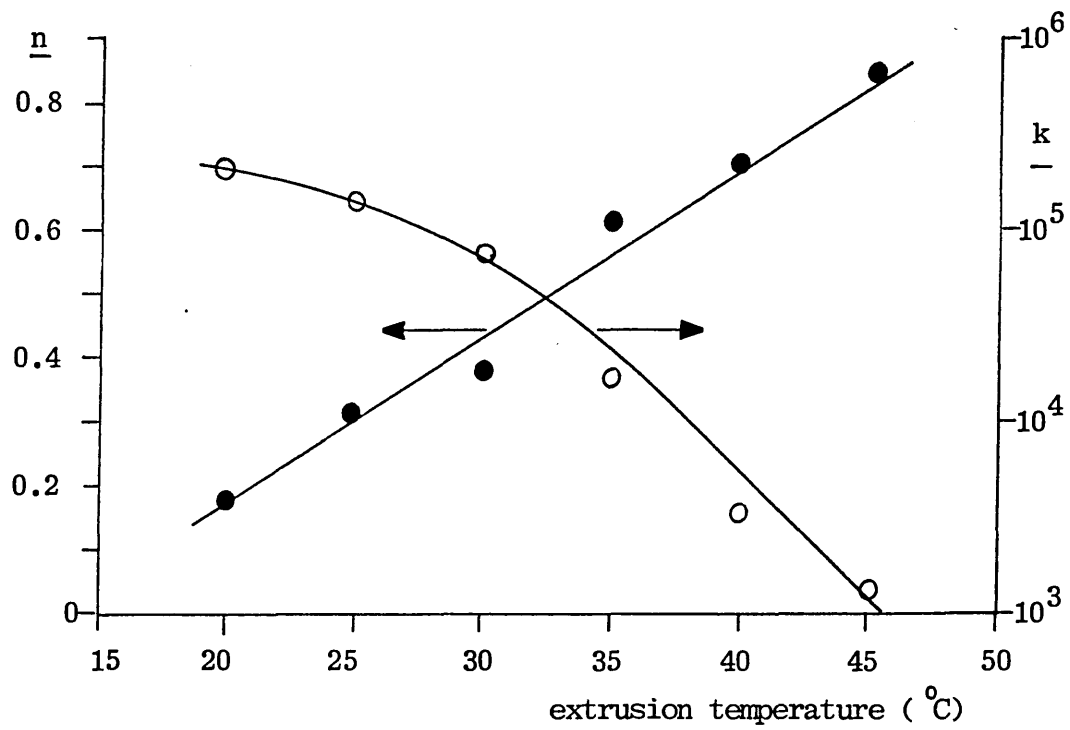


Fig. 4.12 Relative change of the flow behaviour index and consistency index as a function of extrusion temperature

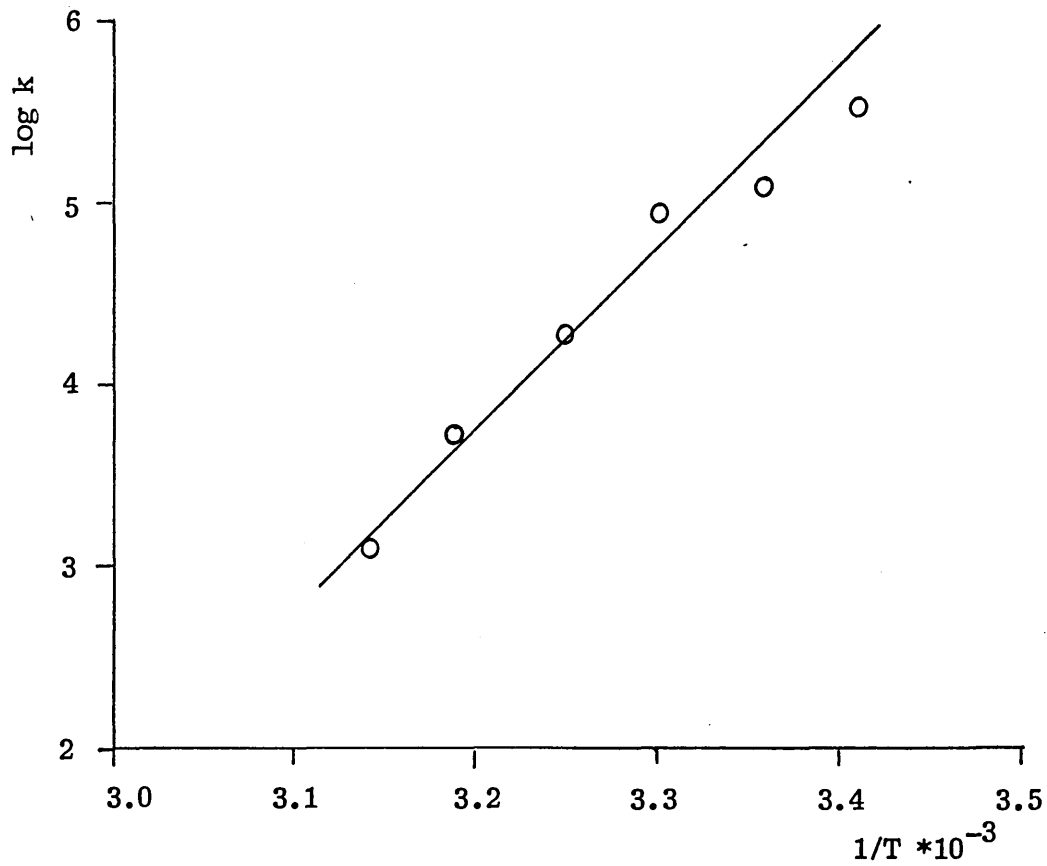


Fig. 4.13 Temperature dependence of the consistency index of CA dough

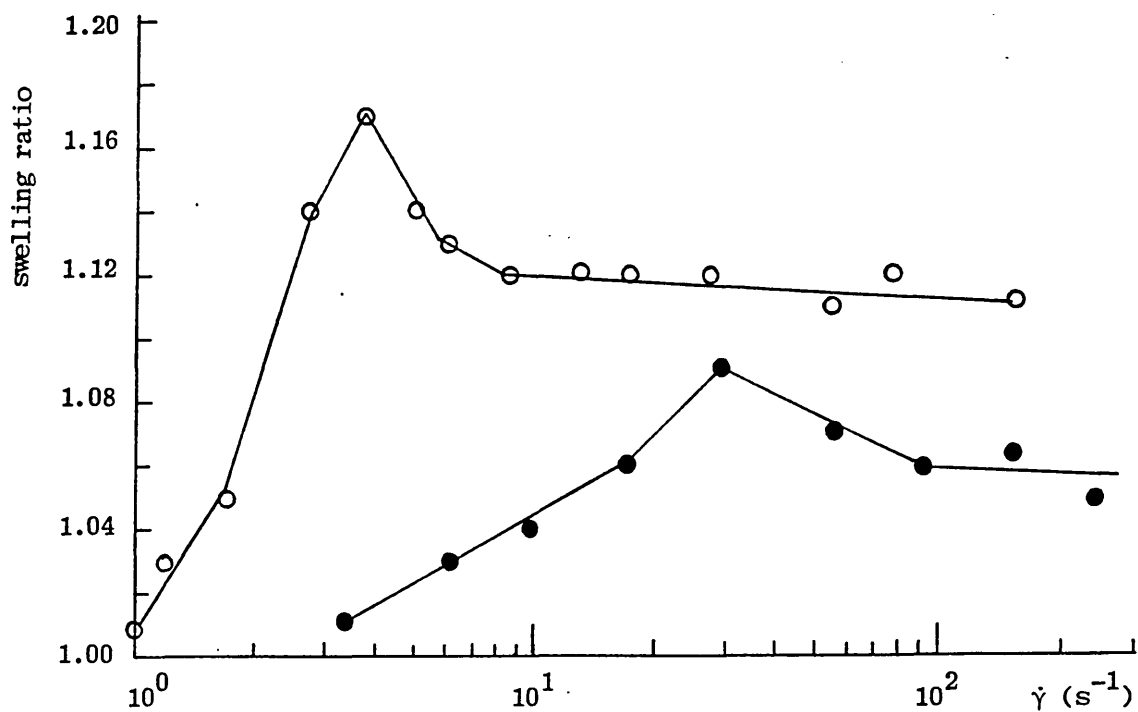


Fig 4.14 Effect of extrusion temperature on swell ratio of CA dough ( ● — 20 °C, ○ — 30 °C)

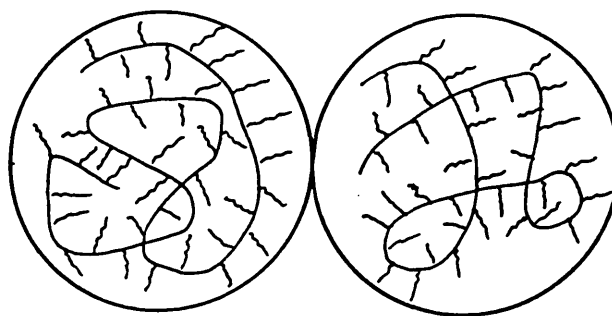


Fig. 4.15 Model of well solvated CA chains at high temperatures  
 (a) side chains extend from the main chain  
 (b) large hydrodynamic volume

#### 4.6 Effect of mixing parameters

The influence of mixing parameters such as mixing time, temperature and solvent concentration on the mixing and extrusion processes were examined by means of varying only one of the mixing parameters at a time in the mixing process. Details of the mixing parameters and the composition code are given in Table 4.2. All the doughs were mixed in the torque rheometer and were extruded at 30 °C in the capillary extrusion rheometer.

Table 4.2 Composition code and mixing conditions of CA doughs

Composition Code	Time /min	Temperature /°C	Solvent pph
MT1	1	20	70
MT5	5	20	70
MT20	20	20	70
MT60	60	20	70
MT120	120	20	70
MC10	20	10	70
MC20	20	20	70
MC30	20	30	70
MC40	20	40	70
MS50	20	20	50
MS60	20	20	60
MS70	20	20	70
MS80	20	20	80
MS90	20	20	90

\* For clarity, a composition with Spph solvent consists of:

CA            100 parts by wt.  
MEK            S parts by wt.

##### (A) Effect of mixing time

By visual inspection of the CA doughs, undispersed CA powder is observed on the surface of the dough MT1 only. The mixing curves for different mixing times are shown in Fig. 4.16. From this figure, it may be noted that the control of mixing temperature was fairly easy regardless of the duration of mixing. The area under

the mixing curve, corresponding to the work unit at different specific times, was measured. Fig. 4.17 shows the variation of maximum torque value and work unit as a function of mixing time. It can be seen that the torque level increases most rapidly in the initial mixing period. In fact a fairly high torque value can be achieved even after 1 minute. Following this initial mixing period, the rate of increase in torque level decreases considerably until about 20 minutes of mixing, and thereafter the torque remains fairly constant. Also, this result shows that there is a linear relationship between the work unit and mixing time, in agreement with Baker et al [47]. Mixing time can be used as a measure of work input in this particular system, and the experimentally determined relationship is :

$$Wu = 0.115t$$

Fig 4.18 illustrates the logarithmic flow curves for CA doughs as a function of mixing time. It should be noted that the flow process of the dough MT1 is fairly unstable as indicated by the fluctuation of shear stresses. This may probably be due to the presence of unsolvated CA powder of the poorly gelatinised doughs. This figure shows that the effect of mixing time on the flow properties of CA doughs is not significant. Therefore the maximum torque level can be used as a measure of the viscosity of the dough. Also, shear heating effects appear at shear stresses above  $5 \times 10^5 \text{ Nm}^{-2}$ .

#### (B) Effect of solvent concentration

Solvent content plays an important role in the dough-up of the CA/MEK system. It has been found that for solvent contents below 30% by weight of CA dough-up becomes more difficult. This is easy to understand because dough-up proceeds by a shear mechanism that distributes the solvent in thin layers so that it can be distributed uniformly over the surface of the solid. Clearly, dough-up is impossible for some formulations if the solvent is present in very low concentrations. There must be a critical

solvent content to provide a surface layer over all the solid particles and to fill the space between them.

Visual inspection of the CA doughs shows that the degree of transparency of the mix increases as the solvent content in the mix increases.

The typical torque versus time curves for different solvent concentrations are shown in Fig. 4.19. These curves indicate that the value of torque generated by the mix increases as solvent content decreases, i.e. the dough becomes stiffer. In addition, the width of the trace is considerably larger for low solvent concentrations. Temperature is more difficult to control for a low solvent concentration because of the tremendous internal viscous heat generated by the stiffer materials inside the mixer. The variation of maximum torque level and work unit with solvent content is shown in Fig. 4.20. This figure shows that the work unit decreases in a linear manner while the maximum torque level decreases exponentially with increasing solvent concentration. However, a plot of logarithmic maximum torque level against solvent concentration gives a linear relationship as shown in Fig. 4.21. The experimentally determined relationships are :

$$Wu = 6.83 - 0.067 * C$$

$$\text{Log (Tor)} = 1.70 - 0.018 * C$$

It should be noted that Baker et al found a logarithmic-linear relationship between work unit and solvent content in the range of 10 to 20 pph of the gun propellant system. However, such a relationship is not observed in the present study as shown in Fig. 4.21. The reason for this variation is not clearly understood. It may be due to the difference in the components inside the doughs or the difference in the range of solvent concentration. A linear relationship is observed only in the region of low solvent content as shown in Fig. 4.21, and this correlated quite well with the observation that Baker had found.

Flow curves of CA doughs with different solvent contents are shown in Fig. 4.22. For a constant shear rate, the shear viscosity of the dough decreases as a function of solvent content. These results correlate well the relationship between maximum torque value with solvent content as shown in Fig. 4.21, indicating that the torque level is an indirect measure of the viscosity of the dough. Viscous heating is related to the product of shear stress and shear rate. Doughs with lower viscosities would show heating effects at lower shear stresses and at higher shear rates. Well solvated doughs have lower shear stresses than poorly solvated doughs. Therefore, it can be observed from Fig. 4.22 that there is a change of slope for the 70 pph line and 80 pph line at shear stresses above  $5 \times 10^5 \text{ Nm}^{-2}$  and  $3 \times 10^5 \text{ Nm}^{-2}$  respectively. This change in slope is attributed to shear heating, which also causes the low value of the flow behaviour index for the dough with 60 pph solvent content. Unfortunately the critical shear stress is higher than the shear stress range covered in the MS90 doughs. The narrow shear stress range was due to the fluctuation of the extrusion pressures, so that much longer times were required before the pressure reached equilibrium for each piston speed. The limited amount of material inside the rheometer also account for a much narrower shear stress range.

Some die swell measurements were made on the extrudate at two solvent concentrations as shown in Table 4.3. This table shows that the values of die swell ratio are small and there are no obvious differences in the die swell values of the doughs with solvent content of 70 pph and 80 pph. This shows that the die swell ratio is not sensitive to the solvent content because there have already sufficient amount of solvent to gelatinise the dough.

Table 4.3 Effect of solvent content on die swell

80 pph		70 pph	
shear rate	swell ratio	shear rate	swell ratio
1.0	1.01	1.0	1.05
1.2	1.03	1.4	1.07
1.7	1.05	1.6	1.11
2.7	1.14	1.7	1.10
3.7	1.17	2.7	1.11
4.9	1.14	4.8	1.10
6.0	1.13	6.0	1.12
12.8	1.12	8.5	1.11
16.9	1.12	12.7	1.11
26.8	1.12	16.6	1.11
43.6	1.13	21.5	1.12
54.6	1.11	33.6	1.13
77.0	1.12	58.4	1.10
151.6	1.11	89.9	1.12
241.3	1.13	311.4	1.01
393.5	1.12	438.4	1.06

Logarithmic-linear plots between viscosity and reciprocal solvent concentration are shown in Fig. 4.23 for doughs at low shear rates to avoid shear heating effects and at an extrusion temperature of 30 °C. These plots are linear, indicating that the relationship is somehow similar to that of the Arrhenius-Frenkel-Eyring expression. The empirical equation for such a relationship may be written as follows:

$$\eta = K \exp (A/C)$$

where K and A = constants  
C = solvent concentration

### (C) Effect of mixing temperature

The mixing curves of the doughs as a function of mixing temperature are shown in Fig. 4.24. This figure shows that the effect of mixing temperatures on mixing behaviour is very similar to that of solvent concentration on mixing behaviour. The maximum torque level and the width of the trace increases as the mixing temperature decreases. In addition, mixing temperature is more difficult to control for a mix at low mixing temperature because of the shear heating effects. It should be noted that the torque

level follows the small fluctuations of the mix temperature during the mixing process. This indicates that the viscosity of the dough is very sensitive to temperature. The variation of work unit and maximum torque level with mixing temperature is illustrated in Fig. 4.25. From this figure, it can be seen that the work unit and the maximum torque level decrease in a linear manner as the mix temperature increases. The experimentally determined relationships are:

$$Wu = 3.33 - 0.06 T_c$$

$$Tor = 4.33 - 0.08 T_c$$

where  $T_c$  is the Celsius temperature

However, Baker et al found that the torque level generated by a material for a given mixer speed was more sensitive to temperature as the level of solvent in the dough decreased. A linear relation is observed with well solvated NC doughs, which is in good agreement with present results for the CA doughs of relatively higher solvent concentration than those employed in the NC doughs (Fig. 4.25).

As the solvent content in the doughs of the MC series are the same, and they are extruded at the same temperature ( $30^{\circ}\text{C}$ ), the flow properties of these materials should be similar. Indeed, the flow curves of the doughs mixed at  $10^{\circ}\text{C}$  and  $20^{\circ}\text{C}$  are very similar as shown in Fig. 4.26. However, the extrusion pressures of the dough mixed at  $30^{\circ}\text{C}$  are higher than those of doughs mixed at lower temperatures. This may be due to the process of solvent evaporation during the transfer stage of the dough from the torque rheometer to the capillary extrusion rheometer, as it has been observed that there is some condensed solvent on the surface of the doughs. The migration of solvent towards the surface of the doughs may be due to the temperature gradient between the temperature of the dough and the ambient temperature. Again, shear heating effects occur at shear stresses above  $5 \times 10^5$  Pa and this critical value is roughly the same for all the doughs mixed at different temperatures.

In conclusion, analysis of all the flow curves as a function of mixing parameters is difficult because of the presence of shear heating effects. As a result, the data at high shear rates are not considered during the analysis in order to eliminate the shear heating effects. A best line according to the power law model is fitted over the shear stresses at low shear rates. Also, the curve fitted equations of flow of all CA doughs covering the full range of shear rates are obtained. A summary of the results is reported in Table 4.4.

By comparison of the flow parameters, it can be seen that solvent content is the most pronounced factor affecting the rheological properties of CA doughs. The flow behaviour index increases significantly but there is a significant drop in the consistency index with increasing solvent content. It is because some of the intermolecular attraction between CA molecules is broken down due to the presence of solvent molecules. As a result, the CA chains are pushed farther apart, resulting in the corresponding change in  $k$  and  $n$  values.

The flow behaviour index decreases while the consistency index increases in a gradual way as a function of mixing time. As mentioned in Chapter 3, there is a gradual decrease in crystallinity of CA with mixing time. The increase in the amorphous region during mixing will affect the overall degree of solvation of the dough. This may lead to the observed change in the  $k$  and  $n$  values.

The flow parameters of the doughs mixed at 10 °C and 20 °C are reasonably constant, and a slight variation of the flow parameters in the dough mixed at 30 °C is observed. Evaporation of solvent from the surface of the dough as mentioned before may account for this variation. Therefore, it indicates that the mixing temperature is not an important factor governing the flow of CA doughs.

Table 4.3 Variation of the flow parameters and the curve fitted equation of flow as a function of mixing parameters

Composition code	k (10 <sup>4</sup> )	n	curve fitted equation of flow
MT1	4.28	0.55	$Y=3.526+1.985X-0.455X^2$
MT5	5.69	0.49	$Y=3.881+1.602X-0.344X^2$
MT20	5.37	0.46	$Y=4.095+1.221X-0.225X^2$
MT60	6.20	0.46	$Y=3.893+1.541X-0.322X^2$
MT120	9.08	0.36	$Y=4.480+0.929X-0.165X^2$
MC10	5.04	0.49	$Y=3.630+1.774X-0.375X^2$
MC20	5.37	0.46	$Y=4.095+1.221X-0.225X^2$
MC30	8.42	0.41	$Y=3.970+1.532X-0.322X^2$
MS60	22.2	0.33	$Y=4.620+1.285X-0.309X^2$
MS70	5.37	0.46	$Y=4.102+1.213X-0.222X^2$
MS80	2.30	0.50	$Y=3.825+1.114X-0.169X^2$
MS90	0.58	0.69	$Y=3.470+1.034X-0.099X^2$

NOTE:  $Y = \log \tau$   
 $X = \log \dot{\gamma}$

At first, the effect of mixing parameters on the consistency and flow behaviour indices of CA doughs appear to contradict the results of Baker and Carter for NC doughs. A careful consideration of their NC system, however, reveals that there are four components to consider, i.e. fibrous NC, solvent, plasticiser, picrite; while only two components are present in this study. The breakdown of the NC fibres during the mixing process may account for the different variations of both the flow behaviour and consistency indices with mixing parameters as compared with the present results in which no fibrous structure was broken down.

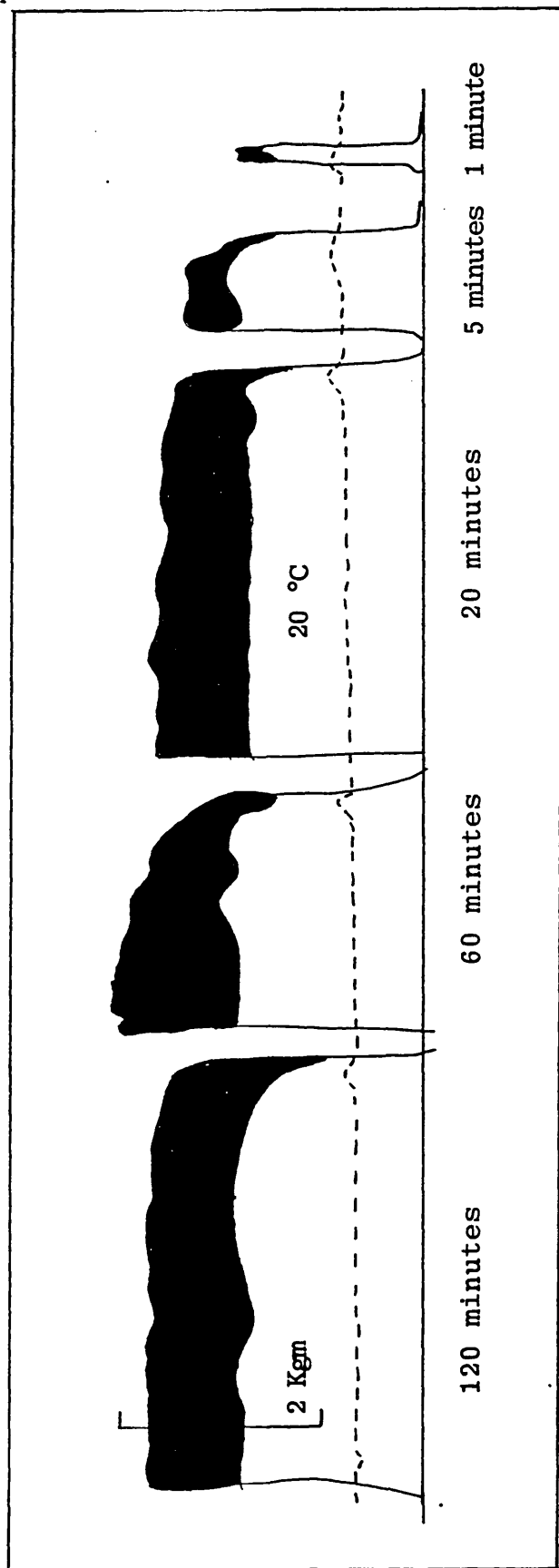


Fig. 4.16 Mixing curves of CA doughs with 70 pph solvent at 20 °C as a function of mixing time

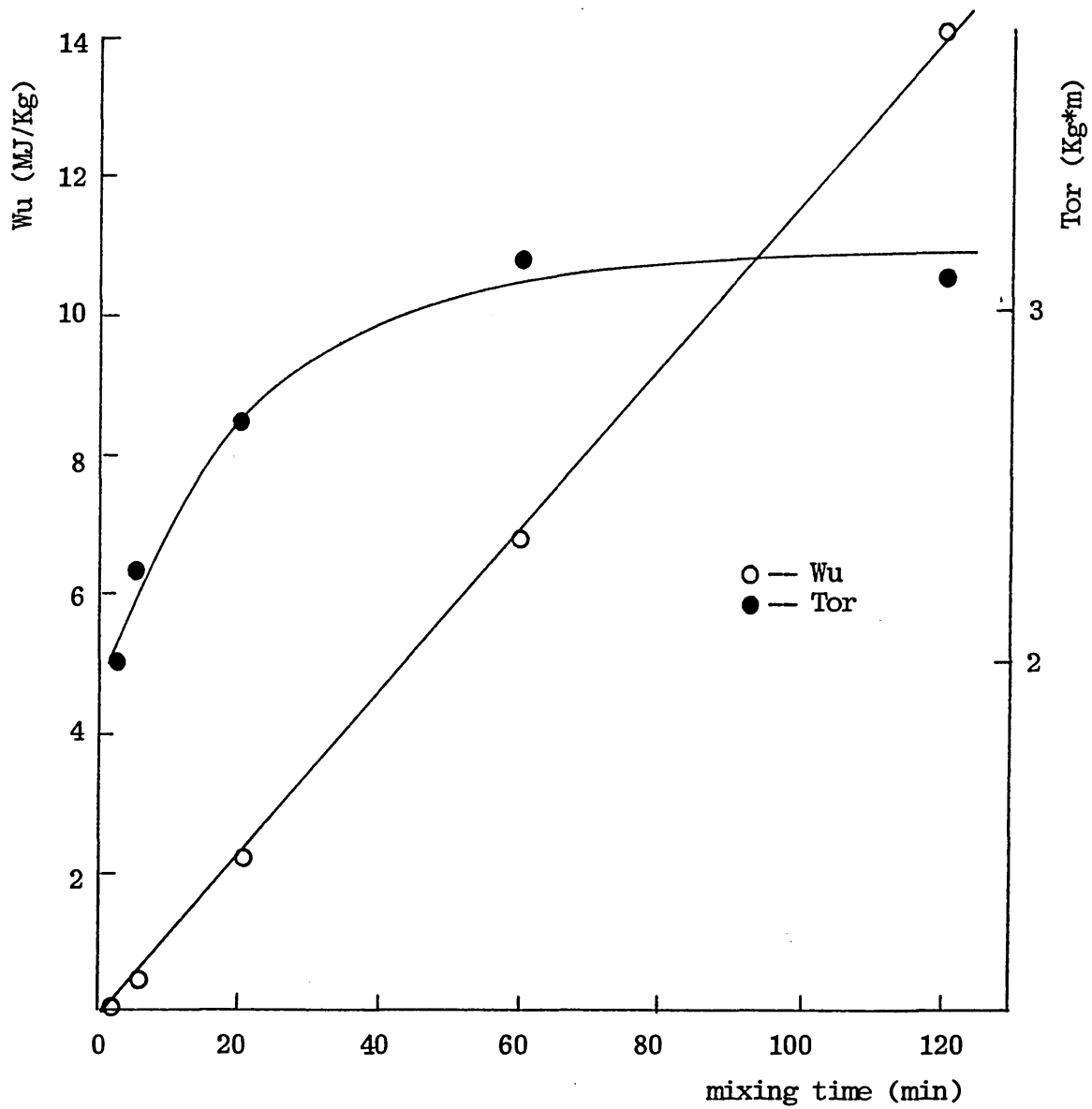


Fig. 4.17 Effect of mixing time on work unit and maximum torque of the mixing curves

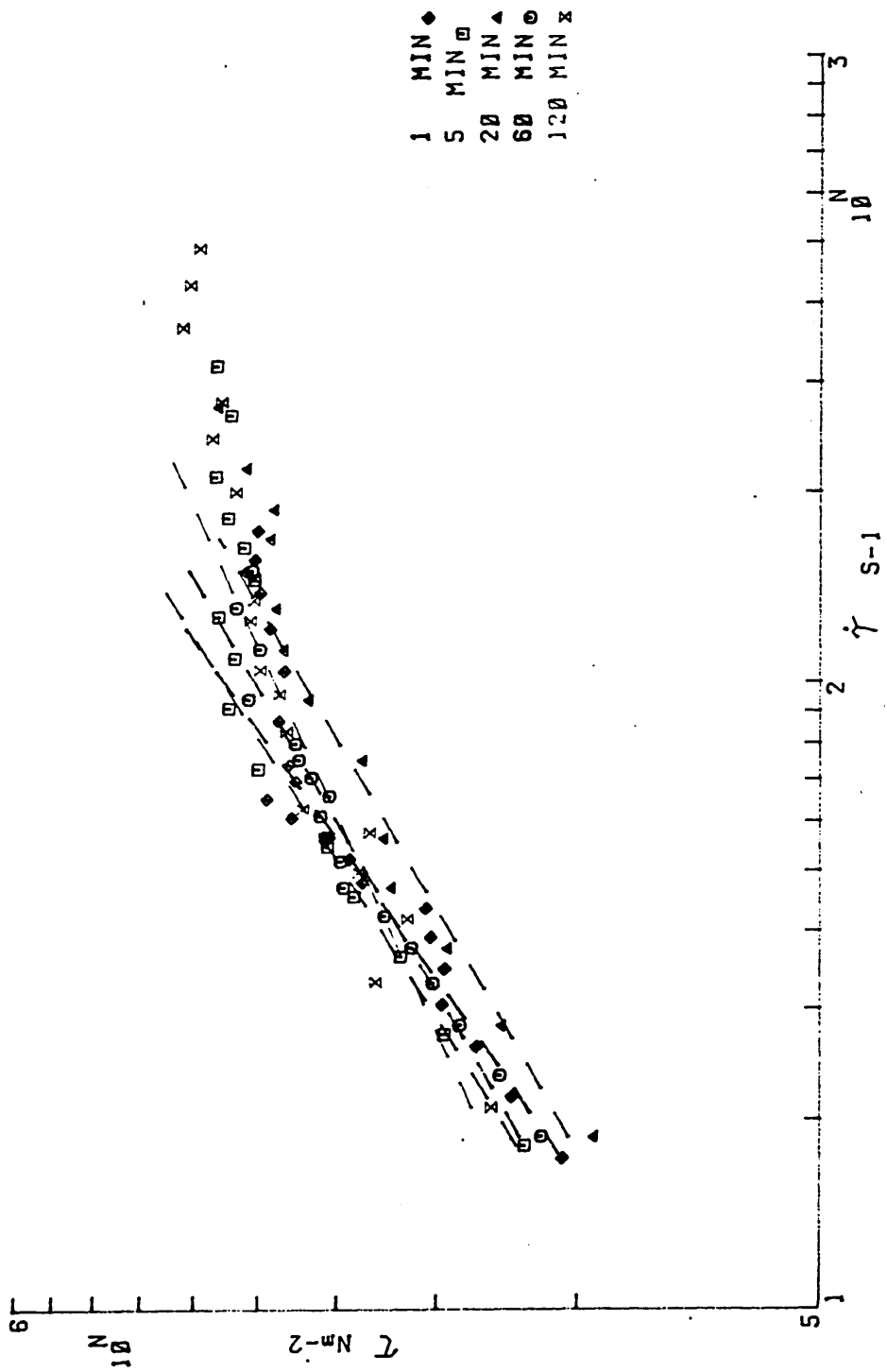


Fig. 4.18 Effect of mixing time on the flow properties of CA doughs at 30°C

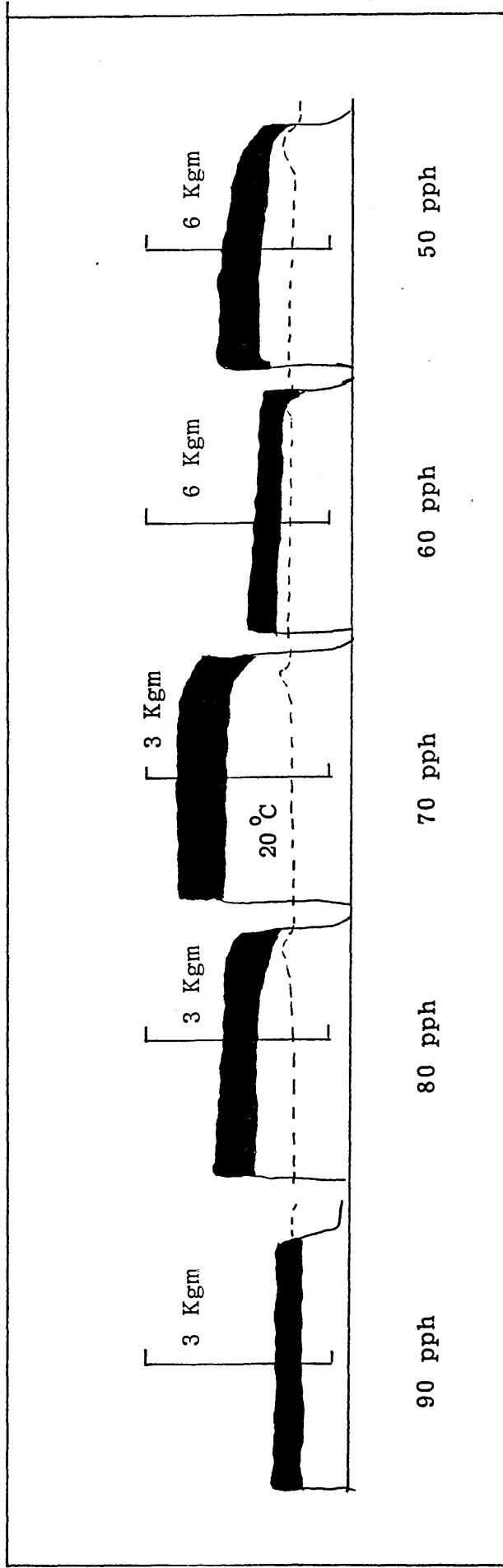


Fig. 4.19 Mixing curves of CA dough at 20°C for 20 minutes as a function of solvent content

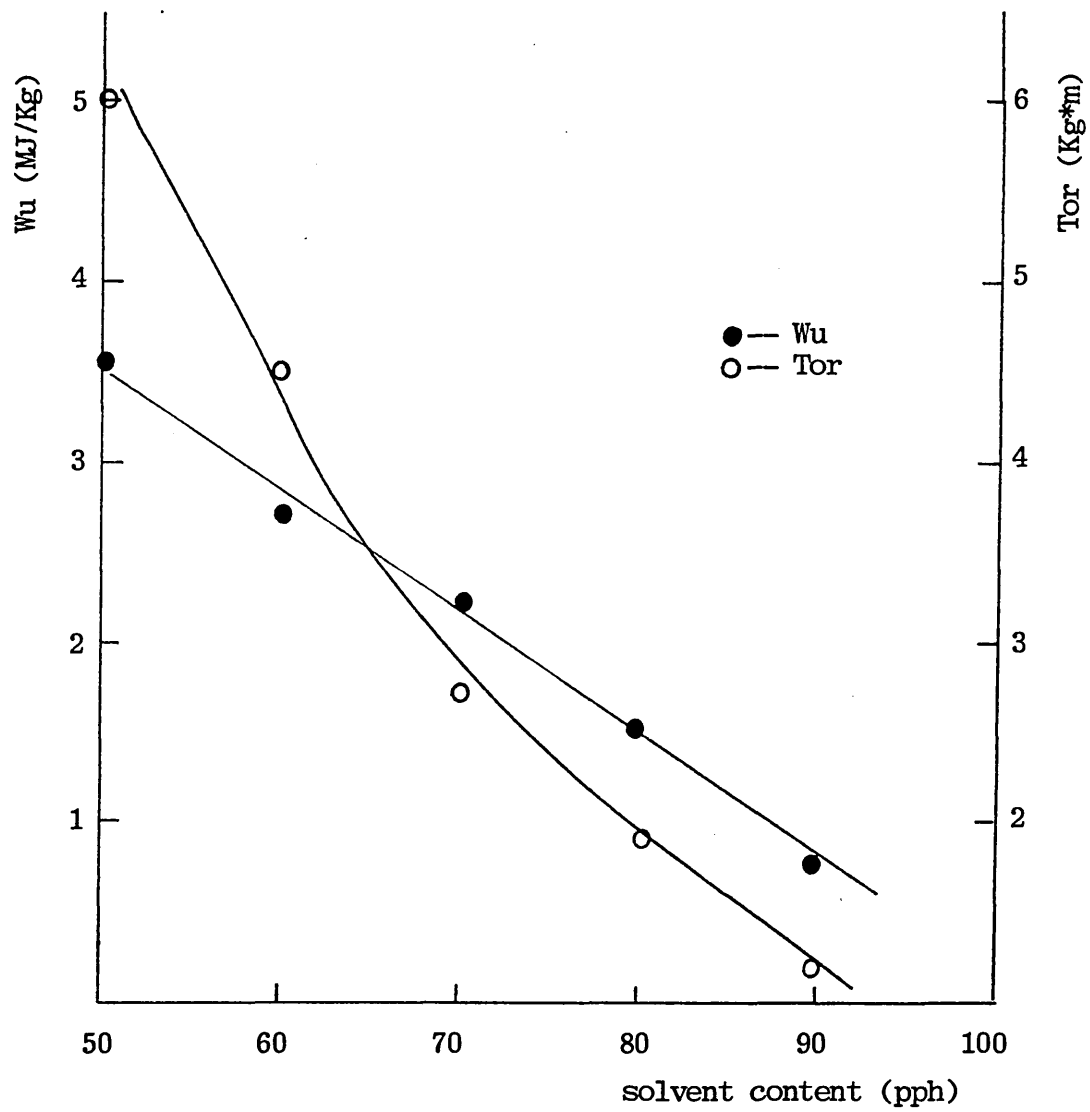


Fig. 4.20 Effect of solvent content on work unit and maximum torque of the mixing curve

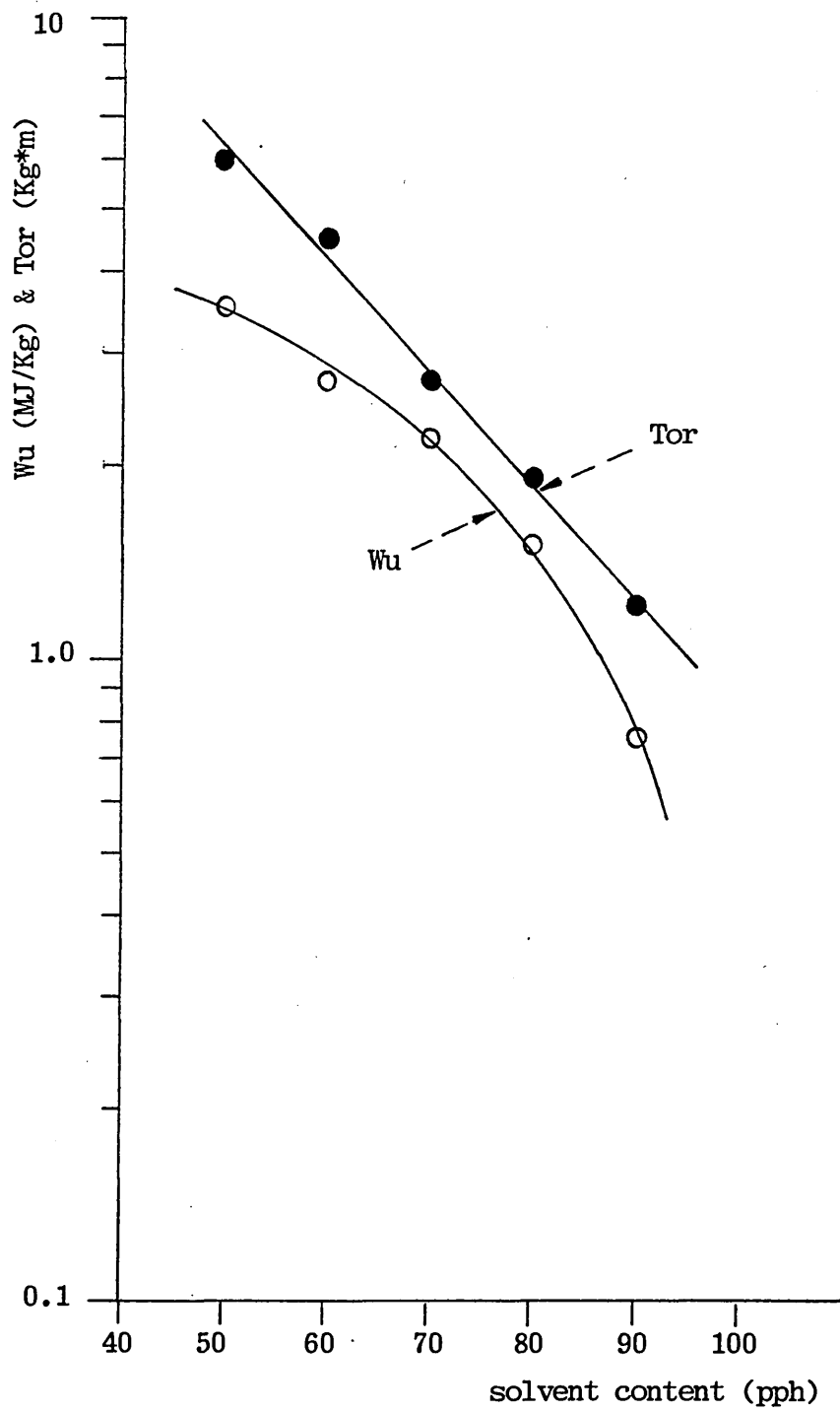


Fig. 4.21 Effect of solvent content on work unit and maximum torque on the linear-logarithmic plots

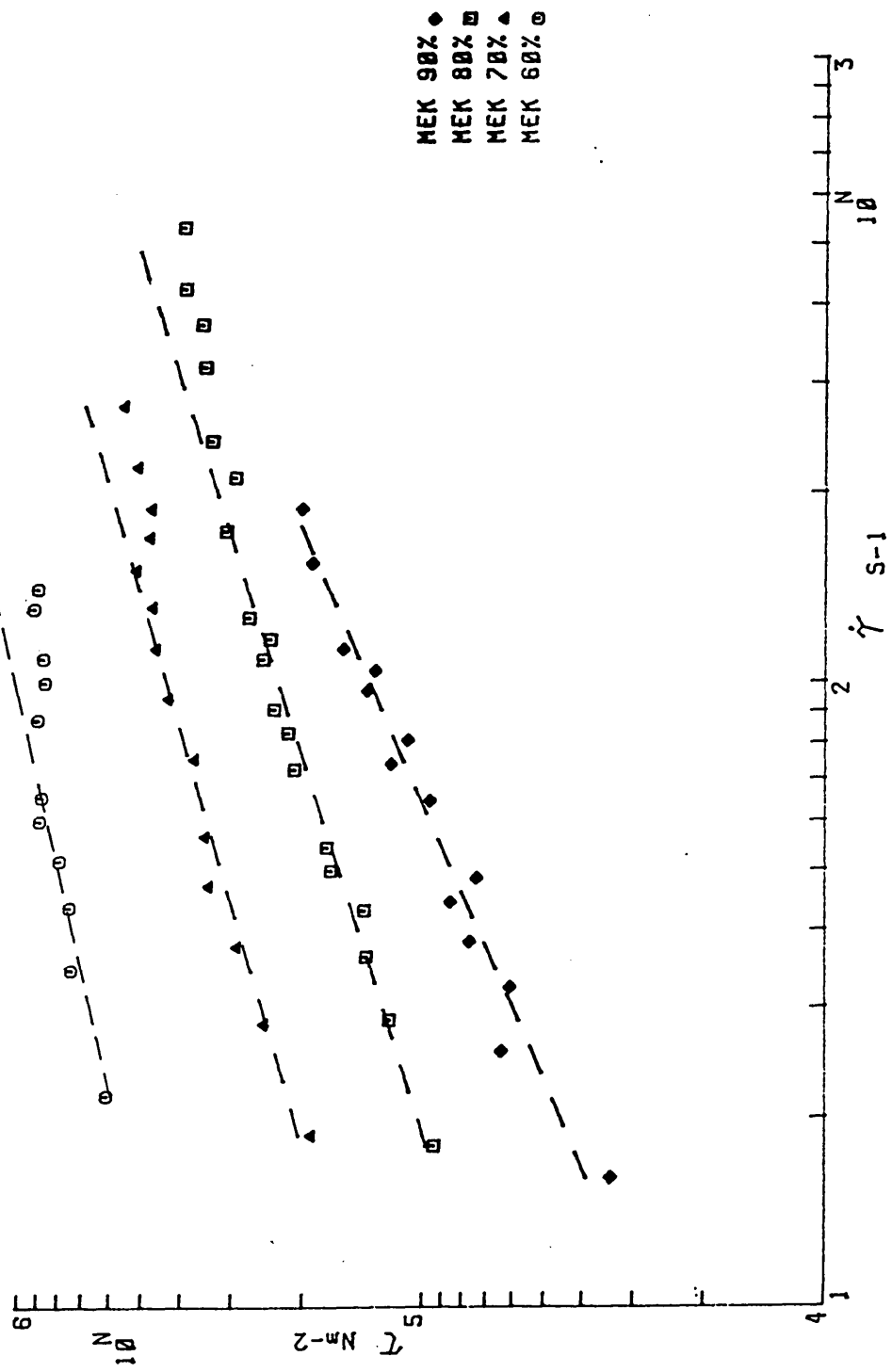


Fig. 4.22 Effect of solvent content on the flow properties of CA doughs at 30°C

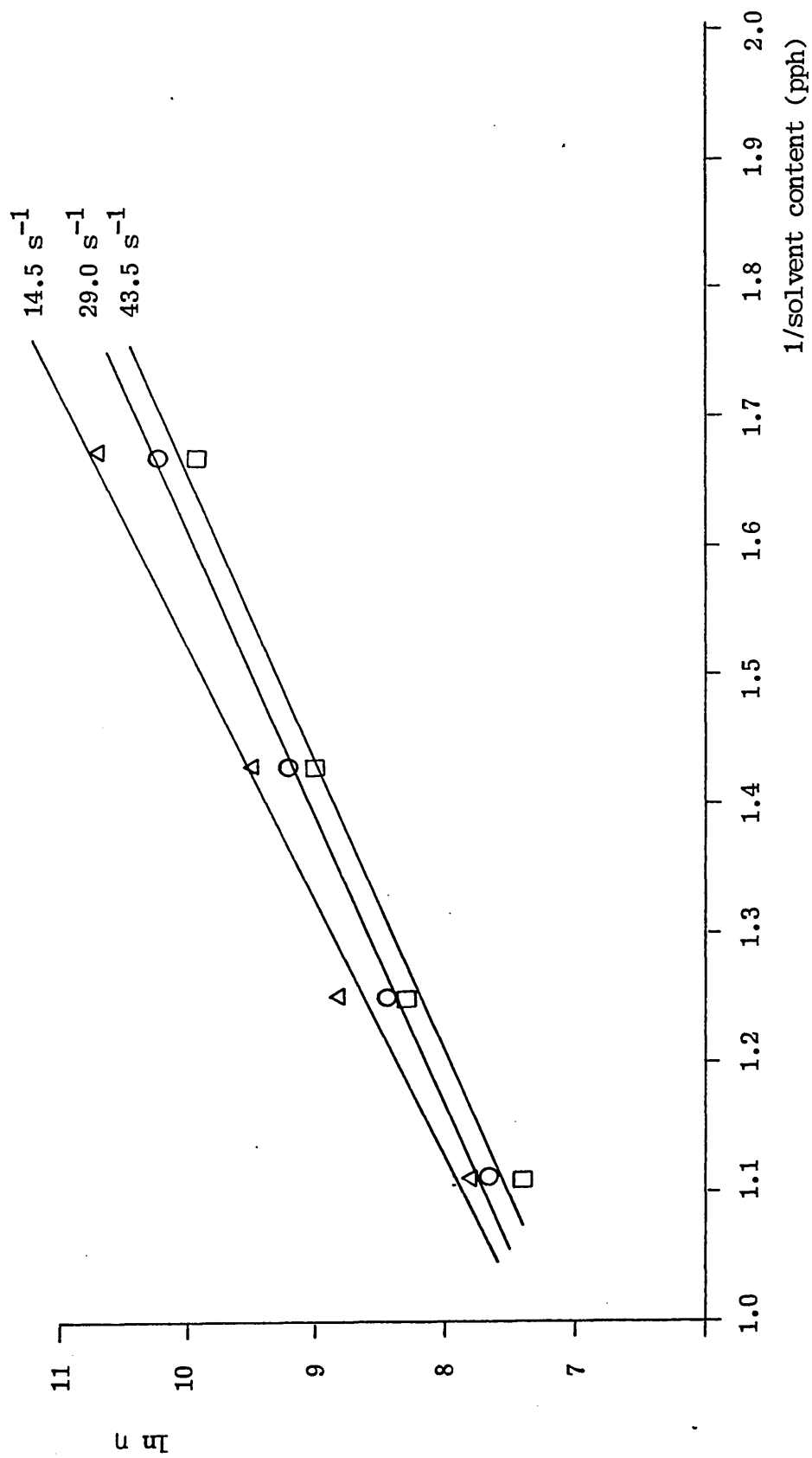


Fig. 4.23 Solvent content dependence of viscosity at constant shear rate

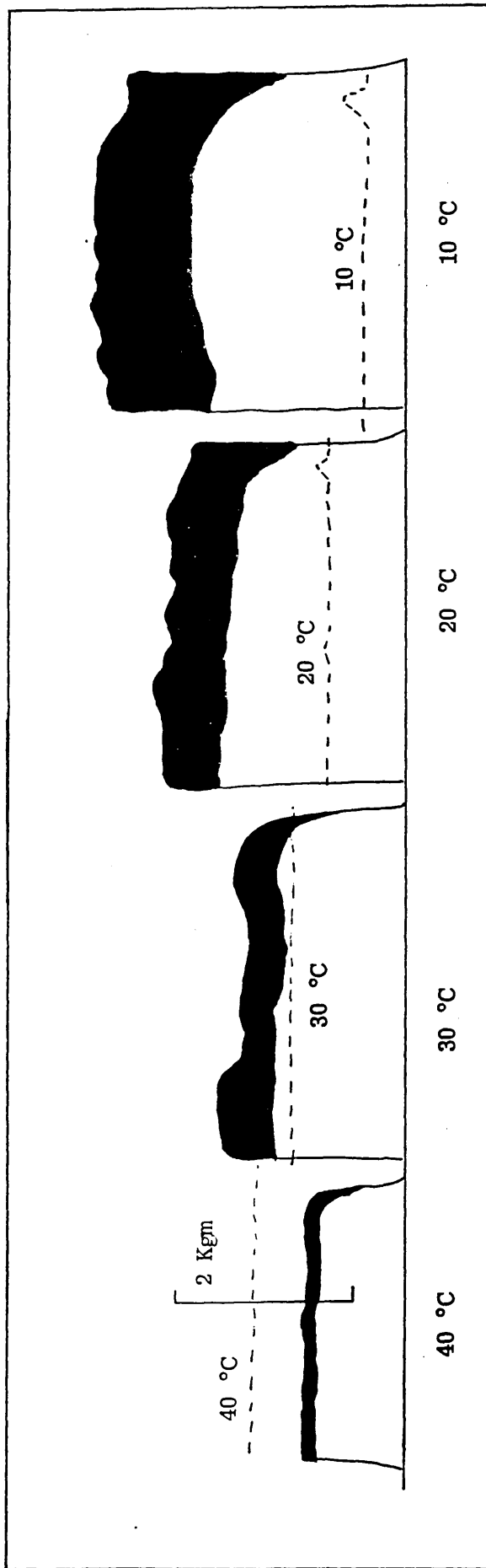


Fig. 4.24 Mixing curves of CA doughs with 70 pph solvent for 20 minutes as a function of mixing temperature

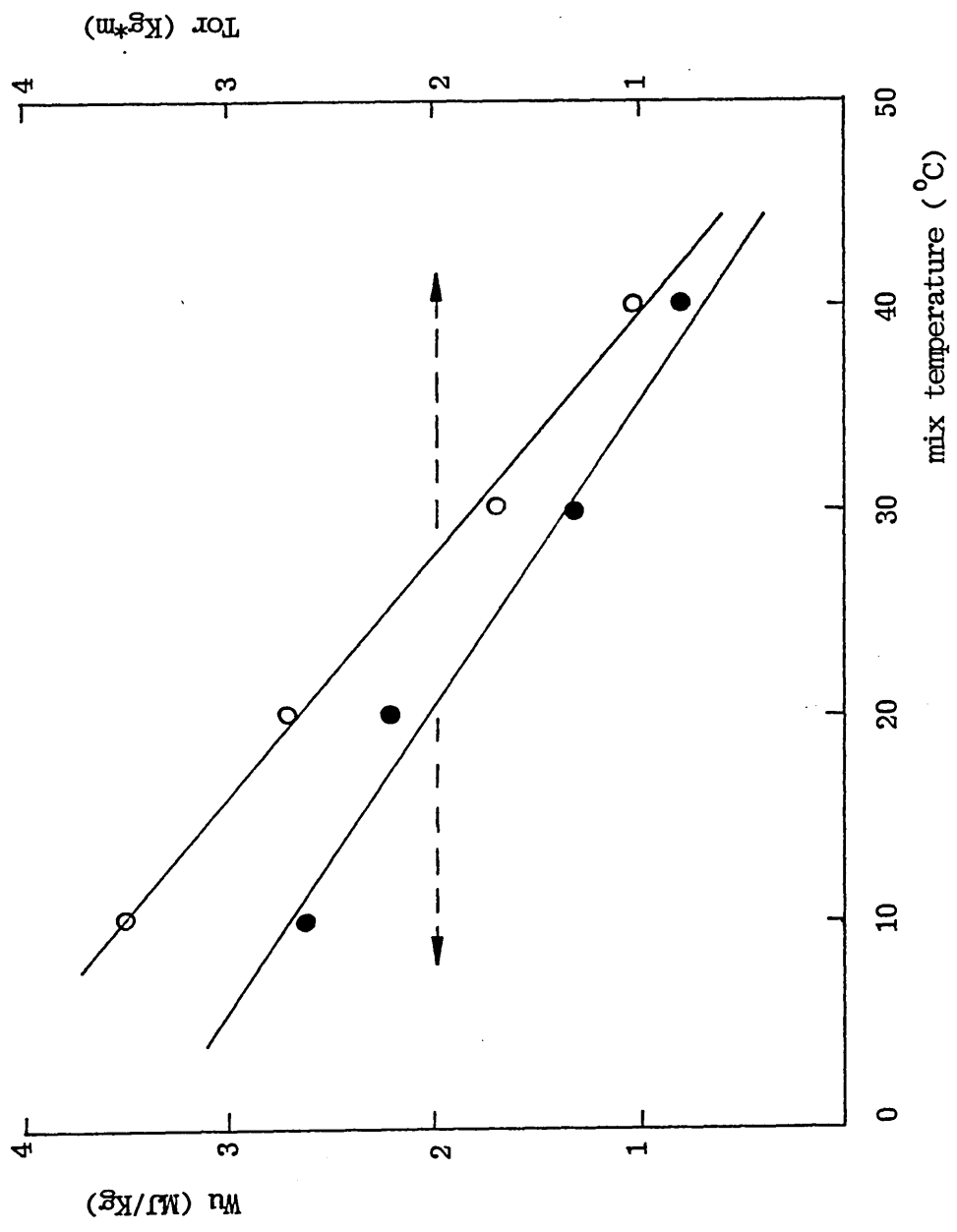


Fig. 4.25 Effect of mixing temperature on work unit and maximum torque of the mixing curve

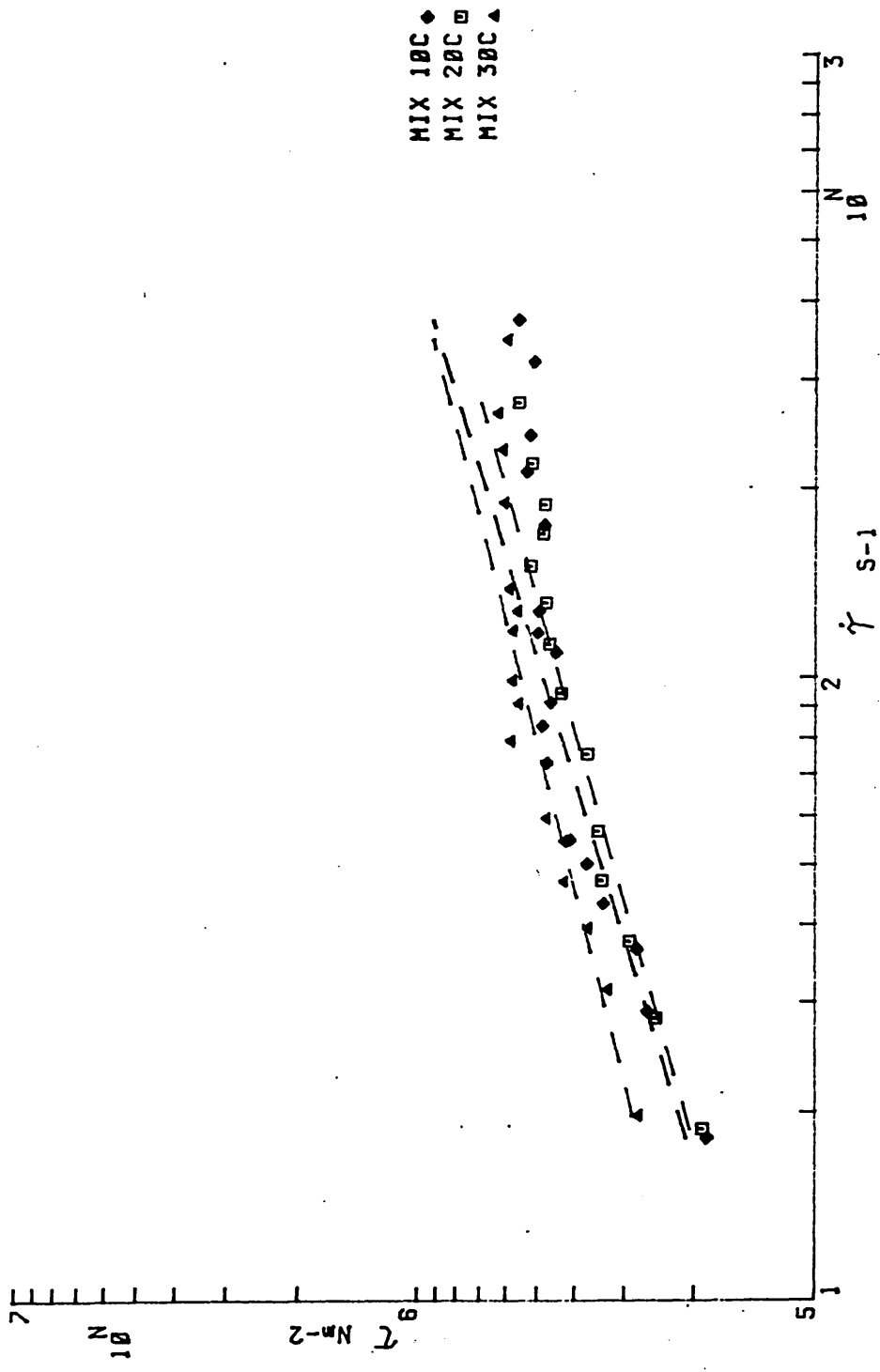


Fig. 4.26 Effect of mixing temperature on the flow properties of CA doughs at 30°C

A mixture of fibrous CA and commercial CA was employed in order to simulate the effect of fibre structure on the flow properties of gun propellants. The fibrous CA was kindly supplied by Pethrick et al (University of Strathclyde). CA doughs containing 80% solvent content were mixed with 1%, 5%, 10% and 15% fibrous CA respectively for 20 minutes at 20°C, and they were extruded at 30°C. It should be noted that solvent content of the dough is based on the weight of both fibrous CA and commercial CA. Both the maximum torque value and the energy required for mixing of the doughs containing different amount of fibre content are fairly constant.

Fig. 4.27 shows the logarithmic flow curves as a function of fibre content in the dough. A dough with no fibrous CA was used as a control in this experiment. This figure shows two important features. Firstly, the overall extrusion pressures of the doughs containing fibrous CA are higher than those of the control. Secondly, there are significant changes in extrusion pressures at lower shear rates, while the pressures remain fairly constant at higher shear rates for the doughs with varying fibrous content. The possible explanation for these phenomena is now discussed. Since fibrous CA is not soluble in the solvent medium, the fibres remain in their original form and act as high aspect ratio fillers inside the dough. They are distributed throughout the dough in a way that provides rigidity to the system upon deformation. Thus, at low shear rate, a higher extrusion pressure is required to break down this internal structure of the doughs. Once a steady flow is maintained, the fibres arrange themselves along the streamlines, resulting in the same flow properties at high shear rates. Analysis of the flow curves reveal that the flow behaviour index decreases gradually while the consistency index increases significantly as a function of fibre content as shown in Fig. 4.28. The curve fitted equations of flow of these doughs are summarized in Table 4.5.

Table 4.5 Curve fitted equation of flow for doughs containing various amount of fibrous CA

Fibre content /%	curve fitted equation of flow
0	$Y=3.825+1.114X-0.169X^2$
1	$Y=3.991+0.943X-0.100X^2$
5	$Y=3.774+1.306X-0.226X^2$
10	$Y=3.693+1.458X-0.280X^2$
15	$Y=4.505+0.603X-0.054X^2$

Where  $Y = \log \tau$  and  $X = \log \dot{\gamma}$

Despite the relationship between consistency index and fibre content, there is no direct evidence that a yield stress is likely to occur in doughs with fibrous structures because the rheometer used is not capable of reproducing accurately slow piston speeds, which is essential in order to determine the yield stress. A complementary experiment was carried out at Waltham Abbey to study the relationship between yield stress and fibre content. Doughs containing 20% fibrous CA with 80% solvent content were extruded at 30°C. The apparent flow curves are shown in Fig. 4.29. Again, the flow curve is in good agreement with those curves as shown in Fig. 4.27. The apparent yield stresses for CA doughs containing 0% and 20% fibrous CA were found to be 19.7 and 40.0 kPa respectively, confirming that a fibrous structure inside the dough is essential to give rise to high yield stress values. The logarithmic plot of  $(\tau - \tau_y)$  against  $\dot{\gamma}$  is linearised at low shear rate as shown in Fig. 4.29, indicating the presence of a yield stress responsible for the deviation of flow curve at low shear rates.

CA/MEK doughs containing 5% fibrous CA were mixed for 20 and 60 minutes, and the corresponding flow curves are shown in Fig. 4.30. This figure shows that the flow properties of the doughs are independent of the mixing times. In a similar study, Baker et al observed a change in the rheological properties of the NC system

as a result of the breakdown of the fibrous structure. However, this effect is unlikely to occur in this study because MEK does not dissolve fibrous CA. Therefore, fibrous CA retains its original fibrous structure after the mixing process, and thus the rheological properties of the fibrous doughs under different incorporation times is very similar.

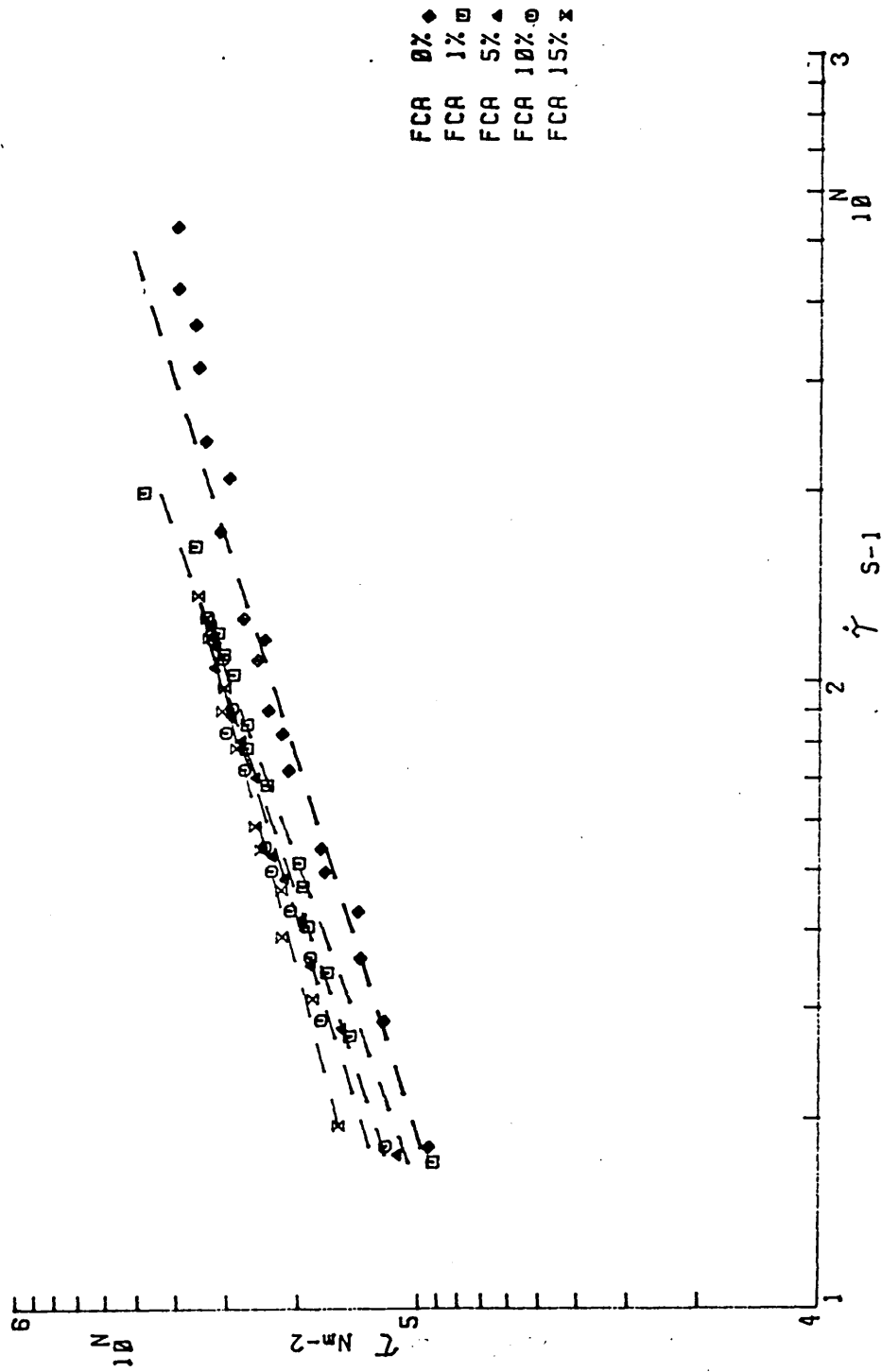


Fig. 4.27 Effect of fibrous CA content on the flow properties of CA doughs at 30°C

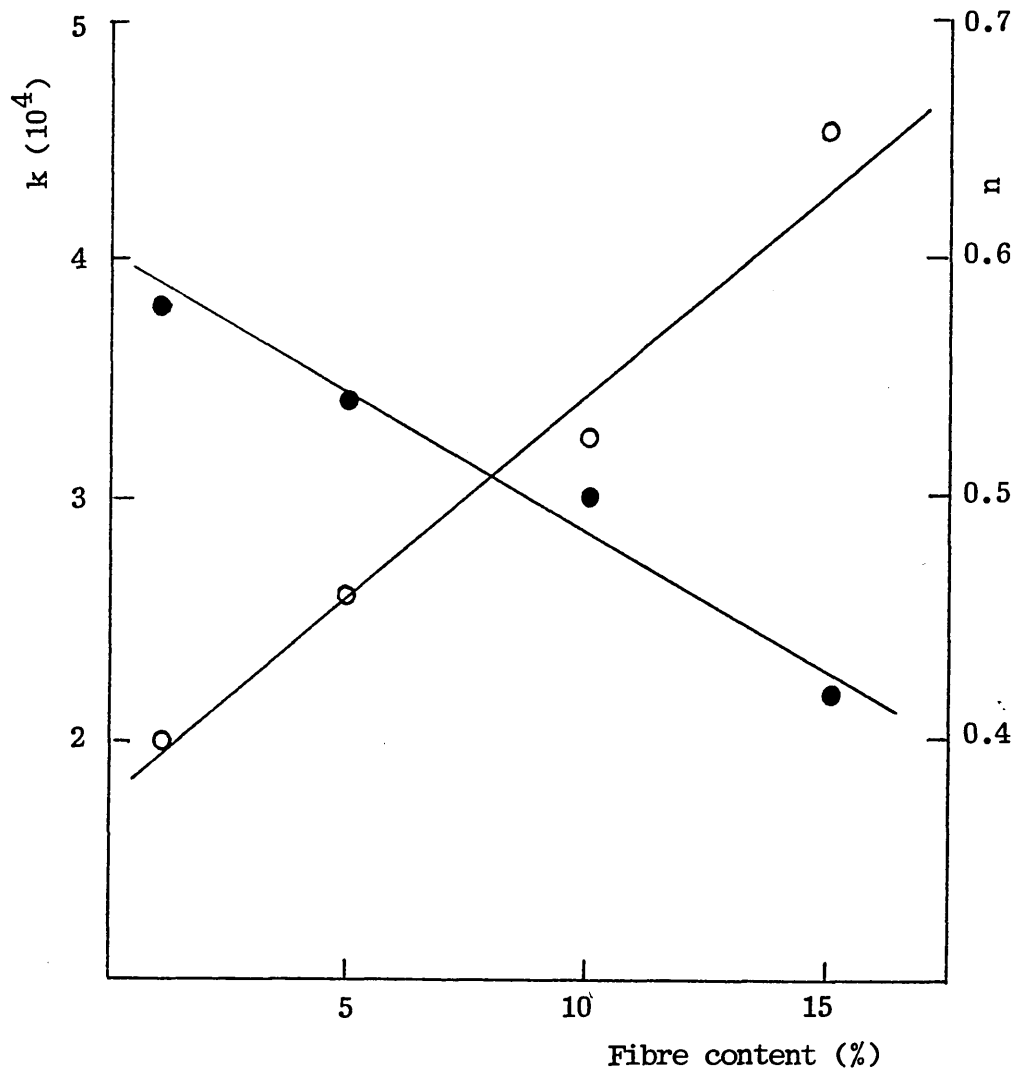


Fig. 4.28 Variation of the flow behaviour index and consistency index as a function of FCA

○ —  $k$     ● —  $n$

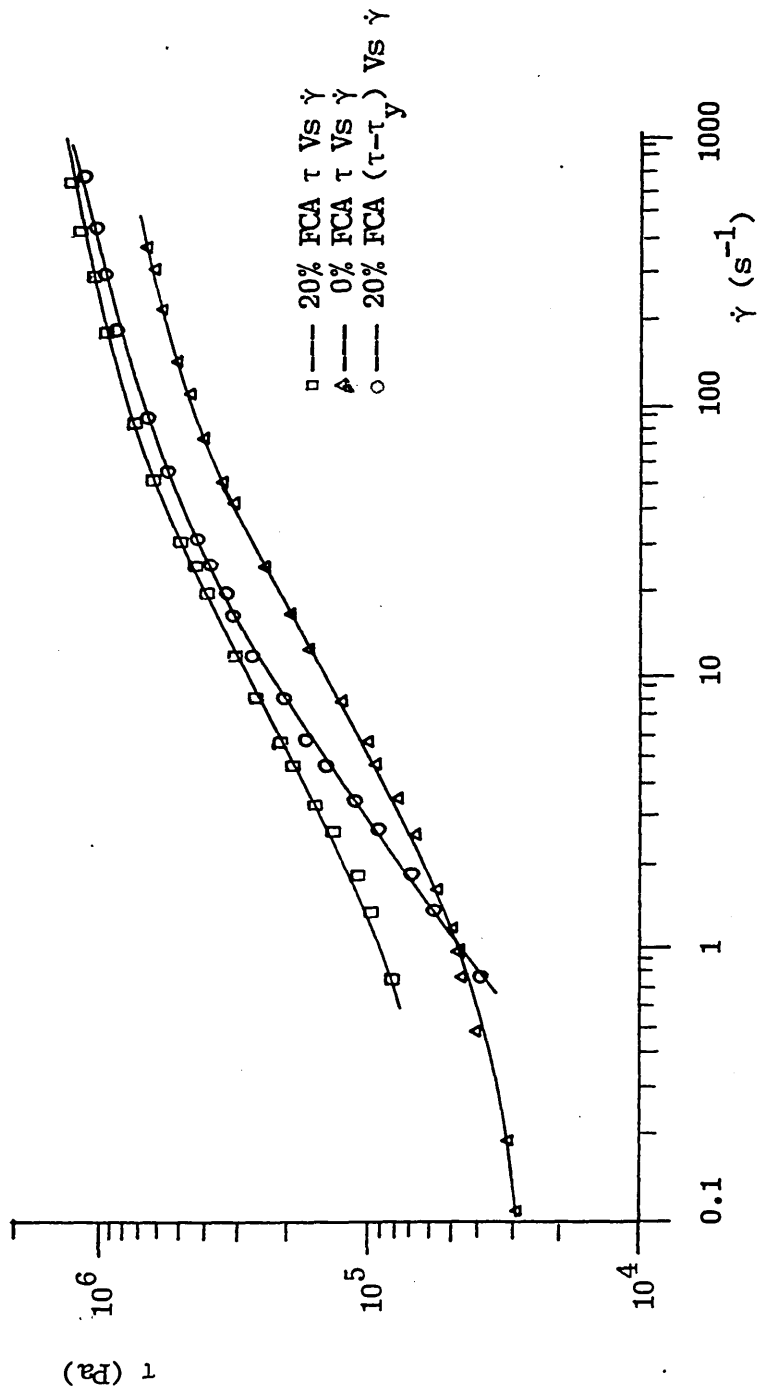


Fig. 4.29 Apparent flow curve of CA doughs containing 0% and 20% fibrous CA

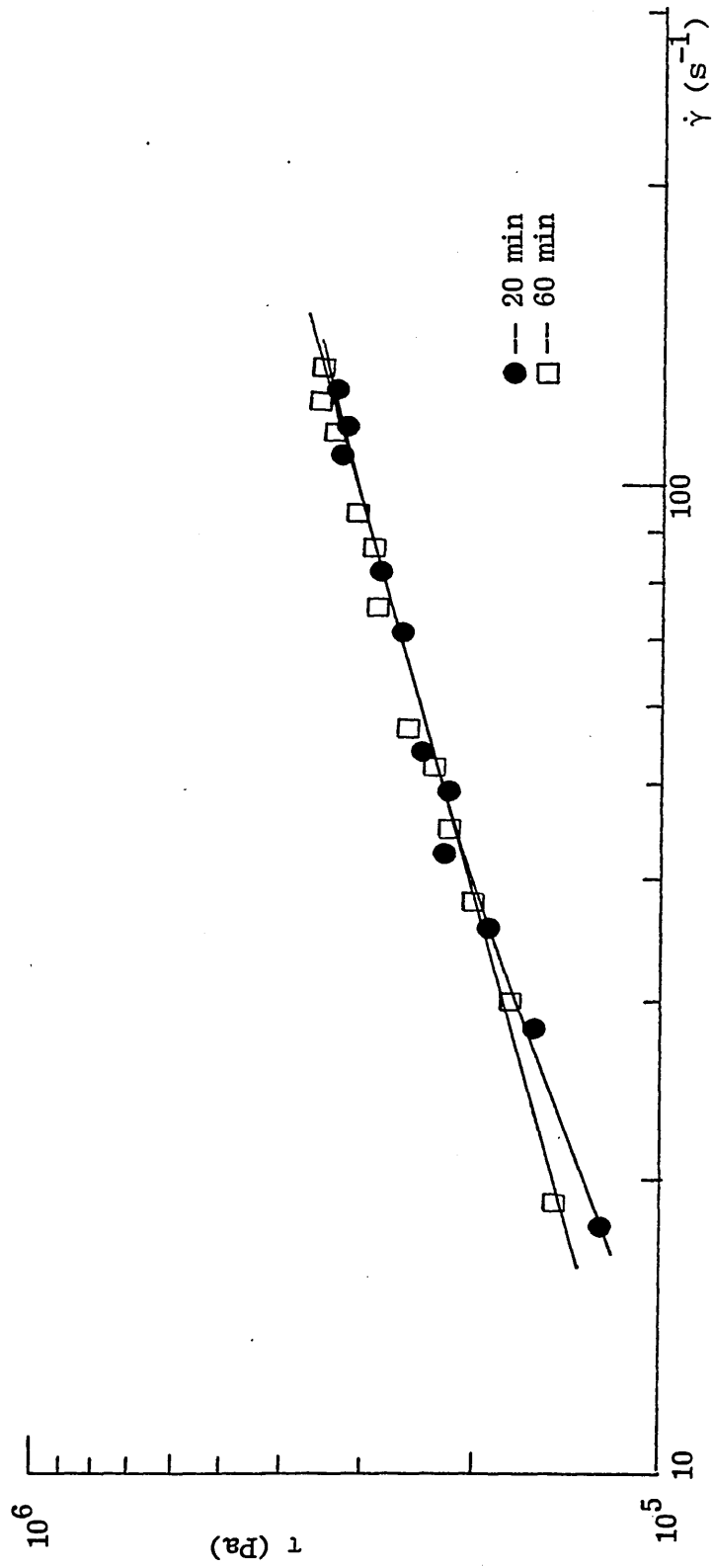


Fig. 4.30 Effect of mixing time on the flow properties of cellulose acetate doughs containing 5% fibrous cellulose acetate

#### 4.8 Effect of plasticisers

To establish the effect of plasticisers on the flow properties of CA doughs, three plasticisers namely dimethyl phthalate (DMP), diethyl phthalate (DEP) and dibutyl phthalate (DBP) were used. Again, details of the mixing conditions and the composition codes are summarized in Table 4.6. Rheological assessments of the test doughs was partly carried out at the Royal Ordnance Factory and the Sheffield City Polytechnic.

Table 4.6 Composition code and mixing condition of plasticised CA doughs

Composition code	DMP /pph	DEP /pph	DBP /pph	Other mixing conditions
MS80	/	/	/	time = 20 min
MP10	10	/	/	
EP10	/	10	/	
BP5	/	/	5	solvent = 80 pph
BP8	/	/	8	
BP10	/	/	10	
BP20	/	/	20	temperature = 20°C
BP30	/	/	30	

Fig. 4.31 shows the apparent flow curves of four doughs, in which three of them contain the same amount of different types of plasticiser. The remaining dough contains no plasticiser and is used as a control only. It can be seen from this figure that the extrusion pressure of the doughs containing 10 pph of DMP and DEP respectively is lower than that of the control for a given extrusion rate. On the other hand, a much higher extrusion pressure is required with doughs containing 10 pph of DBP than for the control, and this was corroborated by the work unit used in the incorporation of the doughs with different types of plasticiser (Table 4.7). Analysis of the apparent flow curves as a function of different types of plasticiser showed that the flow behaviour index remained reasonably constant. The yield stress and the consistency index of the doughs containing DMP or DEP are slightly lower than that of the control. However, there is a significant increase in the yield stress and the consistency index of the dough containing DBP. These results may lead to a

conclusion that DMP and DEP act as a plasticiser while DBP acts as an anti-plasticiser for CA doughs.

Table 4.7 Variations of work unit and apparent flow parameters with different types of plasticiser

Composition code	Work unit /MJ/Kg	n	k /kPa	$\tau_y$ /kPa
MSSO	0.979	0.605	28.7	19.7
MP10	0.603	0.560	19.0	17.4
EP10	0.752	0.580	20.4	11.7
BP10	1.170	0.540	156	49.5

The reasons for this phenomenon are not clearly understood. It may be due to the difference in the compatibility of DMP, DEP and DBP with CA in the presence of MEK. As mentioned in Chapter 1, a three-dimensional approach to the solubility of CA has been set up by Crowley [26] in which the solubility parameter ( $\delta$ ) and dipole moment ( $\mu$ ) are plotted on the X and Y axis respectively, and hydrogen bonding values ( $\gamma$ ) are plotted as contour lines. Three solubility maps are required in order to describe the solubility of CA in solvents or solvent mixtures having  $\gamma$  from 0-5 (Fig. 4.32), 5-9 (Fig. 4.33), and 9-13 (Fig. 4.34). In predicting the solubility of CA in solvents or solvent mixtures by this model, the solubility parameter and dipole moment coordinates of the solvent or solvent mixture is located on the solubility map. If the map in Fig. 4.32 or 4.33 is used, and the hydrogen bonding read from the map is less than the hydrogen bonding of the solvents or solvent mixture, then this solvent or solvent mixture will dissolve CA. However, if Fig. 4.34 is used and the hydrogen bonding from the map is less than the hydrogen bonding of the solvent or solvent mixture, then this solvent or solvent mixture will not dissolve CA.

In the experimental determination of solubility, CA and solvent in a concentration of 1g/dl was made up, and this mixture was shaken occasionally for 48 hours at 25<sup>o</sup>C. A variety of solvents with the three solution parameters as shown in Table 4.8 were used. In

studying the solubility behaviour of CA, six solvents with values of solubility parameter in the range  $19.8 \pm 1.0$  were used, namely methyl formate, acetone, ethyl lactate, methylene chloride, methyl ethyl ketone and chloroform.

Table 4.8 Solubility test of cellulose acetate in various organic solvent

Solvent	3-D solution parameters			Solubility
	solubility parameter	hydrogen bonding	dipole moment	
Propylene carbonate	27.2	4.9	1.0	PS
N,N-Dimethyl formamide	24.7	11.7	3.8	S
Methyl formate	20.9	8.4	1.9	S
Acetone	20.4	9.7	2.9	S
Ethyl lactate	20.4	7.0	1.9	S
Methylene chloride	19.8	1.5	1.5	I
Methyl ethyl ketone	19.0	7.7	2.7	PS
Chloroform	19.0	1.5	1.2	I

Note -- PS = partly soluble  
 S = soluble  
 I = insoluble

From Table 4.8, the existence of a homogenous solution was only observed in solvents with moderate hydrogen bonding values such as methyl formate and acetone. As the hydrogen bonding number decreases gradually, there is a transition from a partially soluble state to an insoluble state, as in the case of MEK, chloroform and methylene chloride respectively. Therefore, it is clear that hydrogen bonding plays an important part in determining the solubility of CA, and the most active solvents for CA are those with moderate hydrogen bonding. Also, it should be noted that propylene carbonate and N,N-dimethylformamide which have solubility parameters of 27.2 and 24.7  $(\text{MJ/m}^3)^{0.5}$  respectively are normally thought to be non-solvents of CA. However, N,N-

dimethylformamide with a relatively higher hydrogen bonding value dissolves CA to form a solution with an intrinsic viscosity of 1.2 dl/g, which is greater than that of acetone (1.1 dl/g). This result suggests that N,N-dimethylformamide is a better solvent than acetone. Therefore, the use of the three-dimensional approach to solubility is essential and, indeed, the results from the solubility test agree very well with the prediction from the solubility maps as mentioned above.

It should be noted that the three-dimensional approach can be extended for use in the polymer-plasticiser system. However, there is no information regarding the hydrogen bonding values for the plasticisers used in this project, from the literature survey. However, a rough idea can be obtained from the molecular structure of the plasticisers. In general, Gordy showed that organic solvents are largely proton acceptors with their order being amines > ethers > ketones > esters > nitro compounds [116]. The typical hydrogen bonding value of MEK (ketone series) and nitrobenzene are 7.7 and 2.8 respectively. Thus, it would be expected that the hydrogen bonding values of DMP, DEP and DBP should lie between these two values. It should also be noted that the hydrogen bonding values of different types of plasticiser decrease in the order DMP > DEP > DBP because of the electron donating power of the alkyl groups. Again, this reasoning is supported by considering the hydrogen bonding values of ACE (9.7) and MEK (7.7).

The solubility maps as shown in Fig. 4.32 and 4.33 reveal that as the hydrogen bonding number decreases (i.e. from DMP to DBP), a progressively higher solubility parameter is necessary for the compatibility of plasticiser with CA. However, it should be noted that the solubility parameters of phthalatic plasticisers decrease with the increasing length of alkyl groups as shown in Table 4.9 [117].

Table 4.9 Solubility parameters of phthalatic plasticisers

plasticiser	$\delta / (\text{MJ/m}^3)^{0.5}$
DMP	21.5
DEP	20.4
DPP	19.8
DBP	19.2
DOP	17.8

As a result, the compatibility of plasticiser with CA decreases in the order of DMP, DEP and DBP as mentioned in Chapter 1. Since DMP is compatible with CA, the introduction of this plasticiser into the solvated dough will further increase the hydrodynamic volume of CA and hence a normal plasticisation effect is observed. As DBP is semi-compatible with CA, there is no direct affinity between these two components. As a result the DBP molecules have to distribute themselves homogeneously throughout the dough by the physical interactions between DBP molecules and solvent molecules because of the similarity in the values of their solubility parameters. Since the affinities of some of the solvent molecules are expended on the plasticiser, the overall effective solvent content for CA is lowered, resulting in a poor gelatinisation of the dough and a consequent increase in the viscosity of the dough. Thus, it should be expected that the doughs containing DMP should have a higher die swell value than the doughs containing DBP because of the difference in the extent of gelatinisation. Indeed, this argument is further supported by the experimental results in which die swell is plotted against shear stress for doughs with different types of plasticiser, as shown in Fig. 4.35. This figure shows that the doughs with DMP have slightly higher die swell values than the doughs with DEP. However, significantly smaller die swell values are observed in poor gelatinised doughs with DBP.

In order to understand the flow mechanism of plasticised CA dough, a series of doughs containing different amounts of DBP were studied, and their flow curves are shown in Fig. 4.36. The flow

parameters and the curve fitted equations of flow of these doughs are given in Table 4.10.

Table 4.10 Variation of the flow parameters and the curve fitted equations for flow as a function of DBP content

Composition code	k (10 <sup>4</sup> )	n	curve fitted equation
BP5	4.72	0.45	$Y=4.045+1.182X-0.208X^2$
BP8	5.15	0.45	$Y=4.318+0.926X-0.142X^2$
BP10	4.97	0.44	$Y=4.092+1.140X-0.194X^2$
BP20	8.22	0.28	$Y=4.776+0.432X-0.042X^2$

Where  $Y = \log \tau$  and  $X = \log \dot{\gamma}$

Again, a plot of logarithmic viscosity versus reciprocal plasticiser concentration shows that the viscosity increases as the concentration of DBP in the dough increases, indicating the phenomenon of antiplasticisation, and there is an inversion at the plasticiser concentration of about 8 pph, after which the viscosity decreases with increasing plasticiser concentration (Fig. 4.37). This observed inversion may be due to slip at the die wall, and is reflected by the low value of the flow behaviour index of the dough containing 20% DBP. The reason for this may involve the displacement of the complex between DBP and solvent molecules from the dough, particularly at high extrusion rates, due to the widely different absorption characteristics of DBP in CA. This argument is further supported by the experimental result that poorly gelatinised doughs are formed when the DBP concentration is 30 pph or above. During extrusion, it was observed that some liquid dripped out of the die when the extrusion started. The extrudate was also opaque with poor mechanical properties, showing poor gelatinisation.

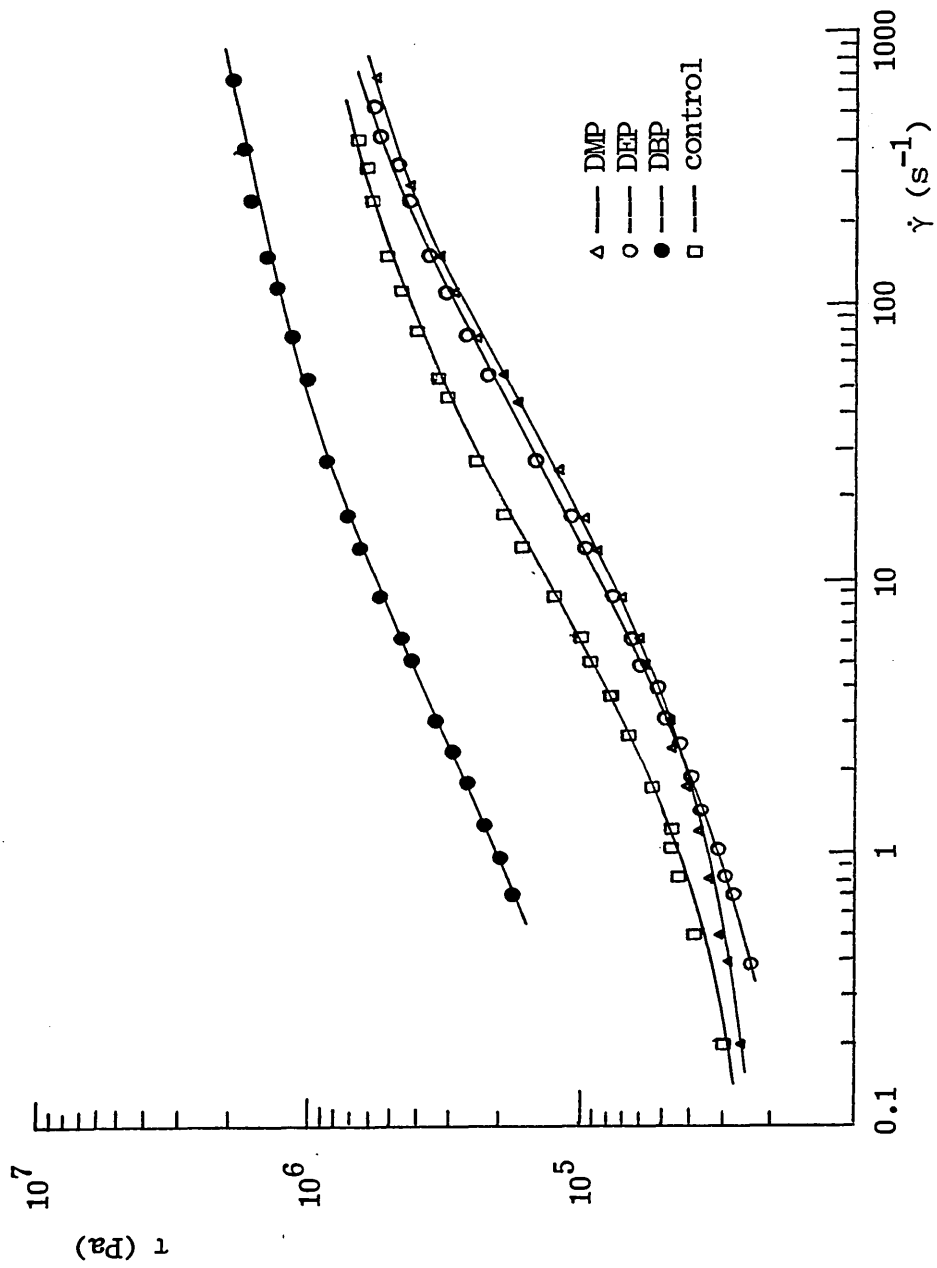


Fig. 4.31 Apparent flow curves of CA doughs with different type of plasticisers

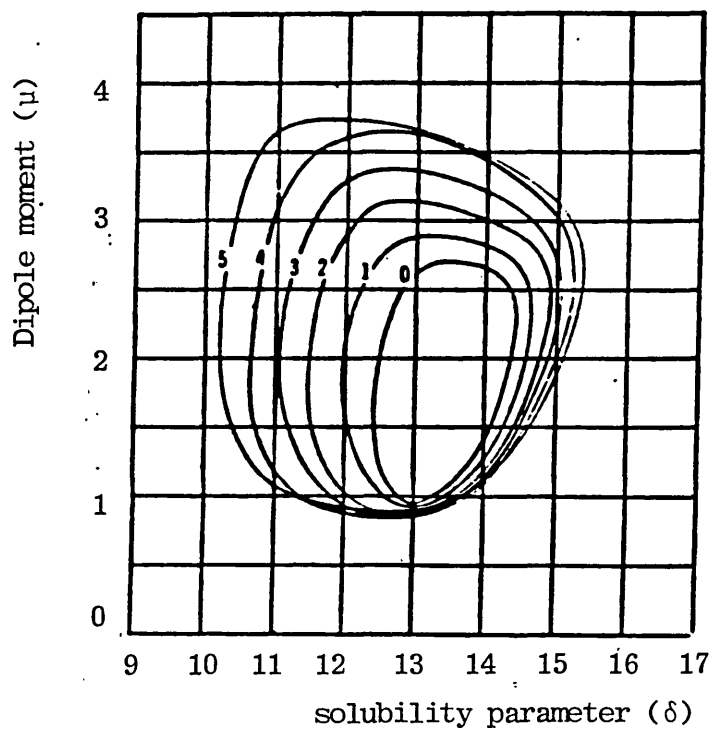


Fig. 4.32 Solubility map of CA with hydrogen bonding values from 0 to 5 ( After Crowley et al )

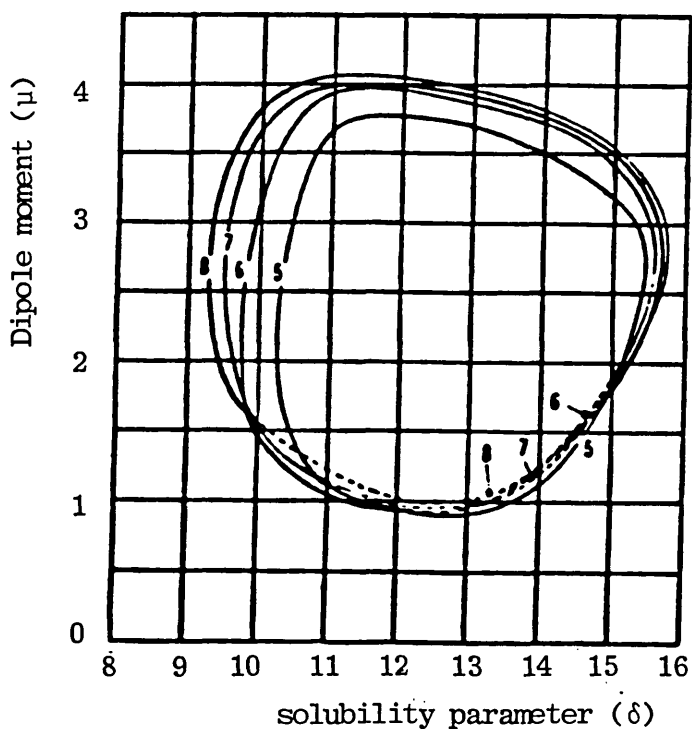


Fig. 4.33 Solubility map of CA with Hydrogen bonding values from 5 to 8 ( After Crowley et al )

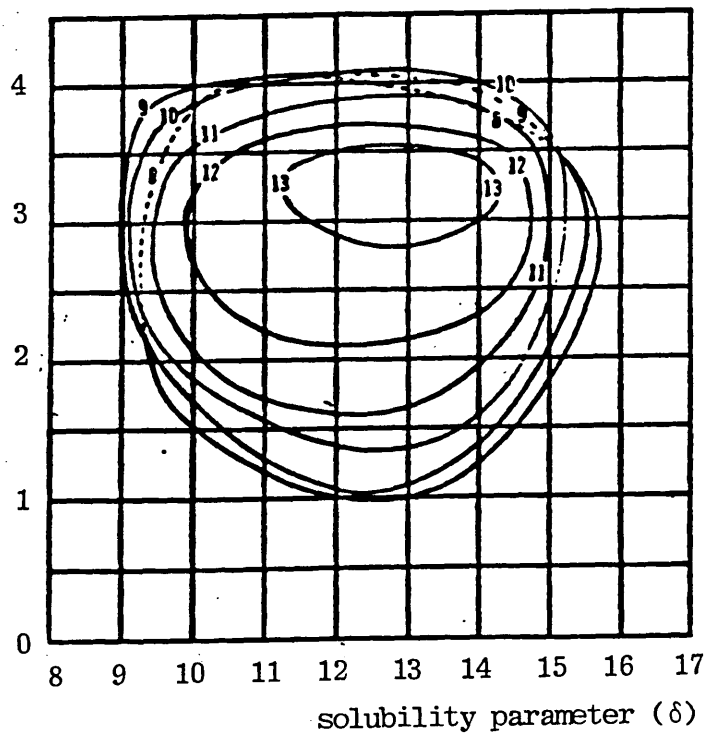


Fig. 4.34 Solubility map of CA with hydrogen bonding values from 9 to 13 ( After Crowley et al)

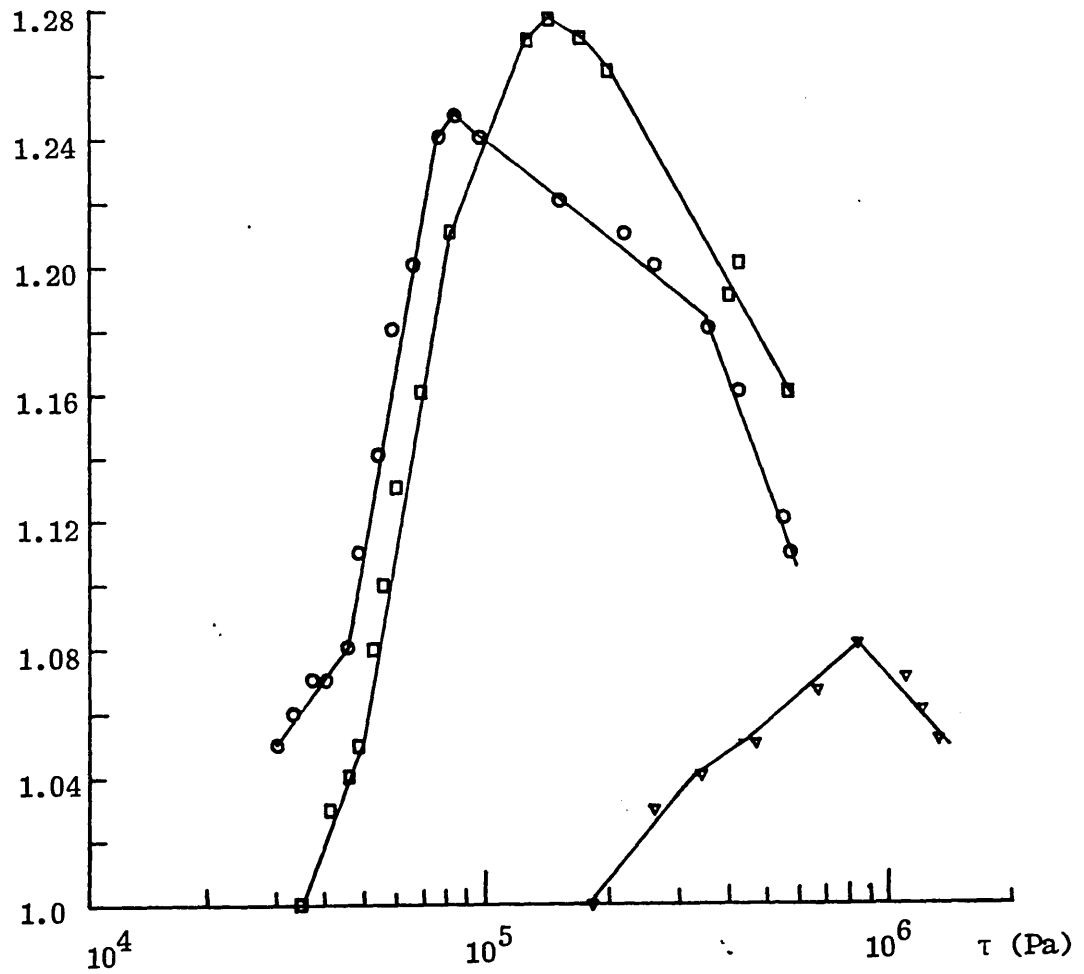


Fig. 4.35 Effect of the nature of plasticiser on swell ratio  
 $\square$  — 10% DMP    $\circ$  — 10% DEP    $\nabla$  — 10% DBP

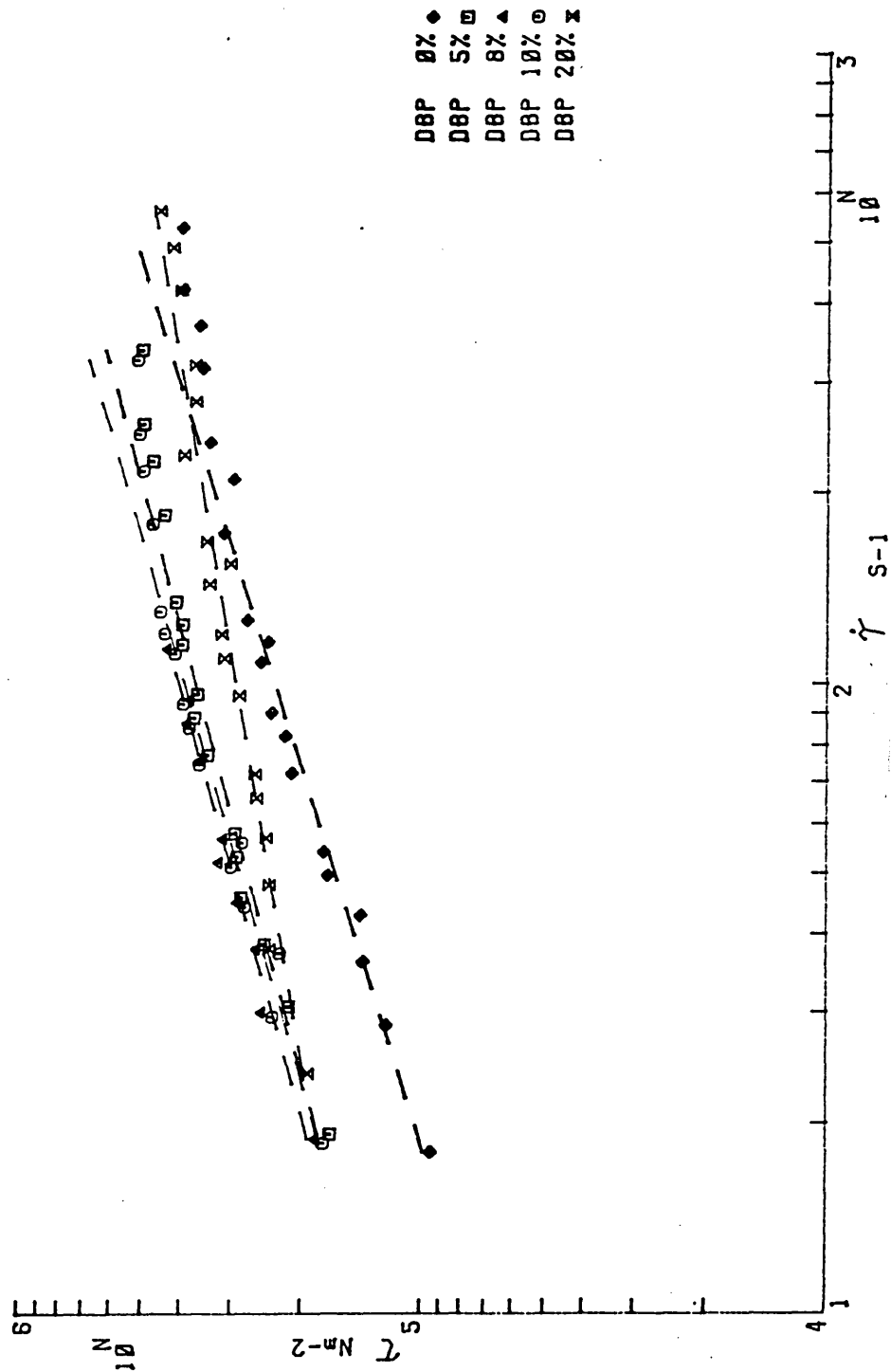


Fig. 4.36 Effect of the concentration of DBP on the flow properties of CA doughs at 30°C

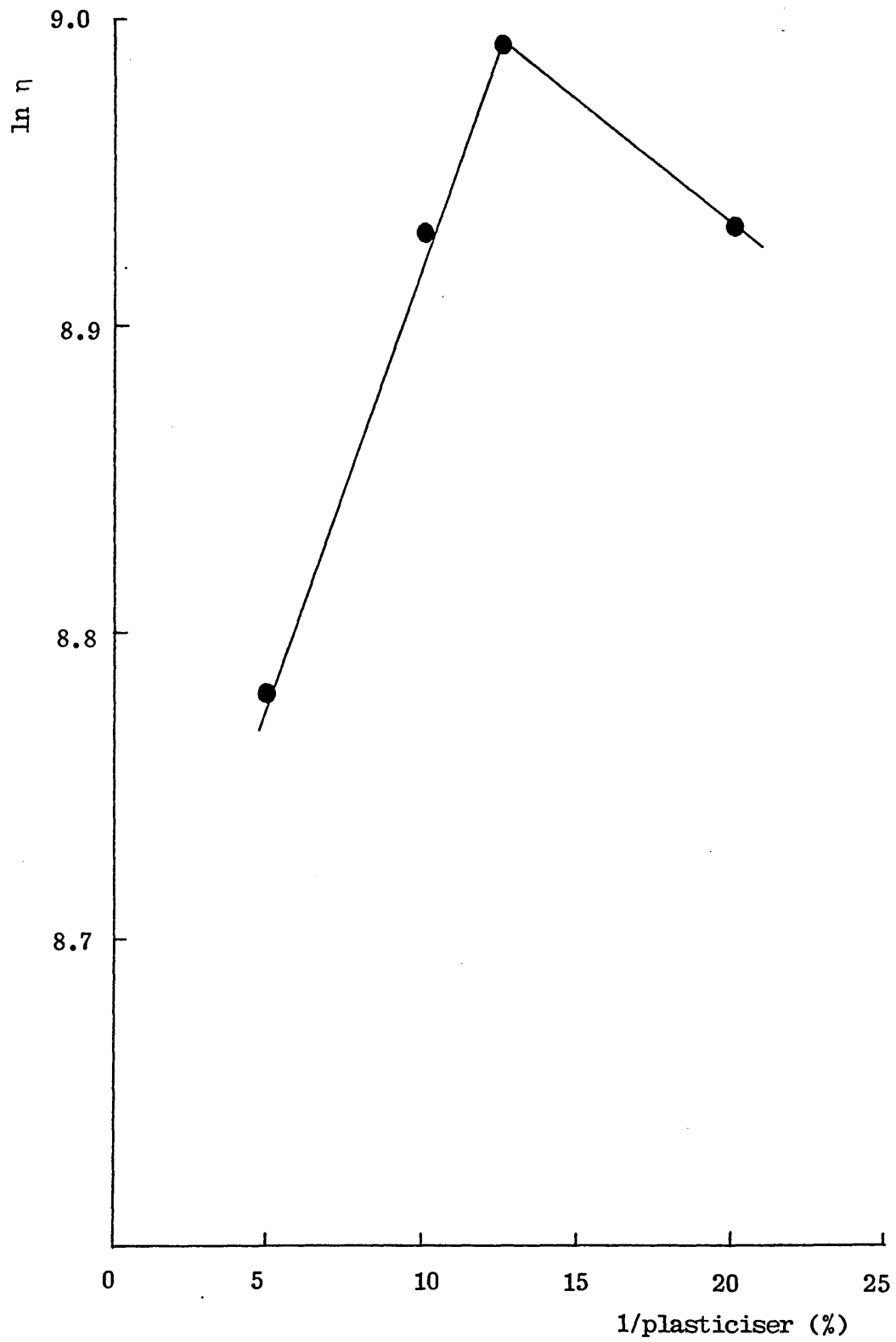


Fig. 4.37 DEP concentration dependence of the viscosity at constant shear rate ( $\dot{\gamma}=40 \text{ s}^{-1}$ )

## CHAPTER 5 : CONCLUSION

The results described in this thesis lead to a fundamental understanding of the processing behaviour of CA and from this an understanding of the effects of the manufacturing process on gun propellant doughs is possible.

On mixing the binary system (cellulose acetate and solvent) in the torque rheometer, it is found that the rate of consolidation of CA powder is quick, and a reasonably coherent dough is formed within 3 minutes. A fill factor of 0.8 is found to give the best dough, with fewer air bubbles present. Temperature is more difficult to control for stiff doughs because of the viscous heating effect. A lower fill factor, a higher solvent content or a higher mixing temperature should be used to reduce viscous heating. When the direction of rotors is changed, and reversed back to the original direction, an immediate increase in the torque is observed. This suggests that more material is being incorporated into the mix and this process can be used to improve the uniformity of the dough.

The regular fluctuations of the torque level in the mixing curve is due to the complex geometry of the mixer head and the difference in rotors' speeds, which give a distribution of shear stresses in the doughs. Three transitions are observed in the mixing curve, which are identified as incorporation, dispersion and homogenization stages. The maximum torque level and the work unit give an indirect measure of the consistency of the dough. It is found that the work unit is directly proportional to mixing time but is indirectly proportional to both solvent concentration and mixing temperature. The maximum torque value increases rapidly in the initial phase of mixing and it remains fairly constant with increasing mixing time. However, the maximum torque value decreases in an exponential manner and a linear manner as a function of solvent concentration and mixing temperature respectively.

All these results corroborate well with the mixing behaviour of NC

doughs in the torque rheometer.

There is an apparent reduction of viscosity average molecular weight of 4% caused by processing. This, however, is attributed to solvent entrapment as indicated from the DSC work. These results suggest that no mechano-degradation of CA is observed as a result of the mixing process. This is further supported by the result from IR studies that no new absorption peak is generated, suggesting that there is no structural transformation of CA after the mixing process.

The micrographs from SEM show that no fibre structure is observed in the CA doughs. The surface texture of CA doughs changes from an undulating to a smooth appearance with increasing degree of gelatinisation.

From the DSC studies on processed doughs, it is found that the reduction in enthalpy of fusion at  $234^{\circ}\text{C}$  ( $T_m$ ) is accompanied by a base line shift at  $190^{\circ}\text{C}$  ( $T_g$ ). This combination suggests that mixing reduces the already low degree of crystallinity or reduces the perfection of the crystallites. Some preliminary x-ray diffraction experiments were made on the processed CA. The results tentatively indicate that the size of the domains decreases with increasing mixing time. A clear-cut conclusion cannot be drawn from these primitive results and further investigation is essential. Nevertheless, these results seem to agree with the results from DSC. However, it is found that the CA possesses a greater degree of crystallinity as determined from DSC thermograms than from the x-ray diffraction patterns.

NC is a fibrous crystalline material, while the present modelling material CA has minimal crystallinity without any fibrous structure. For this reason, the change in the morphological structure such as crystallinity and fibrosity after mixing in CA doughs is small when compared with NC doughs.

The flow behaviour of CA doughs, in common with NC propellant, deviates from the power law at low and high shear rates, giving 'S' shaped flow curves. The causes of the deviations at low and

high shear rates are due to the existence of a yield stress and to the viscous heating effect respectively. The small value of yield stress is attributed to the lack of fibrosity of CA structure. The magnitude of yield stress is found to be a function of the concentration of solvent, filler and plasticiser, which affects the extent of gelatinisation of the dough. The rheological properties of the doughs are not influenced by the mixing time and mixing temperature. This is attributed to the lack of crystallinity and fibrosity in the CA used during these experiments. This confirms the theories of Baker et al that changes induced in NC doughs are due to the breakdown of fibrous NC and picrite crystals. Therefore, it is of paramount importance to control the fibrosity of NC in order to obtain good consistency in NC propellants.

Both extrusion temperature and concentration of solvent used in the mixing of CA dough have an appreciable effect on the rheological behaviour of the dough. At higher temperatures or at higher solvent concentration the flow behaviour index shows less non-Newtonian behaviour of the doughs. Plots of logarithmic viscosity versus reciprocal temperature and reciprocal solvent content give a straight line. This is attributed to the creation of vacant sites and increases in the movement of CA into vacant sites, as in the classic Eyring rate theory. A model is proposed to describe the aforementioned rheological behaviour. In this model, it is assumed that the flow mechanism is totally dependent on the rigidity of macromolecular chains and molecular interactions such as van der Waal forces, polar and hydrogen bonding forces. The addition of solvent to the system can reduce the strength of intermolecular interactions and increase the molecular mobility of CA. Since MEK is not a good solvent for CA, the solvation behaviour of such a system is greatly influenced by temperature. At higher temperatures, the interaction between MEK and CA is increased, leading to an increase in the segregation of

the polymer chains.

The increase in yield value with the incorporation of fibrous CA is attributed to the build up of a three dimensional network. The slumping of the extrudates is attributed to a slow loss of solvent, which while present allowed the material to flow under gravity. This seems to back up the notion of Walters [118] that yield value is a myth. Under processing condition it is real-enough because the Deborah number would be large; at process times of half an hour, the Deborah number would be very small, permitting the extrudates to flow.

Addition of DMP and DEP into the CA doughs will lower the viscosity of the dough and they act as a classic plasticiser for CA. The increase in the viscosity with the incorporation of DBP is attributed to the poor gelatinisation of the dough due to the difference in compatibility between CA and DBP, indicating the phenomenon of antiplasticisation. The results from the mechanical relaxation studies of the CA/DBP system show that the addition of DBP reduces the  $\alpha$  relaxation temperature but increases the  $\beta$  relaxation temperature.

Some die swell measurements were made on the extrudates as a function of shear stress, shear rates, extrusion temperature, solvent content and plasticiser. The values are small, 1.28 being the largest. In general, die swell is found to be a function of the degree of gelatinisation of the dough, which affects elasticity.

## CHAPTER 6 : FUTURE WORK

In the present modelling system, solvated CA dough is mixed individually with plasticiser or fibres in order to determine the effect of each on both the rheological and morphological behaviour of CA. However, in an actual propellant system, two more components are present such as filler and stabiliser. Therefore, a study of other combinations of the dough is required in order to isolate the effect of each on the rheological and morphological behaviour of the doughs.

Nitrocellulose, used in the propellant system, is a highly substituted cellulose with nitrate groups. It exists in a fibrous form and is highly crystalline. The degree of crystallinity and fibrosity of such a material is liable to change during the solvation process. At present, CA is a low crystalline material without any fibre structure, and hence it is unlikely to show any significant changes in the morphology during the solvation process. Thus, a better model for the propellant, such as fibrous CA, with high crystallinity and fibrosity, is needed once the influence of amorphous matter has been established.

In order to have a fundamental understanding of the effect of compatibility of solvent and plasticiser with CA, a series of solvents and plasticisers with different three-dimensional solubility parameters should be used to investigate the rheological changes that occur.

During mixing in the torque rheometer, it was found that not all the input energy goes into the mix. Some of it is used in heating the water inside the thermocirculator. Thus, this viscous heating effect should be investigated to correct the value of the work unit input to the material during the mixing process.

It is hoped that with the installment of an optical encoder into the drive shaft of the capillary extrusion rheometer it will be possible to obtain better measurements at low shear rates. This will have dual functions. Firstly, the viscous heating effect will be reduced and secondly, the slower shear rates will provide

a means to determine the yield stress. Also, a semi-automatic mode for the computer-controlled program should be developed, which allows the operator to determine when the extrusion pressure has reached an equilibrium value. This will reduce the fluctuations of the extrusion pressure in the flow curve.

It would be interesting to study other cellulosic systems to build up an understanding of the influence of solvation, side groups, plasticisers and fillers on rheological properties of the doughs. We want a basic model that works for all cellulosic materials in order to predict rheological behaviour of the doughs.

REFERENCE

- (1) J.E. Dolan, Chemistry in Britian, p.732, Aug. 1985.
- (2) P. Tooley, Fuels, Explosives & Dyestuffs, Chapter 4, John Murry, 1971.
- (3) F.S. Baker, R.E. Carter & R.C. Warren, Rheology, Vol.3, 1980.
- (4) E.D.T. Atkins, Applied Fibre Science, Vol. 3, F. Happy. (Ed.), Academic Press, London, 1978.
- (5) A.J. Pertsin, O.K. Nugmanov, G.N. Marchenko and A.I. Kitaigorodsky, Polymer 1984, Vol 25, P.107.
- (6) A.J. Pertsin, O.K. Nugmanov & G.N. Marchenko, Polymer 1986, Vol 27, p.597-601.
- (7) N. Bikalas & L. Segal (Eds.), Cellulose & Cellulose Derivatives, Wiley Interscience, N.Y. ,1971.
- (8) J.A. Brydson, Plastics Materials, 4th Edition, Butterworth Scientific, Chapter22, p.546,1982.
- (9) V.E.Yarsley, Cellulosic Plastics, Iliffe Books Ltd., 1964, Chapter 2.
- (10) J.D. Wilson & J.K. Hamilton, J. of Chemical Education, Vol 63, No. 1, p.49-53, 1986.
- (11) L.J. Tanghe, L.B. Genung & J.W. Merich, Eastman Kodak Company, Rochester, N.Y.
- (12) O.H. Ray, Cellulose Esters-Organic, Encyclopedia of polymer science, Vol 3, 1965.
- (13) S. Doyle & R.A. Pethrick, British Polymer J., Vol 16 1984, p.15-20.
- (14) P.H. Hermans & A. Weidinger, J. polym. Sci. 1949, Vol. 4, p.135.
- (15) J.O. Warwicker & H. Spedding, J. Appl. Polym. Sci., 1965, Vol.9, p.1913.
- (16) C.M. Conrad & P. Harbrink, Textile Research J., Oct. 1963, p.784.
- (17) E. Roche, M. Bondeulle & R.H Marchessault, Macromolecules, Vol II, 1978.
- (18) P. Zugenmaier, J. Appl. Polym. Sci. (APS), Vol. 37 p.223, 1983.
- (19) S. Watanabe, M. Takai & J. Hayushi, J. of Polym. Sci., Part C, P.825-835, 1968.
- (20) R.E. Boy & R.M. Schulken, J. Appl. Polym. Sci., p.2453, 1967.
- (21) H.C. Trivedi, K.C. Patel & R.D. Patel, J. Macromol Sci.-Chem., A 19(1), p.85-95, 1983.
- (22) M. Scandola & G. Ceccorulli, Polymer, 1985, Vol 26, p.1958.

p.1958.

- (23) D.W. Woods, Nature, 174, 753 (1954).
- (24) K. Nakamura, Chem. of High Polymer (Japan), 13, 47, 1956.
- (25) P.A. Small , J. Appl. Chem., 3 (1953) 71.
- (26) J.D. Crowley, G.S. Teagul & J.W. Lowe, J. of Paint Technology, 38, p.269.
- (27) Encyclopedia of Polym. Sci., Vol. 10, p.274, **1969**.
- (28) G. Matthews, Polymer Mixing Technology, 1982.
- (29) M.F. Edwards, Mixing in the Process Industries, 1985 Butterworths.
- (30) H. Palmgren, European Rubber J., Part 1, May, 1974, p.30-44.
- (31) P. Hold, Advances in Polym. Technol., Vol. 2, p.141, 1982.
- (32) P.K. Freadley & W.Y. Wan Idris, Rubber Chem. Technol. Vol. 52, p.134, 1979.
- (33) H. Palmgren, Rubber Chem. & Technol., Vol. 48, p.462 1975.
- (34) P.R. Van Biskirk, S.B. Turetzky & P.F. Gunberg, Rubber Chem. & Technology, Vol. 48, p.577, 1975.
- (35) J.T. Bergen, Processing of thermoplastic materials, Reinhold Published Co., N.Y., p.405-446.
- (36) J.M. Mckelvey, Polymer Processing, John Wiley & Son, N.Y., 1962, Chapter 12.
- (37) W.D. Mohr, Processing of thermoplastic Materials, Reinhold Published Co., N.Y., 1959, p.135-6.
- (38) F.N. Cogswell, Polymer Rheology, George Godwin Limited, 1981.
- (39) J.A. Brydson, Flow Properties of Polymer Melts, 2nd edition, George Godwin Limited, 1981.
- (40) R.J. Crawford, Plastic Engineering, Pergaman Press, 1981.
- (41) J.R. Van Wazer, Viscosity & flow measurement, Interscience publishers, 1963.
- (42) L.E. Nielsen, Polymer Rheology, Marcel Dekker, 1977.
- (43) C.D. Han, Rheology in Polymer Processing, Academic Press, 1976.
- (44) S.D. Holdsworth, J. Texture Stud., 2, p.393, 1971.
- (45) F.S. Baker & R.E. Carter, The development of modern gun propellants as a function of basic research, Presented ADPA, New Jersey, USA 1984.

- (46) F.S. Baker & R.C. Carter, Rheology, Vol. 3, p.591, 1980.
- (47) F.S. Baker & R.C. Carter, Propellants, Explosives & Pyrotechnics, Vol. 7, p.139-147, 1982.
- (48) Hampden Equipment Ltd., Hampden Variable Torque Rheology (Model TR-1), Operation Manual.
- (49) F.S. Baker, PERME Technical Report 119, Nov. 1979.
- (50) Daventest Equipment Ltd., Davenport Capillary Extrusion Rheometer (Serial No. ZR406/31), Operation Manual.
- (51) R.E. Carter, PERME Technical Report 137, Nov. 1979.
- (52) F.S. Baker & R.C. Carter, U.K. Patent Application 7941423, Nov. 1979.
- (53) E.B. Bagley, J. of Appl. Physics, Vol. 28, No. 5, 1957.
- (54) J.T. Marsh & F.C. Wood, Introduction to Chemistry of Cellulose, P.213, D.Van Nostrand Co., 1939.
- (55) F. Howlett & E. Martin, J. of Textile Institute, Jan 1944, p.T1-T6.
- (56) L.B. Genung & R.C. Mallatt, Ind. Eng. Chem., Vol. 13, No. 6, 1941, p.369-374.
- (57) C.R. Fordyce, L.B. Genung & M.A. Pile, Ind. Eng. Chem., Anal. Ed., Vol. 18, 547 (1946).
- (58) Manuscript of Mettler TA3000 operation manual.
- (59) N.D. Baker, C.S. Fuller & N.R. Pape, J. AM. Chem. Soc., Vol. 64, p.776 (1942).
- (60) R.J. Mosely & W.F. Watson, Mechanochemistry of polymers, Maclaren & Sons Ltd., 1964.
- (61) H.Staudinger, Die hochmolekularenorganischen Verbindungen, Springer, Berlin, 1932.
- (62) N.C. Billingham, Molar mass measurements in polymer science, Kogan Page Limited, 1977.
- (63) H.J. Philipp & C.F. Bjork, J. of Polym. Sci., Vol VI, No. 5, p.549-562, 1950.
- (64) H.K. Johnston, J. Appl. Polym. Sci., Vol. 16, p.3375, 1972.
- (65) F. Howlett, E. Minshall & A.R. Urguhart, J. Text. Inst., Vol. 35, T133, 1944.
- (66) B.T. Hofreiter, J.O. Ernst & W.L. Williams, J. Appl. Polym. Sci., Vol. 17, p.1449-1454 (1973).
- (67) R.G. Zhabankov, translated by A.B. Densham, I.R spectra of cellulose and its derivatives, Consultants Bureau, N.Y., 1968.

- (68) G. Arneri & J.A. Sauer, Polym. Eng. Sci., 1975, Vol. 15, p.795.
- (69) R.T. O'Conner, E.F. DuPie & D. Mitchoum, Text. Res. J., Vol. 28, p.382, 1958.
- (70) H.G. Shinouda & A.A. Hanna, J. of Appl. Polym. Sci., Vol. 21, p.1479-1488, 1977.
- (71) P.J. Goodhew, Electron microscopy & analysis, Wykeham Sci. Series, 1975.
- (72) P.J. Grundy & G.A. Jones, Electron microscopy in study of materials, Arnold, 1976.
- (73) M.H. Loretto, Electron beam analysis of materials, Chapman & Hall, 1984.
- (74) V. Peck & W. Kaye, Text. Res. J., Vol. XXIV, No. 4, p. 300-306, April 1954.
- (75) S. Doyle, PhD thesis, The physical characteristic and dielectric behaviour of cellulose acetate polymers, 1985. Univ. of Strathcyde.
- (76) J.R. White, Rubber Chem. & Technol., Vol. 57, p.457, **1984**.
- (77) Aklonis, Macknight & Shen, Introduction to polymer viscoelasticity, Wiley-Interscience 1972.
- (78) R.A. Pethrick & R.W. Richards, Static & dynamic properties of the polymer solid state, Reidel Publishing Company, 1982.
- (79) T. Murayama, Dynamic mechanical analysis of polymeric material, 1978, Elsevier Publishing Company.
- (80) P. Burroughs & M.G. Lofthouse, Plastics & Rubber International July/August, Vol. 4, No. 4, **1979**.
- (81) C.W. Fong, J. Appl. Polym. Sci., Vol. 27, p.3585, 1982.
- (82) L. Mandelkem & P.J. Flory, J. Am. Chem. Soc., 1951, Vol. 73, p.3206.
- (83) J. Rwsell & R.G. Van Kerpel, J. Polym. Sci., 1957, Vol. 25, p.77.
- (84) A.F. Klarman, A.V. Galanti & L.H. Sperling, J. Polym. Sci (A-2), Vol. 7, P.1513, 1969.
- (85) T. Morooka, M. Noramoto & T. Yamada, J. Appl. Polym. Sci., Vol. 29, p.3981, 1984.
- (86) M. Scandola & G. Ceccorulli, Polymer 1985, Vol. 26, p. 1953.
- (87) M. Scandola & G. Ceccorulli, Polymer 1985, Vol. 26, p. 1958.
- (88) M. Scandola & G. Ceccorulli, Polymer 1986, Vol. 27, p. 228.

- (89) S.A. Bradley & S.H. Carr, J. Polym. Sci., Polym. Phys. Ed., Vol. 14, p.111, 1976.
- (90) M. Kimura & J. Nakano, J. Poly. Sci., Polym. Lett. Ed., Vol. 14, p.741, 1976.
- (91) R.W. Seymour, S. Wemhold & S.K. Haynes, J. Macromol. Sci.-Phys., B16(3), p.337, 1979.
- (92) D.J. Crafton & R.A. Pethrick, Polymer 1981, Vol. 22, p.1048.
- (93) W.J. Jackson & J.R. Caldwell, J. Appl. Polym. Sci., Vol. 11, p.211, 1967.
- (94) W.J. Jackson & J.R. Caldwell, J. Appl. Polym. Sci., Vol. 11, p.227, 1967.
- (95) A.D. Jenkins, Polymer Science, North-Holland Publishing company, 1972.
- (96) L.E. Alexander, X-ray diffraction methods in polymer science, John Wiley, N.Y., 1969.
- (97) R.W. James, The optical principles of diffraction of x-rays, G. Bells & Sons Ltd., 1965.
- (98) Private communication with Dr. R. Wood.
- (99) J.E. Goodrich & R.S. Porter, Polymer Eng. & Sci., Jan. 1967, p.45-51.
- (100) P.K. Freakley & S.R. Patel, Rubber Chem & Techno., Vol. 58, p.751-773, **1985**.
- (101) Dizon & Papazian, Rubber Chem. & Techno., Vol. 52, p.765, 1977.
- (102) G.E.O. Conner & J.B. Putman, Rubber Chem & Techno., Vol. 51, p.299-816, **1978**.
- (103) P.T. Dolezal & P.S. Johnson, Rubber Chem. & Techno., Vol. 53, p.252-269, **1980**.
- (104) R.S. Porter & J.F. Johnson, J. Polym. Sci., Part C, No. 15, p.365-371, 1966.
- (105) E.A. Collins, Transaction of the Soci. of Rheology, Vol. 11:2, p.225-242, 1967.
- (106) H. Pohl & K. Lund, Can. J. Chem. Eng., Vol. 43, p.231, 1965.
- (107) G.J. Drennes & F.O. Dexter, J. Colloid Sci, Vol. 4, p.181, 1949.
- (108) A.B. Bestal & H.V. Belcher, J. Appl. Phys., Vol. 24, p. 696, 1953.
- (109) C.K. Shih, Trans. Soc. Rheol., Vol. 14, p.83, 1970.
- (110) A. Casale, R.S. Porter & J.F. Johnson, J. Macromol. Sci., C5, p.387, 1971.
- (111) R.A. Mendelson. Polym. Eng. Sci., Vol. 8, p.235,

1968.

- (112) R.A. Mendelson, Polym. Eng. Sci., Vol. 9, p.350, 1969.
- (113) R.A. Mendelson, Trans. Soc. Rheology, Vol. 9, p.53, 1965.
- (114) K.K. Chèe & A. Rudin, Trans. Soc. Rheology, Vol. 18:1, p.103-121, 1974.
- (115) R.E. Carter & R.C. Warren, Extrusion stresses, die swell & viscous heating effects in double-base propellant, submitted to J. Rheology, Dec. 1984.
- (116) W. Gordy, Chem. Phys., Vol. 7, p.93, 1939.
- (117) J. Brandup & E.H. Immergot, Polymer Handbook, Vol. IV, 1975, Wiley.
- (118) H.A. Barnes & K. Walters, Rheologica Acta, Vol. 24, No. 4, 1975.

APPENDIX A

COMPUTER PROGRAM FOR EXTRUSION RHEOMETER

```

10  !*****
20  !           CONTROL OF DAVENPORT EXTRUSION RHEOMETER
30  !*****
40  !
50  !
60  !
70  ! This program will control the Davenport rheometer and take 10 readings
80  ! off pressure and the corresponding piston speed. It will then store
90  ! this data in a binary file on disc for calculations to be performed
100 ! at a later time.
110 OPTION BASE 0           ! Specifies the default lower
120                       ! bound of the arrays
130 DIM Scan_data(301),Press(240),Speed(240),F(25,25),Atemp(240),Spd(25),Wa(11
)
140 Init=0
150 Miss=0
160 Auto=0
170                       ! packing of the rheometer barrel
180 Mi=0                   ! Variable for non printing of
190                       ! die swell data
200 Sd=0                   ! Variable set for temperature
210 Done=0                 ! Variable for non calc of results
220 GOSUB Space           ! 5540-5560
230 GOSUB Mrz             ! 330-590
240 GOSUB Space
250 GOSUB Check           ! 3390-4090
260 GOSUB Data            ! 1150-1410
270 GOSUB Calib           ! 5900-6040
280 GOSUB Instr1         ! 600-790
290 GOSUB Init1          ! 2250-2610
300 GOSUB Instr2         ! 800-1140
310 GOSUB Init2          ! 2620-2950
320 GOSUB Done2          ! 4820-5530
330 Mrz: !*****          ! loads MRZ and performs self-test
340 ASSIGN @Multi TO 723 ! Assigns an I/O path to a device
350 CLEAR 723            ! Clears Multi frame
360 WAIT 4               ! Waits for self test to end
370 REM LOADING MULTIPROGRAMMER PROGRAM
380 PRINT "MRZ PROGRAM BEING LOADED"
390 ALLOCATE Ascii$(80)
400 ASSIGN @Disc TO "MRZ"
410 ON END @Disc GOTO Eof
420 Rd_file: ENTER @Disc;Ascii$ ! This routine transfers the
430         OUTPUT @Multi;Ascii$ ! MRZ file from the disc
440         GOTO Rd_file         ! to Multi mainframe memory
450 Eof:OFF END @Disc
460     ASSIGN @Disc TO *
470     DEALLOCATE Ascii$
480 G=SPOLL(723)         ! Performs an HPIB serial poll
490 IF G<>64 THEN        ! then checks to see if the
500 PRINT "MULTI DIDN'T INTERRUPT" ! Multi set SRQ, If not print
510 PAUSE                ! error message and pause
520 END IF
530 ENTER 72310;A
540 IF A<>16384 THEN
550 PRINT "SELF TEST DIDN'T SET SRQ"
560 PAUSE
570 END IF
580 ON INTR 7 GOTO Interrupt ! Sets up interrupt branch
590 RETURN
600 Instr1: !*****          ! Instructions for long die
610 Sd=1                 ! Initial temp reading
620 PRINT "*****"
630 PRINT "*           PUT THE LONG DIE IN AND PACK THE BARREL      *"
640 PRINT "*"
650 PRINT "*"
660 PRINT "*"
670 PRINT "*"
680 PRINT "*****"
690 PRINT "*           PRESS ANY KEY TO ABORT RUN                    *"

```

```

700 PRINT "*****"
710 PRINT "*"
720 PRINT "*"
730 PRINT "*"
740 PRINT "*"
750 PRINT "*"          TO START RUN PRESS CONTINUE
760 PRINT "*****"
770 PAUSE
780 IF Auto=2 THEN GOSUB Initm
790 RETURN
800 Instr2: !*****! Instructions for short die
810 Sd=2          ! Final temp reading
820 PRINT "DO YOU WISH TO TAKE READINGS WITH THE SHORT DIE?"
830 INPUT S$
840 GOSUB Space
-850 IF S$="N" THEN GOSUB Done1
860 PRINT "          IS THERE SUFFICIENT POLYMER LEFT JUST"
870 PRINT "          TO CHANGE THE DIE?"
880 INPUT S$
890 IF S$="N" THEN GOSUB Short
900 Cvl=1          ! Sets Cvl to 1 to miss ram proc
910 GOSUB Space
920 PRINT "DO YOU WISH TO CHANGE THE TRANSDUCER?(Y/N)"
930 INPUT S$
940 IF S$="N" THEN GOTO 1000
950 GOSUB Space
960 GOSUB Calib
970 GOSUB Space
980 PRINT "INPUT THE MAXIMUM TRANSDUCER PRESSURE IN P.S.I"
990 INPUT Transd2
1000 Transd2=Transd1
1010 GOSUB Space
1020 PRINT "*****"
1030 PRINT "*WHEN SHORT DIE INSTALLED PRESS CONTINUE TO START*"
1040 PRINT "*"
1050 PRINT "*"
1060 PRINT "*"
1070 PRINT "*"
1080 PRINT "*"
1090 PRINT "*****"
1100 PRINT "*"          PRESS ANY KEY TO ABORT RUN
1110 PRINT "*****"
1120 PAUSE
1130 IF Auto=2 THEN GOSUB Initm
1140 RETURN
1150 Data: !*****! Routine for checking file name
1160 REM INPUTING MANUAL DATA VALUES ! and inputing data on the melt
1170 GOSUB Space
1180 PRINT "INSERT DATA DISC "
1190 PRINT ""
1200 PRINT "PRESS CONTINUE WHEN READY"
1210 PAUSE
1220 GOSUB Space
1230 PRINT "WHAT IS THE NAME OF THE DATA FILE TO BE CREATED?"
1240 ON ERROR GOTO File          ! Checks to see if file
1250 INPUT Melt$          ! name is OK
1260 GOSUB Space          !
1270 STORE Melt$          !
1280 PURGE Melt$          !
1290 OFF ERROR          !
1300 PRINT "FILENAME IS O.K."          !
1310 WAIT 3          ! Delay to read screen
1320 GOSUB Space
1330 I=0
1340 Rx=0
1350 PRINT "INPUT TEMP,R,RL,RSL"          ! Inputs variables for store
1360 INPUT Temp,R,Rl,Rsl          ! and later calculations
1370 GOSUB Space
1380 PRINT "INPUT MAXIMUM TRANSDUCER PRESSURE IN P.S.I"
1390 INPUT Transd1
1400 GOSUB Space
1410 RETURN
1420 Input: !*****! Takes readings of speed and pressure
1430 ENABLE INTR 7;2          ! Enable interrupt
1440 OUTPUT @Multi;"CY2T"          ! Enable control card
1450 GOSUB Space
1460 OFF KEY
1470 REM TAKING 200 READINGS(FULL DETAILS PAGE3-6 IN THE HIGH SPEED FET SCANNI
NG BOOKLET
1480 OUTPUT @Multi;"WF2.0,0T"          ! Selects start channel
1490 OUTPUT @Multi;"WF2.1,2T"          ! Set stop channel
1500 OUTPUT @Multi;"WF2.3,5T"          ! Set mode register
1510 OUTPUT @Multi;"WF2.2,80T"          ! Set pacer delay in us

```

```

1520 OUTPUT @Multi;"CC8T" ! Clear memory registers
1530 OUTPUT @Multi;"WF8.0,300T" ! Sets interrupt word
1540 OUTPUT @Multi;"AC8T" ! Arm the memory card
1550 OUTPUT @Multi;"CY2T" ! Start pacer
1560 Wait: !*****
1570 DISP "WAITING FOR INTERRUPT"
1580 GOTO 1610
1590 Interrupt: !***** ! Interrupt routine
1600 G=SPOLL(723) ! Perform an HPIB serial poll
1610 IF G=64 THEN ! then checks to see if Multi
1620 ENTER 72310;A,B,C ! set SRQ (also clears SRQ)
1630 IF C<>0 THEN ! Read SRQ status to see that a
1640 ENTER 72312;Address ! card caused the interrupt
1650 IF Address<>8 THEN ! Check the address of the card
1660 PRINT "NOT A MEMORY ADDRESS" ! if not the right address then
1670 PAUSE ! print error message and pause
1680 END IF
1690 OUTPUT @Multi;"WF7.1,21T" ! Set FIFO in mode with handshakes
1700 ! Lockout to stop handshakes
1710 OUTPUT @Multi;"DC8T" ! Disarms card to avoid interrupt
1720 OUTPUT @Multi;"WF2.2,0T" ! Turn off the pacer
1730 OUTPUT @Multi;"MR7,301T" ! MR command to get the data
1740 REM ENTERS DATA
1750 ENTER 72305 USING "%,W";Scan_data(*) ! Enter and format the data
1760 Scan_data(201)=0 ! In FIFO mode the last memory
1770 END IF
1780 ELSE ! location has invalid data ,
1790 PRINT "MULTI DIDN'T INTERRUPT" ! therefore set to a known value
1800 PAUSE
1810 END IF
1820 DISP "UPDATING ARRAY"
1830 FOR K=1 TO 300
1840 NEXT K
1850 REM END OF DATA RUN
1860 REM FINDS MEAN OF THE 300 READINGS
1870 J=0 ! Zeros all the variables
1880 Xms=0
1890 Xmp=0
1900 Xts=0
1910 Xtp=0
1920 FOR K=3 TO 300 STEP 3 ! Sorts the data and
1930 J=J+1 ! converts the digital reading
1940 Speed(J)=Scan_data(K-2)*.005 ! to volts
1950 Press(J)=Scan_data(K)*.005
1960 Atemp(J)=Scan_data(K-1)*.005
1970 NEXT K
1980 FOR J=1 TO 100 ! Adds the 100 speed readings
1990 Xts=Xts+Speed(J) ! and calculates the mean
2000 NEXT J
2010 Xms=Xts/100
2020 FOR J=1 TO 100 ! Adds the 100 pressure readings
2030 Xtp=Xtp+Press(J) ! and calculates the mean
2040 NEXT J
2050 Xmp=Xtp/100
2060 Sp=Xms
2070 Pr=Xmp
2080 IF D<1 THEN GOTO 2100
2090 IF D>4.5 THEN GOTO 2170
2100 IF Sd=2 THEN GOTO 2230
2110 Atemp1=0
2120 FOR J=1 TO 100
2130 Atemp1=Atemp1+Atemp(J)
2140 NEXT J
2150 Atemp1=Atemp1/100
2160 GOTO 2230
2170 IF Sd=1 THEN GOTO 2230
2180 Atemp2=0
2190 FOR J=1 TO 100
2200 Atemp2=Atemp2+Atemp(J)
2210 NEXT J
2220 Atemp2=Atemp2/100
2230 GOSUB Space
2240 RETURN
2250 Init1: !***** ! Long die routine
2260 Init=1
2270 ON KBD GOSUB Abort ! Branch when a key is pressed
2280 GOSUB Sence
2290 OUTPUT @Multi;"OP,1",-2,"T" ! Multi outputs -2Volts
2300 WAIT 1
2310 I=1
2320 D=1
2330 OUTPUT @Multi;"OP,1",Spd(D),"T" ! Multi outputs array value
2340 IF I>11 THEN GOTO 2360

```

```

2350 WAIT Wa(I)
2360 F=1
2370 REPEAT
2380 GOSUB Input
2390 F=F+1
2400 UNTIL F=4
2410 IF Pr>5.0 THEN GOSUB Trans
2420 P(I,1)=Sp
2430 P(I,2)=Pr
2440 WAIT 2
2450 GOSUB Input
2460 IF Pr>5.0 THEN GOSUB Trans
2470 X=ABS(Pr-P(I,2))
2480 IF X>.01 THEN GOTO 2420
2490 P(I,1)=Sp
2500 P(I,2)=Pr
2510 BEEP
2520 N1=I
2530 I=I+1
2540 D=D+1
2550 IF N1=Decss THEN GOTO 2590
2560 L=Spd(D-1)
2570 GOSUB Rep
2580 GOTO 2330
2590 OUTPUT @Multi;"OP,1",-5,"T"      ! Multi outputs -5 volts
2600 OFF KBD
2610 RETURN
2620 Init2: !*****! Short or zero die routine
2630 Init=2
2640 ON KBD GOSUB Abort      ! Branch when key is pressed
2650 GOSUB Sence
2660 OUTPUT @Multi;"OP,1",-2,"T"      ! Outputs -2 volts to rheometer
2670 I=1
2680 D=1
2690 WAIT 1
2700 OUTPUT @Multi;"OP,1",Spd(D),"T"      ! Outputs array value
2710 IF I>11 THEN GOTO 2730
2720 WAIT Wa(I)
2730 F=1
2740 REPEAT
2750 GOSUB Input
2760 F=F+1
2770 UNTIL F=4
2780 IF Pr>5.0 THEN GOSUB Trans
2790 P(I,3)=Pr
2800 WAIT 2
2810 GOSUB Input
2820 IF Pr>5.0 THEN GOSUB Trans
2830 X=ABS(Pr-P(I,3))
2840 IF X>.01 THEN GOTO 2790
2850 P(I,3)=Pr
2860 N1=I
2870 I=I+1
2880 D=D+1
2890 IF N1=Decss THEN GOTO 2930
2900 L=Spd(D-1)
2910 GOSUB Rep
2920 GOTO 2700
2930 OUTPUT @Multi;"OP,1",-5,"T"      ! Outputs -5 volts to rheometer
2940 OFF KBD
2950 RETURN      ! to normal
2960 Short: !*****! Allows for packing of the barrel
2970      ! with the short or zero lenght die
2980 Sd=2
2990 OUTPUT @Multi;"OP,1",-5,"T"      ! Outputs -5 volts to rheometer
3000 GOSUB Space
3010 PRINT "DO YOU WISH TO CHANGE THE TRANSDUCER?(Y/N)"
3020 INPUT S$
3030 IF S$="Y" THEN GOTO 3080
3040 GOSUB Space
3050 PRINT "HAS PART OF THE DATA HAS JUST BEEN LOADED (Y/N)?"
3060 INPUT S$
3070 IF S$="N" THEN GOTO 3140
3080 GOSUB Space
3090 GOSUB Calib
3100 GOSUB Space
3110 PRINT "INPUT THE MAXIMUM TRANSDUCER PRESSURE IN P.S.I"
3120 INPUT Transd2
3130 GOTO 3150
3140 Transd2=Transd1
3150 GOSUB Space

```

```

3160 PRINT "*****"
3170 PRINT "*"          PUT THE SHORT OR ZERO LENGHT DIE IN  "*"
3180 PRINT "*"          AND PACK THE BARREL                  "*"
3190 PRINT "*"          "*"                                  "*"
3200 PRINT "*"          "*"                                  "*"
3210 PRINT "*"          "*"                                  "*"
3220 PRINT "*****"
3230 PRINT "*"          PRESS ANY KEY TO ABORT RUN           "*"
3240 PRINT "*****"
3250 PRINT "*"          "*"                                  "*"
3260 PRINT "*"          "*"                                  "*"
3270 PRINT "*"          "*"                                  "*"
3280 PRINT "*"          "*"                                  "*"
3290 PRINT "*"          TO START RUN PRESS CONTINUE         "*"
3300 PRINT "*****"
3310 PAUSE
3320 IF Auto=2 THEN GOSUB Initm
3330 GOTO 310
3340 RETURN
3350 Check: ! *****! Checks if part data already taken
3360 DATA 24,38,48,57,66,72,96,110,120,144,155,168,230
3370 FOR N=1 TO 13
3380 READ Q
3390 Spd(N)=(5*Q)/2400
3400 NEXT N
3410 DATA 280,320,420,490,560,700,860,1120,1260,1440,1550,1700
3420 FOR N=14 TO 25
3430 READ Q
3440 Spd(N)=(5*Q)/2400
3450 NEXT N
3460 DATA 60,35,28,23,20,18,13,11,10,7,4
3470 FOR N=1 TO 11
3480 READ Wa(N)
3490 NEXT N
3500 PRINT "          *MENU*"
3510 PRINT ""
3520 PRINT ""
3530 PRINT "          1    FULLY AUTO-LONG/ZERO DIE"
3540 PRINT ""
3550 PRINT "          2    SEMI-AUTO LONG/ZERO DIE"
3560 INPUT S
3570 IF S=1 THEN Auto=1
3580 IF S=2 THEN Auto=2
3590 GOSUB Space
3600 PRINT "HOW MANY DECADES OF SHEAR RATE DO YOU REQUIRE?"
3610 INPUT Decs
3620 IF Decs=1 THEN Decss=13
3630 IF Decs=2 THEN Decss=25
3650 IF Decs>2 THEN GOTO 3600
3660 GOSUB Space
3670 PRINT "DO YOU WISH TO LOAD DATA FROM A PREVIOUS RUN?(Y/N)"
3680 INPUT S$
3690 IF S$="N" THEN RETURN
3700 Miss=1
3710 GOSUB Space
3720 PRINT "WHAT WAS THE NAME OF THE FILE?"
3730 INPUT Melt$
3740 GOSUB Space
3750 ASSIGN @Path1 TO Melt$           ! Opens apath for the file
3760 ENTER @Path1;Temp,R,RI,Rsl,N1,Mi,Atempl ! Enters temperature, radius
3770 PRINT "TEMPERATURE=";Temp       ! length of long and short dies and
3780 PRINT "RADIUS OF THE DIE=";R    ! the number of readings
3790 PRINT "LENGHT OF LONG DIE=";R1  ! and prints them
3800 PRINT "LENGHT OF SHORT DIE=";Rsl !
3810 PRINT "INITIAL TEMPERATURE WAS=";Atempl
3820 PRINT ""
3830 DISP "PRESS CONTINUE"
3840 PAUSE
3850 FOR I=1 TO N1
3860 ENTER @Path1:P(I,1),P(I,2)     ! Fetchs from the disc the speed
3870 NEXT I
3880 IF Mi=1 THEN GOTO 3920
3890 FOR I=1 TO N1
3900 ENTER @Path1:P(I,20),P(I,21)
3910 NEXT I                          ! pressure and die swell data
3920 GOSUB Space
3930 PRINT " P(I,1)   P(I,2)"       ! Displays the speed and pressure
3940 PRINT "-----"
3950 PRINT ""
3960 FOR I=1 TO N1
3970 PRINT P(I,1),P(I,2)
3980 NEXT I
3990 IF Mi=1 THEN GOTO 4090
4000 DISP "PRESS CONTINUE"
4010 PAUSE
4020 GOSUB Space
4030 PRINT " P(I,20) P(I,21)"       ! Display die swell data
4040 PRINT "-----"
4050 PRINT ""

```

```

4060 FOR I=1 TO N1
4070 PRINT P(I,20),P(I,21)
4080 NEXT I
4090 DISP "PRESS CONTINUE"
4100 PAUSE
4110 ASSIGN @Path1 TO *
4120 GOSUB Space
4130 PURGE Melt$
4140 GOSUB Short
4150 RETURN
4160 Done1: ! *****! This creates a binary file
4170 ! for a single run and
4180 ! inputs the data for die swell and
4190 ! tensile die swell calculations
4200 OUTPUT @Multi;"OP,1",-5,"T"
4210 Done=1
4220 PRINT "*****"
4230 PRINT "*" DO YOU WISH TO PERFORM DIE SWELL AND "*"
4240 PRINT "*" TENSILE DIE SWELL CALCULATIONS? (Y/N) "*"
4250 PRINT "*****"
4260 INPUT S$
4270 GOSUB Space
4280 IF S$="N" THEN GOTO 4580
4290 PRINT ""
4300 PRINT "*****"
4310 PRINT "*" THE EXTRUDATE DIAMETER MUST NOT "*"
4320 PRINT "*" EQUALL THE DIE DIAMETER "*"
4330 PRINT "*****"
4340 PRINT ""
4350 PRINT "ENTER THE EXTRUDATE DIAMETER IN mm"
4360 PRINT ""
4370 PRINT "IF NO READING AVAILABLE ENTER 0"
4380 PRINT ""
4390 PRINT "TO ENTER DATA PRESS CONTINUE"
4400 OUTPUT @Multi;"OP,1",0,"T"
4410 PAUSE
4420 GOSUB Space
4430 PRINT ""
4440 PRINT "P(I,20)/P(I,21) , EXTRUDATE DIA"
4450 PRINT "-----"
4460 PRINT ""
4470 PRINT ""
4480 FOR I=1 TO N1 ! Inputs N1 data points
4490 INPUT S
4500 IF S=2*R THEN GOTO 4280 ! Checks to see if equall to die dia
4510 P(I,20)=S ! Sets P(I,20) to die diameter
4520 P(I,21)=S ! Sets P(I,21) to die diameter
4530 PRINT "P(";I;"20) = ",S ! Prints the data
4540 NEXT I
4550 PRINT "IS THE DATA CORRECT? (Y/N)"! Allows for correction of data
4560 INPUT S$
4570 IF S$="N" THEN GOTO 4420
4580 Mi=1
4590 GOSUB Conver
4600 PRINT " P(I,1) P(I,2)" ! Prints data from a single run
4610 PRINT "-----"
4620 PRINT ""
4630 FOR I=1 TO N1
4640 PRINT P(I,1),P(I,2)
4650 NEXT I
4660 PRINT ""
4670 PRINT " Temp1=";Atemp1
4680 PRINT ""
4690 PRINT "PUT IN YOUR DATA DISC AND WHEN YOU WANT TO LOAD"
4700 PRINT "PRESS CONTINUE"
4710 PAUSE
4720 GOSUB Space
4730 PRINT "LOADING FILE"
4740 CREATE BDAT Melt$,8 ! Creates binary file of lenght 8
4750 ASSIGN @Path1 TO Melt$ ! Opens apath to disc drive
4760 OUTPUT @Path1;Temp;R;R1;Rsl;N1;Mi;Atemp1 ! Outputs data
4770 FOR I=1 TO N1
4780 OUTPUT @Path1;P(I,1),P(I,2)
4790 NEXT I ! Outputs speed,pressure and die swell
4800 IF Mi=1 THEN GOTO 4840
4810 FOR I=1 TO N1
4820 OUTPUT @Path1;P(I,20),P(I,21)
4830 NEXT I
4840 DISP "*****LOAD ENDED*****"
4850 ASSIGN @Path1 TO *
4860 STOP
4870 RETURN

```

```

4880 Done2: ! *****! Creates a binary data file and
4890 ! inputs the data for die swell and
4900 ! tensile die swell calculations.
4910 ! for a double run
4920 PRINT "*****"
4930 PRINT "* DO YOU WISH TO PERFORM DIE SWELL AND *"
4940 PRINT "* TENSILE DIE SWELL CALCULATIONS? (Y/N) *"
4950 PRINT "*****"
4960 INPUT S$
4970 IF S$="N" THEN GOTO 5300
4980 GOSUB Space
4990 PRINT ""
5000 PRINT "*****"
5010 PRINT "* THE EXTRUDATE DIAMETER MUST NOT *"
5020 PRINT "* EQUALL THE DIE DIAMETER *"
5030 PRINT "*****"
5040 PRINT ""
5050 PRINT "ENTER THE EXTRUDATE DIAMETER IN mm"
5060 PRINT ""
5070 PRINT "IF NO READING AVAILABLE ENTER 0"
5080 PRINT ""
5090 PRINT "TO ENTER DATA PRESS CONTINUE"
5100 WAIT 3
5110 OUTPUT @Multi;"OP,1",0,"T"
5120 PAUSE
5130 GOSUB Space
5140 PRINT ""
5150 PRINT "P(I,20)/P(I,21) , EXTRUDATE DIA"
5160 PRINT "-----"
5170 PRINT ""
5180 PRINT ""
5190 FOR I=1 TO N1 ! Inputs N1 data points
5200 INPUT S
5210 IF S=2*R THEN GOTO 4980 ! Checks to see if equall to die dia
5220 P(I,20)=S ! Sets P(I,20) to die diameter
5230 P(I,21)=S ! Sets P(I,21) to die diameter
5240 PRINT "P(;"I;"20) = " ,S ! Prints the data
5250 NEXT I
5260 PRINT "IS THE DATA CORRECT? (Y/N)"! Allows for the correction of data
5270 INPUT S$
5280 IF S$="N" THEN GOTO 5130
5290 GOTO 5310
5300 Mi=1
5310 GOSUB Space
5320 GOSUB Conver
5330 PRINT " P(I,1) P(I,2) P(I,3)"!
5340 PRINT "-----"
5350 PRINT "" ! Prints the data and pauses for
5360 FOR I=1 TO N1 ! the correct disc to be inserted
5370 PRINT P(I,1),P(I,2),P(I,3)
5380 NEXT I
5390 PRINT ""
5400 PRINT " Temp1=";Atemp1;" Temp2=";Atemp2
5410 REM LOADS DATA INTO FILE Melt$
5420 PRINT "DO YOU WISH TO CHANGE THE VALUE OF N1 (Y/N)?"
5430 INPUT S$
5440 IF S$="N" THEN GOTO 5460
5450 INPUT N1
5460 PRINT ""
5470 PRINT "PUT IN YOUR DATA DISC AND WHEN YOU WANT TO LOAD"
5480 PRINT " PRESS CONTINUE"
5490 PAUSE
5500 DISP "LOADING FILE "
5510 CREATE BDAT Melt$,8 ! Creates a binary file and stores
5520 ASSIGN @Path1 TO Melt$ ! the data on disc for a double run
5530 OUTPUT @Path1;Temp;R;Rl;Rsl;N1;Mi;Atemp1;Atemp2
5540 FOR I=1 TO N1
5550 OUTPUT @Path1;P(I,1),P(I,2),P(I,3)
5560 NEXT I
5570 IF Mi=1 THEN GOTO 5610
5580 FOR I=1 TO N1
5590 OUTPUT @Path1;P(I,20),P(I,21)
5600 NEXT I
5610 DISP "*****LOAD ENDED*****"
5620 ASSIGN @Path TO *
5630 STOP
5640 Space: ! *****! Clears the screen
5650 OUTPUT 2 USING "E,B";255,75.
5660 RETURN
5670 File: ! *****! If computer will not accept the name
5680 ! of a file then it performs this
5690 ! routine and repeats
5700 PRINT "THE COMPUTER WILL NOT ACCEPT THIS FILENAME"
5710 PRINT "TRY ANOTHER"

```

```

5720      GOTO 1230
5730 Trans: ! *****! Transducer protection routine
5740      GOSUB Space
5750      PRINT "THE MAX TRANSDUCER PRESSURE HAS BEEN REACHED "
5760 Abort: !*****
5770      OUTPUT @Multi;"OP,1",-2,"T"      ! Multi outputs -2 volts to back the
5780      BEEP 1220.7,2                      ! piston off, beeps to warn operator
5790      OUTPUT @Multi;"OP,1",0,"T"
5800      PRINT ""
5810      PRINT "                                *MENU*"
5820      PRINT ""
5830      PRINT "      1  CONTINUE THE RUN"
5840      PRINT "      2  ABORT THE RUN"
5850      PRINT "      3  SAVE THE DATA TAKEN"
5860      INPUT S
5870      IF S=1 THEN GOTO 5920
5880      IF S=2 THEN GOTO 5980
5890      GOSUB Space
5900      IF Init=1 THEN GOSUB Done1
5910      GOSUB Done2
5920      IF I=1 THEN GOTO 5950
5930      I=I-1
5940      D=D-1
5950      OUTPUT @Multi;"OP,1",Spd(D),"T"      ! Multi outputs voltage
5960      WAIT 2
5970      RETURN
5980      OUTPUT @Multi;"OP,1",-5,"T"      ! Multi outputs -5 volts
5990      STOP
6000 Calib: !*****! Allows for calibration of computer
6010      PRINT "CALIBRATE TRANSDUCER FOR ZERO AND 80% DEFLECTION"
6020      PRINT ""
6030      PRINT "TO CALIBRATE PRESS CONTINUE"
6040      PRINT ""
6050      PRINT "TO EXIT CALIBRATION ROUTINE PRESS ANY KEY"
6060      PAUSE
6070      GOSUB Input
6080      ON KBD GOTO 6120
6090      PRINT Pr
6100      WAIT .5
6110      GOTO 6070
6120      OFF KBD
6130      GOSUB Space
6140      RETURN
6150 Conver: !*****!Convert the voltage into pressure
6160      !piston speed and temperature
6170      FOR I=1 TO N1
6180      IF Miss=1 THEN GOTO 6220
6190      P(I,1)=(240*Spd(I))/5
6200      P(I,2)=((P(I,2)*.8)/4)*Transd1
6210      P(I,2)=(P(I,2)*200)/2842
6220      IF Done=1 THEN GOTO 6250
6230      P(I,3)=((P(I,3)*.8)/4)*Transd2
6240      P(I,3)=(P(I,3)*200)/2842
6250      NEXT I
6260      IF Miss=1 THEN GOTO 6280
6270      Atemp1=(Atemp1*400)/5.6
6280      Atemp2=(Atemp2*400)/5.6
6290      RETURN
6300 Sence: !*****!Lowers the ram and sences pressure
6310      OUTPUT @Multi;"OP,1",5,"T"
6320      GOSUB Input
6330      IF Pr<.1 THEN GOTO 6320
6340      RETURN
6350 Rep: !*****!Increases voltage slowly
6360      REPEAT
6370      OUTPUT @Multi;"OP,1",L,"T"
6380      L=L+.002
6390      UNTIL L>Spd(D)
6400      RETURN
6410      END

```

APPENDIX B

COMPUTER PROGRAM FOR TORQUE RHEOMETER

SID 3

```

10 HINEM: 24576
20 DEF FN DB(X) = PEEK (SA + 2 * X) + 256 * PEEK (SA + 1 + 2 * X)
25 DEF FN DC(X) = PEEK (SH + 2 * X) + 256 * PEEK (SH + 1 + 2 * X)
30 DEF FN B(Z) = FN DB(Z) / 4096
40 DEF FN CY(D) = (5 * D ^ 3 + 10 * D * D + 10 * D + 184) * .9846 / 1000000
50 DEF FN T1(K) = K * FN CY(DV)
60 DEF FN T2(K) = ((K < = N1) * K * FN CY(D1) + (K > N1) * (N1 * FN CY(D1)
+ (K - N1) * FN CY(D2)))
70 DEF FN T3(K) = TN + FN CY((INT (I% + I * K) * (I% + I * K < 256)))
80 DEF FN HT(Z) = FN DC(Z) / 40.96
90 DEF FN T(K) = FN T1(K) * (DT = 1) + FN T2(K) * (DT = 2) + FN T3(K) * (DT
= 3)
95 DEF FN E(Z) = FN B(Z) * 20
100 DS = CHR$(4):RD = 768:SA = 24576
110 PRINT DS;"BLOAD SIDCODE.A";RD
200 HOME : PRINT "SLOT NUMBER OF A113 --> ";
210 GOSUB 2320:U = U - ASC ("0"): IF U < 1 OR U > 7 THEN 210
220 SN = U: POKE 8,128 + 16 * SN: PRINT SN
230 POKE 9,192
240 PRINT : PRINT "ENERGY CHANNEL --> ";
250 GOSUB 2320:U = U - ASC ("0"): IF U < 0 OR U > 15 THEN 250
260 EC = U: PRINT EC: POKE 6,EC + 16
270 PRINT : PRINT "TEMPERATURE CHANNEL --> ";
280 GOSUB 2320:U = U - ASC ("0"): IF U < 0 OR U > 15 OR U = EC THEN 280
290 TC = U: PRINT TC: POKE 7,TC + 16
300 PRINT : PRINT "CK? (Y/N)"
310 GOSUB 2320: IF US$ = "Y" THEN 340
320 IF US$ = "N" THEN 200
330 GOTO 310
340 HOME
350 INPUT "NUMBER OF READINGS --> ";NR:NR = INT (ABS (NR)): IF NOT NR THEN
PRINT CHR$(7): GOTO 350
360 POKE 253,NR - INT (NR / 256) * 256: POKE 254, INT (NR / 256)
400 HOME : PRINT : PRINT "EXPERIMENTAL CONDITIONS"
410 PRINT : INPUT "FILL FACTOR --> ";FF
420 PRINT : INPUT "CONCENTRATION (%) --> ";CO
430 PRINT : INPUT "TEMPERATURE (DEG. C) --> ";TE
440 PRINT : INPUT "RAM PRESSURE (BAR) --> ";RP
450 PRINT : INPUT "MASS (G) --> ";M
460 PRINT : INPUT "ROTOR SPEED (RPM) --> ";RS
470 PRINT : INPUT "DATE DD/MM/YY --> ";DD$
480 PRINT : INPUT "MIX --> ";MX$
490 HOME : PRINT : PRINT "EXPERIMENTAL CONDITIONS"
500 PRINT : PRINT "FILL FACTOR --> ";FF
510 PRINT : PRINT "CONCENTRATION (%) --> ";CO
520 PRINT : PRINT "TEMPERATURE (DEG. C) --> ";TE
530 PRINT : PRINT "RAM PRESSURE (BAR) --> ";RP
540 PRINT : PRINT "MASS (G) --> ";M
550 PRINT : PRINT "ROTOR SPEED (RPM) --> ";RS
560 PRINT : PRINT "DATE DD/MM/YY --> ";DD$
570 PRINT : PRINT "MIX --> ";MX$
580 PRINT : PRINT "OK?";
590 GOSUB 2320
600 IF US$ = "N" THEN 400
610 IF US$ < > "Y" THEN PRINT CHR$(7): GOTO 590
620 HOME : PRINT "DELAY TYPE :- ?"
630 PRINT : PRINT "1 - FIXED DELAY THROUGHOUT"
640 PRINT : PRINT "2 - SPLIT DELAY"
650 PRINT : PRINT "3 - INCREASING DELAY"
660 GOSUB 2320:U = U - ASC ("0"):DT = 0
670 ON U GOSUB 2000,2110,2030
680 IF NOT DT THEN 620
690 HOME : PRINT "PRESS ANY KEY TO COMMENCE READING": GOSUB 2320: CALL RD
695 SH = 24576 + 2 * NR
700 BU = 1: ONERR GOTO 720
710 DIM V(2,NR): POKE 216,0: GOTO 730
720 BU = BU + 1:NR = INT (NR / 2): GOTO 710
730 PRINT BU,NR
740 LV = BU
750 WU = 0:TN = 0
760 PRINT : FLASH : PRINT "          CALCULATING          " : NORMAL
800 FOR K = 0 TO NR - 1: GOSUB 2270

```

```

810 J = K + 1
820 V(0,J) = FN T(J):TN = V(0,J)
830 EN = 2 * 3.1415926 * 9.8 * RS / 60 * FN E(K) * DL / M / 1000
840 V(1,J) = EN / DL:WU = WU + EN
850 V(2,J) = FN HT(K)
860 IF NOT TN THEN TN = 256
870 NEXT K
880 IF LV = BU THEN INPUT "FILE? ";FS: PRINT D$:"OPEN":FS: PRINT D$:"WRITE":FS
: PRINT NR * 2 (BU - 1)
890 FOR K = 1 TO NR: PRINT V(0,K): PRINT V(1,K): PRINT V(2,K): NEXT K
900 LV = LV - 1: IF LV THEN SA = SA + 2 * NR:SH = SH + 2 * NR: GOTO 800
910 PRINT WU
920 PRINT RS: PRINT FF: PRINT CO: PRINT TE: PRINT RP: PRINT M: PRINT DD$: PRINT
MX$
930 PRINT D$:"CLOSE"
940 PRINT D$:"RUN SIDLINK"
950 END
2000 HOME :DT = U: PRINT "DELAY VALUE --> ";: INPUT "":DV:DV = INT ( ABS ( DV ))
: IF DV < 1 OR DV > 256 THEN 2000
2010 FOR K = 0 TO 2 * NR STEP 2: POKE SA + K,DV: NEXT K
2020 TT = FN T1(NR): GOTO 2220
2030 HOME : PRINT "INCREASE IN DELAY VALUE PER READING --> ";: INPUT "":I
2040 I = ABS (I):TT = 0:DT = U:DV = I%:TN = 0
2050 PRINT : INPUT "INITIAL DELAY VALUE -->":I%
2060 I% = ABS (I%): IF I% < 1 OR I% > 256 THEN GOTO 2050
2070 FOR K = 0 TO NR * 2 STEP 2
2080 DV = ( INT (I% + I * K) * (DV < 256)):TN = FN T3(K)
2090 POKE SA + K,DV
2100 NEXT K:TT = TN: GOTO 2220
2110 HOME : PRINT "FIRST SECTION:--"
2120 PRINT : PRINT "DELAY VALUE --> ";
2130 INPUT "":D1:D1 = INT ( ABS ( D1 )): IF NOT D1 OR D1 > 256 THEN 2120
2140 PRINT : PRINT "NO. OF READINGS --> ";: INPUT "":N1:N1 = INT ( ABS ( N1 )):
IF N1 < 1 OR N1 > = NR THEN 2140
2150 N1 = N1 - 1
2160 HOME : PRINT "LAST SECTION:--"
2170 PRINT : PRINT "DELAY VALUE --> ";: INPUT "":D2:D2 = INT ( ABS ( D2 )): IF D
2 < 1 OR D2 > 256 THEN 2170
2180 FOR K = 0 TO NR * 2 STEP 2
2190 POKE SA + K,D1 * (K < = (N1 - 1) * 2) + D2 * (K > = N1 * 2)
2200 NEXT K:DT = 2
2210 TT = FN T2(NR)
2220 HOME : PRINT "TOTAL RUN TIME --> ";TT:"S"
2230 PRINT : PRINT "OK?"
2240 GOSUB 2320: IF US$ = "Y" THEN RETURN
2250 IF US$ < > "N" THEN 2240
2260 ON DT GOTO 2000,2110,2030
2270 IF DT = 1 THEN DL = FN CY(DV): RETURN
2280 IF DT = 3 THEN 2300
2290 IF K > N1 THEN DL = FN CY(D2): RETURN
2295 DL = FN CY(D1): RETURN
2300 DV = ( INT (I% + I * (K - 1)) * (DV < 256) + 256 * (DV > = 256))
2310 DL = FN CY(DV): RETURN
2320 POKE - 16368,0
2330 U = FRE (0):U = PEEK ( - 16384)
2340 IF U < 128 THEN 2330
2350 U = U - 128:US$ = CHR$ (U)
2360 POKE - 16368,0
2370 RETURN

```

0300-	7B	SEI	
0301-	A9 00	LDA	£\$00
0303-	B5 F9	STA	£F9
0305-	A9 60	LDA	££60
0307-	B5 FA	STA	£FA
0309-	A5 FD	LDA	£FD
030B-	1B	CLC	
030C-	2A	ROL	
030D-	B5 FB	STA	£FB
030F-	A5 FE	LDA	£FE
0311-	2A	ROL	
0312-	1B	CLC	
0313-	69 60	ADC	££60
0315-	B5 FC	STA	£FC
0317-	A5 FD	LDA	£FD
0319-	49 FF	EOR	££FF
031B-	1B	CLC	
031C-	69 01	ADC	££01
031E-	0B	PHP	
031F-	B5 FD	STA	£FD
0321-	A5 FE	LDA	£FE
0323-	49 FF	EOR	££FF
0325-	2B	PLP	
0326-	69 00	ADC	££00
032B-	B5 FE	STA	£FE
032A-	A0 00	LDY	££00
032C-	B1 F9	LDA	(£F9),Y
032E-	B5 19	STA	£19
0330-	A5 06	LDA	£06
0332-	91 0B	STA	(£0B),Y
0334-	A2 04	LDX	££04
0336-	CA	DEX	
0337-	D0 FD	BNE	£0336
0339-	B1 0B	LDA	(£0B),Y
033B-	91 F9	STA	(£F9),Y
033D-	0B	INY	
033E-	B1 0B	LDA	(£0B),Y
0340-	91 F9	STA	(£F9),Y
0342-	E6 F9	INC	£F9
0344-	E6 F9	INC	£F9
0346-	D0 04	BNE	£034C
034B-	E6 FA	INC	£FA
034A-	D0 04	BNE	£0350
034C-	F0 00	BEQ	£034E
034E-	EA	NOP	
034F-	EA	NOP	
0350-	BB	DEY	
0351-	A5 07	LDA	£07
0353-	91 0B	STA	(£0B),Y
0355-	A2 04	LDX	££04
0357-	CA	DEX	
035B-	D0 FD	BNE	£0357
035A-	B1 0B	LDA	(£0B),Y
035C-	91 FB	STA	(£FB),Y
035E-	CB	INY	
035F-	B1 0B	LDA	(£0B),Y
0361-	91 FB	STA	(£FB),Y
0363-	E6 FB	INC	£FB
0365-	E6 FB	INC	£FB
0367-	D0 04	BNE	£036D
0369-	E6 FC	INC	£FC
036B-	D0 04	BNE	£0371
036D-	F0 00	BEQ	£036F
036F-	EA	NOP	
0370-	EA	NOP	
0371-	BB	DEY	
0372-	A4 19	LDY	£19
0374-	A5 19	LDA	£19
0376-	B5 1A	STA	£1A
037B-	A6 19	LDX	£19
037A-	CA	DEX	
037B-	D0 FD	BNE	£037A
037D-	C6 1A	DEC	£1A
037F-	D0 F7	BNE	£037B
0381-	BB	DEY	
0382-	D0 F0	BNE	£0374
0384-	E6 FD	INC	£FD
0386-	D0 06	BNE	£038E
038B-	E6 FE	INC	£FE
038A-	D0 9E	BNE	£032A
038C-	5B	CLI	
038D-	60	RTS	
038E-	EA	NOP	
038F-	1B	CLC	
0390-	90 9B	BCC	£032A

### SIDCODE PROGRAM

APPENDIX C

COMPUTER PROGRAM FOR THE DETERMINATION OF INTRINSIC VISCOSITY

```

DIMENSION FLOWS(10),FLOW(10),DIFLN(9),RLVIS(9),SPVIS(9)
DIMENSION X(9),Y(9),ST(7)
DATA ST(7),ST(6),ST(5),ST(4),ST(3),ST(2),ST(1)
1/2.3646,2.4469,2.5706,2.7764,3.1625,4.3027,12.706/
200 READ(3,205)NOSLN,MOSET,GBSOL,VOLML,PCTM
205 FORMAT(211,F6.4,F5.2,F5.5)
IF (NOSLN) 295,295,210
210 ACONC=(GBSOL-PCTM*GBSOL/100.)*100./VOLML
WRITE(2,208)
208 FORMAT('1',20X,'INTRINSIC VISCOSITY')
WRITE(2,212)GBSOL,VOLML,PCTM
212 FORMAT('0 GRAMS SAMPLE',F6.4,' VOLUMETRIC',F6.1,'ML MOISTURE',
1F6.2,' PERCENT'/,' FLOW TIMES, SEC.'/'0 AVERAGE',11X,'DATA')
DO 250 J=1,NOSLN
IF (MOSET) 214,211,214
211 IF (J-1) 227,214,227
214 READ(3,215)FLOWS
215 FORMAT(10F5.1)
NO=0
TFLOS=0.
DO 220 I=1,10
IF (FLOWS(I)) 220,220,218
218 NO=NO+1
TFLOS=TFLOS+FLOWS(I)
220 CONTINUE
TFLOS=TFLOS/NO
WRITE(2,225)TFLOS,(FLOWS(I),I=1,NO)
225 FORMAT(3X,F6.1,4X,'SOLVENT',10F6.1)
227 READ(3,232)DIFLN(J),FLOW
232 FORMAT(F5.2,10F5.1)
NO=0
TFLO=0.
DO 240 I=1,10
IF (FLOW(I)) 240,240,235
235 NO=NO+1
TFLO=TFLO+FLOW(I)
240 CONTINUE
TFLO=TFLO/NO
WRITE(2,230)TFLO,J,(FLOW(I),I=1,NO)
230 FORMAT(3X,F6.1,4X,'SOLN C',I1,10F6.1)
X(J)=ACONC/DIFLN(J)
RLVIS(J)=TFLO/TFLOS
SPVIS(J)=RLVIS(J)-1
Y(J)=SPVIS(J)/X(J)
250 CONTINUE
WRITE(2,255)
255 FORMAT('0SUMMARY'/14X,'DILN',8X,'VICOSITY'
1/3X,'CONC.PCT FACTOR REL SPECIFIC REDDCED'/1X)
WRITE(2,245)(X(J),DIFLN(J),RLVIS(J),SPVIS(J),Y(J),J=1,NOSLN)
245 FORMAT(1X,F9.4,F6.1,F10.4,F6.4,F9.4)
N=NOSLN
IF (N-1) 200,200,3
3 EN=N
SIGX=C.0
SIGY=0.0
DO 101 I=1,N
SIGX=SIGX+Y(I)
SIGY=SIGY+Y(I)
SIGXX=SIGXX+Y(I)*Y(I)
SIGYY=SIGYY+Y(I)*Y(I)
101 CONTINUE
A=(SIGY*SIGXX-SIGX*SIGYY)/(EN*SIGXX-SIGX*SIGY)
B=(EN*SIGYY-SIGX*SIGY)/(EN*SIGXX-SIGX*SIGY)
EBA=0.
DO 70 I=1,N
YEA=X(I)*B+A
YEA=Y(I)-YEA
EBA=EBA+YEA*YEA
70 CONTINUE
NDF=N-2
DF=NDF
IF (NDF) 340,340,342
340 C1=0
GOTO 346
342 C1=SQR(EBA/DF*(1./EN+SIGX*SIGX/(EN*EN*SIGXX-EN*SIGX*SIGX)))
C1=C1*ST(NDF)
346 WRITE(2,260)A,C1
260 FORMAT('0 INTRINSIC VISCOSITY=',F8.3,' DL/GRAM',5X,'C I =',F6.3)
GOTO 200
295 CONTINUE
END

```